MICROTUBULE DEPOLYMERIZING COMPOUNDS

AS NOVEL POTENTIAL ANTIVASCULAR AGENTS

IN CANCER THERAPY

Direttore della Scuola: Ch.mo Prof. Giuseppe Basso

Coordinatore d'indirizzo: Ch.mo Prof. Giuseppe Basso

Supervisore: Dott. Giampietro Viola

Dottoranda: Dott.ssa Elena Porcù

INDEX

2. NOSCAPINE DERIVATIVES AS ANTIMITOTIC AGENTS

3. SMALL MOLECULES AS WNT INHIBITORS IN COLON CANCER

SOMMARIO

Negli ultimi anni la ricerca biomedica si è interessata principalmente di patologie oncologiche, le quali causano un'elevata incidenza di morte nei Paesi sviluppati. Sebbene siano stati identificati numerosi target molecolari, risulta ancora necessario trovare nuove strategie per migliorare la chemioterapia tradizionale.

I tumori crescono in maniera aberrante, e la loro espansione necessita dell'apporto di nuovi vasi sanguigni. Alcuni approcci terapeutici nella lotta contro i tumori prevedono l'utilizzo di farmaci antiangiogenici, tra i quali sono comprese le molecole che legano la tubulina (TBA). Questo studio riguarda la valutazione farmacologica di molecole con struttura simile alla combretastatina (TR-644, TR-764, 3b) che sono in grado di legarsi alla tubulina con alta affinità. E' stata studiata l'attività di questi composti sul citoscheletro di cellule endoteliali, e su processi legati all'angiogenesi, quali la motilità cellulare o la permeabilità. Essi alterano la struttura dei microtubuli e inducono un'elevata disorganizzazione dei microfilamenti di actina. Tali effetti danneggiano le proteine che costituiscono le adesioni focali o le giunzioni aderenti, compromettendo le vie di segnale di FAK/Src e VE-caderina/β-catenina.

È stata valutata l'attività antivascolare anche in modelli *in vivo*, sulla membrana corioallantoidea di pollo (CAM) e in modelli di allotrapianto tumorale nel topo. I composti testati agiscono in maniera significativa sia riducendo la densità microvascolare, sia inibendo la crescita tumorale. Inoltre, in cellule endoteliali, il composto TR-764 è in grado di contrastare stimoli ipossici, che sono stati descritti come possibili responsabili dell'insorgenza di meccanismi di resistenza del tumore.

Questi nuovi TBA vengono quindi proposti come potenziali agenti terapeutici per la monoterapia di tumori altamente vascolarizzati.

Oltre a derivati della combretastatina è stato studiato un altro sottotipo di TBA non tossici, le noscapine. Una serie di derivati della noscapina è stata sintetizzata ed è

stato analizzato il l'effetto antimitotico su linee cellulari tumorali. Questi composti bloccano il ciclo cellulare in fase G2/M, e di conseguenza inducono l'apoptosi, attivando la via mitocondriale. Essi agiscono riorganizzando la struttura radiale dei microtubuli e portano alla formazione di fusi mitotici multipolari. Queste modificazioni stimolano l'insorgenza di danni al DNA, e l'attivazione di caspasi-9 e PARP, effetti già dimostrati per altri derivati della noscapina.

Tuttavia in questo studio viene proposto un nuovo metodo molto efficace per la sintesi chimica dei composti (Suzuki cross-coupling).

Infine, è stata svolta una valutazione farmacologica di una serie di piccole molecole, con potenziale attività inibitoria della via di segnale di Wnt/β-catenina in una linea cellulare di cancro al colon (HT-29). I composti più attivi inibiscono questa via di segnale, compromettendo l'attività del fattore di trascrizione β-catenina, inibendo i suoi geni target, quali la ciclina D1 e c-myc, e alterando l'attività dei suoi cofattori TCF-1/4. Il trattamento quindi comporta la riduzione della proliferazione cellulare *in vitro*. Gli effetti di inibizione dell'attività trascrizionale della β-catenina sono stati confermati anche *in vivo*, tramite saggi reporter di Wnt, in modelli di zebrafish.

Gli studi farmacologici riportati in questa tesi possono essere utili per migliorare gli approcci terapeutici per il trattamento di alcuni tumori.

SUMMARY

In the last years, biomedical research was focused on cancer, since it is a leading cause of death in the developed countries. However several molecular targets were identified thus making necessary to find new strategies to improve the traditional chemotherapy.

Aberrant tumors grow and spread, and they require their own blood supply. Some approaches of anticancer therapy utilize antiangiogenic drugs, including tubulin binding agents (TBAs). Here we focused our studies on several combretastatin-like molecules (TR-644, TR-764, 3b) which bind to tubulin with high affinity. We report the activity of our TBAs on endothelial cell cytoskeleton, cell motility, permeability, and other processes involved in angiogenesis. Our compounds strongly induce microtubules derangement, and alter the actin microfilaments organization. These effects result in focal adhesions and adherens junctions impairment, by affecting FAK/Src and VE-cadherin/β-catenin molecular pathways. We also evaluated the antivascular activity *in vivo* both in the chick embryo chorioallantoic membrane (CAM) and in an allograft mouse tumor model. These compounds induce a significant decrease in microvascular density, and strongly inhibit the tumor growth. Additionally, compound TR-764 is endowed with the ability to counteract *in vitro* hypoxic stimuli on endothelial cells, which usually give rise to resistance mechanisms. Thus we propose our molecules as potential single agents against highly vascularized tumors.

A subtype of non-toxic TBAs is represented by noscapines. Some derivatives were synthesized and we investigated their antimitotic effect, on cancer cell lines. They induce cell cycle arrest in G2/M phase and consequently they stimulate apoptosis, following the mitochondrial way. Radial organization of microtubules is altered and

multipolar spindles occur after treatment. These modifications trigger DNA damage, and caspase-9/PARP activation. Here we report a new effective method for chemical synthesis (Suzuki cross-coupling), even though the biological activity of our compounds is comparable to other known noscapine derivatives.

Another part of the study concern the pharmacological evaluation of a series of small molecules as potential inhibitors of the Wnt/β-catenin pathway. The most potent compounds induce Wnt repression, in a colon cancer cell line (HT-29). They impair β-catenin activity as transcription factor, by downregulating its target genes cyclin D1 and c-myc and altering TCF-1/4 co-factors. Therefore the treatment leads to a reduction of cell proliferation *in vitro*. Finally we confirmed the inhibitory effects on β-catenin transcriptional activity *in vivo*, in Wnt-reporter zebrafish models.

All these pharmacological studies could be helpful to improve potential approaches for an effective anticancer therapy.

1. TUBULIN BINDING AGENTS AND ANGIOGENESIS

1.1 INTRODUCTION

1.1.1 Development of vasculature

In vertebrate development, one of the primitive processes for embryonic progression is the formation of circulating system, necessary to supply the growth of the other organs[1]. Starting from mesoderm, angioblasts differentiate in endothelial cells, giving rise to the "vasculogenesis" process. Key factors such as fibroblast growth factor 2 (FGF2) and bone morphogenetic protein 4 (BMP4) are involved in endothelial commitment, resulting in *de novo* blood vessels formation, which progressively maturate in arteries, venules and capillaries[2]. A second event, known as "angiogenesis", includes the remodeling of primitive vessels into a mature vascular network, by growth, expansion and sprouting of endothelial cells. In the final stage, during "arteriogenesis", pericytes or smooth muscle cells cover endothelial cell channels, providing the development of stable blood vessels and control perfusion[3].

Numerous processes and signaling pathways were described as mediators of vasculature development, and all of these inputs are precisely synchronized to produce functional blood vessels[4]. Particularly, growth factors and cytokines, such as vascular endothelial growth factor (VEGF), fibroblast growth factor (FGF), tumor necrosis factor-alpha (TNF-α), transforming growth factor-beta (TGF-β), the angiopoietins (ANG), and platelet-derived growth factor (PDGF) are direct contributors in the angiogenic process, and their activity is selectively regulated through ligand-receptor interaction systems[5,6]. Other mechanisms involved in angiogenesis regulation are the proteolysis and remodeling of the ECM, operated by the activity of proteolytic enzymes, such as metalloproteinases and plasmin, which are critical in the endothelial cells migration, the invasion into the perivascular

tissue, the morphological formation of luminal structures. These mechanisms are essential in angiogenesis regulation since the extracellular matrix is an important mediator for angiogenesis during development, oncogenesis and wound healing, and endothelial cells have been shown to require appropriate cell-matrix interactions[7],[8]. The contacts to the extracellular matrix are mediated by integrins, transmembrane heterodimeric receptors, which transduce environmental signals to cytoskeletal remodeling and intracellular signaling pathways, involved in phenotypic modulation, cell proliferation, motility and mechanotransduction[9],[10].

The signals are transduced at intracellular level and stimulate the activation of a plethora of signaling pathways, comprehending the Rho GTPases family, protein kinase C (PKC), Notch, focal adhesion kinase (FAK)/steroid receptor coactivator (Src)[11],[12],[13],[14],[15].

Besides the interactions between endothelial cells and the extracellular matrix, also cell-to-cell contacts are essential for vascular development and maturation. Perivascular cells, smooth muscle cells and adventitial fibroblasts are associated with the endothelium capillaries and contribute to stabilize vessels during the later stages of angiogenesis. However it has been described that they are involved in early events of vascular development, since they stimulate the deposition of protein of the extracellular matrix, or the secretion of soluble factors, such as VEGF[5].

Therefore paracrine stimuli regulate the local microenvironment, controlling also the development of cell polarity during lumen formation, vascular integrity and permeability. These processes are strictly regulated by the interaction between VE-cadherin (vascular endothelial) and its intracellular binding partners, such as β-catenin[16],[17].

Vascular development is a highly complex process which requires the participation of numerous molecules, such as growth factors, cytoskeleton proteins or kinases, and other cell types which cooperate with endothelial cells to vessel maturation.

1.1.2 Physiological and pathological angiogenesis

The development of new blood vessels from existing vasculature is a process relatively rare in the healthy human adult, since it occurs only in wound healing and during the female menstrual cycle.

Generally, vasculogenesis and angiogenesis are processes which appear physiologically at embryonic stages, during mammalian development, but they are critical in many pathologies. Excessive or deficient angiogenesis is essential in different pathological conditions, such as diabetic retinopathy, arthritis, athero-sclerosis, psoriasis, but it is extensively investigated in human neoplasia[18].

According to Folkman and Hanahan[19], the equilibrium between physiological and pathological conditions is regulated by a balance of several pro- and anti-angiogenic factors, as well the tumor progression.

Angiogenesis is a critical phenomenon not only for tumor invasiveness, but also for the early events which determine tumorigenesis[20].

Table I. Angiogenesis-dependent diseases (adapted from Ref.[21])

Disease	*Symptoms*
Diabetic retinopathy	Loss of vision
Rheumatoid arthritis	Pain and immobility from destroyed cartilage
Atherosclerotic plaques	Chest pain, dyspnoea
Endometriosis	Abdominal pain from intraperitoneal bleeding
Crohn's disease	Intestinal bleeding
Psoriasis	Persistent severe
Uterine fibroids	Vaginal bleeding, abdominal pain
Benign prostatic hypertrophy	Urinary retention
Cancer	Bleeding, thrombosis, anaemia, abdominal ascites, bone pain, seizures from cerebral oedema around a tumor and others

1.1.3 Tumor angiogenesis

Tumor angiogenesis was deeply studied, and it can occur following different mechanisms. Most tumors start growing in a dormant form, as avascular nodules, until cancer cells keep a balance between proliferation and apoptotic stimuli. Secondly, to ensure the tumor growth, the "angiogenic switch" has to occur, and the unvascularized tumor mass can expand in a hypervascularized proliferating tumor. Pro-angiogenic molecules are stimulated and prevail on antiangiogenic factors, promoting the development of tumor blood vessels[22].

Tumor vessels differ from normal blood vasculature in terms of structure, permeability and stability. They are not characterized by the classical layout arteries-capillaries-veins, but they can have dead ends. The organization is highly chaotic and vessels are tortuous, leaky and haemorrhagic, rich in proangiogenic factors like VEGF. The blood flow is irregular and oscillating, leading to dysfunctional capillaries. Sprouting of new vessel is continuously stimulated and uncontrolled[23].

Several mechanisms were identified as determiner of the tumor vasculature: angiogenic sprouting, vasculogenesis, intussusception, vessel co-option, vascular mimicry, tumor stem cell to endothelial cell differentiation[24].

Sprouting of new vessels from preexisting ones involves the loss of junctions between endothelial cells, degradation of basement membrane, and migration of endothelial cells. In particular, migrating cells which respond to angiogenic stimuli are "tip cells", while "stalk cells" constitute the wall of blood vessels and proliferate in order to expand the tube[1]. This process is strictly mediated by VEGF and its receptors, and by the Delta/Notch pathway[15],[25].
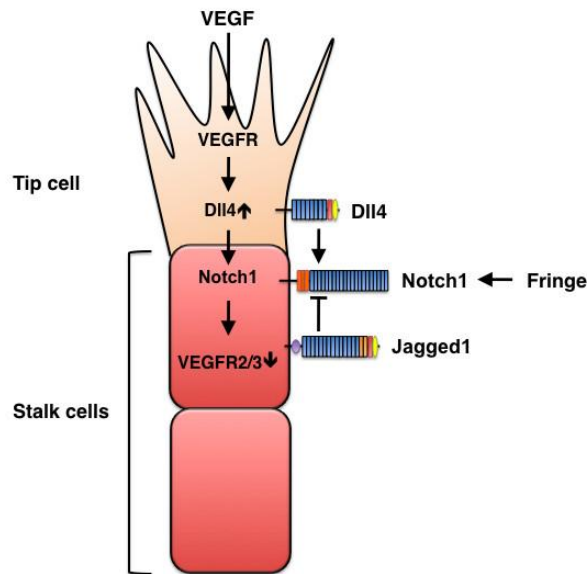
Figure 1. Molecules involved in sprouting angiogenesis (adapted from Ref.[26])

Vasculogenesis is the formation of blood vessels from circulating cells. It is a *de novo* production of endothelial cells, derived from their progenitor cells, the angioblasts, which are stimulated to migrate from bone marrow to peripheral blood, where they differentiate to form new blood vessels. The term angiogenesis is strictly defined as the development of blood vessels from pre-existing ones, whereas vasculogenesis is used when there are no pre-existing vessels. Neverthenless, vasculogenesis can occur, and then vessels are extended by angiogenesis[27].

Intussusception is a more rapid and energically more economic way to generate new capillaries. It does not require the immediate proliferation of endothelial cells, but rather the rearrangement of the structure of the pre-existing vessels. Opposing microvascular walls protrude into the capillary lumen, creating a contact between endothelial cells. A perforation of the endothelial bilayer occurs, and an interstitial core is formed. To expand the vessel myoblasts and perycites invade the lumen, leading to a deposition of collagen fibrils. The new capillaries result less leaky than the vessels formed by other mechanisms[28],[29]. Sprouting and intussusception can be

complementary and sequential processes in angiogenesis, but they can occur autonomously. Moreover it has been reported that muscle capillary growth results after an increase in blood flow through intraluminal splitting, and in absence of sprouting[30].

Vessel co-option, firstly described in brain, is the tumor cells migration along the preexisting vessels, in order to use them[31]. It occurs tipically in highly vascularized tissues, and it represents a mechanism of microcirculation provided lacking sprouting or angiogenesis. Tumors can grow and metastasize without a real formation of blood vessels, but by hijacking the existing vasculature. This characteristic makes vasculature hidden to therapy and could explain resistance mechanisms of the antiangiogenic drugs[32].

Vascular mimicry is a mechanism of angiogenesis independent from endothelial cells. It is described as the differentiation of highly aggressive tumor cells into multiple cellular phenotypes, which form a vascular channel for blood circulation. Vascular-like structured are formed by tumor cells and laminin, and they contain plasma and red blood cells. Vascular mimicry is associated to an increase risk of metastasis and poor prognosis, even if its occurrence in patients is relatively rare.

It has been described that VE-cadherin is essential in vascular mimicry, and other factors involved in this phenomenon are FAK, phosphoinositide 3-kinase (PI3K), Notch and hypoxia-inducible factor-1α (HIF-1α). On the other hand, bFGF and VEGF were found to be unable to induce these vascular-like structure[33].

Finally, **tumor stem cells can differentiate to endothelial cells**, and participate to the developing of tumor vasculature. Thanks to their ability to undergo asymmetric division, cancer stem cells can program themselves to assume several phenotypes, among which they can be committed to the endothelial lineage. Consequently, these cells can be recruited for tumor vascularization[34].
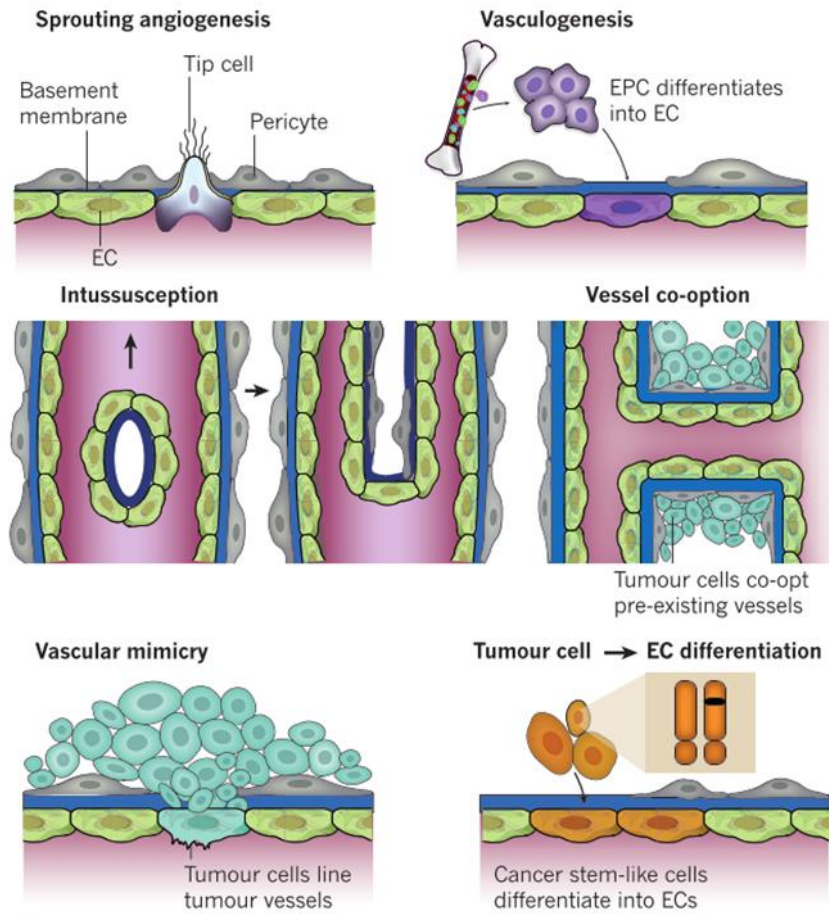
Figure 2. Mechanisms of vessel formation (adapted from Ref.[2])

1.1.4 Hypoxia and tumor angiogenesis

Hypoxic microenvironment is necessary to regulate homeostatic equilibrium between vascular oxygen supply and metabolic demand, both in physiological and in pathological conditions[35],[36].

HIF is the key molecule regulating hypoxic-mediated processes, and it was found upregulated in many cancers[37]. Aberrant tumor growth requires additional oxygen supply, and HIF pathway is activated in order to stimulate neovascularization. HIF system activates multiple signaling pathways regulating both angiogenesis and

tumorigenesis, as well as the progression of tumors to malignancy[38]. It induces and in turn is amplified by a wide range of growth factors and oncogenic stimuli, and many HIF target genes belong to the angiogenic pathway. These evidence support the HIF system as an antiangiogenic and anticancer target.

Table II summarized the main molecules involved in angiogenesis, directly regulated by hypoxia.

Table II. Action of hypoxia on some molecules involved in angiogenesis (adapted from Ref.[36])

Steps in angiogenesis	Stimulatory factors	Inhibitory factors
Vasodilation Increased vascular permeability	Nitric oxide synthases VEGF, Flt-1, Kdr	Angiopoietin-1 Tie-2
Extravasation of plasma proteins Endothelial sprouting	VEGF Angiopoietin-2, Tie-2	Angiopoietin-1 Tie-2
Degradation of extracellular matrix	Balance between MMPs and TIMPs Collagen prolyl-4-hydroxylase	TIMP-1 PAI-1
Liberation of growth factors (including VEGF, IGF-1and bFGF)	uPA receptor	Thrombospondin-1 PAI-1
Endothelial cell proliferation & migration	Interplay between VEGFs, angiopoietins and FGFs, MCP-1, PDGF	
Pericyte and smooth muscle recruitment Endothelial assembly and lumen acquisition	PDGF, VEGF Angiopoietin-1 Tie-2 Integrins	VEGF Thrombospondin-1
Stabilization of nascent vessels Maintenance, differentiation and remodeling PAI-1	PAI-1 Angiopoietin-1 Tie-2	Angiopoietin-2 Tie-2

1.1.5 Antiangiogenic therapy

Since tumor growth requires blood vessel supply, targeting angiogenesis could be a strategy to optimize cancer therapy. Most approaches are based on combination treatments, focused on the inhibition both of tumor mass and its vasculature[39].

The VEGF signaling system, constituted by ligands, receptors and intracellular downstream molecules, is the most common target used in antiangiogenic therapy, together with other proangiogenic factors (i.e. FGFs, PDGFs).

Several methods such as antibodies, soluble receptors, aptamers or peptides which bind the ligand, are used and tested to specifically counteract the angiogenic stimuli of tumors. Moreover, the receptors can be masked by decoy molecules or key components of the intracellular signalling cascades can be inhibited by small lipophilic molecules that cross the plasma membrane of the cells[40]. A list of drugs approved by FDA in March 2013 is reported in Table III.

Table III. List of drugs approved by FDA for anti-angiogenic cancer treatment - March 2013 (adapted from Ref.[40])

Name	*Target*	*Type of cancer*
Bevacizumab	VEGF-A	Metastatic colorectal cancer Metastatic non-squamous Metastatic breast cancer Recurrent GBM Metastatic RCC (with IFN-a)
Aflibercept	VEGF-A and partially for PlGF	Metastatic colorectal cancer (second-line)
Axitinib	VEGFRs, PDGFR, and cKIT	Advanced renal cell carcinoma
Pazopanib	TKIs	Renal cell carcinoma Advanced soft tissue sarcoma that has received chemotherapy

Regorafenib	VEGFRs, PDGFR, FGFRs, Tie2, DDR2, Trk2A, Eph2A, RAF-1, BRAF, BRAFV600E, SAPK2, PTK5, and Abl	Metastatic colorectal cancer (refractory disease)
Sorafenib	VEGFRs, PDGFRs, Raf, KIT	Advanced renal cell carcinoma Unresectable hepatocellular carcinoma
Sunitinib	VEGFRs, PDGFs. KIT, RET, CSF-1R and flt3	Gastrointestinal stromal tumour Advanced renal cell carcinoma Unresectable locally advanced or metastatic pancreatic neuroendocrine tumours
Vandetanib	VEGFRs, EGFRs and RET	Unresectable locally advanced or metastatic medullary thyroid cancer
Everolimus	mTOR	Advanced HER2-negative Breast Cancer Progressive Neuroendocrine Tumours of Pancreatic Origin (PNET) Subependymal Giant Cell Astrocytoma (SEGA) Advanced renal cell carcinoma
Temsirolimus	mTOR	Advanced renal cell carcinoma

FDA approved drugs include also small molecules with low specificity. Tyrosine kinase inhibitors (TKIs) are not directed to a single protein, but they target multiple pathways and several receptors. They act at intracellular levels, interfering with receptors kinase activity, and blocking the signal transductions necessary for the pro-angiogenic effect. TKIs are represented by compounds that bind to the ATP binding site of the tyrosine kinase receptor, preventing its activation, or by antibodies that block the contact between the growth factors and their receptors[41].

Table IV. Examples of Kinase Inhibitors (adapted from Ref.[41])

INHIBITOR	*OTHER NAMES*	*INHIBITS*
Axitinib	AG013736	VEGFR, PDGFR, and c-kit
Canertinib	CI-1033	EGFR, HER2, HER3, and HER4
Cediranib	Recentin, AZD2171	VEGFR, PDGFR- , and c-kit
Dasatinib	Sprycel, BMS- 354825	Abl, Src, and Tec
Erlotinib	Tarceva, OSI-774	EGFR/HER1
Gefitinib	Iressa	EGFR/HER1
Imatinib	Gleevec, STI571	Abl, PDGFR, and c-kit
Lapatinib	Tykerb, GW-572016	EGFR and HER2
Leflunomide	Arava, SU101	PDGFR (EGFR and FGFR)
Motesanib	AMG 706	VEGFR, PDGFR, and c-kit
Neratinib	HKI-272	EGFR and HER2
Nilotinib	Tasigna	Abl, PDGFR, and c-kit
Pazopanib	Armala, GW786034	VEGFR, PDGFR and c-kit
Regorafenib	BAY 73-4506	VEGFR-2 and Tie-2
SemAxinib	SU5416	VEGFR
Sorafenib	Nexavar, BAY 43- 9006	Raf, VEGFR-2 and -3, PDGFR, and c-kit
Sunitinib	Sutent, SU11248	VEGFR, PDGFR, Flt-3, c-kit, RET, and CSF-1R
Tandutinab	MLN518, CT53518	PDGFR, Flt-3, and c-kit
Toceranib	Zactima, ZD6474	
Vandetanib	PTK787	VEGFR-2, PDGFR- , EGFR, and RET
Vatalanib		VEGFR, PDGFR- , and c-kit

In addition to VEGF, FGFs, PDGFs pathways, angiopoietins, epidermal growth factor receptor (EGFR), phosphoinositide 3-kinase (PI3K)/AKT/mammalian target of rapamycin (mTOR), mitogen-activated protein kinases (MAPK), Delta/Notch and

HIF signaling pathways were deeply studied in order to identify specific targets for antiangiogenic therapy[42].

Since angiogenesis is a process regulated by multiple signaling pathways, more wide approaches are still optimized, in order to target the tumor vasculature at more levels. Nevertheless, by targeting multiple pathways, resistance mechanisms and potential side effects can occur, like gastrointestinal perforations, impaired wound healing, bleeding, hypertension, proteinuria, and thrombosis[41].

All these drugs and others were simply categorized by D. Siemann *et al.* in two different classes: angiogenic inhibitors (AIs), or vascular disrupting agents (VDAs).

AIs are cytostatic molecules which prevent the formation of new blood vessels, while VDAs are cytotoxic and target the pre-existing tumor vasculature[43].
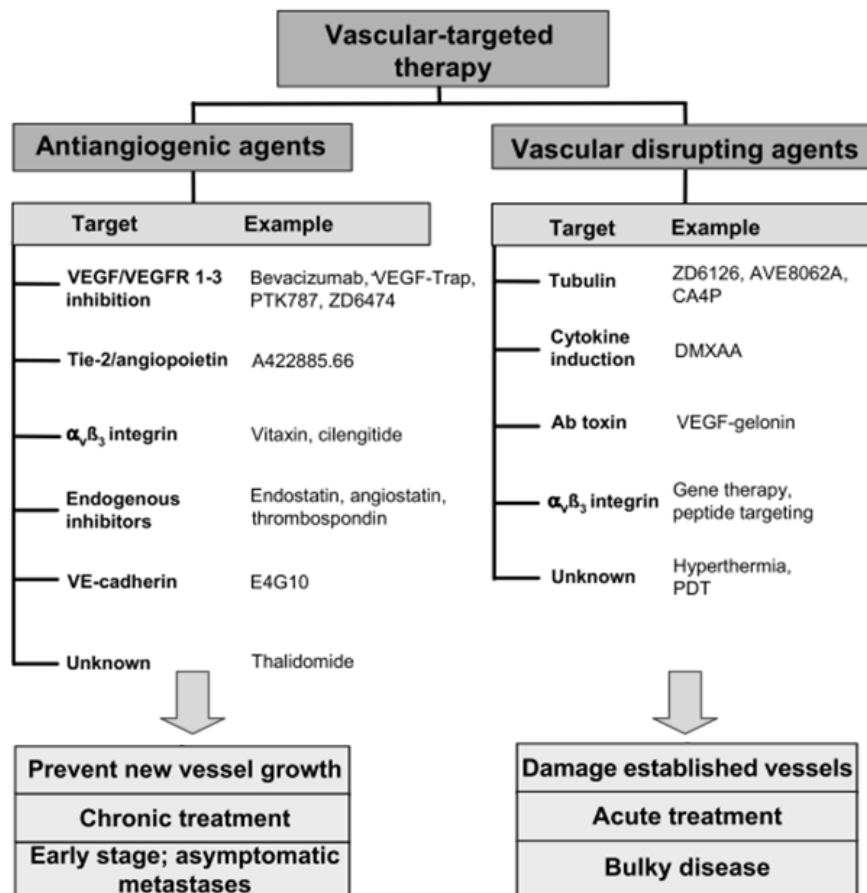
Figure 3. Examples of vascular-targeted therapy (adapted from Ref.[43])

Treatment with these agents shows different responses. AIs therapy results in vessel normalization, whereas VDAs which disrupt the vasculature. AIs allow efficient delivery of chemotherapeutic drugs and increased oxygenation, which aid radiotherapy. VDAs therapy leads to the formation of extensive central necrosis, and it leaves a rim of surviving viable cells targetable with standard treatments[23],[44].
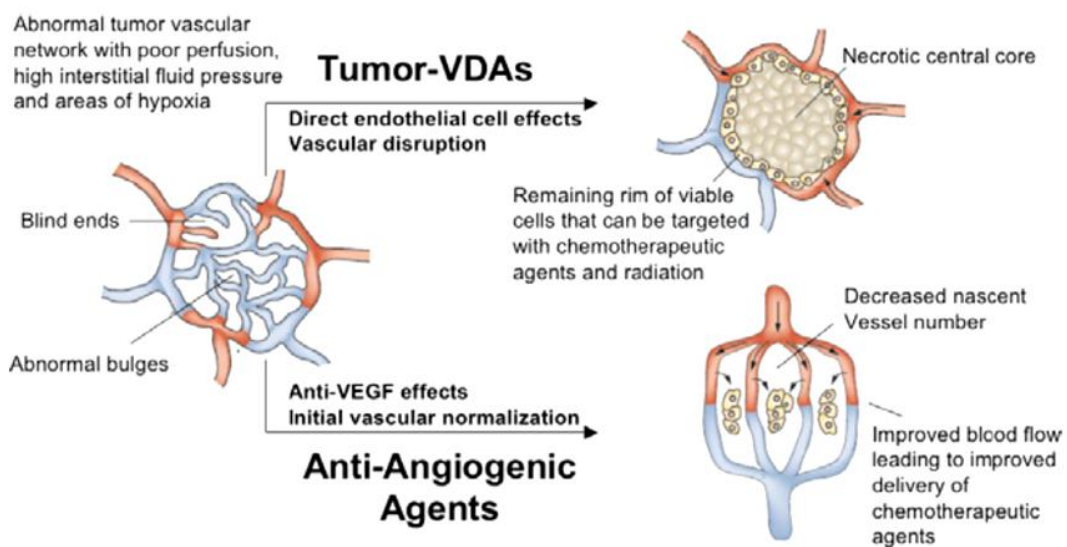
Figure 4. Preclinical effects of AIs and VDAs on abnormal tumor blood vessels (adapted from Ref.[23])

1.1.6 VDA: Vascular Disrupting Agents

VDAs are ligand-directed or small molecules which selectively target pre-existing tumor vasculature. They rapidly shutdown the blood flow of tumor tissue, causing ischaemia and secondary tumor cell death.

It has been demonstrated that they have insufficient activity as single agents. Several resistance mechanisms occur, such as the resistance of the tumor rim cells, while promising results has been described in combination with other chemotherapeutics.

Moreover, their efficacy is dependent on tumor type and a moderate variability in patients was observed[45],[46]. The susceptibility to VDAs treatment is primarily dependent on fragility, instability and cell-to-cell endothelial junctions defectiveness of tumor blood vessels. Secondly, the high proliferative index of tumor endothelial cells make them more sensitive to VDAs disruption. Finally, tumors have less pericytes and mural cells in contact with endothelial cells, compromising the vascular stability[47].

Ligand-specific VDAs are represented by antibodies, peptides or growth factors which selectively bind to the endothelium. They are conjugated with a toxin or a pro-coagulant factor which induce endothelial cell death.

Concerning small molecule VDAs, they can be divided in two essential categories: flavonoids and tubulin binding agents (TBAs)[48],[49]. Flavonoids cause partial derangement of the actin cytoskeleton, DNA strands breaks and apoptosis of endothelial cells, with macrophages activation and cytokines release[50]. TBAs induce tubulin depolymerisation and dysorganisation of both tubulin and actin cytoskeleton, due to their binding to different sites of tubulin.

1.1.7 Tubulin Binding Agents (TBAs) as antiangiogenic drugs

Many conventional chemotherapeutics actually have unknown antiangiogenic activity, such as tyrosine kinase inhibitors, hormonal ablation therapies, and cytotoxic drugs[41].

TBAs were originally used as antimitotics against cancer, but antivascular activities were reported.

Binding to tubulin, they can promote microtubules polymerization and stabilization (i.e. taxanes, epothilones), or microtubules depolymerization and instability (i.e. colchicine, Vinca alkaloids, combretastatins)[51],[52].

The cytoskeleton organization of endothelial cells can be directly altered by these agents with consequent changes in endothelial shape and vessel blockage, reduction in blood flow and disruption of the endothelial cell layer. The basement membrane is exposed, triggering the coagulation cascade, and increase in vessel permeability[50].

On endothelial cells, at low concentrations, TBAs produce subtle effects on microtubules dynamics, preventing their contact to transient subcellular assemblies, such as focal adhesion and adherens junctions. In that way, TBAs inhibit endothelial cell adhesion, motility and cell-to-cell interactions, acting on specific signaling pathways[51].

Moreover, they interfere with the normal organization of actin in stress fibers, causing the loss of cell polarity and they inhibit cell contractility, due to an increased myosin light chain phosphorylation, preventing the formation of cell protrusions such as lamellipodia.

Cell shape is impaired and, in some cases, it assumes a "blebbing" and rounded morphology[53],[54].

Migration dynamics and contacts between lamellipodia and extracellular matrix are processes highly regulated by integrin-dependent anchoring to the extracellular matrix, and by focal adhesions, transiently assembled at the cell surface, to link plasma membrane to the intracellular cytoskeleton.

TBAs give rise not only to a defective or reduced focal adhesion assembly, but also disrupt adherens junctions formation, respectively acting on FAK and VE-cadherin signaling pathways[55],[11].

Several proteins, like VE-cadherin, p120-catenin, β-catenins, plakoglobin, vinculin, functionally contribute to form adherens junctions at cell surface, which provide a direct connection to the actin cytoskeleton, and they are principle mediators of endothelial cell engagement with other endothelial cells[56],[57]. These homotypic

interactions, critical for angiogenic sprouting and for maintenance of vascular integrity, are disrupted by TBAs[58].

Finally, all these molecules are interconnected to VEGF receptors, simplifying the integration of multiple extracellular signals, necessary for the response to pro-angiogenic stimuli, and ultimately prevented by the action of TBAs[51].
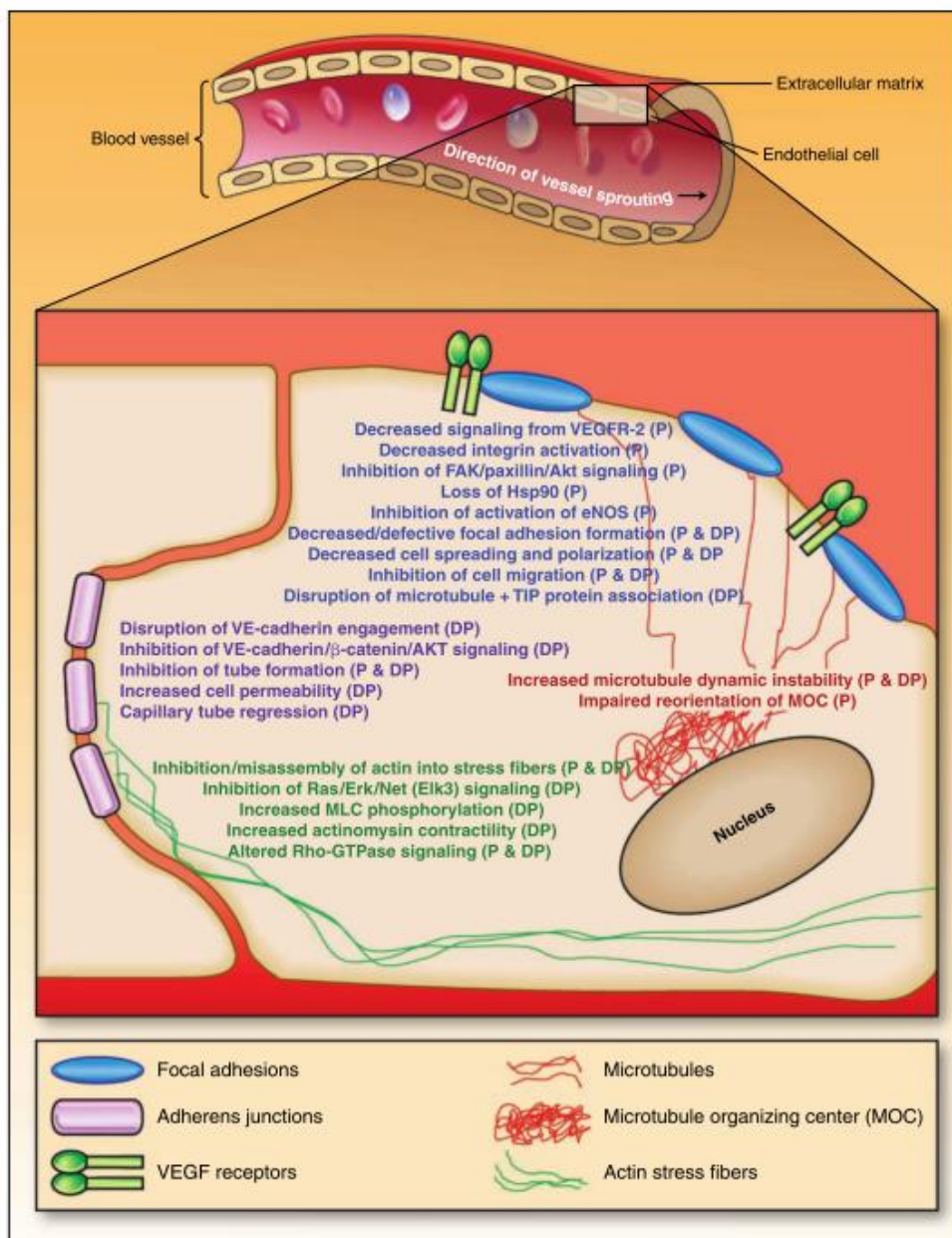

Figure 5. Effects of TBAs on endothelial cells (adapted from Ref.[51])

Among the different TBAs, we are particularly interested on combretastatin. Combretastatin-A4 (**CA-4**), isolated from the African tree Combretum caffrum, is structurally related to colchicine, which is too toxic for clinical use. **CA-4** emerged as a promising VDA, and its structure was optimized in order to obtain a soluble pro-drug, **CA-4P**[46]. Its activity was deeply studied and the mechanism of action was investigated *in vitro*, as well as the antivascular effect in various tumor models was described[59],[60],[61].

Nevertheless several **CA-4** analogues were synthesized with the aim to increase the anticancer and antiangiogenic activity, reduce the side effects and overcome resistance mechanisms[62],[63].

Untreated endothelial cells	VDA-treated endothelial cells	VDA-treated endothelial cells
• intact microtubules	• disrupted microtubules	• disrupted microtubules
• non-contractile cells	• contractile cells	• contractile-blebbing cells
• tight VE-cadherin junctions	• actin stress fibers	• actin-lined surface blebs
• low permeability	• strong focal adhesions	• misassembled focal adhesions
	• disrupted VE-cadherin junctions	• lost VE-cadherin junctions
• low RhoA-GTPase activity	• high permeability	• high permeability
• low Rho kinase activity		
		• necrotic cells
	• high RhoA-GTPase activity	
	• high Rho kinase activity	• high RhoA-GTPase activity
	• high SAPK-2/p38 activity	• high Rho kinase activity
	• high ERK activity?	• high SAPK-2/p38 activity
		• low ERK activity?

Microtubules
Actin stress fibers
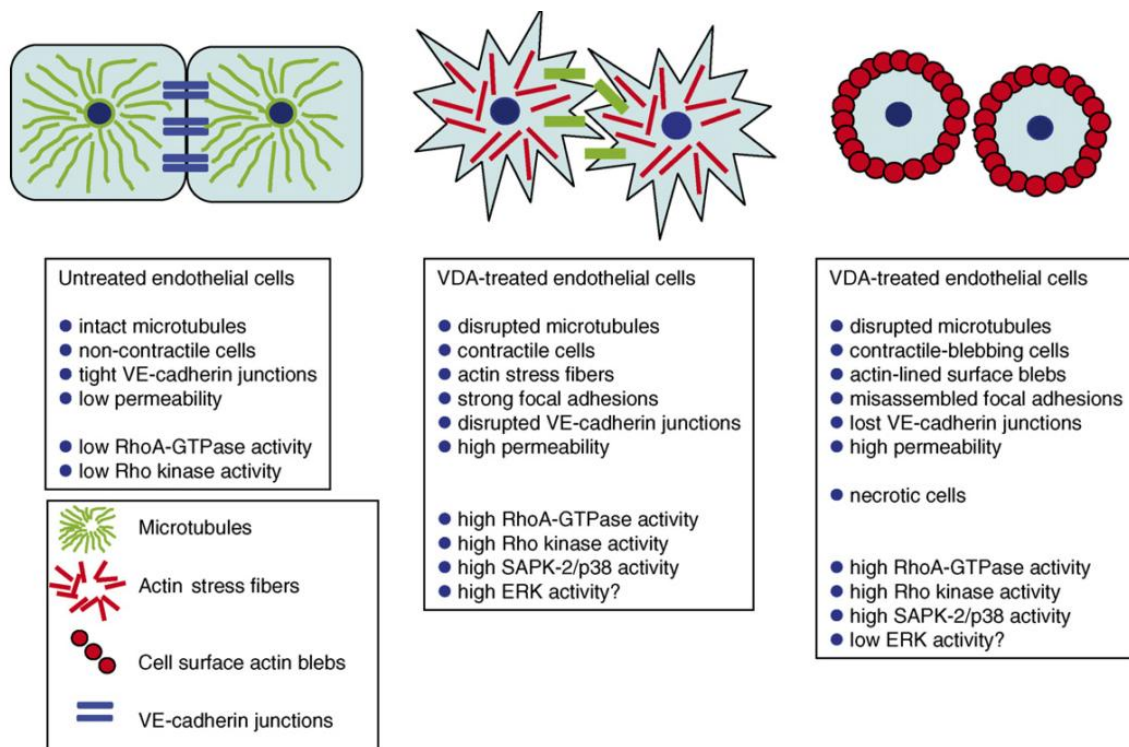Cell surface actin blebs
VE-cadherin junctions

Figure 6. Endothelial morphological and signaling responses to **CA-4P**, associated with a rise in permeability (adapted from Ref.[47])

1.1.8 Resistance to antiangiogenic therapy

Angiogenesis is a very dynamic process, apt to continuous modifications and adaptive mechanisms. These compensatory effects gave rise to resistance mechanisms to the anti-angiogenic therapies, explaining the numerous unsatisfactory results of the last clinical trials with antiangiogenic drugs. New approaches should be directed to arrest the communications between vascular components and cells which gradually change the tumor microenvironment. It has been described that resistance phenomena are due to different mechanisms. The redundance of angiogenic factors (VEGF, FGFs, PDGFs, TNF-α), mostly related to hypoxia, is one of the cause of resistance. Secondly, as described before, several mechanisms can induce neovascularization and angiogenesis, so it is hard to arrest all of the involved signaling pathways[64]. Both stromal cells, which secrete pro-angiogenic factors and stimulate paracrinally tumor cells to grow, and perycites, involved in vessel maturation and regulation of perfusion, are implicated in resistance mechanisms. Moreover, genetic instability and multiple mutations were found in tumor endothelial cells, particularly in glioblastomas[65]. These genomic modifications originated in endothelial cells, derived from cancer stem cell abnormal proliferation and differentiation and are associated to resistance to the antiangiogenc therapies[40].

1.2. AIM OF THE STUDY

The fight against cancer is one the main research focus of the last century, because of its high incidence, aggressiveness and inability to control.

Aberrant tumor growth requires its own blood supply, so inhibiting angiogenesis could be an effective strategy to arrest tumor development and progression.

Several strategies were studied to inhibit the formation of tumor vessels, and one of them is the use of tubulin binding agents. These drugs, binding to tubulin, cause cytoskeleton alterations and are able to impair endothelial cells functionality.

This study is focused on three molecules, **TR-644**, **TR-764** and **3b** which have strong antimitotic activity on hyperproliferating cancer cells.

TR-644 (2-amino-4-(3',4',5'-trime-thoxyphenyl)-5-aryl thiazole) is a derivative of combretastatin-A4, while **TR-764** (2-aryl-4-amino-5-(3′,4′,5′-trimethoxybenzoyl) thiazole) and **3b** (4-amino-2-(thiophen-3-yl)thiazol-5-yl)(3,4,5-trimethoxyphenyl)-methanone) are new molecules.

All of them were syntesized in order to improve **CA-4** effects as anticancer and antivascular agent, and to overcome resistance mechanisms and side effects.

We have investigated the role and the efficacy of **TR-644**, **TR-764**, **3b** as vascular disrupting agents, and to examine in depth their mechanism of action as regards their antiangiogenic activity.

Since an high anti-tumoral activity was already reported, our aim is to demonstrated their antivascular effects, thus to propose these molecules as drugs which target both the tumor vasculature and the tumor mass.

CA-4

TR-644

TR-764

3b

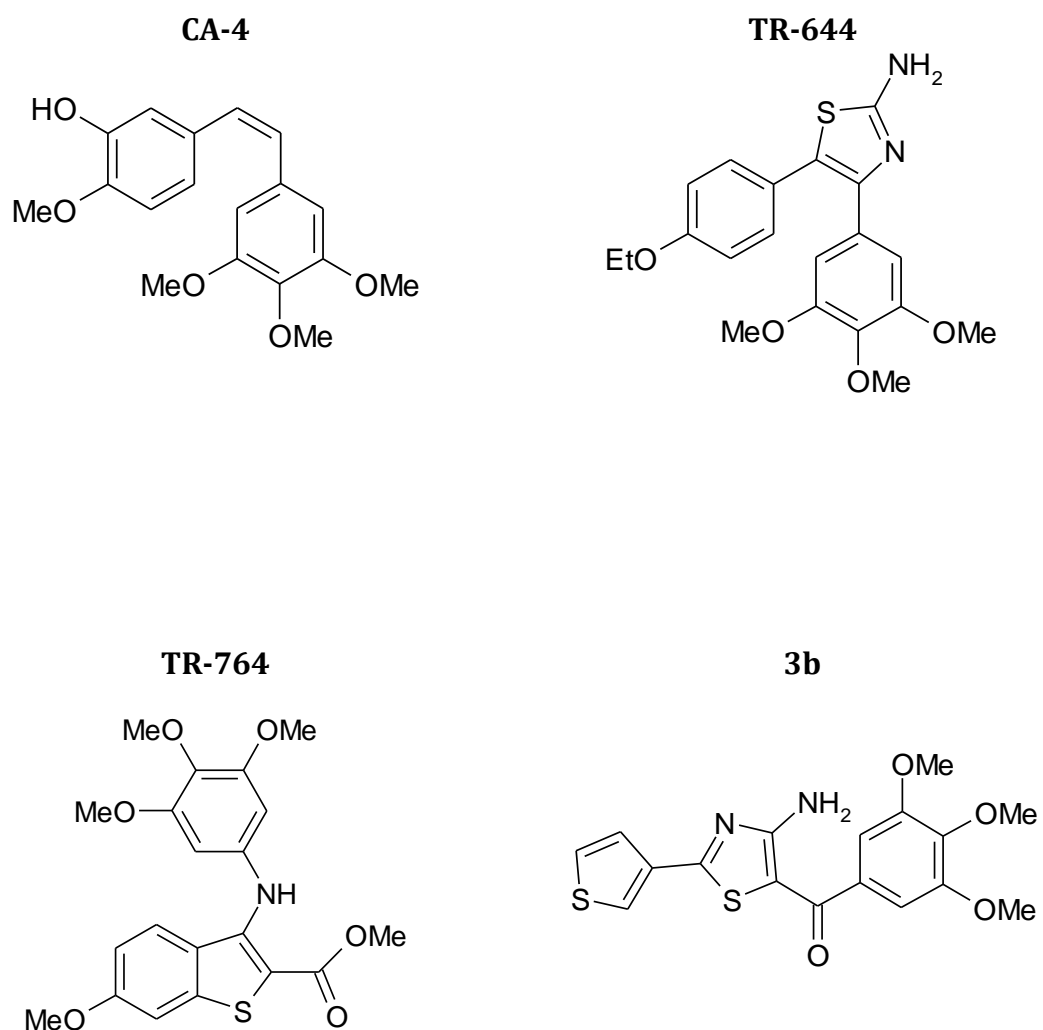**Figure 1.** Chemical structures of compounds.

1.3. RESULTS

1.3.1. TR-644 A NOVEL POTENT TUBULIN BINDING AGENT INDUCES IMPAIRMENT OF ENDOTHELIAL CELLS FUNCTION AND INHIBITS ANGIOGENESIS

Elena Porcù[*], Giampietro Viola[*], Roberta Bortolozzi, Luca Persano, Stefania Mitola, Roberto Ronca, Marco Presta, Romeo Romagnoli, Pier Giovanni Baraldi, Giuseppe Basso

Equal contributing Authors

1.3.1.1. Abstract

TR-644 is a novel combretastatin (**CA-4**) analogue endowed with potent microtubule depolymerizing activity superior to that of the lead compound and it also has high affinity to colchicines binding site of tubulin. We tested **TR-644** anti-angiogenic effects in human umbilical endothelial cells (HUVEC). It showed no significant effects on the growth of HUVEC cells at concentrations below 1000nM, but at much lower concentrations (10-100nM) it induced inhibition of capillary tube formation, inhibition of endothelial cell migration and affected endothelial cell morphology as demonstrated by the disruption of the microtubule network. **TR-644** also increased permeability of HUVEC cells in a time dependent manner.

The molecular mechanism for the anti-vascular activity of **TR-644** was investigated in detail. **TR-644** caused G2/M arrest in endothelial cells and this effect correlated with downregulation of the expression of Cdc25C and Cdc2^{Tyr15}. Moreover **TR-644** inhibited VEGF-induced phosphorylation of VE-cadherin but did not prevent the VEGF-induced phosphorylation of FAK. In chick chorioallantoic membrane *in vivo* assay, **TR-644** (1 pmol/egg) efficiently counteracted the strong angiogenic response induced by FGF2. Also **CA-4**, used as reference compound, caused an antagonistic effect, but in contrast, it induced per se, a remarkable angiogenic response probably due to an inflammatory reaction in the site of treatment. In a mice allogenic tumor model, immunohistochemical staining of tumors with anti-CD31 antibody showed that **TR-644** significantly reduced the number of vessel, after 24hours from the administration of a single dose (50mg/Kg).

1.3.1.2. Introduction

The microtubule system of eukaryotic cells is a critical element in a variety of fundamental cellular processes, such as cell division, formation and maintenance of cell shape, regulation of motility, cell signalling, secretion and intracellular transport[67]. Among the various strategies developed to block mitosis, microtubules represent an attractive target for numerous small natural and synthetic molecules that inhibit the formation of the mitotic spindle[67,68]. Besides the ability to inhibit tumor cell proliferation, microtubule-targeting drugs have also been shown to have activity against the vasculature in tumors[51,61]. Since the tumor vasculature differs from that of normal tissues, in recent years, the abnormal structure and function of tumor blood vessels have been studied in the attempt to attack and destroy solid tumors. These vascular abnormalities consist of temporary occlusions, a rapidly dividing endothelial population, blind ends, leaky vessels, and a reduction in blood vessel coverage by pericytes. In addition, the structure of the tumor blood vessel wall is also abnormal, which is evident by uneven vessel diameter and defects in their endothelial lining, as well as the presence of endothelial cells undergoing apoptosis. In contrast, normal vasculature is organized with vessels close enough to each other to ensure adequate nutrient and oxygen supply to all cells. Tumor-vascular disrupting agents (VDAs) are a new class of anti-cancer drugs that show strong promise in treating a variety of solid tumors[51]. In contrast to antiangiogenic therapy, which inhibits the outgrowth of new blood vessels, VDAs treatments selectively attack the existing tumor vasculature. Several low-molecular-weight VDAs are currently in clinical trials or undergoing preclinical testing. One of the most important antimitotic agents and vascular disrupting agents (VDA) is combretastatin A-4 (**CA-4**, Figure 1). **CA-4**, isolated from the bark of the South African tree *Combretum caffrum* is one of the well-known natural molecules that

strongly inhibits tubulin polymerization by binding to the colchicine binding site. **CA-4** shows potent cytotoxicity against a wide variety of human cancer cell lines, including those displaying multidrug resistant. A water-soluble disodium phosphate derivative of **CA-4** (named **CA-4P**) has shown promising results in human cancer clinical trials. The proposed mechanism of **CA-4P** for rapid tumor vascular shutdown assumes that the compound induces changes in endothelial-cell shape, plasma membrane blebbing, and increases the permeability of cell monolayers. These changes in endothelial cells result in increases in vascular resistance to blood flow and increases vascular permeability and in vasoconstriction, subsequently leading to vascular shutdown. **CA-4** has tumor vascular damaging effects at well-tolerated doses of **CA-4P** in animal models[69]. Recently, **CA-4P** has received orphan drug designation for the treatment of anaplastic thyroid cancer, medullary thyroid cancer, and stage IV papillary or follicular thyroid cancer. Despite its efficacy **CA-4P** presents some side-effects in particular tumor pain.

Therefore, many synthetic analogues were synthesized making structural modification of the **CA-4** in order to develop new compounds with more activity and fewer adverse reactions. Previous structure-activity relationship studies demonstrated that both the 3',4',5'-trimethoxy substitution pattern on the A-ring and the *cis*-olefin configuration at the bridge were fundamental requirements for optimal activity, while B-ring structural modifications were tolerated by the target[70]. However, the *cis*-configuration of **CA-4** is prone to isomerize to the thermodynamically more stable *trans*-form during storage and metabolism, resulting in a dramatic decrease in its activity[71]. Thus, to retain the appropriate geometry of the two adjacent aryl groups required for a potent bioactivity, chemically stable *cis*-restricted derivatives of **CA-4** were obtained by incorporating the olefinic double bond with vicinal diaryl-substituted five-member aromatic heterocyclic rings, such as pyrazole[72], imidazole[73], thiazole[74], furazan (1,2,5-

oxadiazole)[75], isoxazole[76], oxazole[72], 1,2,3-thiadiazole[77], triazole[78] and 1,2,3,4-tetrazole[74]. We recently synthesized[79] a new series of 2-amino-4-(3',4',5'-trimethoxyphenyl)-5-aryl thiazoles in which we identified compound **TR-644** as the most active compound (Figure 1). It has been shown that this compound is endowed with high antiproliferative effects with IC_{50} values in the nanomolar range in different cancer cell lines. Here we show that this compound is endowed with pronounced *in vitro* antivascular effects at sub-toxic concentrations and appears to disrupt the vasculature *in vivo* both in tumor tissue and in the chick chorioallantoic membrane, without any evident toxic effect.
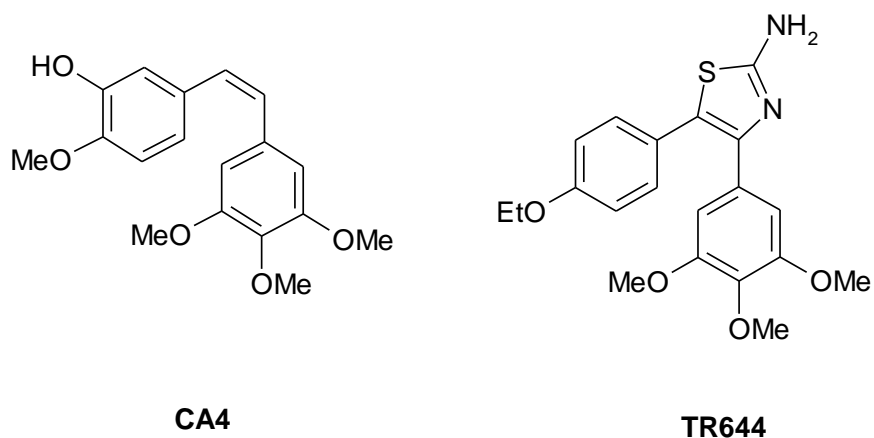

CA4   **TR644**

Figure 1. Chemical structures of compounds

1.3.1.3. Results

TR-644 inhibits HUVEC migration and tube formation

To investigate the effects of **TR-644** on endothelial cell migration, we scraped confluent monolayers of HUVEC to clear space for motile cells to move into. As shown in Figure 2 (panels A and B) we observed that **TR-644** inhibited HUVEC migration in a concentration and time-dependent manner. For comparison, we studied the effects of **CA-4** in the same experimental conditions. **CA-4** treatment displayed similar effects, with a more pronounced inhibition of cell migration at the concentration of 5nM (Figure 2, panel C) at which **TR-644** is barely effective.
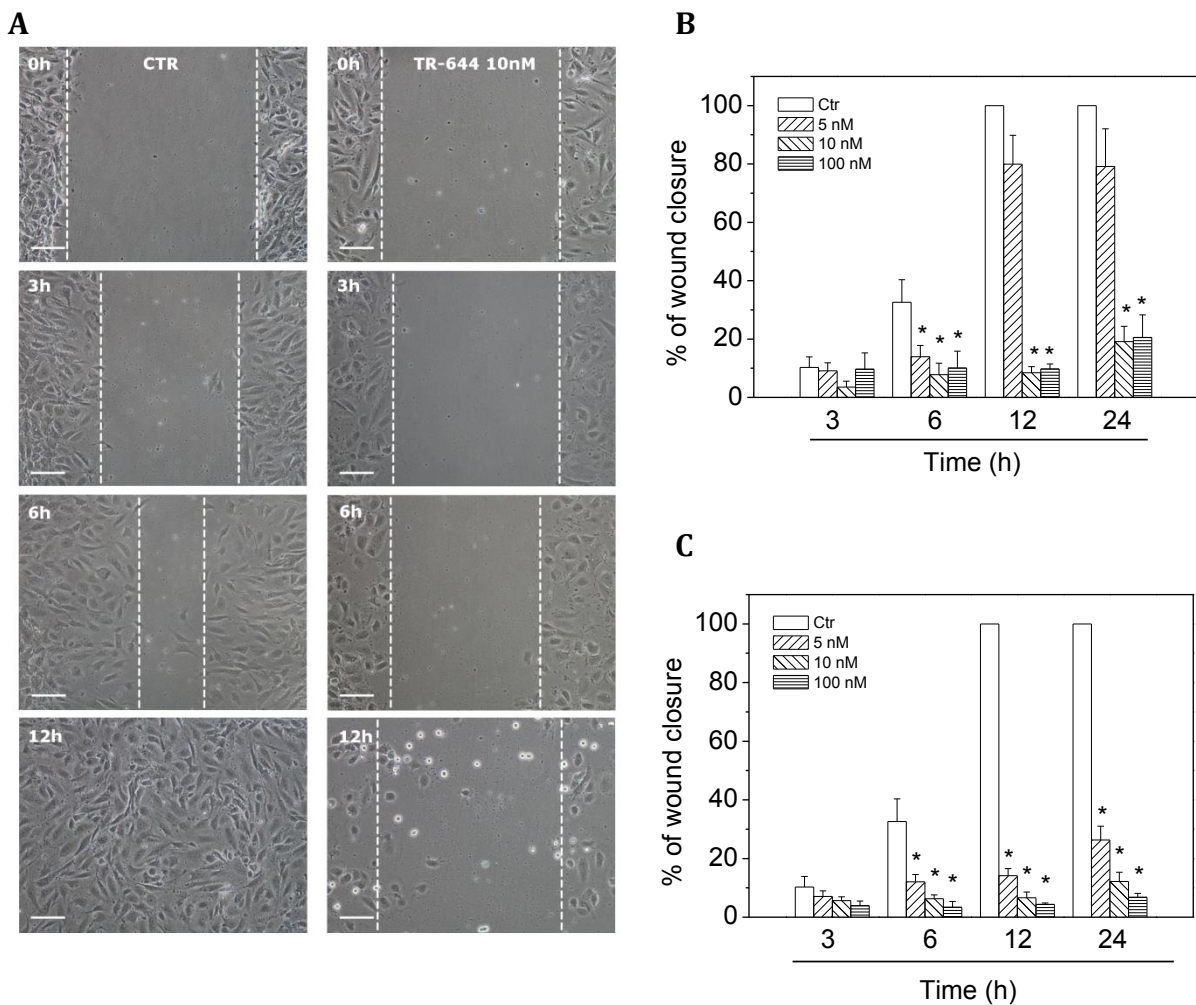

Figure 2. TR-644 inhibits HUVEC migration. Panel A. Confluent HUVEC monolayer were scratch wounded and the cells were treated with different concentration of

TR-644 or **CA-4** and at different times cells were photographed, 40x magnification; Bar=10µm. The dotted lines define the areas lacking cells. Panels B and C. Graphs show the quantitative effect of **TR-644** (B) and **CA-4** (C) chosen as reference compound. Migration was quantified by measuring the gap closure at the indicated times as showed in panel A. Data were represented as mean ± S.E.M. of three independent experiments. *p<0.01 vs control.

We also tested the effects of **TR-644** on tubules formation assay, a well known *in vitro* angiogenesis test. After 18hours from cells seeding on Matrigel, HUVEC form a rich meshwork of branching capillary-like tubules with multicentric junctions. In the presence of **TR-644**, at different concentration and after 3hours of incubation, we observed that the capillary-like tubes were interrupted (1-10nM) and at higher concentration (100nM) most cells were spherical either isolated or aggregated in small clumps (Figure 3, panel A). These effects started to occur after 1hour of incubation and further increased after 6hours of incubation (Data not shown).

Quantitative image analysis showed that **TR-644** (10-100nM), significantly decreased both dimensional (percent of area covered by HUVECs, total length per field) and topological parameters (number of meshes per field, and number of branching points) of the capillary-like network (Figure 3, panel B). Similar results were obtained with **CA-4** (Figure 3, panel B).

Moreover we evaluated the inhibitory effects of **TR-644** on tube formation. In this case, drugs were added simultaneously at the time of seeding. After 3hours of incubation we found a strong inhibition of capillary formation in comparison to untreated cells, in which we observed the polygonal structures (mesh) already formed (Figure 3, panel C). It is interesting to note that in this case the effect of **TR-644** was evident and significant also at the lowest concentration used (1nM) and was higher than that of **CA-4** (Figure 3, panel D), suggesting that **TR-644** strongly interfere with the ability of HUVEC to form capillary-like structures *in vitro*.

31

A
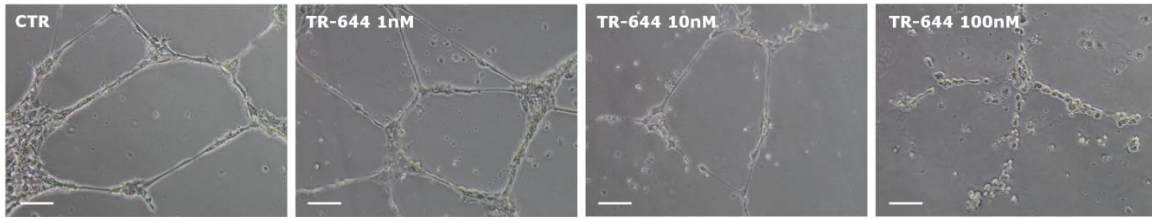
B
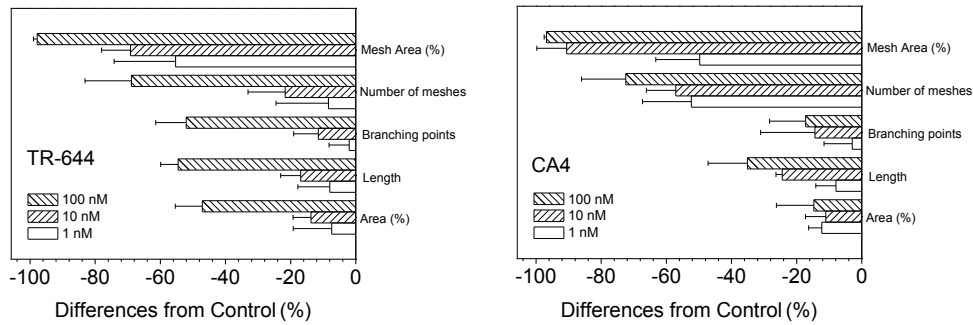
C
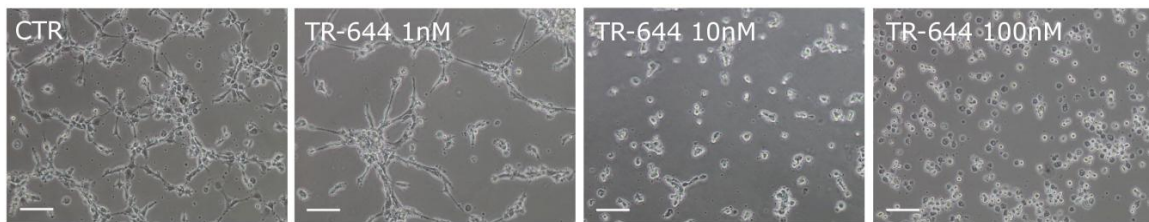
D
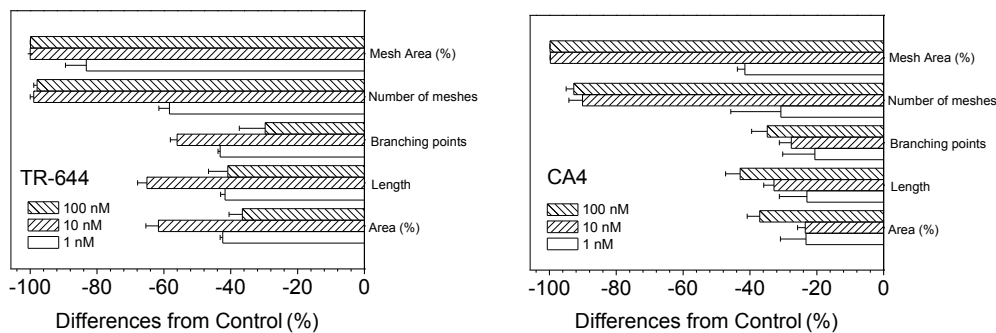
Figure 3. Inhibition of endothelial cell capillary-like tubules formation by **TR-644**. Tubules formation on Matrigel was carried out as described in Materials and methods. Panel A. Representative pictures (10x magnification; Bar=10μm) of preformed capillary-like tubules treated with increasing concentration of **TR-644** for 3hours. Panel B quantitative analysis of the effects of **TR-644** and **CA-4** on the dimensional and topological parameters of the preformed capillary-like tubules network. Data were represented as mean ± S.E.M. of three independent experiments. Panel C Representative pictures (10x magnification; Bar=10μm) of HUVEC in

Matrigel treated with increasing concentration of **TR-644** for 3hours. Panel D quantitative analysis of the effects of **TR-644** and **CA-4** on the dimensional and topological parameters of the capillary-like tubules network. Data were represented as mean ± S.E.M. of three independent experiments.

TR-644 increases permeability of the vascular endothelial monolayer

Changes in endothelial cell monolayer permeability also provide an *in vitro* model of tumor vascular disruption. The increase in permeability induced by the tested compounds, was evaluated in 24-well cell culture, where a confluent HUVEC monolayer was formed and monitoring the fluorescent signal of FITC-dextran in the lower chamber as a function of time. As shown in Figure 4, a significant increase in endothelial cell permeability was observed when the confluent monolayers were treated with 10 and 100nM **TR-644** (panel A) whereas **CA-4** (panel B) displayed a similar profile.

A
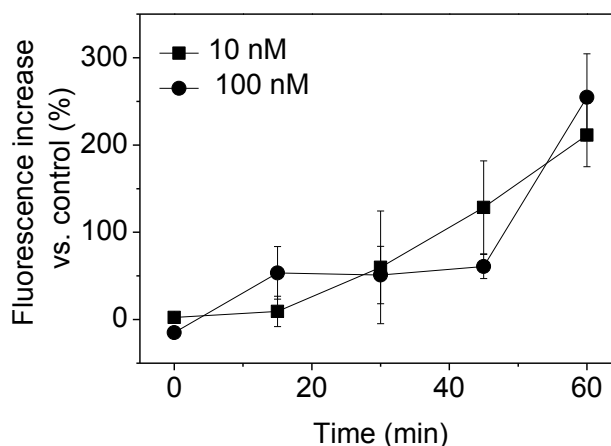
B
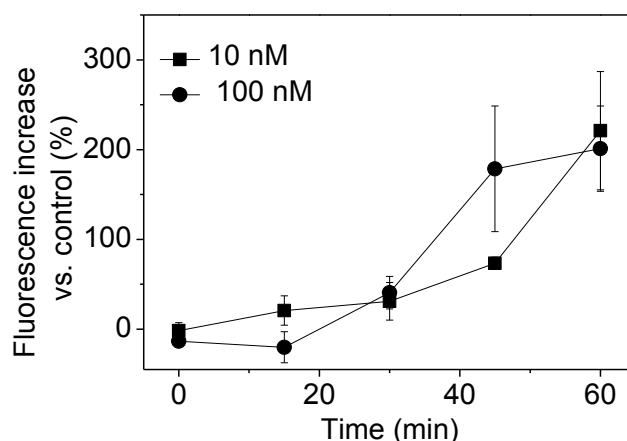
Figure 4. TR-644 increased the permeability of an endothelial cell layer. HUVEC cells were seeded onto 0.1% collagen-coated 24-well insert wells in complete medium until a confluent monolayer was formed. They were then treated with the indicated concentrations of **TR-644** (Panel A) or **CA-4** (Panel B). Simultaneously FITC-dextran was also added and its passage into the lower chamber was monitored at the indicated times. Data were represented as mean ± S.E.M. of three independent experiments.

TR-644 is not cytotoxic at the concentrations that induce vascular effects

To evaluate if the inhibition of cell migration and tube formation are due to a cytotoxic action of the drug we analyzed cell proliferation at different times of incubation by trypan blue count.

As shown in Figure 5 (panel A), with **TR-644** we observed a modest reduction of the number of cells occurring only at longer times of incubation (48-72hours). At lower concentration (10nM), after 24hours of incubation, no reduction of the viability was found while at 48 and 72hours of incubation the viability decrease to 38% and 43% respectively. For comparison **CA-4** was also evaluated (Figure 5, panel B) and we observed a marked reduction of cell number also at the concentration of 10nM for which we note a reduction of about 45% after 24hours incubation relative to untreated cells. We also carried out a clonogenic assay in which we observed that

TR-644 had no effect at concentration lower than 10nM in comparison to **CA-4** which was more toxic than **TR-644** of an order of magnitude (Figure 5, Panel C).

To further confirm that **TR-644** is not cytotoxic for endothelial cells we performed flow cytometric Annexin-V/PI assay of HUVEC cells. As showed in Figure 5 (panel D), we observed only a slight reduction of the cell viability at time points in which, as described above, we observed antivascular effects of the drug. Even at longer times of incubation (24hours) and highest concentration (100nM) no sign of apoptosis were detected.

A

B

C
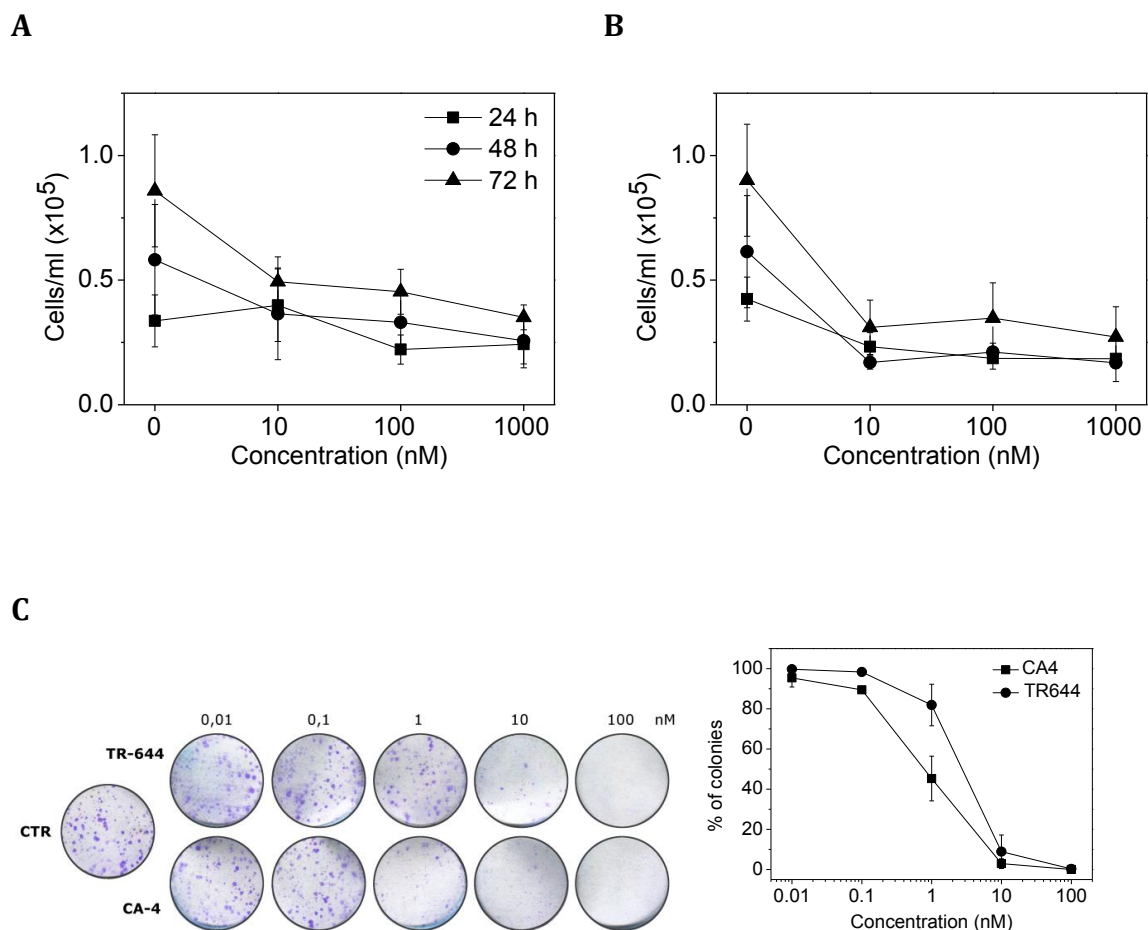
D
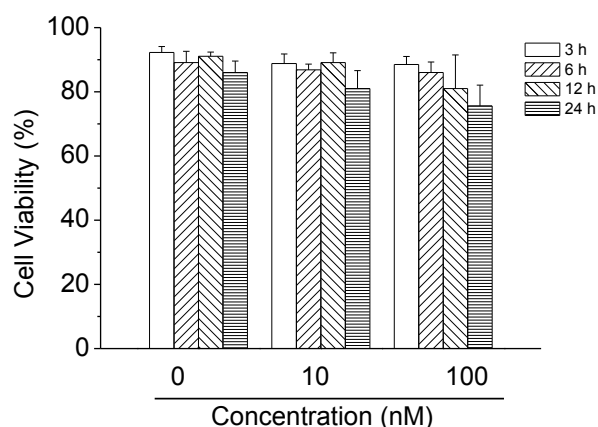
Figure 5. Effects of **TR-644** on HUVEC cells viability. HUVEC were plated on onto 0.1% collagen-coated 24-wells and then treated with the indicated concentrations of **TR-644** (panel A) or **CA-4** (panel B). At different times (0, 24, 48 and 72hours) cells were trypsinized and viability was determined by trypan blue exclusion assay. Data were represented as mean ± S.E.M. of three independent experiments. Panel C. Representative dishes and quantitative data on the inhibitory effects of **TR-644** and **CA-4** on HUVEC proliferation evaluated by clonogenic assay. Data were represented as mean ± S.E.M. of three independent experiments. Panel D. HUVEC plated as described above were assayed for apoptosis by flow cytometry using an Annexin-V/PI assay kit.

TR-644 induce G2/M arrest of the cell cycle in HUVEC cells

The effect of **TR-644** on cell cycle progression was examined by flow cytometry. **TR-644** treatment resulted in the accumulation of cells in the G2/M phase, with a concomitant reduction in the proportion of cells in the G1 phase after 24hours of treatment. These changes started to occur at the concentration of 10nM (Figure 6, panel A). A small decrease, although not significant, of cells in the S phase was also observed.

Next, we investigated the association between **TR-644**-induced G2/M arrest and alterations in G2/M regulatory protein expression. Cell arrest at the prometaphase/metaphase to anaphase transition is normally regulated by the

mitotic checkpoint. In eukaryotic cells the activation of Cdc2 kinase is necessary for occurrence of the G2/M transition of the cell cycle. Activation of the kinase requires its dephosphorylation at Tyr15 and Thr14 by the phosphatase Cdc25 and accumulation of the cyclin B protein. As shown in Figure 6 (panel B), **TR-644** caused a decrease in cyclin B1 expression at 10nM while at 100nM we observed a significant increase. $Cdc2^{Tyr15}$ and Cdc25 levels decreased both at 10 and 100nM. Altogether these results indicate that arrest at G2/M induced by **TR-644** is accompanied by a decreased expression of cyclin B1 at lower concentration whereas at higher concentration by an increase and by a remarkable decrease of Cdc25c and p-$Cdc2^{Tyr15}$.

A

B

0   1   5   10   100 nM

Cyclin B1

Cdc2 (Y15)

Cdc25C

β-actin
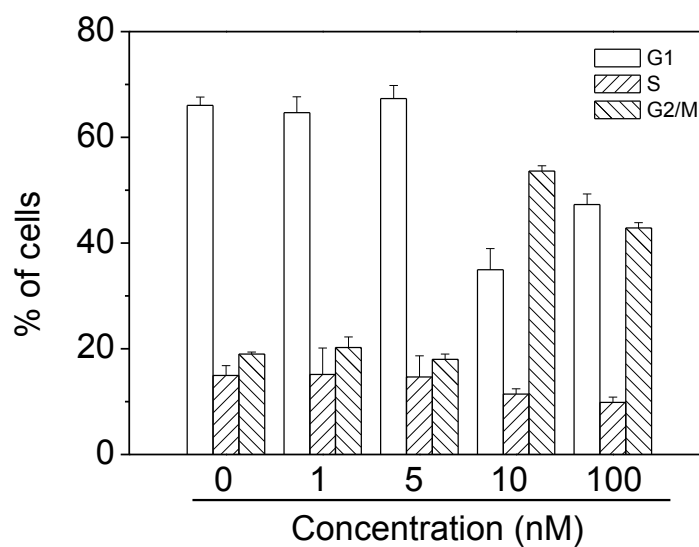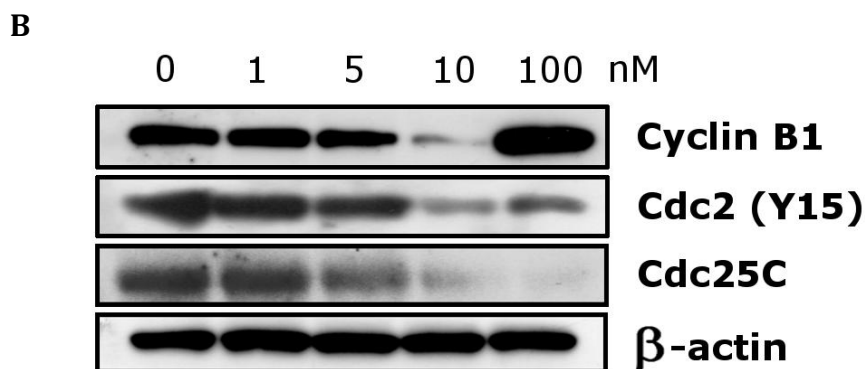
Figure 6. Panel A. Effect of compound **TR-644** on cell cycle distribution of HUVEC cells. Cells were treated with different concentrations, ranging from 1 to 100nM for 24hours. Then the cells were fixed and stained with PI to analyze DNA content by flow cytometry. Data are presented as mean ± SEM of three independent experiments. (Panel B). Effect of **TR-644** on G2/M regulatory proteins. HUVEC cells were treated for 24hours with the indicated concentrations. The cells were harvested and lysed for the detection of cyclin B, p-cdc2^{Tyr15} and cdc25c expression by western blot analysis. To confirm equal protein loading, each membrane was stripped and reprobed with anti-β-actin antibody.

Effects of TR-644 on microtubules and actin microfilament in HUVEC cells

We investigated the effects of **TR-644** on the cytoskeleton proteins microtubules and actin micrfilaments. As shown in Figure 7, the microtubule network exhibited normal arrangement and organization in HUVEC cells in the absence of drug treatment as well as when the cells were incubated with the lower concentration of drug (1nM). In contrast, 24hours of exposure to 10nM **TR-644** caused microtubule disassembly, with induction, in about 20% of the cells, of spherical morphology. Exposure to the compound at 100nM resulted in an almost complete loss of microtubules. Similar results were obtained for **CA-4** although the observed changes were more marked. In agreement to the changes in cellular microtubules, cells treated with **TR-644** showed minimal effects in the arrangement and amount of F-actin (Figure 8), at low concentration (1nM) respect to the untreated cells. On the

contrary the actin cytoskeleton started to disorganize both with **TR-644** and **CA-4** (10nM), resulting in the disappearance of actin fibers and in their relocalization and reorganization in intracellular focal adhesion regions, whereas the cytoskeleton was completely altered at higher concentration of both **TR-644** and **CA-4**.
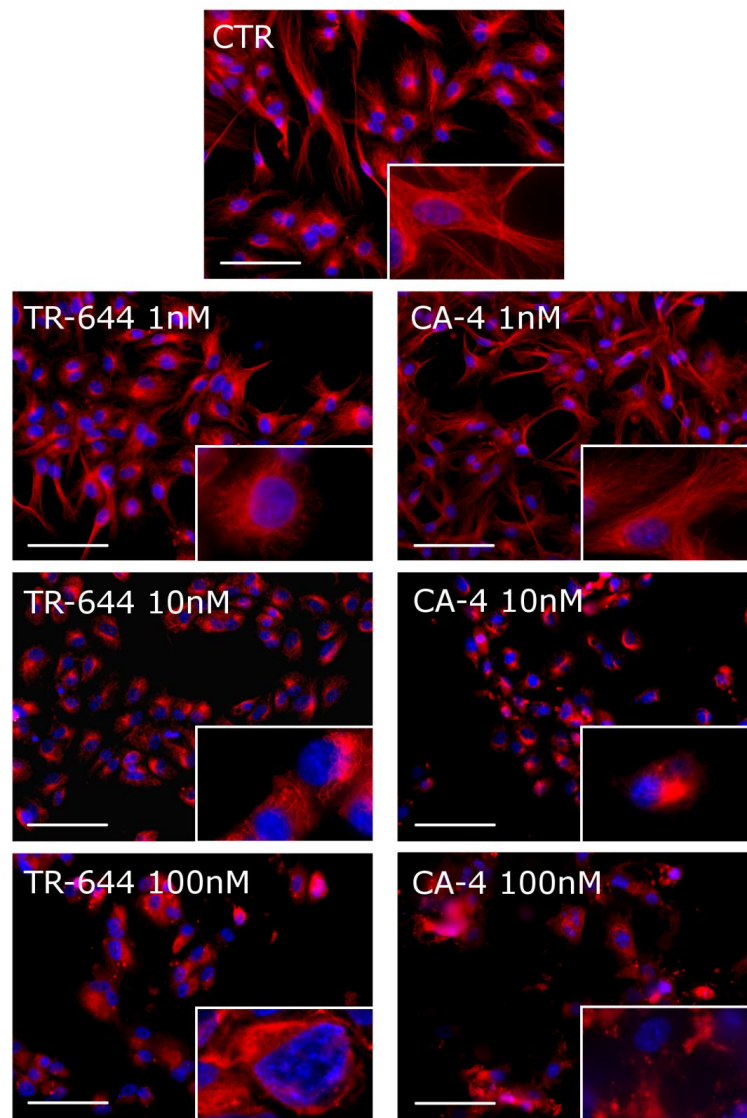
Figure 7. Effect of **TR-644** on microtubules in HUVEC. Cells were incubated for 24hours with the indicated concentration of **TR-644** or **CA-4** as comparison and stained with anti-β-tubulin primary antibody and secondary Alexa-conjugated antibody and then observed by confocal microscopy. (magnification 20x Bar= 10μm). Cells were also counterstained with DAPI to visualize the nuclei. Insets represent magnification at 60x, of a portion of the field.
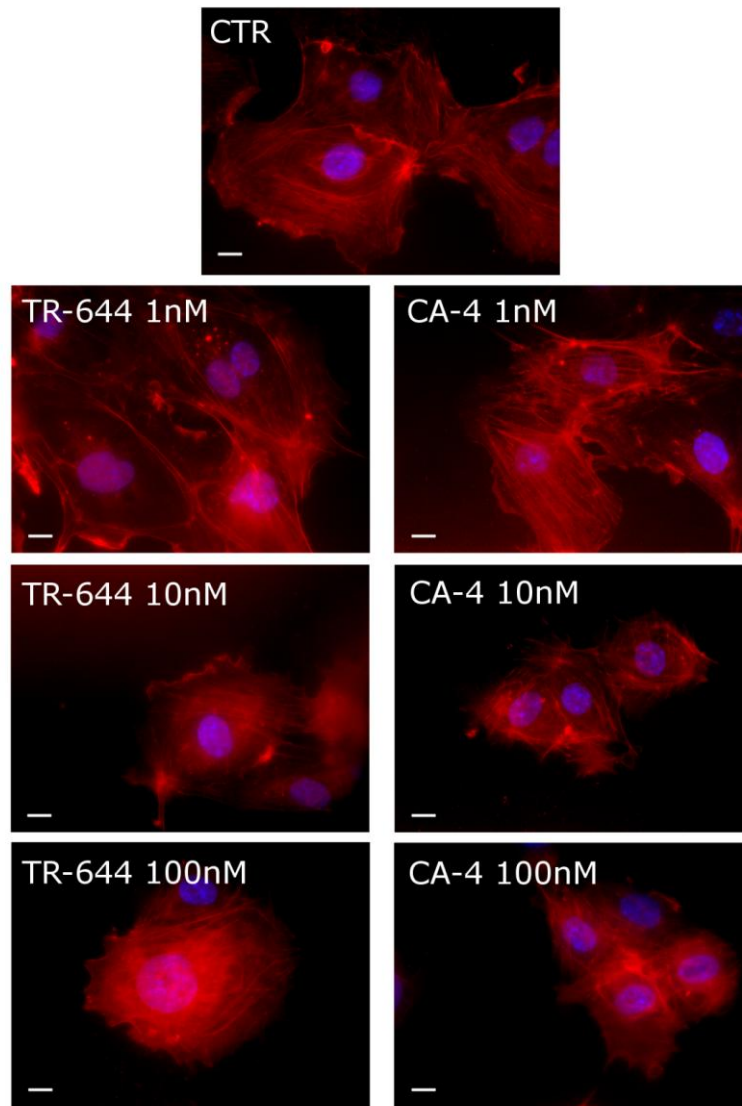
Figure 8. Effect of **TR-644** on actin microfilaments in HUVEC. Cells were incubated for 24hours with the indicated concentration of **TR-644** or **CA-4** as comparison and stained with phalloidin-tetramethylrhodamine B isothiocyanate conjugate Cells were also counterstained with DAPI to visualize the nuclei (magnification 60x).

TR-644 reduces VE-cadherin phosphorylation

VE-cadherin is a member of cadherin superfamily, expressed by vascular endothelial cells[80]. In these cells, it is the major adherence junction protein, which, by modulating cell-cell adhesion, regulates angiogenesis, and vascular permeability. It is also required for differentiation into vasculature-like structures by endothelial

cells *in vitro*[81,82]. Since VE-cadherin is crucial for controlling the state of adherence junctions, which in turn regulate endothelial cell-cell adhesion, cell motility, morphogenesis and intracellular signaling pathways, this molecule has many clinical implications. As showed above, **TR-644** increased HUVEC permeability and VE-cadherin was mainly non-phosphorylated in quiescent vessels, thus we evaluated if this compound was able to reduce VE-cadherin phosphorylation following VEGF stimuli. VEGF rapidly induced the phosphorylation of VE-cadherin, triggering modifications of the adherence junction that is thought to allow for the loosening of cell–cell contacts that would be required for the sprouting of a new vessel[83]. As shown in Figure 9 (panel A), **TR-644** remarkably reduced the VEGF-induced VE-cadherin phosphorylation at Tyr658, both at 10 and 100nM. In comparison also **CA-4** reduced the phosphorylation as previously demonstrated[58].

VE-cadherin is linked to the actin–myosin cytoskeleton via β-catenin. The cytoskeleton plays a central role in the regulation of endothelial permeability and cell migration by controlling cell shape[51,84]. Activation of the endothelial contractile machinery and generation of contractile forces by endothelial cells can cause adjacent cells to retract from each other.

The linkage of the cytoplasmic region of VE-cadherin with the actin cytoskeleton is mediated by a number of proteins, including α- and β-catenin, p120, and plakoglobin, and their interactions with VE-cadherin tend to strengthen adherens junctions[83]. Immunofluorescent analysis revealed a partial co-localization of VE-cadherin and β-catenin in untreated cells at the junctions between cells (Figure 9, panel B). On the other hand, the expression of VE-cadherin was strongly reduced in the presence of **TR-644** both at 10 and 100nM. More importantly, the cell-cell contacts appeared destroyed by the treatment and in control cells, VE-cadherin staining occurs on the surface suggesting that **TR-644** is able to disrupt the

cadherin/catenin complex and that the disruption of this complex may be responsible for the disruption in cell-cell adhesion.
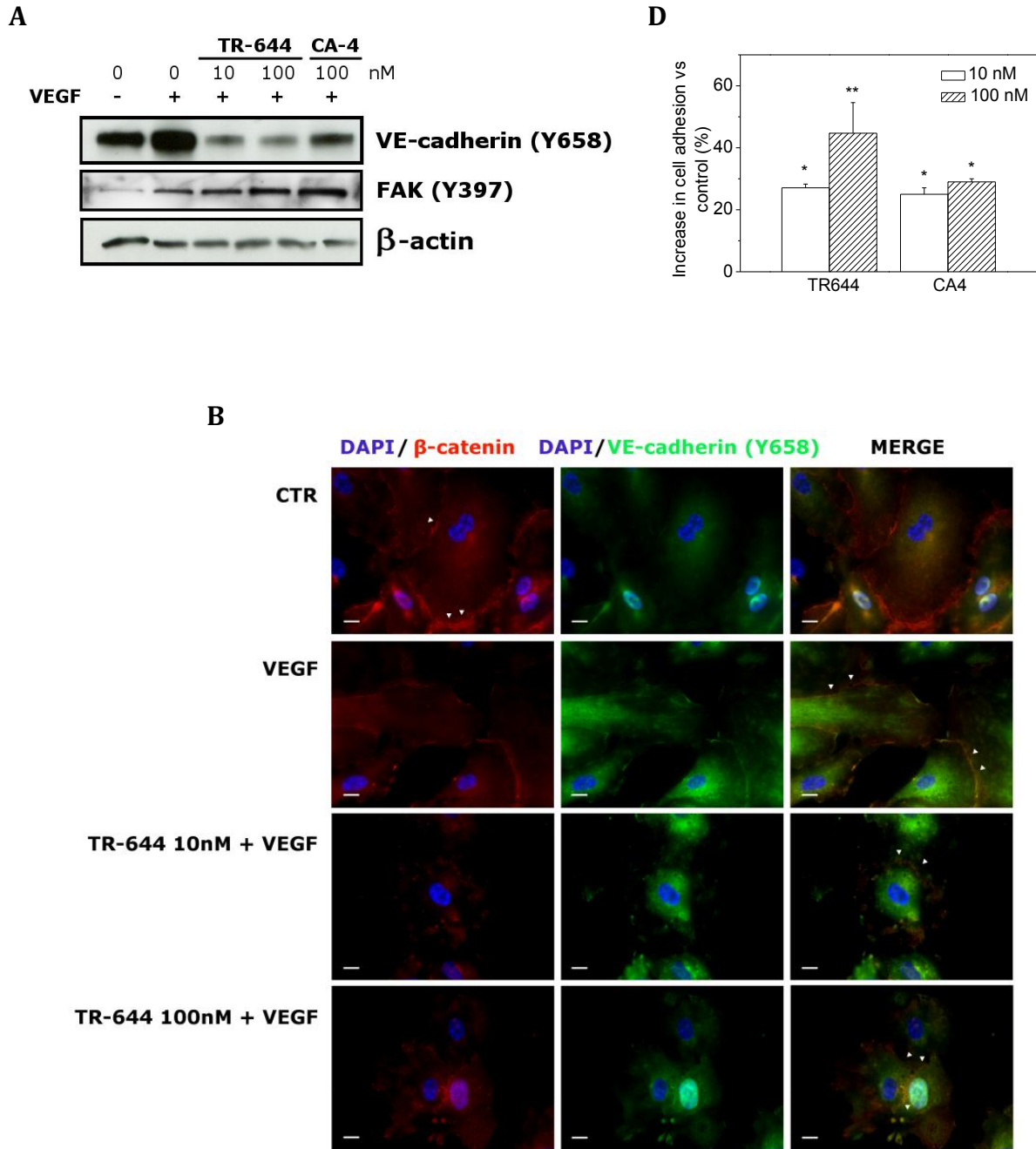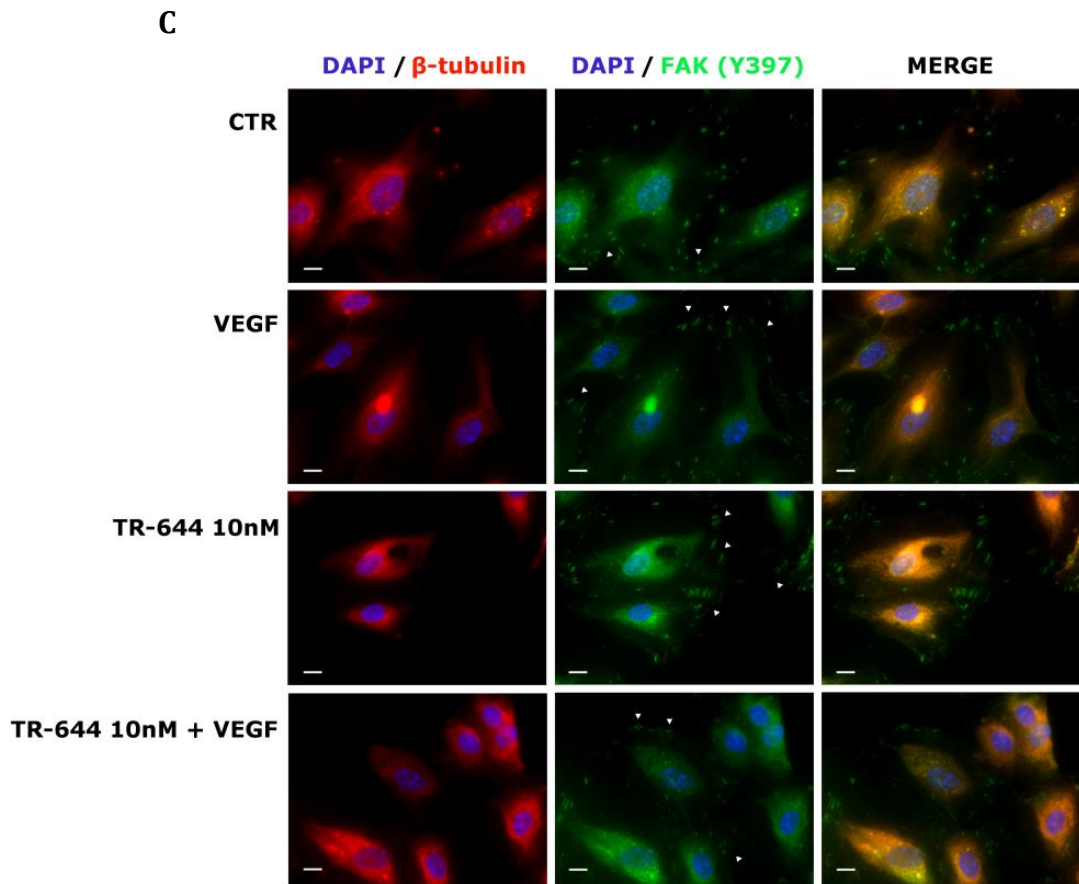
Figure 9. Effect of **TR-644** on VE-cadherin and FAK. Panel A. Western blot analysis of VE-Cadherin^{Tyr658} and FAK^{Tyr397} after 6hours of treatment with **TR-644** and **CA-4** at the indicated concentration in the presence of VEGF. Panel B. Immunofluorescence analysis of HUVEC cells treated with the indicated concentration of **TR-644** for 6hours and then stained with anti β-catenin antibody and anti VE-cadherin^{Tyr658} antibody. Cells were also counterstained with DAPI to visualize the nuclei (magnification 40x). Panel C Immunofluorescence analysis of HUVEC cells treated with the indicated concentration of **TR-644** for 6hours and then stained with anti β-tubulin antibody and anti FAK^{Tyr397} antibody. Cells were also counterstained with DAPI to visualize the nuclei (magnification 40x). Arrows indicate focal adhesions. Panel D. **TR-644** enhances HUVEC cell adhesion. Data represent mean ±SEM of three independent experiments performed in triplicate.

TR-644 induces increase of cell adhesion without interfering with focal adhesion kinase (FAK)

Focal adhesion kinase (FAK) is a 125-kDa non-receptor tyrosine kinase, which acts as a scaffold at sites of cell attachment to the extracellular matrix and is activated following binding of integrins to ECM or upon growth factor stimulation including VEGF[85–87]. As a result, it regulates cell shape, cell adhesion and cell motility[87]. Since **TR-644** inhibits cell migration, we examined if it is able to inhibit the formation of focal adhesions and the VEGF-induced phosphorylation of FAK. As shown in Figure 9 (panel A), VEGF induce an increase of FAK phosphorylation at Tyr397 while the treatment with **TR-644** slight increase its phosphorylation, both at 10 and 100nM. **CA-4** also increases the expression of FAK[Tyr397]. To further investigate the effect of **TR-644** on FAK we analyzed HUVEC cells by immunofluorescence. As showed in Figure 9 (panel C), we observed that focal adhesions were distributed in a punctiform pattern along the cell periphery and **TR-644** did not change the expression of focal adhesion both in the absence and in presence of VEGF. These results could appear in contrast with the inhibition of cell migration induced by the compound, indeed they are consistent with the increase in HUVEC cells adhesion induced by **TR-644** (Figure 9, panel D).

TR-644 treatment inhibits in vivo angiogenesis in CAM assay.

TR-644 was assessed for its anti-angiogenic activity *in vivo* on the chick embryo chorioallantoic membrane (CAM). To this purpose, alginate beads containing FGF were applied topically on the CAM at day 11 of development in the absence or in the presence of **TR-644** or **CA-4**. As showed in Figure 10 (panels A and B), FGF alone, triggered a potent angiogenic response that was significantly inhibited by **TR-644** (panel A), also at the lowest concentration used (0.01nmol/egg). Interestingly, **TR-**

644 did not induce any effect on the basal vascularization of the CAM and did not affect the development and survival of the chick embryos (data not shown). In contrast, **CA-4** (panel B) in the absence of FGF, induced a significant increase of the basal vasculature at all the concentration used. It has recently been shown, that the formation of new vessels in CAM could be driven by a pro-inflammatory signature, characterized by the upregulation of proinflammatory cytokine/chemokines and their receptors, endothelial cells adhesion molecules, and members of the eicosanoid pathway[88]. Thus, this effect could be due to an inflammatory response triggered by cellular damage induced by **CA-4**. Indeed hematoxylin-heosin staining of the CAM showed a remarkable appearance of multiple site of inflammation along with the recruitment of lymphocytes and macrophages in **CA-4**-treated samples (Figure 10, panel C).
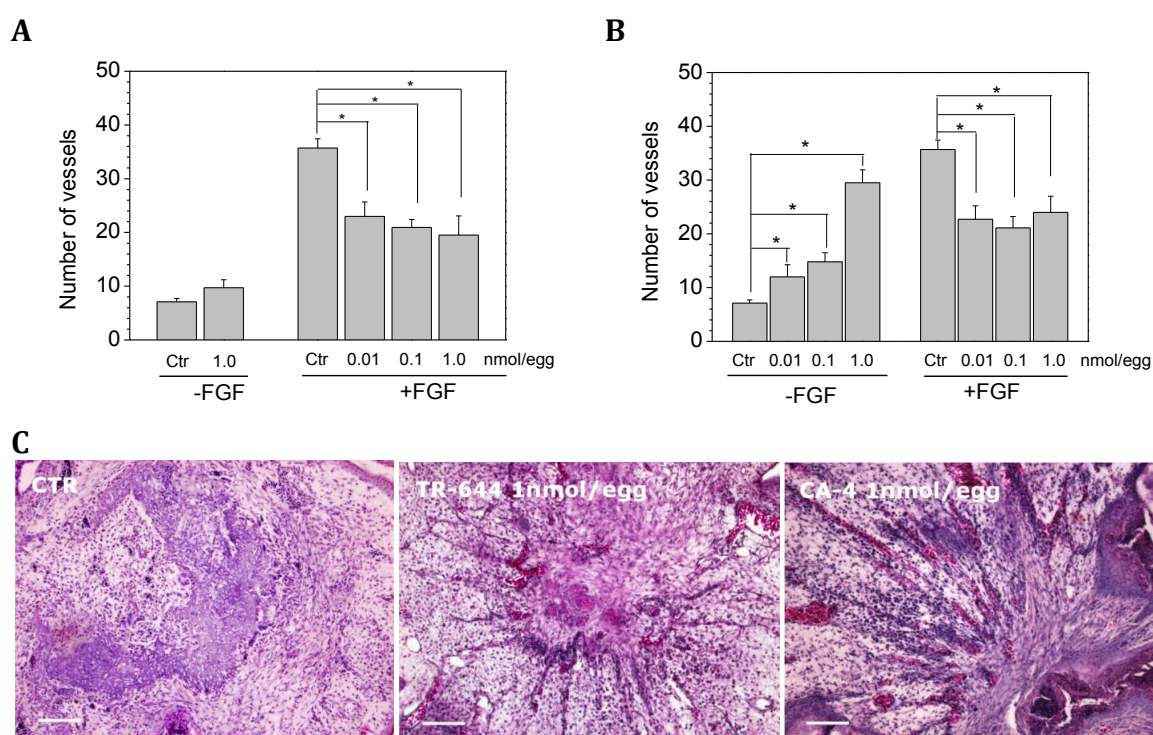
Figure 10. *In vivo* effects of **TR-644** (Panel A) and **CA-4** (Panel B) on chorioallantoic membrane (CAM) assay. A alginate sponges embedded with FGF, a stimulator of blood vessel formation, in the presence of the indicated doses of compounds were implanted on the top of the growing CAM on day 11 of development. On day 14,

newly formed blood vessels converging toward the implants are counted at microscopic levels. Data represent mean ±SEM of at least ten eggs for groups. *p<005 **p<0.01 vs control. Panel C. Histological pictures obtained from the CAM assay in the absence of FGF (hematoxylin-eosin staining 60x magnification).

TR-644 disrupts tumor vasculature in vivo tumor model

BL6-B16 mouse melanoma cell line were injected s.c. in syngeneic C57BL/6 mice. CD31 is expressed on vessels and is the most specific and sensitive endothelial marker currently available. A single i.p. administration of **TR-644** (30mg/Kg) significantly reduced tumor blood vasculature as determined by immunohistochemical staining with the antibody reactive to CD31 in brown color (Figure 11 panel B). Also **CA-4P** significantly reduce the number of CD31 positive cells per field in well agreement with previous reports[58].

Moreover, we also tested whether **TR-644** causes histological changes in tumor tissue by staining with hematoxilin and eosin (HE) and measuring proliferation using PCNA staining. The HE staining suggested that 24hours after a single i.p. injection of **TR-644**, there was a massive area of necrosis within tumor for both compounds. The number of PCNA positive cells, can be used as an index of cell proliferation. As showed in Figure 11 (panel C), cell proliferation in the whole tumor significantly decreased after **TR-644**, while **CA-4P** did not. These results are in well agreement with the higher antiproliferative activity of **TR-644** in many tumor cell lines relative to the lead compound **CA-4**[79].
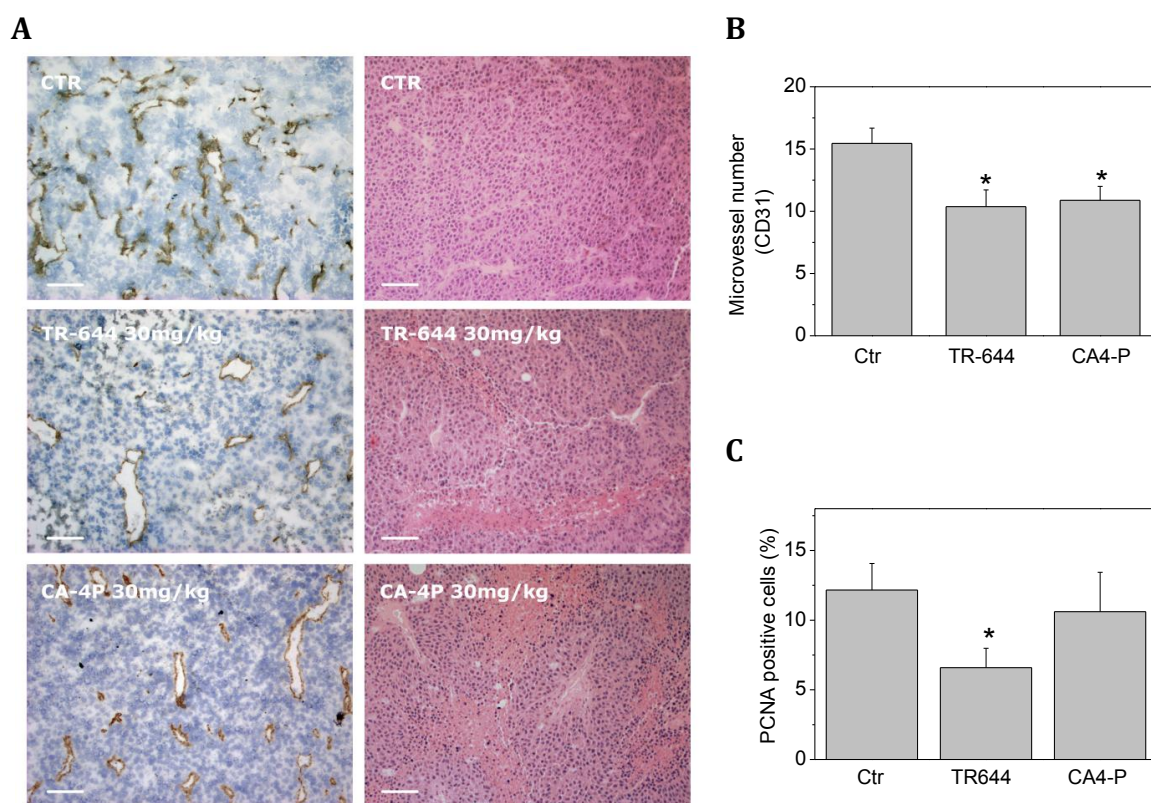
Figure 11. Efficacy *in vivo* of **TR-644** in a syngeneic mouse model. BL6-B16 murine melanoma cells were injected in the right flank of C57BL/6 mice as described in Materials and Methods. Tumor tissues were embedded in OCT-compound and frozen for immunohistochemistry. Panel A CD31 immunohistochemistry and Hematoxylin-Eosin (HE) staining of tumor after i.p. treatment with 30mg/kg of both **TR-644** or **CA-4P** (100x magnification). Panel B. Quantitative analysis of tumor section stained with CD31. Data are represented as mean±SEM of five mouse per group *P < 0.05 versus control. Panel C. Quantitative analysis of tumor section stained with PCNA Data are represented as mean±SEM of five mouse per group *P < 0.05versus control.

1.3.1.4. Discussion

We previously demonstrated that **TR-644** displayed effective antiproliferative activity in numerous cell lines derived from human solid tumors and leukemias, including multidrug resistant cell lines[79]. We also showed that **TR-644** induced depolymerization of tubulin and inhibited normal spindle formation in HeLa cells, resulting in mitotic arrest and cell death. The inhibition of tubulin polymerization was similar to that observed with the reference compound **CA-4**. Examination of the effects of **TR-644** on [^{3}H]colchicine binding to tubulin revealed that colchicine binding was efficiently inhibited, indicating that **TR-644** binds tubulin in the colchicine site.

In this study, we demonstrated that **TR-644** is a potent vascular disrupting agent that exhibit antivascular activity both *in vitro* and *in vivo* experiments. Motility and migration of vascular endothelial cells are important in the angiogenic process. We found that **TR-644**, at namolar concentration range, induces a significant inhibitory effect on endothelial cell migration. In addition, **TR-644** inhibits both the organization of HUVEC into vessel-like tubes and disrupts established endothelial cell tubes in a concentration dependent manner. These effects are similar to that of the lead compound **CA-4**.

Given the correlation between G2/M phase arrest and cytoskeletal dynamics, we investigated the effect of **TR-644** on the cell cycle. As other microtubule-binding agents **TR-644** induces a G2/M phase arrest along with a remarkable reduction of the G1 phase while the S phase is only slight affected. During a normal cell cycle, the progression of cells in the G2 phase to M phase is triggered by the activation of the cyclin B1-dependent Cdc2 kinase[89,90], which is regulated by a series of phosphorylation-dephosphorylation events and protein-protein interactions[91]. At the G2/M phase transition, Cdc2 is dephosphorylated on Tyr[15] and Thr[14] and this

event lead to activation of the Cdc2 kinase and entry of cells into mitosis. Treatment with **TR-644** decreases the phosphorylation of at Cdc2 at Tyr^{15} and the expression of the phosphatase Cd25c both at 10nM and 100nM. Curiously enough we observed a dual effect of **TR-644** on cyclin B1 expression: while at 10nM we observed a down regulation of Cyclin B1 expression at higher concentration we found the opposite. This could be due to the fact that at low concentration a part of the cells are still able to exit from mitosis, while at higher concentration the cell arrest become irreversible and consequently the cyclin B1 expression increased.

TR-644 increases vascular permeability probably by disrupting endothelial cell-cell contact, and preventing organization of cellular connections that are critical for their survival and maintenance. These effects could be attributed to the inhibition of VE-cadherin phosphorylation. Indeed **TR-644** strongly inhibits the phosphorylation of VE-cadherin induced by VEGF and reduces cell-cell contacts. Interestingly such analysis also clearly show a dissociation of the VE-cadherin/β-catenin complex. Since VE-cadherin is linked and interacts with actin fibers via β-catenin, it is reasonable that the effect of **TR-644** on cytoskeleton may contribute to the disconnection of homophilic VE-cadherin/β-catenin–mediated cell-cell interactions. In this context it is worthwhile to note that also **CA-4** was demonstrate to increase endothelial cell permeability through disruption of the VE-cadherin/β-catenin signaling[58].

It is interesting to note that all these effects occur at concentration that per se did not induce significant effects on endothelial cell proliferation while it appears that in HUVEC **TR-644** is endowed with a lower cytotoxicity in comparison to the lead compound **CA-4**.

FAK plays a central role during focal adhesion complex assembly and disassembly, that are critical for cell adhesion and migration. When FAK is activated, it is autophosphorylated at its autophosphorylation site Tyr397, binds to Src, which in

turn phosphorylates other sites on FAK and the FAK-binding proteins, such as Cas and paxillin, which modulates cytoskeleton re-arrangement[85]. Moreover, inhibition of FAK phosphorylation greatly impairs cell spreading and adhesion[85]. Some anti mitotic drugs such as laulilamide[92] and taxotere[93] have been previously found to block the formation of focal adhesion and the autophosphorylation of FAK.

However, in **TR-644**-treated HUVEC, we found that FAK phosphorylation at Tyr397 is slight increased compared with the VEGF-treated cells. These high leves of FAK[Tyr397] could prevent focal adhesion disassembly, leading to impaired cell migration. Recent evidences suggest that the level of phosphorylated FAK increases during focal adhesion formation[94]. The behavior of **TR-644** is similar to JG-03-14, a new substituted pyrrole derivative which has been showed to affect endothelial cells function through inhibition of VE-cadherin but without interfering with FAK phosphorylation or focal adhesion formation[95]. It is worth noting that **TR-644** increases actin stress fiber formation and in a recent study[96], the increased formation of intracellular stress fibers were correlated with enhanced cell adhesion in mammary cells, whereas migrating cells had fewer stress fibers. Indeed we also found that **TR-644** significantly increases HUVEC adhesion suggesting that inhibition of cell migration may be linked to an activation of FAK signaling. To evaluate the ability of the **TR-644** to interfere with the angiogenic process *in vivo*, we used the CAM assay as a model of neovessel formation, and observed that **TR-644** significantly reduces the number of newly formed vessels in the CAM even at very low doses (0.01nmol/egg). The effect was observed in the absence of any effect on embryonic development and survival and **TR-644** had no toxic effects on preexisting vessels (data not shown). This is in accordance with our *in vitro* findings that showed a lower cytotoxicity of **TR-644** respect to **CA-4**. Surprisingly **CA-4** at all concentration tested induces per se a significant increase of the vasculature mimicking the effects of FGF. Recent papers[88,97], indicate that inflammatory

cytokines, as early mediators of inflammation, are a potent angiogenic factors, suggesting that angiogenesis and inflammation are closely integrated processes. In this context the pro-angiogenic effect of **CA-4** in the absence of FGF could be due to a cell damage effect of **CA-4** that in some way induce the recruitment of inflammatory cells that consequently induce neovascularization. Accordingly, histological examination of CAM showed a remarkable monocyte/macrophage infiltrate in the area in which the alginate pellet containing **CA-4** was located. It is worthwhile to note that anti-inflammatory agents exert antiangiogenic effects. Further *in vivo* experiments carried out with mouse melanoma tumor model demonstrated that a single injection of **TR-644** efficiently and selectively destroy vasculature of tumor tissue and induce a significant reduction of tumor cell proliferation as demonstrated by reduction in PCNA positive cells. In summary our study provides for the first time evidence that administration of **TR-644** causes inhibition of angiogenesis both *in vitro* and *in vivo* at a concentration that is not cytotoxic for endothelial cells indicating that **TR-644** may be a promising candidate as inhibitor of angiogenesis.

52

1.3.2. THE NOVEL ANTITUBULIN AGENT TR-764 STRONGLY REDUCES TUMOR VASCULATURE AND INHIBITS HIF-1α ACTIVATION

Elena Porcù, Luca Persano, Roberto Ronca, Stefania Mitola, Romeo Romagnoli, Pier Giovanni Baraldi, Giuseppe Basso, Giampietro Viola

1.3.2.1. Abstract

Tubulin binding agents (TBAs) are drugs commonly used in cancer therapy as antimitotics. **TR-764** is a new inhibitor of tubulin polymerization, based on the 2-(alkoxycarbonyl)-3-(3′,4′,5′-trimethoxyanilino)benzo[*b*]thiophene molecular skeleton, with high antiproliferative activity *in vitro* and *in vivo*. Recently it has been described that TBAs, like combretastatin A-4 (**CA-4**), present also antivascular activity. Targeting both the tumor mass and its blood vessels could be a new strategy to improve the traditional chemotherapy.

TR-764 (1-10nM) antiangiogenic activity was tested *in vitro* on human umbilical endothelial cells (HUVECs), through the Matrigel-based tube formation assay. Tubulin and actin cytoskeleton was observed by immunofluorescence staining, and cell motility was monitored by the wound assay. Immunoblot analyses were helpful to investigate the molecular mechanisms involved in **TR-764** activity on endothelium. Data were confirmed *in vivo*, on the chick embryo chorioallantoic membrane (CAM assay) and on BL16 mice allogenic tumors.

TR-764 binding to tubulin triggers cytoskeleton rearrangement without affecting cell cycle and viability. It leads to capillary tube disruption, increased cell permeability, cell motility reduction and VEGF-stimulated cell adhesion impairment. Signal transduction between extracellular matrix and plasma membrane is arrested by the disruption of adherens junctions and focal adhesions, through mechanisms which involve VE-cadherin/β-catenin and FAK/Src. Importantly, **TR-764** is active in hypoxic conditions and reduces significantly HIF-1α activation. *In vivo* **TR-764** (1-100nmol/egg) remarkably blocks the bFGF proangiogenic activity on CAM and it shows a strong reduction both of tumor mass and microvascular density on a murine allogenic tumor model, at concentrations lower than that of reference compound **CA-4P**.

TR-764 is a novel tubulin binding agent with a strong potential as antivascular and antitumor molecule that could improve the common anticancer therapies, by overcoming hypoxia-induced resistance mechanisms.

1.3.2.2. Introduction

Microenvironment is very important for tumor sustenance, and angiogenesis is essential for tumor growth and spreading. The characterization of this process has been fundamental to design and optimize new therapies targeting both the tumor mass and the tumor blood supply, as supported by recent advanced in chemotherapy, focused on combination treatments[50],[40].

Tumor vasculature presents abnormal and disorganized structures, lacking of the conventional blood vessel hierarchy. Arteries, capillaries and venules are not recognizable, and they are tortuous, hyperpermeable and immature[23]. Therefore the antiangiogenic therapy targeting the vascular endothelium results very efficacious and selective.

Numerous mechanisms regulate tumor angiogenesis, and a series of molecular mediators are involved in this process, including signal transduction systems mediated by growth factors, proteins for cytoskeleton remodeling, paracrine and intracellular signaling pathways[5].

Hypoxia inducible factor-1α (HIF-1α), appears in its active form under low oxygen tension conditions, is the key molecule regulating hypoxic stimuli. It has been described that hypoxic microenvironment gives rise to proangiogenic factors requirement, which in turn recruit endothelial cells and stimulate sprouting, developing new tumor blood vessels. Moreover, hypoxia is responsible for some described resistance mechanisms, which make the therapy ineffective[36],[40].

Several antiangiogenic strategies have been studied, most of them target the VEGF signaling system and are directed to tyrosine kinase receptors (i.e. VEGFR, and PDGFR)[40], inhibiting the proliferation of new blood vessels. Other therapies target pre-existing tumor vasculature, and are principally represented by the so-called vascular disrupting agents (VDAs)[50].

Among this class of compounds tubulin binding agents (TBAs), which are drugs commonly used in cancer therapy as antimitotics, represent an important group, since recently it has been described combretastatin A4 (**CA-4**), presenting in addition to its antimitotic properties also antivascular activity[59].

TR-764 is a new inhibitor of tubulin polymerization, based on the 2-(alkoxycarbonyl) -3- (3′,4′,5′-trimethoxyanilino) benzo[*b*]thiophene molecular skeleton. It was selected among a series of benzothiophenes derivatives for its high antiproliferative activity *in vitro*, being endowed with GI_{50} values in the nanomolar range in different cancer cell lines. Moreover it demonstrated the ability to inhibit significantly *in vivo* the growth of a syngenic hepatocellular carcinoma in Balb/c mice[63].

Here we investigated the antiangiogenic activity of **TR-764** in HUVEC cells, and its strong effect *in vivo* as a vascular disrupting agent, in the chick chorioallantoic membrane and in tumorigenic murine models.

This compound is proposed for deepen its activity as single agent in clinical trials, with a dual effect against cancer cells as an antimitotic, and targeting the tumor vasculature exploiting its antiangiogenic activity. Traditional chemotherapy could be improved without falling back upon combination treatments, and overcoming possible resistance mechanisms.

1.3.2.3. Results

TR-764 has a strong antivascular effect in vitro

HUVEC cells were used as a model for the angiogenic process *in vitro*, and they organize themselves in tubule-like structures when seeded on a Matrigel matrix. **TR-764** (1-10nM) rapidly disrupted the tubes network within 1hour of treatment, as shown in Figure 1A. It was able to reduce the number and the area of meshes, and it decreased the length of tubules and the number of the branching points, formed by HUVECs (Figure 1B-C).

A

B   **C**
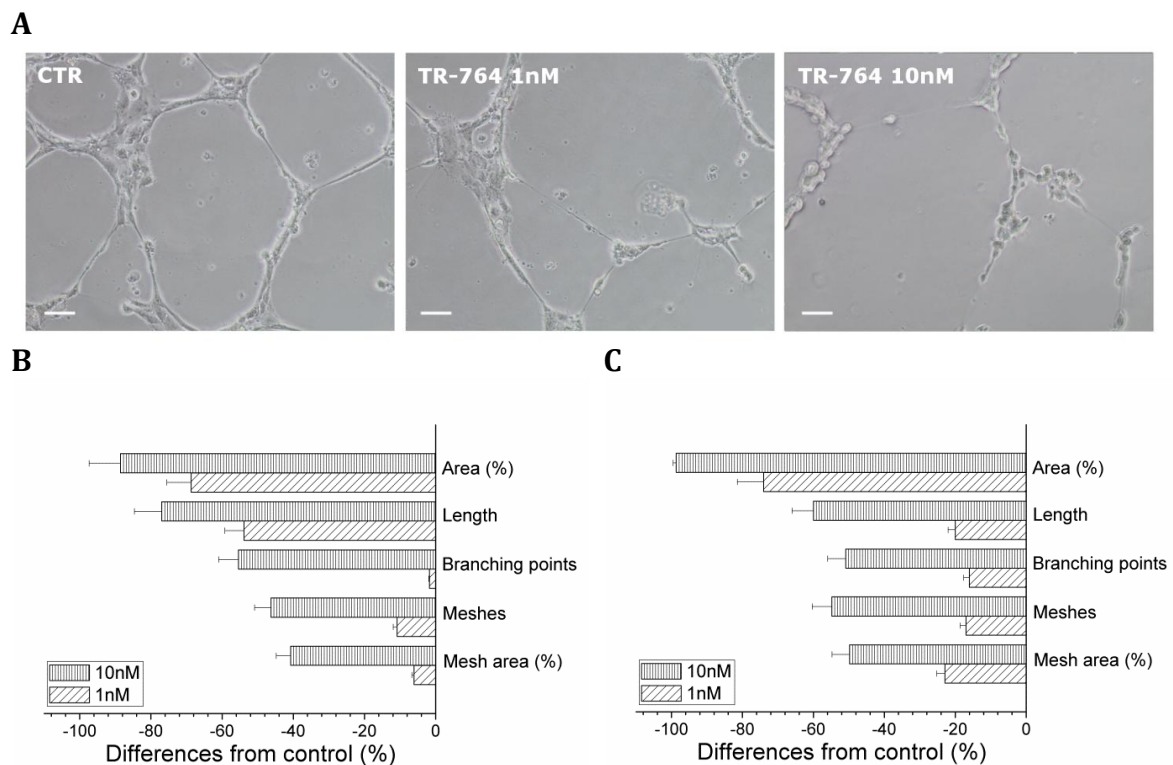
Figure 1: TR-764 disrupts tubule-like structures formed by HUVECs seeded on Matrigel matrix. Representative pictures of HUVECs treated with **TR-764** at the indicated concentrations for 1hour (10x magnification, scale bar = 100μm) (**A**). Quantitative analysis of **TR-764** treatment for 1hour (**B**) or 3hours (**C**) on dimensional and topological parameters of tubule networks. Data were represented as mean ± SEM of three independend experiments.

Endothelial cells motility is arrested by TR-764

Cell motility is a fundamental mechanism involved in angiogenesis. **TR-764** strongly arrested HUVECs motility, preventing the closure of endothelial monolayer after wounding. HUVECs were scratched and cells were allowed to migrate and restore the monolayer. Treated cells were arrested and they were not able to heal the wound, unlike control cells which moved into the scratch. As shown in Figure 2, **TR-764** 1nM reduced the motility, while **TR-764** at the concentration of 10nM definitively arrested the movement. Co-treatment with VEGF did not prevent **TR-764** activity, and the effect on cell motility resulted more statistically significant at 10nM (Figure 2, Panel C).
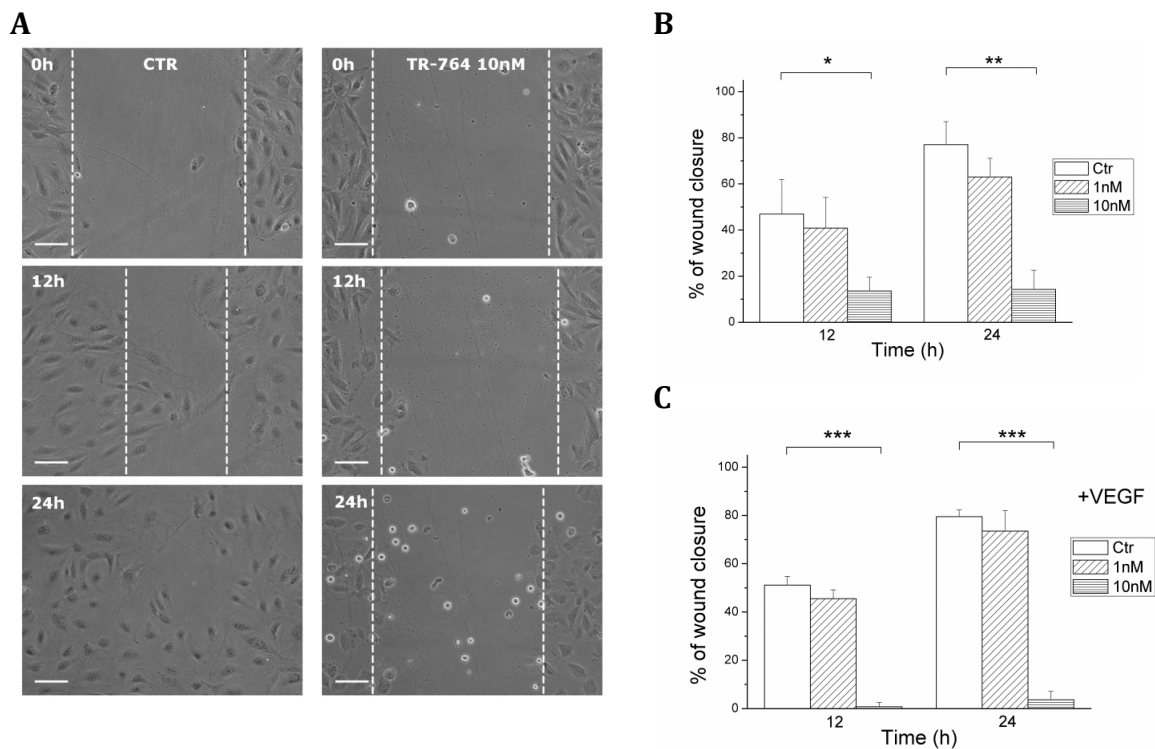
Figure 2. TR-764 impairs HUVECs motility in presence and absence of VEGF. Confluent HUVECs monolayer was scratched and cells were treated with **TR-764**. At different time points cells were photographed (10x magnification, scale bar = 100μm) (**A**). Quantitative analyses of the effects on wound closure after treatment with **TR-764** alone (**B**) or in presence of VEGF (**C**). Cell motility was quantified by measuring the scratch gap at the set times. *$p<0.05$, **$p<0.01$, ***$p<0.001$ vs control.

TR-764 does not alter HUVEC cell cycle and cell viability, although its specific target is tubulin

As previously described[63], a competitive binding cell-free assay revealed that **TR-764** binds tubulin in the same binding site of colchicines, with a very strong affinity constant (IC_{50} = 77±4), comparable to that of reference compound **CA-4**.

α-tubulin staining in HUVEC cells with a specific antibody for immunofluorescence analysis showed as the microtubules were totally disrupted after 6hours of treatment with **TR-764** (Figure 3, microtubules stained in green). Cell nuclei were intact, but tubulin filaments were completely disassembled.
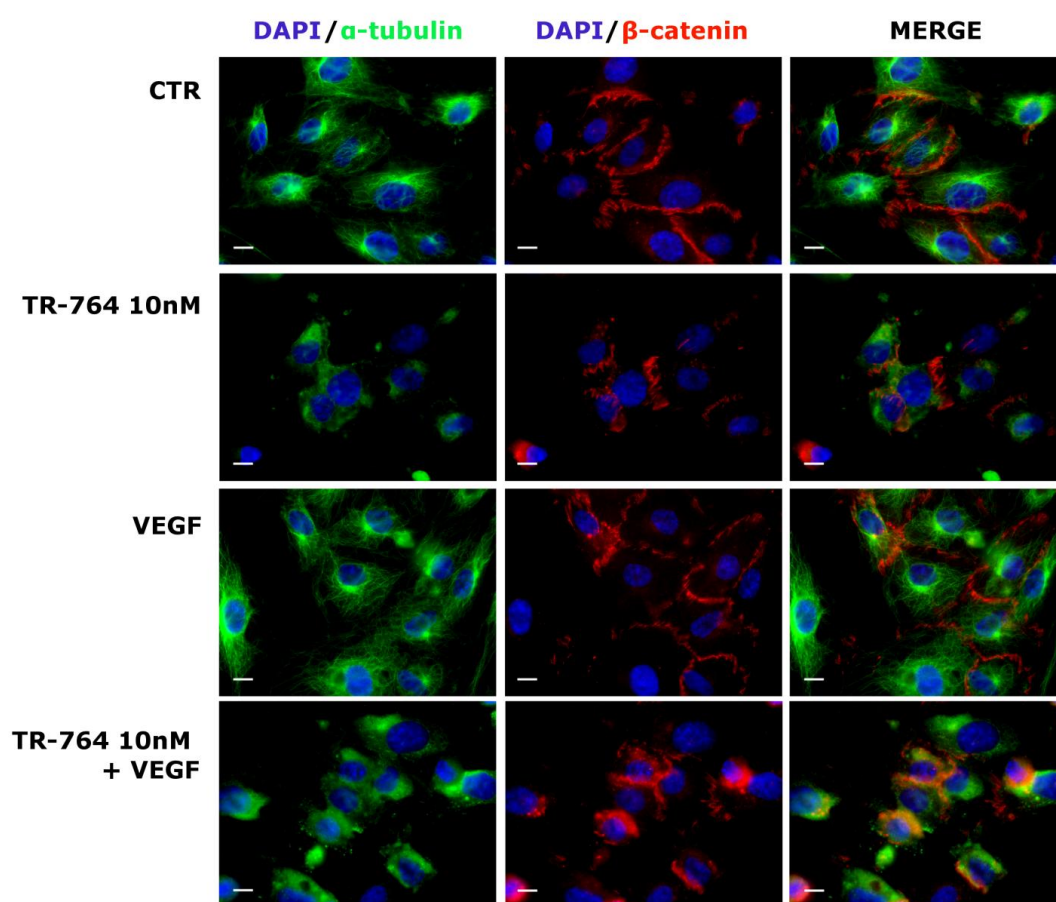
Figure 3. TR-764 disrupts α-tubulin filaments and changes β-catenin organization. Immunofluorescence images of HUVECs treated with **TR-764** 10nM for 6hours in

presence and absence of VEGF. Cells were fixed and stained with primary antibodies anti- α-tubulin (green) and β-catenin (red), and DAPI was used to visualize cell nuclei (60x magnification, scale bar = 10μm).

Although **TR-764** binds to the cytoskeleton, it did not affect cell cycle and cell viability of HUVEC cells. As shown in Figure 4, no cell cycle phases, assayed by PI staining, were modified after 24hours of treatment. Secondly, cell viability, measured using MTT dye, was only slightly impaired after 72hours. It was not possible to calculate the GI_{50} value in HUVECs because cell proliferation was only 30% reduced, at the higher concentration used (100μM). Moreover clonogenic assay confirmed the scarse toxicity of **TR-764**, which presented an increased number of colonies at 1nM respect to **CA-4**, while in the other concentrations the effect was comparable. Altogether these results indicate that **TR-764** is not toxic for HUVECs at the set doses and times, although it rapidly impairs cell cytoskeleton.

A

B

C

D
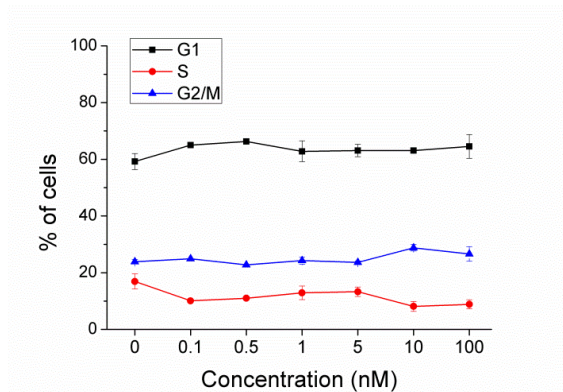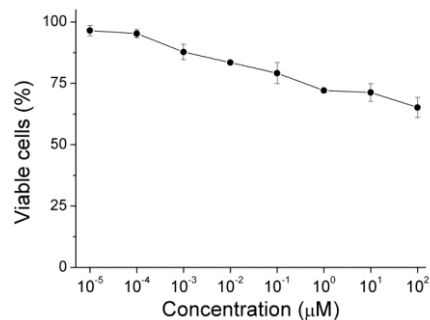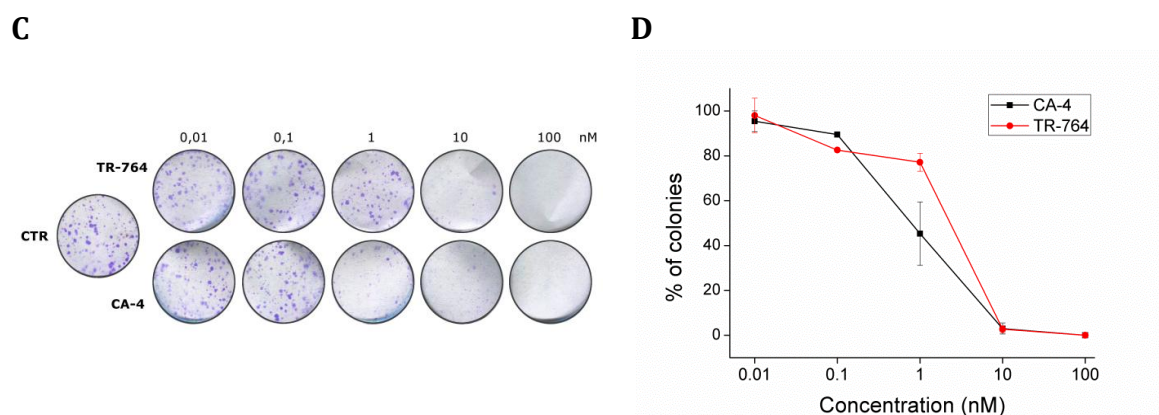
Figure 4. TR-764 is not toxic for HUVEC cells. Cell cycle was analyzed after 24hours of treatment with **TR-764** at the indicated concentrations (**A**). MTT test was performed after 72hours of treatment with **TR-764** to evaluate cell proliferation (**B**). Effects of **TR-764** compared to **CA-4** on cell proliferation was investigated by colony assay. Representative images (**C**) and quantitative data (**D**) are reported.

Actin cytoskeleton is rearranged by TR-764 treatment

TR-764, targeting specifically tubulin, was able to disrupt microtubules, but it also induced microfilaments rearrangement. HUVECs monolayer was scratched and cells were stimulate to move into the wound. As reported in Figure 5, after 6hours of treatment with the compound, endothelial cells showed a reorganization of actin filaments, marked by phalloidin in red. **TR-764** increased the number of stress fibers and it caused blebbing, a characteristic phenomenon of cytoskeleton uncoupling to the extracellular matrix. In addition, control cells were able to move and they formed lamellipodia, projections of actin cytoskeleton on the leading edge of cell migration. Treated cells did not show these structures, indicating that all processes linked to cytoskeleton functionality could be compromised.

61
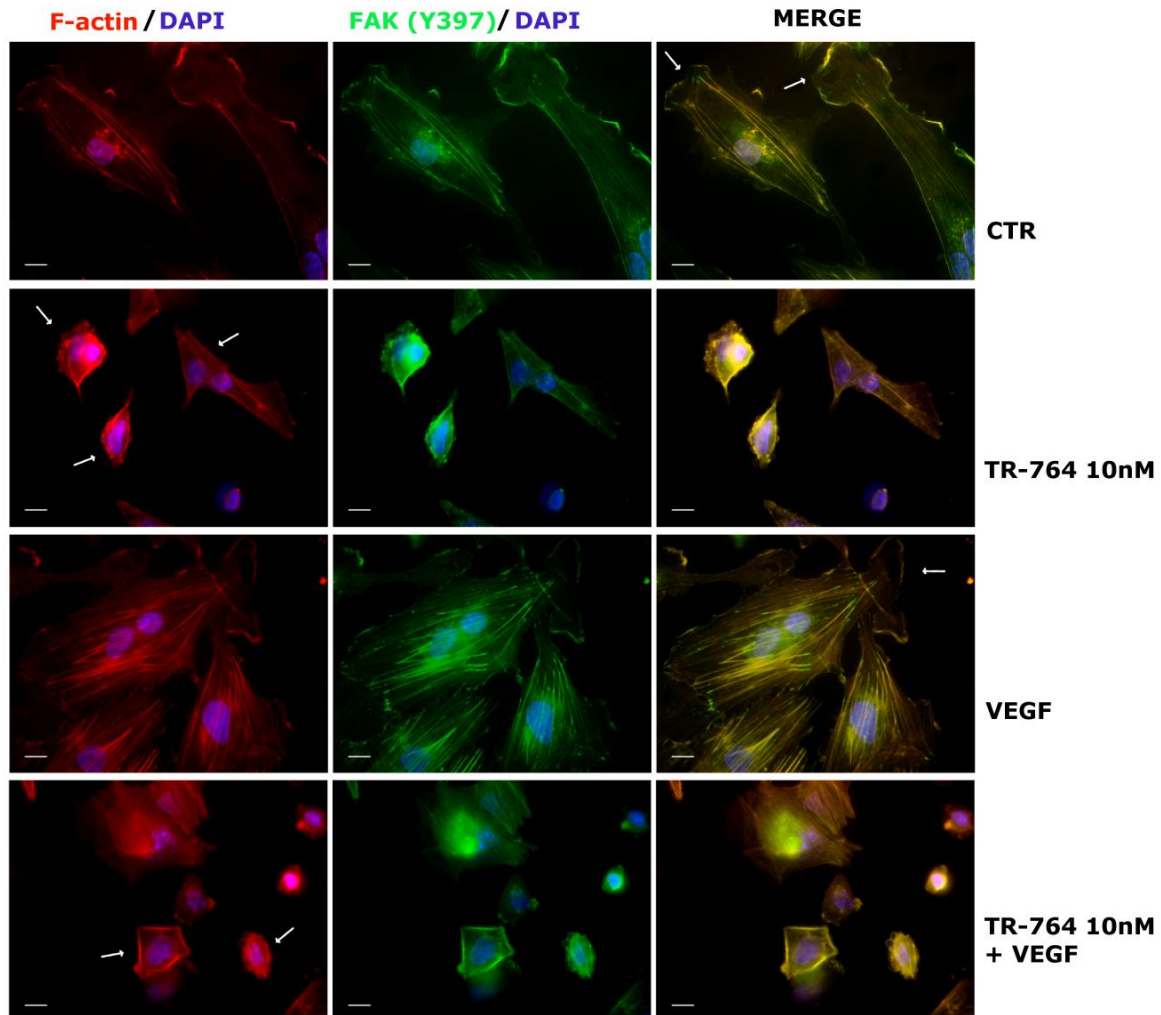
Figure 5. TR-764 induces cytoskeleton rearrangement. HUVECs monolayer was scratched and cells were treated with **TR-764** ± VEGF. After 6hours cells were fixed and stained with phalloidin- tetramethylrhodamine B isothiocyanate conjugate to mark F-actin (red) and with primary antibody anti-FAK^{Tyr397} (green). DAPI was used to visualize cell nuclei (60x magnification, scale bar = 10μm).

In control cells lamellipodia are visible, while in treated cells blebbing occurs. Actin stress fibers are induced by **TR-764** treatment.

Cell spreading is reduced with a mechanism which involves FAK/Src pathway

Focal adhesions are necessary for cell adhesion and cell migration, particularly regulating endothelial cell spreading. As already observed in Figure 2, cells ability to heal empty areas was impaired after **TR-764** treatment. Cell spreading reduction was due to focal adhesion kinase (FAK) inhibition. FAK activating phosphorylation in Tyr397, as well as total FAK, decreased after 6hours of treatment, and steroid receptor coactivator (Src), which regulates the focal adhesions, is dephosphorylated in Tyr416 by the treatment with **TR-764** (Figure 6). Total level of Src was not modified. Proangiogenic factors, such as VEGF, are described as inducer of cell motility, and activators of several molecules among which are FAK and Src. **TR-764** treatment, in particular at 10nM dose, carried out its activity also in presence of VEGF. Focal adhesions are hard-wired to actin microfilaments, as shown in the control cells in Figure 7B. VEGF did not impair these connections, but after treatment with **TR-764** the normal conformation of focal adhesions is modified, and they seem to lose the direct contact with actin, and they assume a more enlarged shape. Concurring with this fact, cell adhesion is increased after treatment with **TR-764**, as showed by other TBAs[66], and it was significantly increased by VEGF, but the co-treatment restored the normal amount of adherent cells (Figure 7A). Thus, focal adhesion expanded shape induced by **TR-764** can be considered as a dysfunctional form of adhesions to the extracellular matrix.
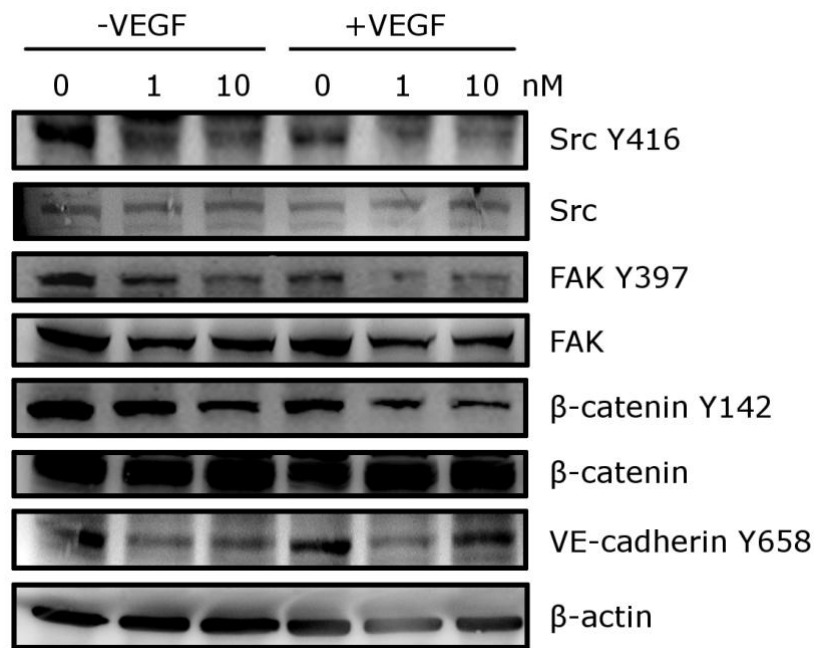
Figure 6. TR-764 effects on several proteins, after 6hours of treatment. Protein lysates were analyzed by western blot and β-actin was used as reference protein for equal loading.

A

B
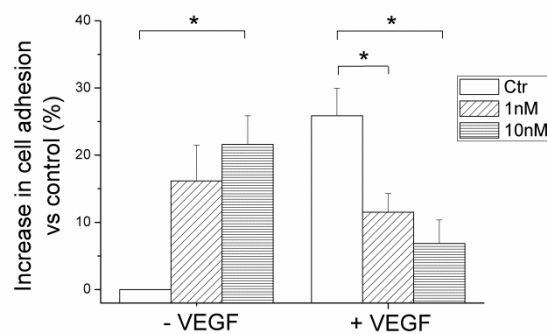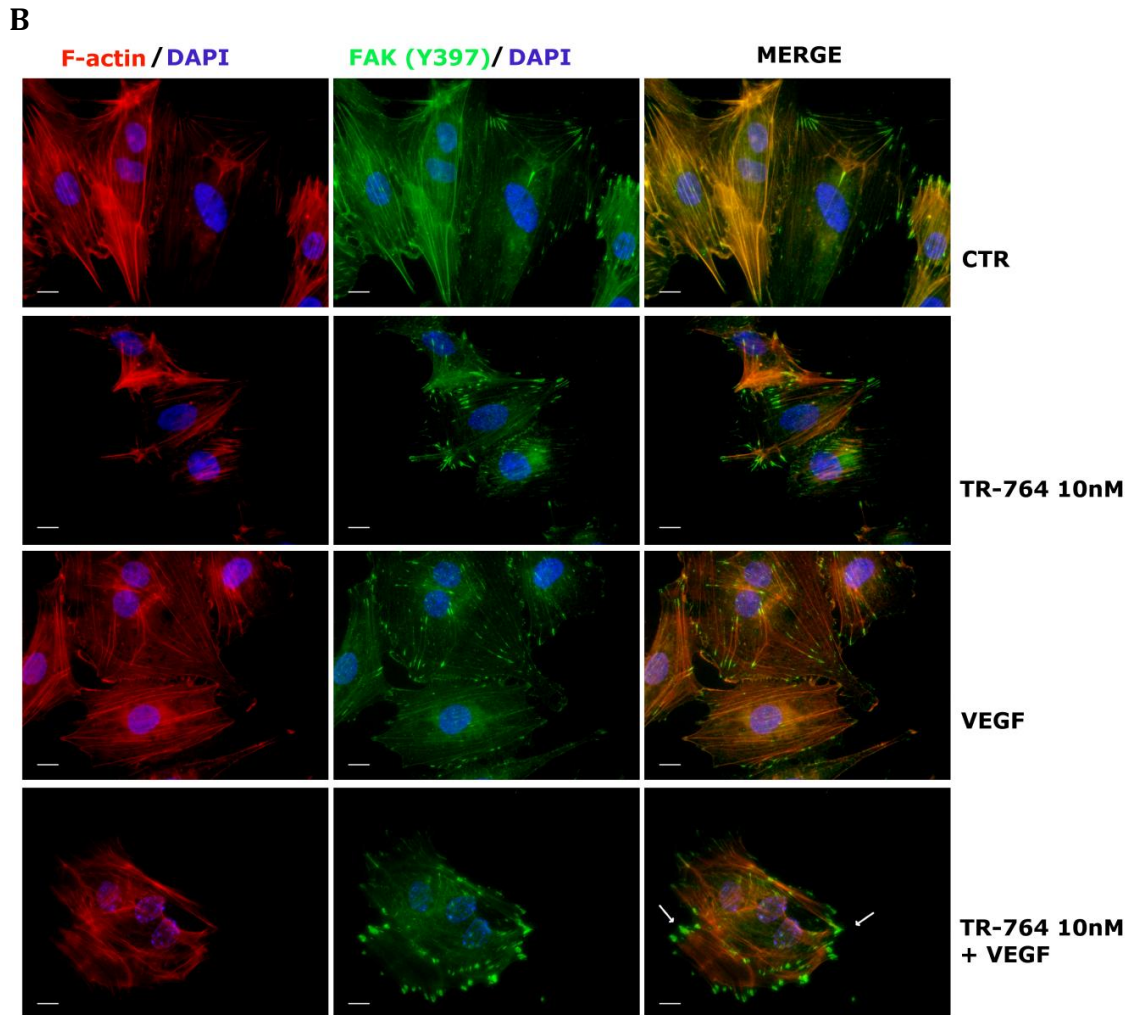
Figure 7. TR-764 alters cell adhesion impairing focal adhesions. Cells were treated with **TR-764** ± VEGF for 6hours, removed from the plate and left to adhere for 30min. Data represent mean ± SEM of three independent experiments. *p<0.05 vs control. (**A**). HUVECs were fixed after 6hours of treatment with **TR-764**, and stained with phalloidin- tetramethylrhodamine B isothiocyanate conjugate to mark F-actin (red) and with primary antibody anti-FAK^{Tyr397} (green). DAPI was used to visualize cell nuclei (60x magnification, scale bar = 10μm). In control cells and after VEGF treatment focal adhesions are well structured and strictly in contact with actin filaments. They are altered by **TR-764** treatment, and they assume a more enlarged morphology (**B**).

TR-764 strongly increases cell permeability, inhibiting VE-cadherin functionality and impairing cadherin- β-catenin interaction

The permeability of a HUVEC cells monolayer was assayed monitoring the ability of a macromolecule, dextran-FITC, to pass through the intercellular spaces, within 90min (Figure 8). With the passing of time, treated cells increased progressively the permeability to dextran-FITC, in contrast to the control.

The observed increase in cell permeability could be explained by the reduction of Tyr658 phosphorylation of VE-cadherin. VE-cadherin functions as a linker between endothelial cells and constitutes the adherens junctions. As reported in Figure 6, VEGF treatment induced VE-cadherin activation, increasing its phosphorylation. In contrast, **TR-764** reversed VE-cadherin status, restoring the normal level of phosphorylated protein.

Adherens junctions are constituted not only by VE-cadherin, but also by β-catenin. β-catenin is directly phosphorylated by FAK in Tyr142, to simplify the dissociation between VE-cadherin and β-catenin and disrupt the adherens junctions[87]. **TR-764** gave rise to a reduced β-catenin Tyr142 phosphorylation, maintaining the same level of the total β-catenin, as demonstrated by western blot analysis (Figure 6). In well agreement the integrity of β-catenin seemed preserved after treatment, as shown in Figure 3. In fact, β-catenin pattern was not altered, but it was relocalized, from an ordered structure mainly linked to the adherens junctions to a more diffused disposition inside the cell.
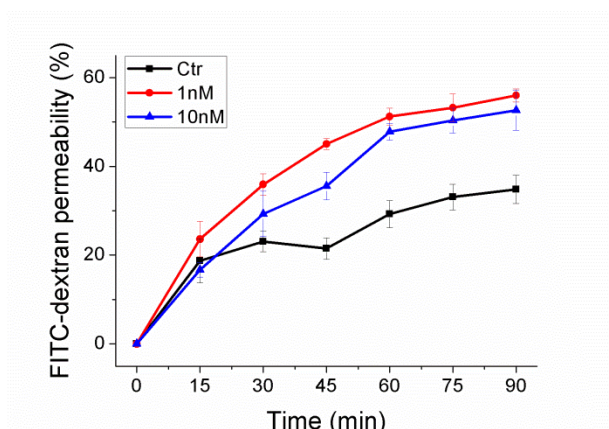
Figure 8. TR-764 increases endothelial cells permeability. HUVEC cells were seeded onto 24-well insert wells until a confluent monolayer was formed. They were then treated with **TR-764** at the indicated concentrations. Simultaneously FITC-dextran was added and its passage into the lower chamber was monitored at the indicated times. Data were represented as mean ± SEM of three independent experiments.

FGF-induced vascularization in CAM is highly reduced by TR-764 treatment

Chick embryo chorioallantoic membrane (CAM) is a highly vascularized structure, usually utilized for angiogenesis experiments *in vivo*. Through alginate beads applied on the CAM, **TR-764** (1-10-100nmol/egg) was slowly distributed within the membrane, starting from day 11 post egg fertilization, in the presence or absence of FGF (100ng/egg). As shown in Figure 9, **TR-764** alone at the highest concentration used did not induce blood vessels increase. On the other hand, treatment with FGF gave rise to a massive production of new-formed blood vessels, which were strongly arrested by **TR-764** treatment, in a significant manner also at the lowest tested concentration (1nmol/egg).
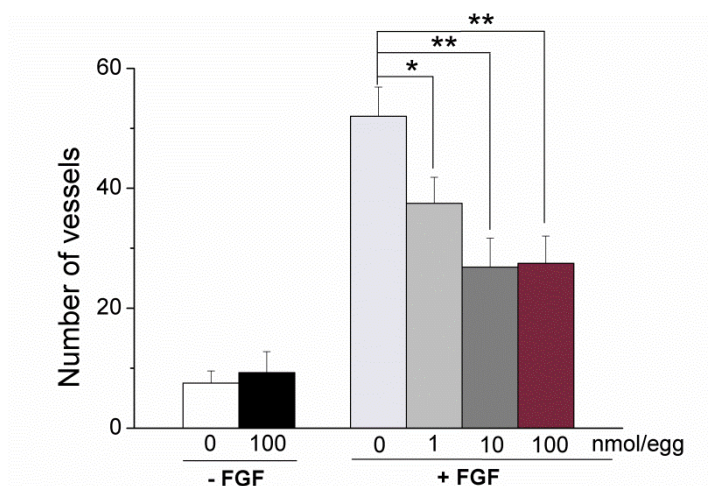
Figure 9. TR-764 reduces the number of vessels on chorioallantoic membrane (CAM) assay. Alginate sponges embedded with **TR-764** at the indicated doses ± FGF (150ng) were implanted on the top of the growing CAM on day 11 of development. On day 14, newly formed blood vessels converging toward the implants are counted at microscopic levels. Data represent mean ± SEM of at least 10 eggs for groups. *p<0.05, **p<0.01 vs control.

Both tumor vasculature and tumor growth are significantly inhibited by TR-764 in a tumorigenesis murine model

TR-764 was further evaluated in a tumor model developed in mice (Figure 10). BL6-B16 mouse melanoma cell lines, injected s.c. in syngeneic C57/BL6 mice, are able to proliferate and generate tumor masses. After 8 days, **TR-764** was daily i.p. administrated at different doses (7.5, 15, 30mg/kg), and the hydrosoluble **CA-4P** (30mg/kg) was used as reference compound. Figure 10D shows the reduction of tumor mass after treatment. **CA-4P** slightly decreased the tumor growth, but its effect was not significant, while **TR-764** significantly arrested tumor developing. The maximum dosage (30mg/kg) reduced by 50% of the tumor mass, and the minimum concentration (7.5mg/kg) shrinked the tumor by more than 30%, after 10days of treatment.

TR-764 endowed an antivascular effect also on the murine model. Blood vessels were stained with an antibody against the endothelial marker CD31 and counted. After 24hours of treatment with **TR-764** 30mg/kg, the number of vessels was significantly reduced by 40%, and this effect was duplicated respect to that of **CA-4P** (Figure 10A-B). After 10days of treatment, the microvessel number is 50% reduced by **TR-764** 30mg/kg, while it is about 40% decreased by the treatment with **TR-764** 7.5mg/kg and **CA-4P** 30mg/kg (Figure 10C).

A

B

C

D
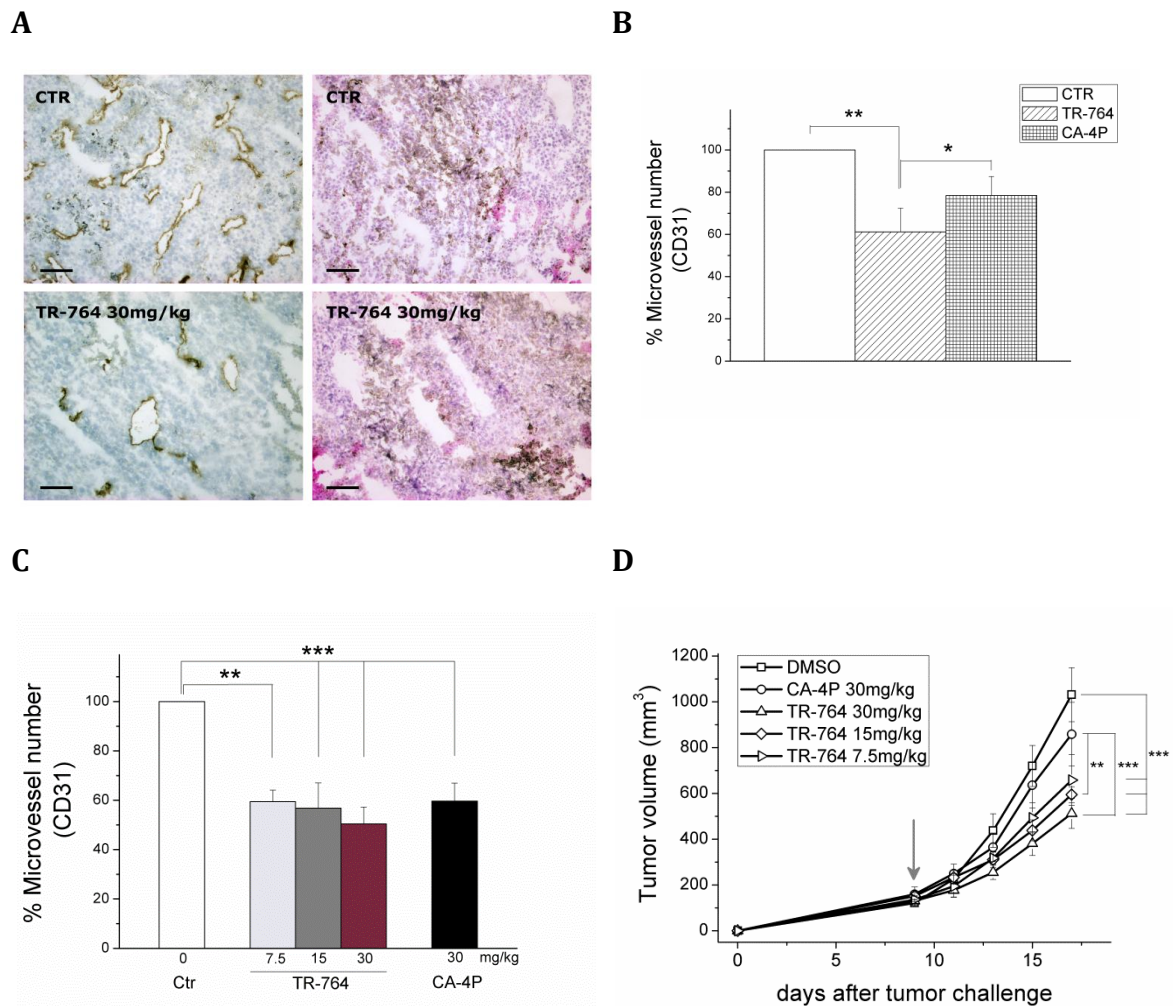
Figure 10. TR-764 significantly reduces the vasculature and inhibits the growth of tumor mass *in vivo*.

BL6-B16 murine melanoma cells were injected in the right flank of C57BL/6 mice. Tumor tissues were embedded in OCT-compound and frozen. CD31 immunohistochemistry and hematoxylin–eosin (HE) staining of tumor after i.p.

treatment with **TR-764** or **CA-4P** at the indicated doses, for 24hours (10x magnification, scale bar = 100μm) (**A**). Quantitative analysis of tumor section stained with CD31, after treatment for 24hours (**B**) or after daily injection for 10days (**C**). Tumor growth was monitored, and the arrow indicates the day of the first treatment (**D**). Data are represented as mean ± SEM of five mouse per group versus control. *$p < 0.05$, **$p < 0.01$, ***$p < 0.001$ vs control.

HIF-1α activation under hypoxic conditions is impaired by TR-764 and its activity on HUVEC is preserved

It has been described that antitubulin agents stimulate hypoxic environment, and consequently resistance mechanisms are activated[98]. In this context we evaluated if **TR-764**, compared to **CA-4**, is able to inhibit the activation of hypoxic stimuli. HUVEC cells, maintained at 2% oxygen for 3-6hours are able to produce the stable form of HIF-1α, which is degraded in normoxic conditions. Simultaneous treatment with **TR-764** (10nM) for 6hours prevented HIF-1α induction, as shown in Figure 11. Moreover, after 3hours pre-incubation of HUVECs at hypoxic conditions, HIF-1α is induced in the control, and further 3hours of treatment the protein activation is reduced.
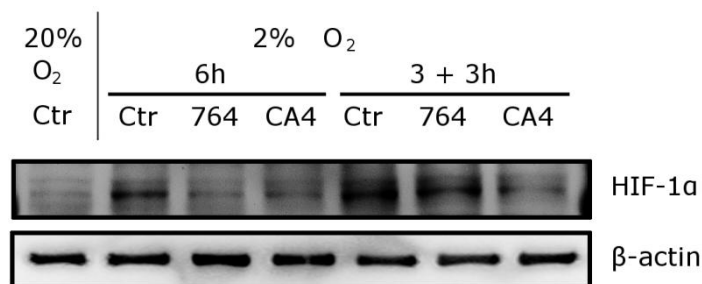
Figure 11. TR-764 and **CA-4** inhibit HIF-1α activation. Western blot analysis was performed on protein lysates of HUVECs maintained in normoxic (20%O_2) and hypoxic (2%O_2) conditions. On the left side of the image, treatment was simultaneously performed when HUVECs were placed in hypoxia. On the right side HUVECs were maintained in hypoxia for 3hours and subsequently treated with **TR-764** and **CA-4** both at 10nM.

TR-764 activity on endothelial cells was preserved also in hypoxic conditions. As shown in Figure 12A-E. the tubule-like structures, formed by HUVEC on Matrigel, were rapidly disrupted by **TR-764**, similarly to **CA-4**. Furthermore, hypoxia remarkably increased HUVEC migration speed, respect to normoxia (see for comparison Figure 2), and **TR-764** is significantly more active to arrest cell motility, in particular at 10nM (Figure12F).

A

B

C

D

E

F
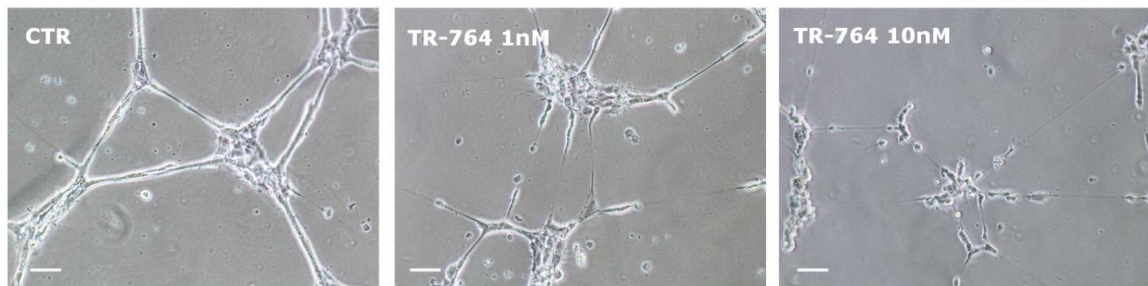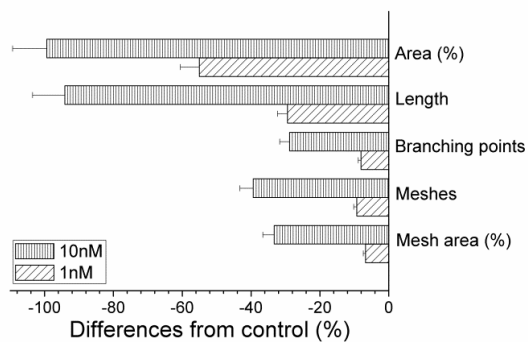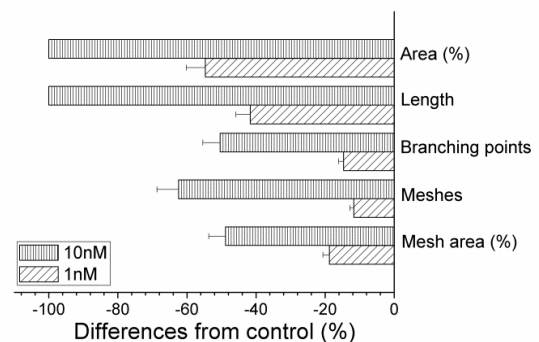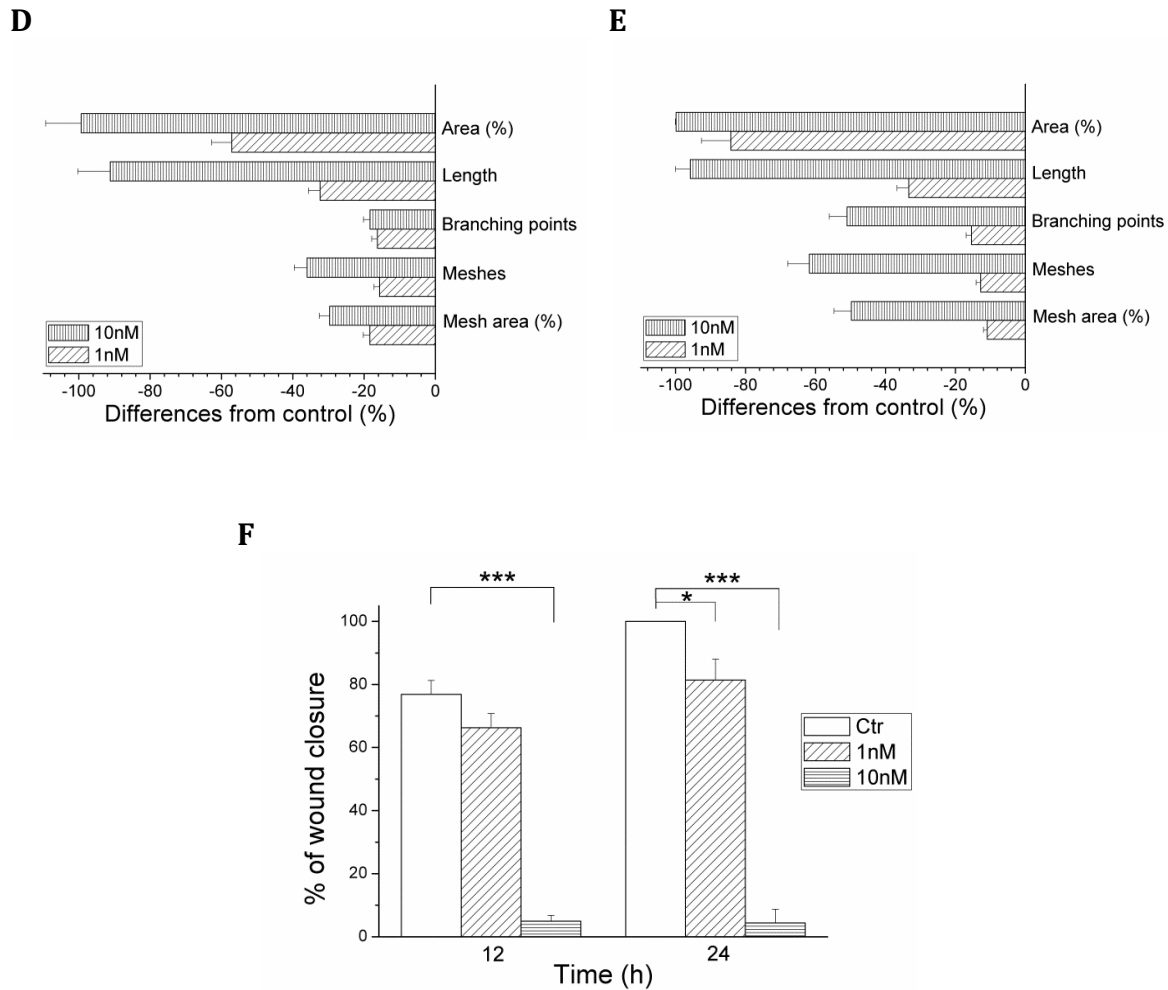
Figure 12. Effects of **TR-764** on HUVECs in hypoxic conditions. **TR-764** disrupts tubule-like structures formed by HUVECs seeded on Matrigel matrix, in hypoxia. Representative pictures of HUVECs treated with **TR-764** at the indicated concentrations for 1hour (10x magnification, scale bar = 100μm) (**A**). Quantitative analysis of treatment with **TR-764** for 1hour (**B**) or 3hours (**C**), and **CA-4** for 1hour (**D**) or 3hours (**E**), on dimensional and topological parameters of tubule networks. Data were represented as mean ± SEM of three independend experiments.

Confluent HUVECs monolayer in hypoxic conditions was scratched and cells were treated with **TR-764**, which impairs cell motility. The ability to move into the wound was measured at the indicated times, and data represent mean ± SEM of three independend experiments (**F**).

1.3.2.4. Discussion

Tubulin binding agents are commonly used in cancer therapy as antimitotic drugs, and recently antivascular effects were described. Here we investigated the antiangiogenic activity of a new tubulin binding agent, **TR-764**, which showed a very strong activity in inhibiting the proliferation of several tumor cells *in vitro* and the tumor growth *in vivo*[99]. **TR-764**, binding to tubulin, triggers a series of events resulting in endothelial cells dysfunction. **TR-764** revealed a marked ability to disrupt the tubule-like structures formed by HUVEC cells seeded on Matrigel, indicating its antiangiogenic activity *in vitro.* Secondly it significantly arrested endothelial cells motility, both in presence and in absence of VEGF, as well as it caused the increase of cell monolayer permeability. All these effects are independent from **TR-764** toxicity in HUVECs, because it did not impair cell cycle and cell viability. Moreover the effects on cytoskeleton occurred rapidly, within 6hours of treatment. These alterations potentially could affect only the tumor blood vessels, composed by highly disorganized and weak structures, more sensitive to TBAs[23], making **TR-764** a selective molecule against tumor vasculature.

The ability of **TR-764** to interact with tubulin was confirmed also in endothelial cells. This new tubulin binding agent efficiently disrupted microtubules structures, causing a strong rearrangement of cytoskeleton, although microfilaments remained intact. Actin filaments were also reorganized, stress fibers and blebs structures appeared after treatment. Altogether, these effects indicate an uncoupling of plasma membrane to extracellular matrix, and this action ultimately is reported to abrogate the complex system of integrating extracellular signals directed to the endothelial cell[51].

Tubulin and actin filaments are both associated to focal adhesions, integrins and cadherins[100],[101]. All these molecules are involved in several biological mechanisms

such as cell adhesion, migration, permeability. They mediate signals deriving from the extracellular matrix or tyrosine kinase receptors, such as VEGFR2, which activate intracellular cascades, mediated by Src/FAK[102]. Thus, targeting endothelial microtubules could impair this signal transduction, involved in a series of processes which stimulate the vascular development.

Besides, the actin cytoskeleton is connected to the plasma membrane through VE-cadherin and one of its intracellular binding partner, β-catenin[17].

We demonstrated that **TR-764** gave rise to both Src and FAK inactivation, by inducing their dephosphorylation respectively in Tyr416 and Tyr397 residues. β-catenin phosphorylation in Tyr142 decreased after treatment with **TR-764**, leading to its dissociation from VE-cadherin (immunoprecipitation experiments are underway to confirm the direct binding between β-catenin and VE-cadherin). Physiological shape of focal adhesions was impaired and adherens junctions were attenuated by **TR-764**, as indicated by VE-cadherin dephosphorylation in Tyr658. The uncoupling of VE-cadherin with β-catenin, as well as the relocalization of β-catenin far from junctions, explained the elevated cell monolayer permeability induced by the treatment. Moreover it has been reported that Src family kinases stimulate VE-cadherin phosphorylation in adherens junctions, leading to increased vascular permeability[103],[56]. Thus **TR-764**, starting from its binding to tubulin, induced cytoskeleton rearrangements, leading to numerous alterations in cell-to-cell contacts and in the interaction to the extracellular matrix. Accordingly, many processes involved in vascular development, such as migration and VEGF-induced stimulation, resulted impaired.

Vessel growth, arise from pro-angiogenic factors, was efficiently counteracted by **TR-764** also *in vivo*, as demonstrated in CAM assay. Vascular development was massively induced by FGF and the number of vessels was strongly reduced by the treatment with **TR-764**. Importantly, our compound alone showed no pro-

inflammatory activity, unlike **CA-4** which is able to stimulate vessel growth in basal conditions, as we previously described[66]. **TR-764** demonstrated highly significant antivascular activity also in a tumorigenic murine model, respect to **CA-4P**, both in acute and after prolonged treatment. Interestingly, **TR-764** not only prevented vascular development, but also arrested the tumor growth, significantly reducing the tumor volume. This peculiarity suggests **TR-764** as a potential candidate as single agent for both anticancer and antivascular therapy. Moreover, numerous failures in recent pharmacological approaches occur, because of resistance mechanisms, mainly governed by hypoxia. Tumor microenvironment, as well as antiangiogenic therapies, give rise to hypoxic stimuli, and tumor cells adapt themselves by developing resistance[40,38]. Thus there is an emergent need to find new strategies to overcome tumor resistance, and in this context **TR-764** could be a valuable candidate. It preserved its antiangiogenic properties *in vitro* under hypoxic conditions and it is endowed with the ability to inhibit or reduce HIF-1α activation, with the aim to prevent potential adaptive signals. Further *in vivo* experiments are underway, to confirm the anti-hypoxic activity of **TR-764**.

1.3.3. DISCOVERY AND OPTIMIZATION OF A SERIES OF 2-ARYL-4-AMINO-5-(3',4',5'-TRIMETHOXYBENZOYL)THIAZOLES AS NOVEL ANTICANCER AGENTS

Romeo Romagnoli, Pier Giovanni Baraldi, Maria Kimatrai Salvador, Delia Preti, Mojgan Aghazadeh Tabrizi, Andrea Brancale, Xian-Hua Fu, Jun Li, Su-Zhan Zhang, Ernest Hamel, Roberta Bortolozzi, Elena Porcù, Giuseppe Basso and Giampietro Viola

1.3.3.1. Abstract

A new series of tubulin polymerization inhibitors based on the 2-aryl/heteroaryl-4-amino-5-(3',4',5'-trimethoxybenzoyl)thiazole scaffold was synthesized and evaluated for growth inhibition activity on a panel of cancer cell lines, cell cycle effects and *in vivo* potency. Structure-activity relationships were elucidated with various substitutions at the 2-position of the thiazole skeleton. Hydrophobic moieties, such as phenyl and 3-thienyl, were well tolerated at this position, and variation of the phenyl substituents had remarkable effects on potency. The most active compound (**3b**) induced apoptosis through the mitochondrial pathway with activation of caspase-3. We also showed that it has potential anti-vascular activity, since it reduced *in vitro* endothelial cell migration and disrupted capillary-like tube formation at non cytotoxic concentrations. Furthermore, compound **3b** significantly reduced the growth of the HT-29 xenograft in a nude mouse model, suggesting that **3b** is a promising new antimitotic agent with clinical potential.

1.3.3.2. Introduction

Besides being critical for cell architecture, the microtubule system of eukaryotic cells is essential for cell division, since microtubules are key components of the mitotic spindle[104–106]. Microtubules are a dynamic cellular compartment in both neoplastic and normal cells. This dynamicity is characterized by the continuous turnover of αβ-tubulin heterodimers in the polymeric microtubules. The microtubule system is also important in other fundamental cellular processes, such as regulation of motility, cell signaling, formation and maintenance of cell shape, secretion and intracellular transport[107].

In the last decades there has been a continuing interest in the discovery and development of novel small molecules able to inhibit tubulin polymerization[108,109]. Numerous chemically diverse antimitotic agents, many of which are natural products, interact specifically with tubulin[68,110,111]. Among the naturally-occurring derivatives, combretastatin A-4 (**CA-4**, **1**), isolated from the bark of the South African tree *Combretum caffrum*[112], is one of the well-known tubulin-binding molecules affecting microtubule dynamics, and compound **1** strongly inhibits the polymerization of tubulin by binding to the colchicine site[113]. Compound **1** shows potent cytotoxicity against a wide variety of human cancer cells, including those that are multidrug resistant[114].

In the course of our search for new synthetic tubulin inhibitors, we recently reported the synthesis and biological characterization of a series of 2-alkylamino-4-amino-5-aroylthiazoles with general structure **2**, prepared by an easy one-pot four step procedure[115]. Among the synthesized compounds, the 2-(pyrrolidin-1-yl)-4-amino-5-(3',4',5'-trimethoxybenzoyl)thiazole derivative **2a** was the only compound of this series active at submicromolar concentrations against a panel of five cancer cell lines, with IC_{50} values ranging from 0.2 to 0.4μM. Compound **2a** was 10- to 100-

fold less active than the reference compound **1** as an antiproliferative agent, while it was comparable to **1** as an inhibitor of tubulin polymerization. Structure-activity relationship studies indicated that the pyrrolidine is the only substituent tolerated at the 2-position of thiazole scaffold. This finding led us to assume that the tubulin binding pocket for this portion of the molecule is quite small and that tubulin only tolerated the presence of hydrophobic substituents, indicating the possibility for further improvement in activity. Thus, once the 4-amino-5-(3',4',5'-trimethoxybenzoyl) thiazole scaffold was identified as minimum structural requirement for activity in this new series of compounds, our strategy for further development of active antimitotic agents was to perform modifications at the 2-position of the thiazole ring. The first round of optimization included replacement of the pyrrolidine ring of compound **2a** with a phenyl or bioisosteric 3-thienyl ring, to furnish derivatives **3a** and **3b**, respectively. As shown in Table 1, phenyl or 3'-thienyl substitutions at the C-2 position of the thiazole ring significantly enhanced antiproliferative activity. Encouraged by the increased potency obtained with **3a**, we then synthesized compounds **3c-o** to determine whether various electron-releasing (Me, Et, $C(CH_3)_3$, OMe, OEt and OCF_3) or electron-withdrawing (F, Cl, CF_3, CN and NO_2) substituents on the *para-* or *meta*-positions of the phenyl ring would further enhance activity. To compare the effects of *para-* and *meta*-substitution, the chloro atom and the methoxy-group were also introduced at the *meta*-position of the phenyl ring. We are including **3b** in this report because it had the best antiproliferative activity (see below) of all the compounds prepared in this study.

We examined the efficacy of the newly synthesized compounds on a panel of human cancer cell lines, including multidrug resistant lines overexpressing the 170-kDa P-glycoprotein drug efflux pump, and we investigated in detail the modalities of cell death induced by these derivatives. Since many antimitotic drugs, such as compound

1, have been shown to possess antiangiogenic and antivascular activities[51,61] we also investigated the effects of these compounds on *in vitro* assays with HUVEC.

1.3.3.3. Results and Discussion

In vitro antiproliferative activities

The 2-aryl/heteroaryl-4-amino-5-(3',4',5'-trimethoxybenzoyl)thiazoles **3a-o** were evaluated for their antiproliferative activity against a panel of six human tumor cell lines and compared with the reference compound **1**. As shown in Table 1, the antiproliferative activities of the tested compounds were generally more pronounced against HeLa and MCF-7 cells as compared with the other cell lines. With the exception of MCF-7 cells, the 3-thienyl derivative **3b** was the most active compound in this series, exhibiting IC$_{50}$ values raging from 2.4 to 78nM against five of the six cancer cell lines and an IC$_{50}$ of 210nM against the A549 cells. Moreover, with the MCF-7 and HT-29 cells, compounds **3a-c**, **3e-f** and **3k** were more potent than **1**, with IC$_{50}$ values in the single- or double-digit nanomolar range. Compounds **3b** and **3e** showed comparable potency to **1** against the HeLa cells. Of the fifteen tested compounds, **3a-b**, **3e** and **3k** possessed the highest overall potency, with IC$_{50}$ values of 2.4-140nM against five of the six cancer cell lines, and IC$_{50}$ values of 200-700nM against the A549 cells. With the exception of MCF-7 and HT-29 cells, the reference compound **1** possessed the highest potency in four of the six cell lines tested.

The bioisosteric replacement of the phenyl ring of compound **3a** with the 3-thienyl group (**3b**) produced a 1.5- to 3-fold increase of potency against A549, Jurkat and HeLa cells, while the differences between **3a** and **3b** were minimal in HL-60 and HT-29 cells. Only in MCF-7 cells **3b** was less active than **3a** (IC$_{50}$ values of 51 and 2.2nM, respectively). Excluding the A549 cells, compounds **3a** and **3b** had IC$_{50}$ values ranging from 24-80nM against the cell lines, compared with a range of 1-3100nM obtained with **1**.

The data shown in Table 1 demonstrated the importance of substituents on the phenyl ring at the 2-position of the thiazole system for activity and selectivity against the different cancer cell lines. In general, all substituents caused a reduction in antiproliferative activity relative to **3a**, except in four cases. The *meta*-chloro substituent of **3e** resulted in enhanced antiproliferative activity against three cell lines (HeLa, A549, and Jurkat cells), while the *meta*-methoxy substituent of **3k** resulted in enhanced activity in one cell line (HL-60 cells). Otherwise, all substituents led to reduced activity, sometimes mild to moderate (e.g., **3c**, **3e**, **3f**), sometimes profound (e.g., **3h-j** and **3l-o**).

Turning specifically to the *para*-substituted phenyl derivatives, these showed highly variable potencies. Generally, it was found that most substituents in the *para*-position resulted in lower activity as compared to the unsubstituted parent compound **3a**, with the least deleterious being fluorine and methyl (compounds **3c** and **3f**, respectively). Comparing the fluorine derivative (**3c**) with the methyl derivative (**3f**), the latter was more active in five of the six cell lines we examined, with the greatest difference observed in the MCF-7 cells. Comparing the fluorine (**3c**) and the chlorine (**3d**) derivative, increasing the size of the halide led to a large loss of activity with all six cell lines. In contrast, as noted above, the *meta*-chloro derivative (**3e**) was much more active than its *para*-congener **3d**, including enhanced activity relative to **3a** in three cell lines. Indeed, the activity of **3e** did not differ greatly from the 3-thienyl analogue **3b** in all cell lines.

Turning to the electronic characteristics of the *para*-substituents, the introduction of a weak electron-releasing methyl group (**3f**) caused a 1.5-4-fold loss in antiproliferative activity in the six cell lines relative to the unsubstituted **3a**. A *para*-ethyl group (compound **3g**) caused a further, major decrease in antiproliferative activity relative to **3a**, **3f** was 14-700-fold less active in the six cell lines. Little

antiproliferative activity was observed with still larger *para*-substituents (**3h-j**, **3m-o**), regardless of their electronic characteristics.

The antiproliferative activities of compounds **3j**, **3k** and **3l** were influenced by the number and position of methoxy substituents on the phenyl ring. The *meta*-methoxy derivative **3k**, as noted above, was relatively active. Relative to the unsubstituted **3a**, **3k** was 1.1-5-fold less active in five cell lines and twice as active in HL-60 cells. In contrast, the *para*-methoxy derivative **3j** was 32-570-fold less active than **3a** when IC_{50} values could be determined. The 3,4-dimethoxy substituted analogue **3l** was generally intermediate in activity between **3j** and **3k**.

In summary, comparing the effects of ERGs and EWGs on the phenyl at the C2-thiazole position, no consistent difference on effects on antiproliferative activity occurred. Overall, all substituents at the *para*-position led to a loss of activity, and profound loss occurred with larger substituents. The effects of the two small *meta*-substitents examined were not dramatic, leading, perhaps, to some enhancement of antiproliferative activity. In different cell lines, moreover, different effects were observed. For example, replacement of the electron-donating methoxy group with the electron-withdrawing chlorine atom (compounds **3k** and **3e**, respectively), resulted in a 3- and 4-fold reduction in activity against HL-60 and MCF-7 cells, while **3k** and **3e** showed comparable potencies against HT-29, and **3e** was 5- and 2-fold more active than **3k** against HeLa and Jurkat cells.

Table 1. *In vitro* cell growth inhibitory effects of compounds **1** and **3a-o**.

Compd	IC$_{50}$ ^{a}(nM)					
	HeLa	A549	HL-60	Jurkat	MCF-7	HT-29
3a	7.6 ± 1.7	367 ± 11.0	80.8 ± 7.1	58.0 ± 5.6	2.2 ± 0.8	13.2 ± 5.4
3b	2.4 ± 0.9	210 ± 38.1	77.9 ± 2.6	26.4 ± 2.3	51.2 ± 9.3	11.4 ± 2.8
3c	24.1 ± 4.3	1082 ± 36.7	384 ± 25.0	582 ± 15.4	29.4 ± 1.5	115 ± 3.5
3d	188 ± 46.0	6730 ± 202	4445 ± 68.2	1749 ± 58.8	845 ± 18.5	2083 ± 50.5
3e	2.8 ± 1.0	326 ± 14.8	137 ± 27.2	35.9 ± 4.4	41.7 ± 3.5	24.0 ± 5.8
3f	22.7 ± 7.8	1223 ± 97.1	295 ± 27.0	201 ± 57.1	3.2 ± 0.7	53.1 ± 14.8
3g	191 ± 44.8	5175 ± 135	1813 ± 244	2328 ± 577	1583 ± 267	1018 ± 135
3h	4148 ± 75.4	>10,000	>10,000	>10,000	508 ± 123	9067 ± 158
3i	1799 ± 27.6	>10,000	>10,000	>10,000	>10,000	>10,000
3j	244 ± 41.3	>10,000	>10,000	2023 ± 75.9	1255 ± 25.7	2806 ± 72.2
3k	13.7 ± 4.5	720 ± 28.3	41.2 ± 5.5	66.6 ± 8.9	11.3 ± 5.1	22.3 ± 4.4
3l	191 ± 35.9	>10,000	1136 ± 74.4	606 ± 45.7	257 ± 65.4	220 ± 18.6
3m	1981 ± 36.0	6253 ± 318	>10,000	4829 ± 64.1	>10,000	>10,000
3n	>10,000	>10,000	>10,000	>10,000	>10,000	>10,000
3o	570 ± 10.2	6106 ± 169.9	>10,000	>10,000	>10,000	4785 ± 83.2
1	4 ± 1	180 ± 50	1 ± 0.2	5 ± 0.6	370 ± 100	3100 ± 100

^{a}IC$_{50}$= compound concentration required to inhibit tumor cell proliferation by 50%. Data are expressed as the mean ± SE from the dose-response curves of at least three independent experiments.

84

Effect of compound 3b on multidrug resistant cells

To investigate whether these derivatives are substrates of drug efflux pumps, one of the most active compounds (**3b**) was tested against a panel of drug resistant cell lines which either overexpress P-glycoprotein (Lovo[Doxo] and Cem[Vbl100])[116,117] or are associated with tubulin gene mutations (A549-T12)[118] that result in modified tubulin with impaired polymerization properties. As shown in Table 2, **3b** exhibited cytotoxic activity in all three of the drug resistant cell lines. The activity in the two P-glycopprotein overexpressing cell lines demonstrated that **3b** is not a substrate for this important drug pump.

Table 2. *In vitro* cell growth inhibitory effects of compound **3b** on drug resistant cell lines.

Compd	IC$_{50}$[a](nM)		
	LoVo	**LoVo[Doxo]**	**Resistance ratio**[b]
3b	18.0 ± 4.5	24.8 ± 5.3	1.4
Doxorubicin[c]	120 ± 30	13150 ± 210	109.6
	CEM	**CEM** [Vbl100]	**Resistance ratio**[b]
3b	273.3 ± 20.3	666.7 ± 12.0	2.4
Vinblastine	0.8 ± 0.1	205 ± 46	256.2
	A549	**A549-T12**	**Resistance ratio**[b]
3b	209.6 ± 38.1	201.5 ± 46.7	0.96
Taxol[c]	7.2 ± 0.1	75.2 ± 12.5	10.4

[a]IC$_{50}$= compound concentration required to inhibit tumor cell proliferation by 50%. Data are expressed as the mean ± SE from the dose-response curves of at least three independent experiments.

[b]The values express the ratio between IC$_{50}$ determined in resistant and non-resistant cell lines. [c] Data from Ref.[115]

Inhibition of tubulin polymerization and colchicine binding

To investigate whether the antiproliferative activities of compounds **3a-c**, **3e-f** and **3k** derived from an interaction with tubulin, these agents were evaluated for their inhibition of tubulin polymerization and for effects on the binding of [^{3}H]colchicine to tubulin (Table 3)[119,120]. For comparison, compound **1** was examined in contemporaneous experiments. In the assembly assay, compounds **3a-b** and **3e-f** was found to be the most active compounds (IC$_{50}$ values, 1.5-1.7μM), with activity comparable with that of **1** (IC$_{50}$, 1.2μM). Compounds **3c** and **3k** were half as active as **1**, although they were more potent than **1** as antiproliferative agents against MCF-7 and HT-29 cells.

When comparing inhibition of tubulin polymerization versus the growth inhibitory effects, we found a positive correlation for most, but not all, of the active compounds. While **3f** was generally less potent than **3b** as an antiproliferative agent, **3f** and **3b** showed equal potency as inhibitors of tubulin assembly. Similarly, **3k** is 1.5-fold less active than **3f** in the tubulin assay, but **3k** is more active than **3f** in five of the cell lines. Nevertheless, we could not exclude the possibility that **3b** and **3k** may affect other molecular targets in addition to microtubules resulting in the enhanced antiproliferative activity.

In the colchicine binding studies, derivatives **3a** and **3b** potently inhibited the binding of [^{3}H]colchicine to tubulin, with 79% and 77% inhibition occurring with these agents. Inhibition of colchicine binding by compounds **3c**, **3e-f** and **3j** was lower, ranging from 45 to 63%. None, however, was quite as potent as **1**, which in these experiments inhibited colchicine binding by 98%.

For the most active compounds **3a** and **3b**, a good correlation was observed between antiproliferative activities, inhibition of tubulin polymerization and inhibition of colchicine binding. In general, inhibition of [^{3}H]colchicine binding to tubulin correlated more closely with antiproliferative than did inhibition of tubulin

assembly. It should be noted, however, that there are much larger differences in antiproliferative activity between cell lines and between compounds with similar antitubulin effects. It has to be considered that the tumor cell growth assay and the tubulin polymerization assay differ in a number of further important issues, such as tubulin concentration present within the cells and during microtubule formation outside a cell, the presence of different types of microtubule-associated proteins and the possible effects of regulatory proteins expressed in the cells but being absent in the tubulin assay. Alternatively, it is possible that cellular tubulin differs from the neural tubulin used in the biochemical assays in its affinities for the tested compounds.

Table 3. Inhibition of tubulin polymerization and colchicine binding by compounds **1**, **3a-c**, **3e-f** and **3k**.

Compound	Tubulin assembly [a] $IC_{50} \pm SD$ (µM)	Colchicine binding [b] % ±SD
3a	1.6±0.2	78±6
3b	1.5±0.2	77±4
3c	2.7±0.2	45±6
3e	1.7±0.2	63±3
3f	1.5±0.1	59±4
3k	2.2±0.3	51±6
1	1.2±0.1	98±0.6

[a] Inhibition of tubulin polymerization. Tubulin was at 10µM.
[b] Inhibition of [3H]colchicine binding. Tubulin, colchicine and tested compound were at 1, 5 and 5µM, respectively.

Molecular Modeling

A series of molecular docking simulations were performed to rationalize the observed SARs for this series of compounds. The proposed binding mode that emerged from these studies is virtually identical to the pyrrolidine analogue **2a** reported previously[115]. Figure 1 shows how the thienyl analogue **3b** sits in a tight hydrophobic pocket defined by β-tubulin residues Val181, Asn258, Met259 and Lys352. It is interesting to note that this pocket can only accommodate an aromatic ring with relatively small substituents, like the ones present in **3a**, **3c-f** and **3k** (Figure 2), while compounds with more sterically hindered substituents (e.g., the *t*-butyl of **3h**) do not dock well in the binding site. In addition to these non-polar interactions, the trimethoxyphenyl ring of **3b** is also in contact with βCys241 while the amino group establishes a hydrogen bond with βThr179. These latter two interactions are often observed in the binding of tubulin inhibitors in the colchicine site[121].
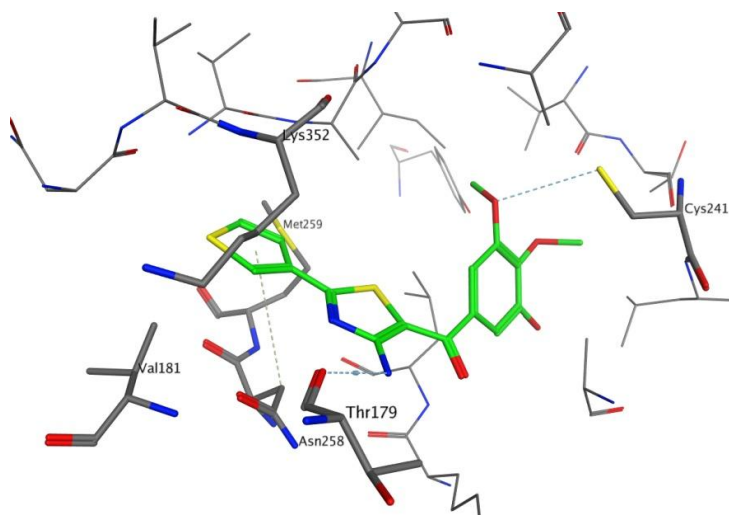
Figure 1. Proposed binding mode of **3b** in the colchicine binding site of β-tubulin.
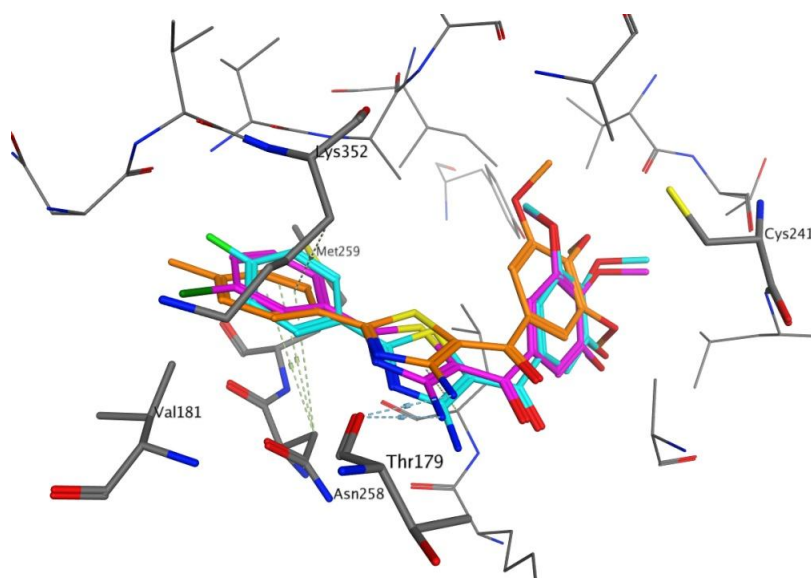
Figure 2. Putative binding mode of **3c** (in cyan), **3e** (in magenta) and **3f** (in orange) in the colchicine site of β-tubulin.

Analysis of cell cycle effects

The effect of **3a** and **3b** on cell cycle progression was examined by flow cytometry in Hela and Jurkat cells. Treatment with the two compounds in HeLa cells, resulted in the accumulation of cells in the G2/M phase, with a concomitant reduction in cells in both the S and G1 phases. These changes occurred in a concentration-dependent manner (Figure 3, Panel A), but changes were observed even at the lowest concentration (62nM) used. A similar behavior was observed also for Jurkat cells (Figure 3, Panel B), except that for compound **3a** we detected a less pronounced G2/M arrest in comparison with **3b** in the same cell lines accompanied with a reduction of the G1 phase while the S phase remain constant.

Next, we investigated the association between **3b**-induced G2/M arrest and alterations in G2/M regulatory protein expression in HeLa cells. As shown in Figure 3 (Panel C), **3b** caused an increase in cyclin B1 expression after 24 and 48hours,

indicating an activation of the mitotic checkpoint following drug exposure. This effect was confirmed by the appearance of slower migrating forms of phosphatase cdc25c at 24hours, followed by a strong reduction at 48hours. The phosphorylation of cdc25c directly stimulates its phosphatase activity, and this is necessary to activate cdc2/cyclin B on entry into mitosis[91]. In good agreement, we also observed at 24hours of incubation, at the concentration of 100nM, a remarkable dephosphorylation at Tyr15 of cdc2 kinase and this effect, although less pronounced also after 48hours of incubation.

A   **B**
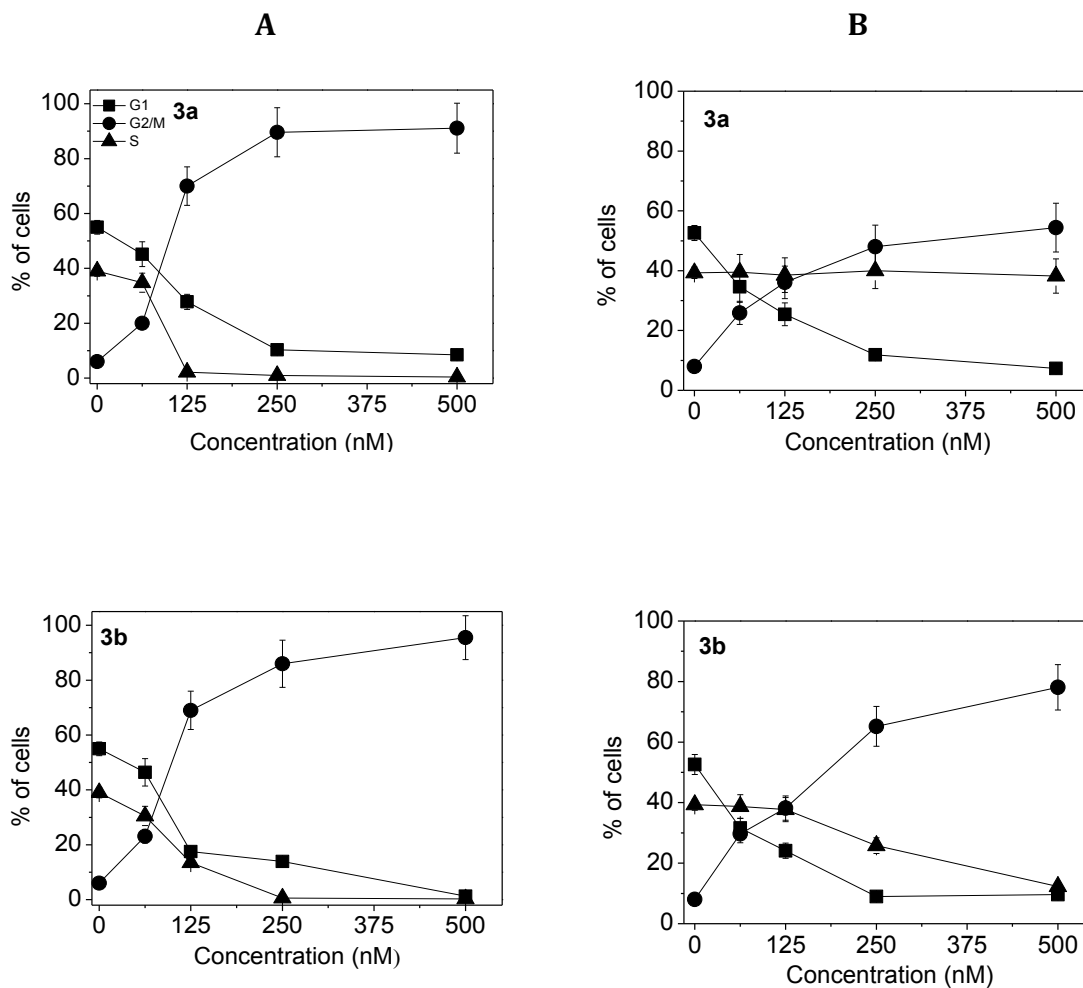
C
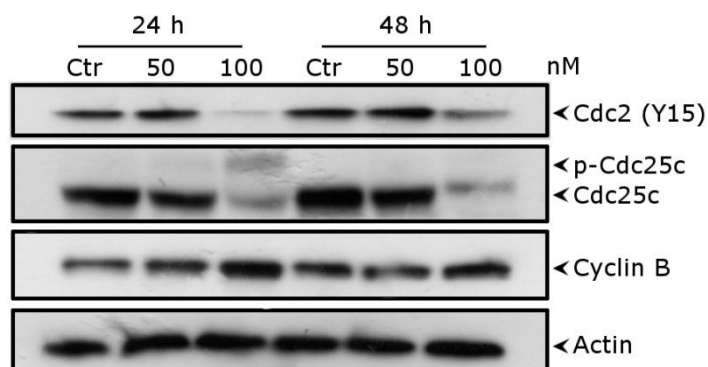
Figure 3. Effect of compounds **3a** and **3b** on cell cycle phase arrest in Hela (panel A) and Jurkat cells (panel B). Cells were treated with different concentrations of **3a** or **3b**, as indicated, ranging from 62.5 to 500nM for 24hours. Then the cells were fixed and stained with PI to analyze DNA content by flow cytometry. Data are presented as mean ± SEM of three independent experiments. Panel C. Effect of **3b** on some G2/M regulatory proteins. HeLa cells were treated for 24 or 48hours with the indicated concentration of the compound. The cells were harvested and lysed for the detection of cyclin B, p-Cdc2^{Tyr15} and Cdc25c expression by Western blot analysis. To ensure equal protein loading, each membrane was stripped and reprobed with anti-β-actin antibody.

Compound 3b induced apoptosis

To evaluate the mode of cell death induced by compound **3b**, we performed a biparametric cytofluorimetric analysis using propidium iodide (PI) and annexin-V-FITC, which stain DNA and phosphatidylserine (PS) residues, respectively.

After treatment with **3b** at 50 or 100nM for 24 or 48hours, HeLa cells were labeled with the two dyes, and the resulting red (PI) and green (FITC) fluorescence was monitored by flow cytometry. As shown in Figure 4 (panel A), **3b** caused a significant induction of apoptotic cells after 24hours. The percentage of annexin-V positive cells then further increased at 48hours (Figure 4, panel B). These findings prompted us to further investigate the apoptotic process after treatment of cells with **3b**.

A

B
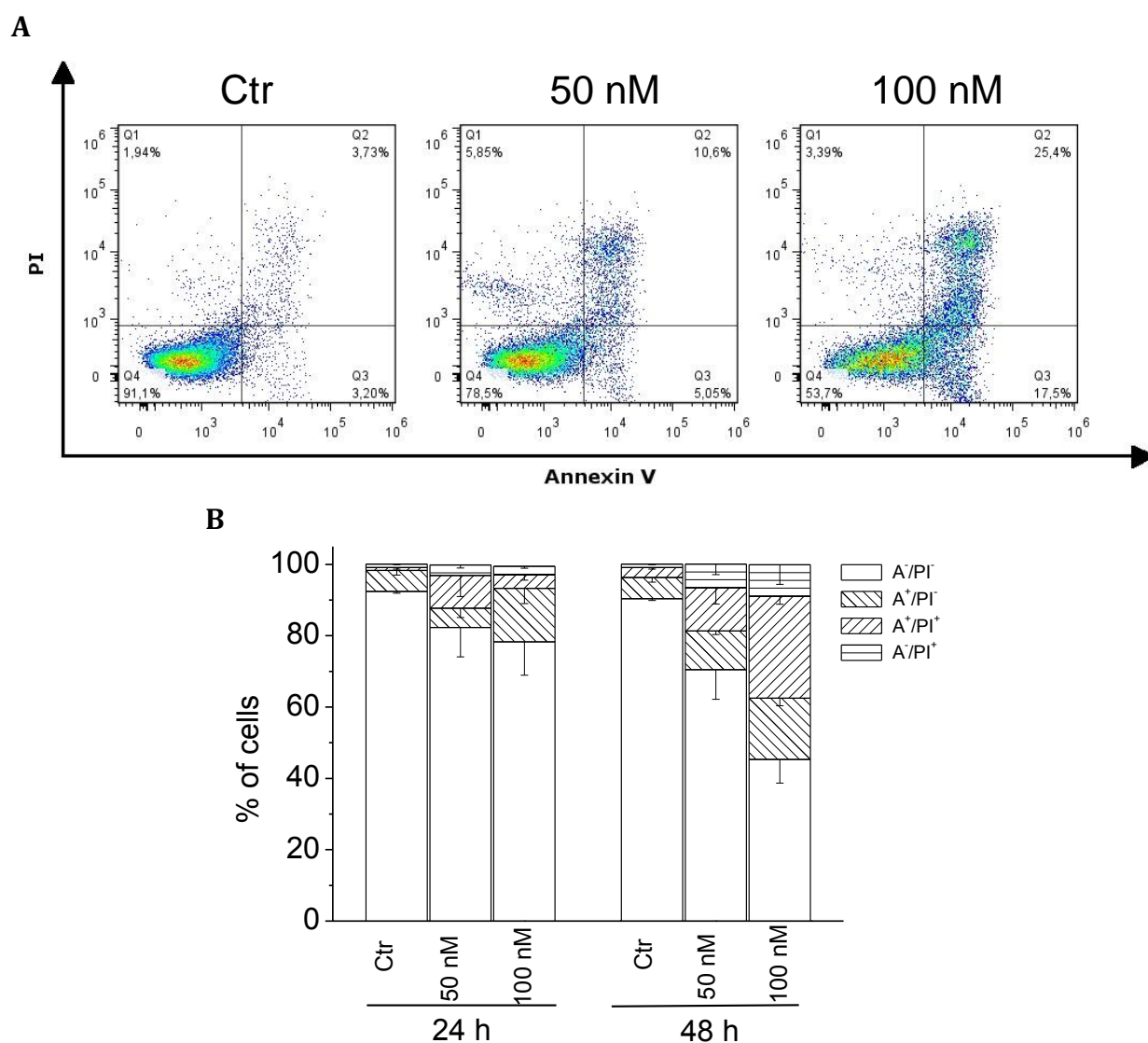
Figure 4. Panel A. Representative flow cytometric histograms of apoptotic HeLa cells after 48hours treatment with **3b.** The cells were harvested and labeled with annexin-V-FITC and PI and analyzed by flow cytometry. Panel B. Percentage of cells found in the different regions of the biparametric histograms after incubation with **3b** for 24 or 48hours. Data are expressed as mean ± S.E.M. for five independent experiments.

3b induced mitochondrial depolarization and ROS production

Mitochondria play an essential role in the propagation of apoptosis[122,123]. It is well established that, at an early stage, apoptotic stimuli alter the mitochondrial transmembrane potential ($\Delta\psi_{mt}$). $\Delta\psi_{mt}$ was monitored by the fluorescence of the dye JC-1[124]. Treated HeLa cells in the presence of **3b** (50 and 100nM) exhibited a marked

shift in fluorescence compared with control cells, indicating depolarization of the mitochondrial membrane potential (data not shown). Following treatment, the percentage of cells with low $\Delta\psi_{mt}$ increased in a time-dependent fashion (Figure 5, panel A). The disruption of $\Delta\psi_{mt}$ is associated with the appearance of annexin-V positivity in the treated cells when they are in an early apoptotic stage. In fact, the dissipation of $\Delta\psi_{mt}$ is characteristic of apoptosis and has been observed with both microtubule stabilizing and destabilizing agents, including **1**, in different cell types[91]. Mitochondrial membrane depolarization is associated with mitochondrial production of ROS[125,126]. Therefore, we investigated whether ROS production increased after treatment with the test compounds. We utilized the two fluorescence indicators hydroethidine (HE), and 2,7-dichlorodihydrofluorescein diacetate (H$_2$-DCFDA) [127]. The results are presented in Figure 5, panels B and C which shown that **3b** induced the production of significant amounts of ROS in comparison with control cells, in agreement with the dissipation of $\Delta\psi_{mt}$ described above.

A

B

C
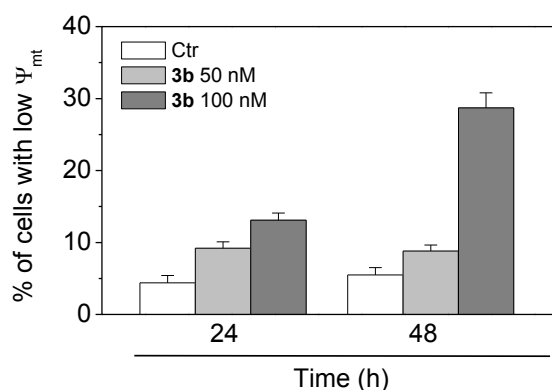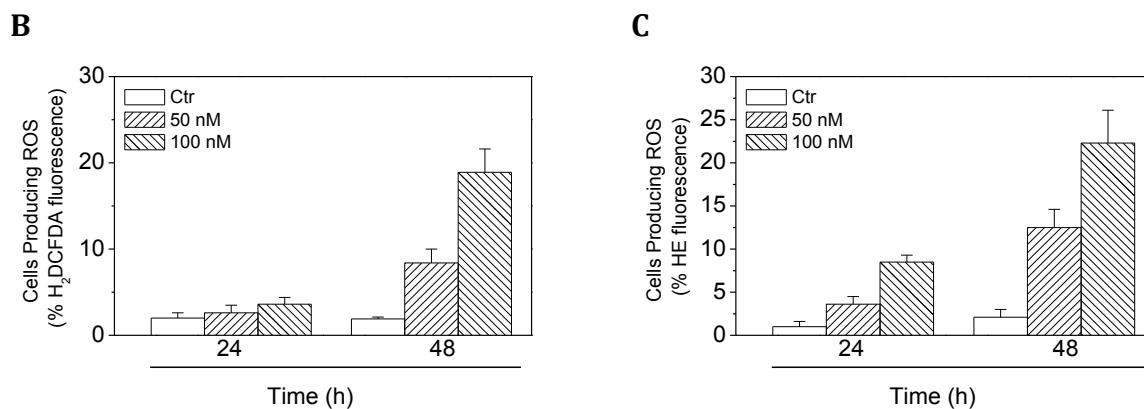
Figure 5. Assessment of HeLa mitochondrial dysfunction after treatment with compound **3b**. Panel A. Induction of loss of mitochondrial membrane potential after 24 or 48hours incubations with compound **3b**. Cells were stained with the fluorescent probe JC-1 and analyzed by flow cytometry. Data are expressed as mean ± S.E.M. for three independent experiments. Panels B and C. Mitochondrial production of ROS in HeLa cells. After 24 or 48hours incubations with **3b**, cells were stained with H_2-DCFDA (panel B) or HE (panel C) and analyzed by flow cytometry. Data are expressed as mean ± S.E.M. of three independent experiments.

Effect of 3b on Bcl-2 and Bax expression and caspase-3 activation

We evaluated the activity of caspase-3 after treatment of HeLa cells with **3b**, since this enzyme is essential for the propagation of the apoptotic signal after exposure to many antimitotic compounds[128]. We observed a clear activation of caspase-3, as well as cleavage of the caspase-3 substrate PARP after 24 and 48hours of **3b** exposure (Figure 6). In addition, after a 48 h exposure to 100nM, we also found an increase in the expression of phospho-γH2AX, a well known marker for cellular DNA double strand breaks[129]. This suggests that DNA damage probably occurred in the unsegregated chromosomes resulting from the stalled replication caused by compound **3b**. There is increasing evidence that regulation of the Bcl-2 family of protein shares the signaling pathways induced by antimicrotubule compounds[91,130]. The proteins of the Bcl family play a major role in controlling apoptosis through the

94

regulation of mitochondrial processes and the release of mitochondrial proapoptotic molecules that are important for the cell death pathway[91]. Our results (Figure 6) showed that the expression of the anti-apoptotic protein Bcl-2 was strongly reduced after 24hours of treatment with 100nM **3b** and after 48hours with either 50 or 100nM **3b**. In contrast, expression of Bax, a proapoptotic protein of the Bcl-2 family, was unchanged.
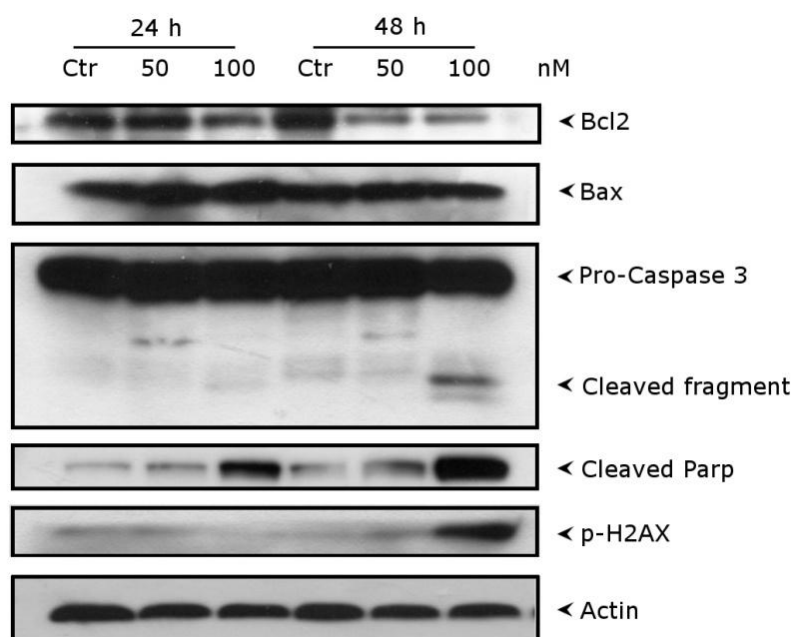
Figure 6. Western blot analysis for caspase-3 activation, PARP cleavage and the expression of Bcl-2, Bax and histone γH2AX in HeLa cells. The cells were treated with the indicated concentration of **3b** for 24 or 48hours. Whole cell lysates were subjected to SDS-PAGE, followed by blotting with the appropriate antibody or an anti-actin antibody.

In vitro evaluation of anti-vascular activity of 3b

Many studies have shown that most microtubule-binding drugs possess vascular disrupting activity, and such data suggest that this class of drugs could be useful as antiangiogenic compounds[51,61]. In this context **CA-4** and its analogues in clinical development have been shown to quickly and selectively shut down the blood flow

of tumors[58,95]. The effect is thought to be mediated by inducing endothelial cell shape change, possibly through disruption of microtubule dynamics[51]. We tested **3b** for its ability to induce rapid endothelial cell shape changes using a human umbilical vein endothelial cell (HUVEC) culture assay. We first investigated the effects of **3b** on endothelial cell migration using an *in vitro* scratch assay[131]. We scraped confluent monolayers of HUVECs to clear space for motile cells to move into. As shown in Figure 7 (panel A), we observed that after 24hours non-treated cells migrated to completely fill the area that was initially scraped. In contrast, **3b** significantly inhibited HUVEC migration in a concentration and time dependent manner (Figure 7, panels A and B).

We also tested the effects of **3b** in a tube formation assay. After being seeded on Matrigel, HUVECs form a rich meshwork of branching capillary-like tubules with multicentric junctions. After just 1 h in different concentration (100-500nM) of **3b**, the capillary-like tubes were interrupted. At the two higher concentrations of **3b**, most cells were spherical and either isolated or aggregated in small clumps (Figure 7, panel C). Quantitative image analysis (Figure 7, panel D) showed that **3b** markedly decreased in a concentration dependent manner both dimensional (percent of area covered by HUVECs, total length per field) and topological parameters (number of mesh per field, number of branching points) of the capillary-like network.

To evaluate if the inhibition of cell migration and tube formation was due to a cytotoxic action of **3b**, we analyzed cell proliferation of the HUVECs by the MTT assay. The calculated GI_{50} after 72hours was $4.4\pm0.9\mu M$, indicating that this compound inhibited proliferation of these cells only at concentrations higher than that required for inhibition of cell migration and tube formation. Altogether, these preliminary observations suggest that **3b**, like **CA-4**, would most likely cause severe vascular disruption *in vitro* although at concentration higher than that of **CA-4**[58,95] and warrant further studies to evaluate in deep its vascular disrupting properties.

A

B

C

D
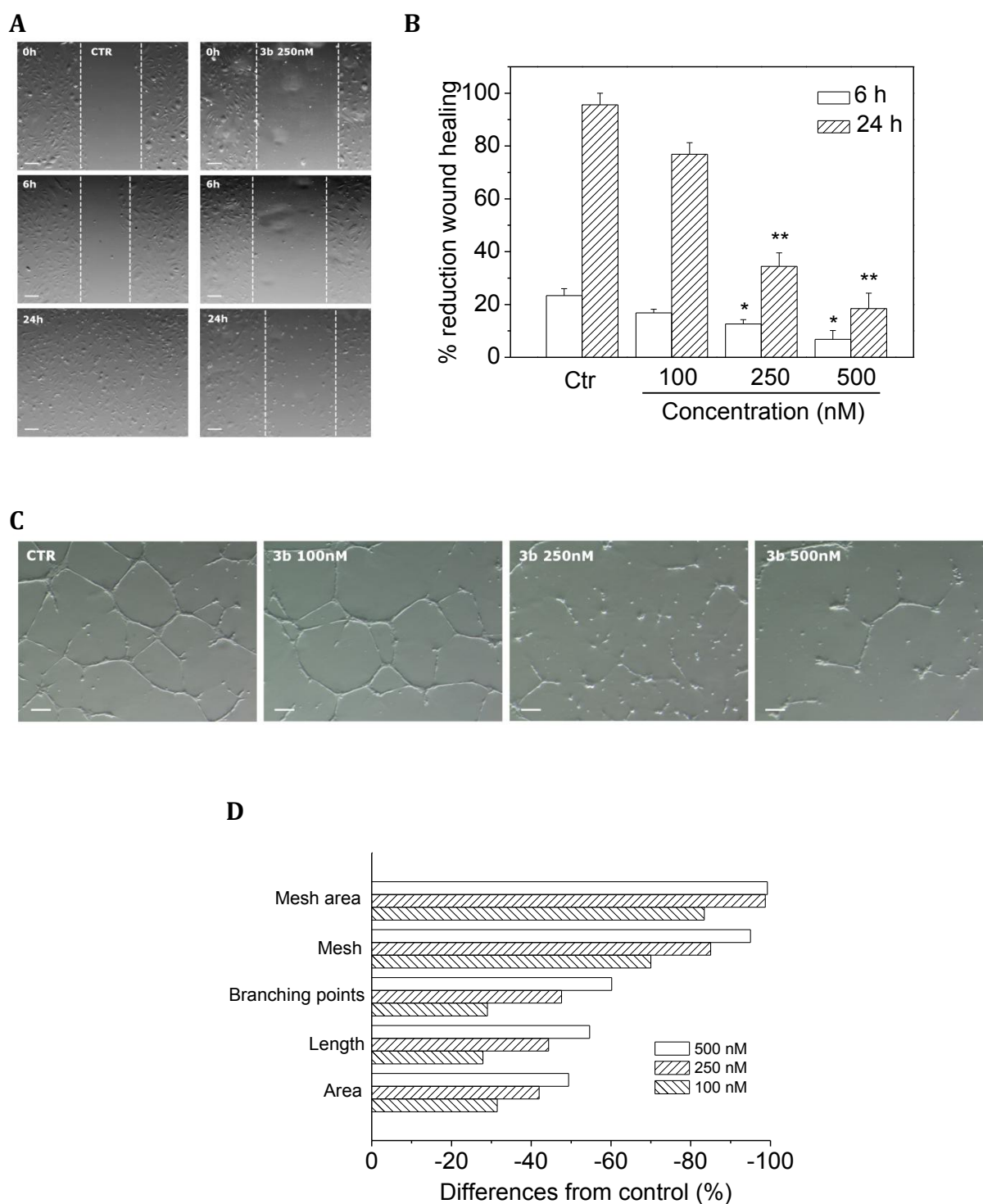
Figure 7. Antivascular activity of compound **3b**. Panel A. **3b** inhibits HUVEC migration. Confluent HUVEC monolayers were scratch wounded. The cells were treated with various concentrations of **3b**, and at different times cells were photographed (40x magnification). The dotted lines define the areas lacking cells. Panel B. Graph shows the quantitative effect of **3b**. Data are presented as mean ± S.E.M. of three independent experiments.*p<0.05 **p<0.01 vs control. Panel C. Inhibition of endothelial cell capillary-like tubule formation by **3b**. Tubule formation on Matrigel was performed as described

in Materials and Methods. Representative pictures (10x magnification) of HUVECs treated with the indicated concentrations of **3b** for 3hours. Panel D. Graph shows the quantitative effects of **3b** on the dimensional and topological parameters of the HUVEC network.

In vivo antitumor activity of compound 3b.

To evaluate the *in vivo* antitumor activity of **3b**, human colon adenocarcinoma xenografts were established by subcutaneous injection of HT29 cells into the backs of nude mice. Once the HT-29 xenografts reached a size of ~300mm³, twelve mice were randomly assigned to one of two groups. In one of the groups, compound **3b** dissolved in DMSO was injected intraperitoneally at doses of 100mg/kg. The drug, as well as the vehicle control, were administered three times a week for one week. As shown in Figure 8 (panel A), compound **3b** caused a significant reduction in tumor growth (58%, p<0.01) as compared with administration of vehicle only.

During the whole treatment period, no significant weight changes or macroscopic signs of toxicity occurred in the treated animals (Figure 8, panel B) suggesting that the administration of **3b** was well tolerated.

A
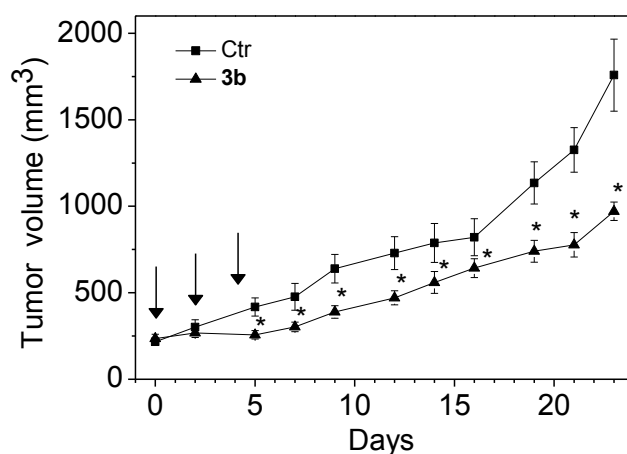
B
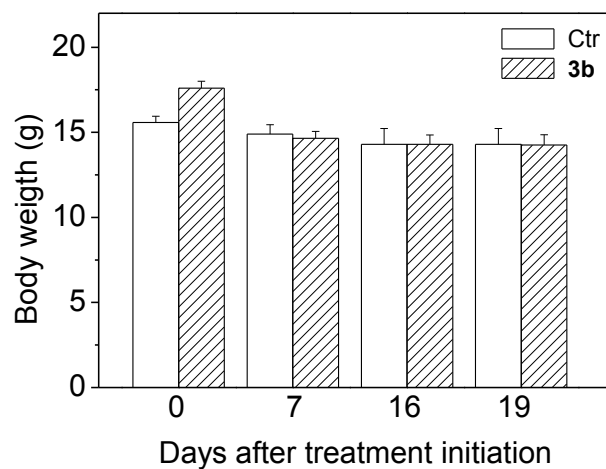
Figure 8. Inhibition of human xenograft growth *in vivo* by compound **3b.** Panel A. HT29 tumor-bearing nude mice were administered either vehicle control or 100mg/kg of **3b** in vehicle intraperitoneally on days 0, 2 and 4 (indicated by arrows). The figure shows the tumor volume (panel A) and body weight (panel B) recorded at the indicated days after treatments. Data are expressed as mean ± SEM of tumor volume and body weight at each time point for six animals per group. *p<0.01 *vs*. control.

1.3.3.4. Conclusions

The structural refinement of compound **2a** led to the discovery of a novel series of synthetic inhibitors of tubulin polymerization with general structure **3**, based on 2-aryl/heteroaryl-4-amino-5-(3', 4', 5'-trimethoxybenzoyl)thiazole molecular skeleton, prepared in a one-step procedure by Liebeskind-Srogl conditions starting from a easily accessible building block **5** bearing an unprotected amino group function. The antiproliferative activity of these compound was highly dependent on the structure modifications on the 2-position of the thiazole ring. The substituents examined included phenyl, 3-thienyl and substituted phenyl bearing EWGs or ERGs. The study revealed that phenyl (**3a**) and 3-thienyl (**3b**) thiazole derivatives exhibited improved growth inhibition activity as compared with the activity of the corresponding pyrrolidine analogue **2a**. Moreover, compounds **3a** and **3b** exhibited the best antiproliferative activity among the compounds synthesized in this study.

Overall, these compounds had greater potency than **1** against MCF-7 and HT-29 cells, comparable activity against HeLa and A549 cells, and less activity against HL-60 and Jurkat cells. Comparing **3a** with the bioisosteric 3-thienyl derivative **3b**, the latter was less active than **3a** only in MCF-7 cells. In general, the introduction of EWGs and ERGs reduced activity compared with the unsubstituted phenyl derivative **3a**, with no clear difference in effect on potency between EWGs and ERGs. At the *para*-position, only fluorine and methyl were tolerated, while the introduction of all other EWGs (Cl, NO_2, CF_3) and ERGs (Et, $C(CH_3)_3$; OCF_3, OEt) significantly reduced antiproliferative activity. For methoxy and chloro substituents, their position on the phenyl ring had a profound influence on potency. Moving the chloro group from the *para*- to the *meta*-position (compounds **3d** and **3e**, respectively), led to a dramatic increase in antiproliferative activity. The same effect was observed for the methoxy substituent (**3j** *vs.* **3k**). In contrast, the insertion of an additional methoxy group, to

100

yield the *m,p*-dimethoxy derivative **3l**, substantially reduced antiproliferative activity. These substituent effects are probably caused by increased steric hindrance, preventing efficient binding in the colchicine site, as observed in the molecular modeling studies. Thus, a selected, single, and small EWG or ERG could be placed on the phenyl ring with relatively minor effects on antiproliferative activity, but no modification improved activity relative to the unsubstuted phenyl or 3-thienyl derivatives **3a** and **3b**, respectively. Moreover, several compounds, such as **3c** and **3f**, characterized by the presence of substituents with opposite electronic effects showed approximately the same potency.

We identified tubulin as the molecular target of the compounds, since derivatives **3a** and **3b**, with the greatest inhibitory effects on cell growth, strongly inhibited tubulin assembly and the binding of colchicine to tubulin. Their potency for inhibition of tubulin polymerization was comparable with that of the reference compound **1**.

We also showed that **3b** had cellular effects typical for microtubule-interacting agents, causing accumulation of cells in the G2/M phase of the cell cycle. Further studies showed that **3b** was a potent inducer of apoptosis in HeLa cells. Apoptosis induced by antimitotic agents has been associated with alterations in a variety of cellular signaling pathways. As with many antimitotic drugs, compound **3b** induced Bcl-2 down-regulation after a 24hours treatment. Bcl-2 prevents the initiation of the cellular apoptotic program by stabilizing mitochondrial permeability. Our results confirmed that the induction of apoptosis by **3b** was associated with down-regulation of Bcl-2, dissipation of the mitochondrial transmembrane potential and activation of caspase-3, which is coupled with terminal events of apoptosis such as PARP cleavage. These effects were in good agreement with the cytotoxic potency of this compound and occur at lower concentrations than was observed with compound **2a**[115]. Compound **3b** was also active in suppressing the growth of drug resistant cells, and, even more importantly, it had significant *in vivo* activity in a

colon cancer xenograft model. Finally, preliminary experiments were performed to assess the potential antivascular activity of compound **3b**. The ability of this compound to inhibit endothelial cell migration and to destroy pre-established vessels using HUVEC is consistent also with antivascular agent utility and warrants further testing *in vivo* cancer models.

1.4. CONCLUSIONS

Solid tumors require vascular supply to grow and expand. The tumor microenvironment stimulates the development of new vessels, which are tortuous, highly disorganized and unstable. Thus they represent a promising target for anticancer therapy, because they result more sensitive to treatment, than normal vasculature.

Here we reported the antivascular activity of three compounds, **TR-644**, **TR-764** and **3b**, with molecular structure similar to **CA-4**. All of them have high binding affinity to tubulin, leading to inhibition of microtubule polymerization. The trimetoxyphenyl group is conserved in the three molecules, and it is responsible for the binding to tubulin.

Since microtubules are the specific target, our compounds can carry out their activity as both antiproliferative molecules against cancer cells and antivascular agents, targeting endothelial cells cytoskeleton.

Recently, cancer therapies are based on combinatorial treatments with antimitotic and antiangiogenic drugs, following precise dosing schedules. Usually antimitotic molecules are used at high doses, necessary to kill cancer cells, while antiangiogenic drugs act at low concentrations to inhibit endothelial cell functions[21].

Our molecules are able to arrest cancer cell proliferation *in vitro* and inhibit *in vivo* the growth of tumor mass, as well as they reduce tumor vasculature at very low concentrations (1-500nM)[66],[63],[79],[132]. These findings suggest that our novel tubulin binding agents could be utilized as single molecules for cancer therapy.

The most active compound is **TR-764**, probably because it is endowed with the highest affinity constant to tubulin, among the reported compounds. As concerning the antivascular effects, **3b**, **TR-644** and **TR-764** were described as inhibitors of cell

motility and angiogenesis *in vitro*. **3b** was mainly described for its ability to induce cell death in cancer cell lines, and secondly its antivascular activity was shortly debated. **3b** was significantly active at 250nM on HUVEC cells, while **TR-644** and **TR-764** at 1-10nM. **TR-644** and **TR-764** strongly impair cell cytoskeleton morphology, altering its role in cell motility and signal transduction. The effects observed *in vitro* explain **TR-764** and **TR-644** ability *in vivo* to significantly reduce the microvessel density of tumor microcirculation.

Unlike **TR-644**, we evaluated **TR-764** action under hypoxic conditions, in order to understand whether this molecule could counteract potential resistance mechanisms induced by tumor microenvironment or by the treatment with antivascular agents. We observed as **TR-764** counteract the hypoxic stimuli, by inhibiting HIF-1α activation.

For that reason, **TR-764** is the most active and promising agent which can improve the traditional chemotherapy against highly vascularized tumors.

2. NOSCAPINE DERIVATIVES AS

ANTIMITOTIC AGENTS

2.1. INTRODUCTION

2.1.1 Microtubule dynamics in cell cycle regulation and apoptosis

In eukaryotes, cell cycle and cell division are processes highly regulated by a series of guardian molecules and microtubule dynamics.

Microtubules are a cytoskeleton element, composed by α-tubulin and β-tubulin filaments associated together by non-covalent interactions at their two ends. They form polarized structures, with a minus and a plus end, terminating respectively with α-tubulin and β-tubulin heterodimers. The main property of microtubules is their "dynamic instability", that is the ability to grow and shrink very rapidly. In mitosis it is necessary for the rapid mitotic spindle assembling and disassembling. Secondly, they give rise to a three-dimensional structure, useful for chromosome capture and alignment at the metaphase plate[133].

Cell cycle is strictly controlled by surveillance mechanisms which arrest the progression in case of damage. During mitosis the spindle assembly and the chromosome segregation are supervised by checkpoint proteins of the spindle assembly checkpoint (SAC), which monitor the correct attachment of chromosomes to the kinetochore. This protein complex is thus considered the guardian of mitotic spindle formation and alignment of chromosome at metaphase[134]. In addition, each transition from a cell cycle phase to another is finely regulated by checkpoint proteins such as cyclins, kinases/phosphatases, DNA damage detectors[135].

A series of alterations, such as mutations and chromosome breaks, can spread if these checkpoints are dysfunctional. The delay in cell cycle progression, due to DNA damage, other stresses and dysregulation of spindle checkpoints trigger programmed cell death.

Many factors are involved in life or death related pathways, and cyclin-dependent kinase (Cdk1) and cyclin B have a crucial role both in mitosis establishment and in apoptosis regulation, by the control of several proteins, such as caspase-9 and surviving, indicating that these two processes are hard-wired. Thus cell fate is established by a balance between pro-survival mechanisms, such as cell-cycle arrest, and death signals which stimulate the activation of apoptotic pathways.
Insufficient regulation of this balance is responsible associated to the development of pathologies and particularly cancer[134],[136].
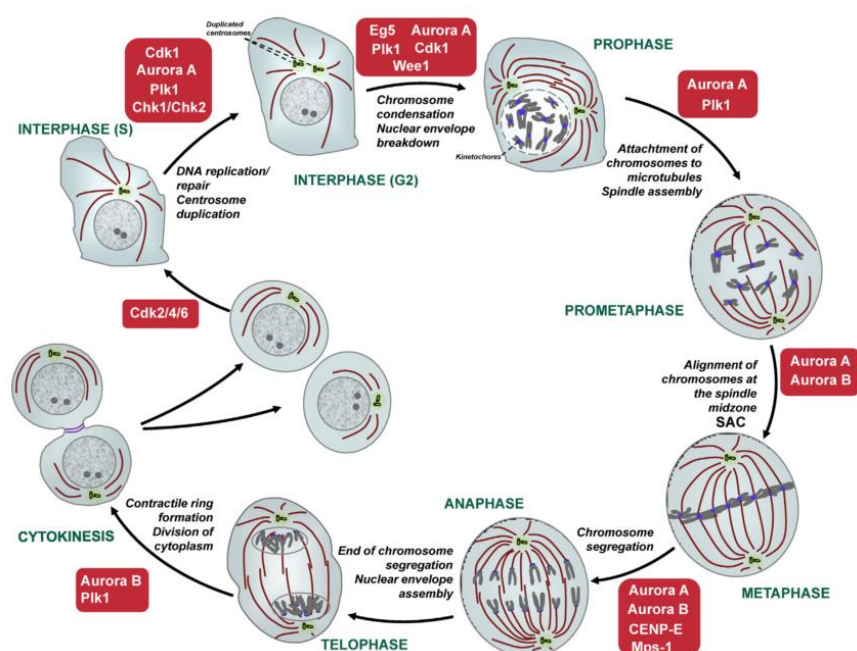
Figure 1. Mitotic proteins as antitumor targets (adapted from Ref.[137])

2.1.2 Tubulin Binding Agents (TBAs) in cancer therapy

Defects in the regulation of cell cycle checkpoints or in microtubule spindle functions lead to an increase proliferation rate, characteristic of tumor cells. In many years a series of antimitotic drugs has been developed to arrest cell cycle and induce apoptosis.

Many antimitotic drugs are molecules that bind to tubulin, and traditionally are classified in two groups: microtubule stabilizing (taxanes and epothilones) and destabilizing agents (Vinca alkaloids and colchicines). The former group stabilizes the pre-existing filaments, preventing the mitotic spindle formation, the latter inhibits the polymerization of microtubules[138].

These kinds of molecules are currently used for the treatment of several neoplastic diseases, such as acute leukemia, Hodgkin's and non-Hodgkin's lymphoma, breast cancer, lung cancer, neuroblastoma, rhabdomyosarcoma.

Nevertheless these drugs showed many side effects, due to their broad action against also non-proliferating cells. Peripheral neuropathy, severe myelosuppression and neutropenia were observed in patients during antimitotic therapy.

For that reason, recently more specific molecules were developed to inhibit mitotic checkpoint kinases, and microtubule-related proteins (Cdks, checkpoint kinases, Aurora A/B/C, polo-like kinase 1, and other mitotic kinesins)[137],[139].
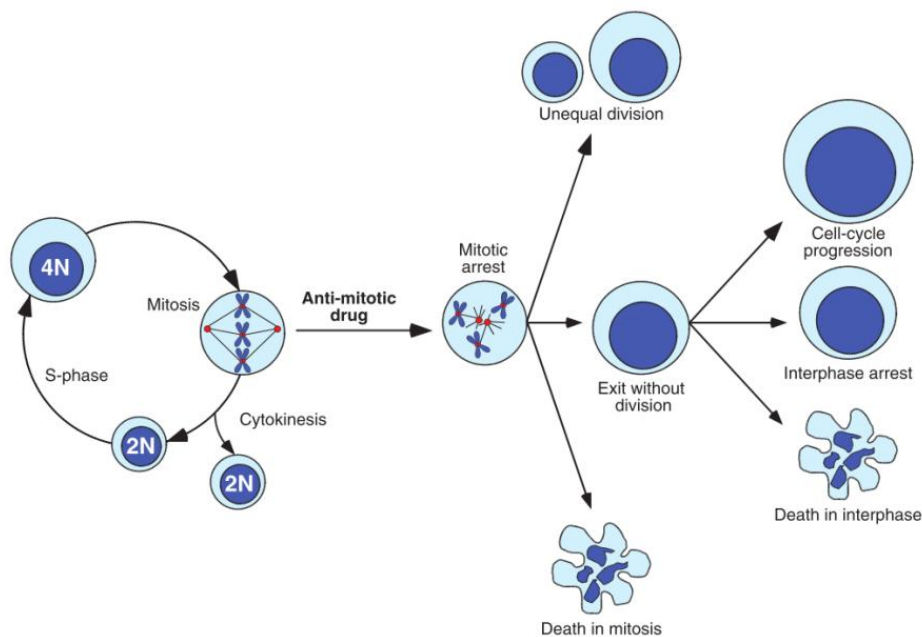
Figure 2. Cell fate in response to anti-mitotic drug treatment (adapted from Ref.[133])

2.1.3 Noscapines as anticancer agents

Among the tubulin binding agents, noscapines represent another class of molecules with anticancer activity.

Noscapine is a phthalideisoquinoline alkaloid extracted from opium, originally used as an antitussive drug. It is water-soluble, orally bioavailable, and endowed with low toxicity. It has been reported that noscapine binds stoichiometrically to tubulin, having a structure alike to that of colchicine and podophyllotoxin. It does not impair the total polymer mass, but it slightly affects the dynamics of cytoskeleton. It slows down the dynamism of microtubules, by increasing the time of the attenuated state to the detriment of the polymerization/depolymerization states. This effect causes alterations in mitotic spindle, by altering the interaction between chromosomes and kinetochore microtubules. Cell cycle is arrested in a metaphase-like state, and consequently cells are induced to a programmed cell death. Thus the growth of numerous cancer cell types is inhibited by the treatment with noscapine[140],[141].

By *in silico* molecular modeling, several derivatives have been developed and optimized in order to increase the binding affinity to tubulin, and to improve the antimitotic activity[142].

This class of molecules represents a potential strategy to overcome the high toxicity induced by tubulin binding drugs, which overall impair the structure of microtubules, unlike noscapines.

The mostly studied analog is **EM011** (9-bromonoscapine), a non-toxic brominated derivative which binds to tubulin with a double binding affinity (K_D = 54 ± 9.1μM) respect to the lead compound noscapine (K_D = 144 ± 1.0μM)[143]. **EM011** is more potent than noscapine, as concerning the inhibition of cell proliferation too. It has been showed that 9-bromonoscapine decrease the proliferation of a panel of cancer cell lines, and it is effective also in tumor models *in vivo*[144],[145].
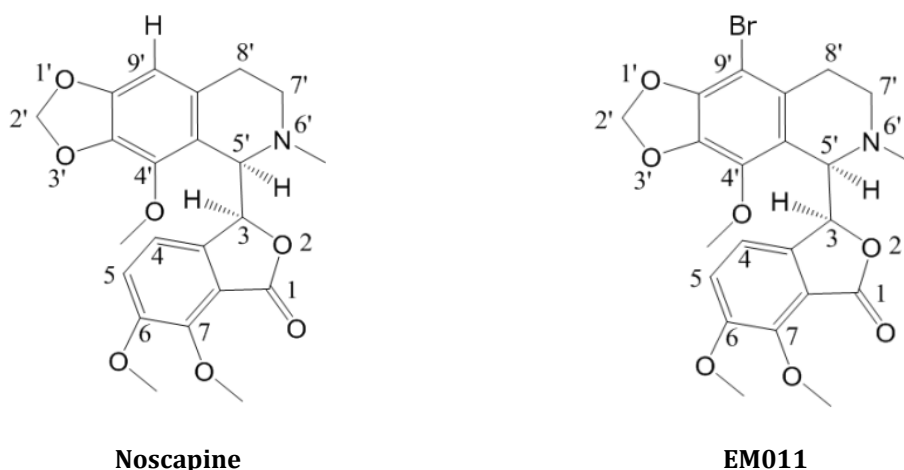
Figure 3. Structures of noscapine and **EM011** (adapted from Ref.[140,146,147])

2.1.4 Noscapines activity on cell cycle and apoptosis induction

It has been described that **EM011** or noscapines significantly alter cell cycle regulation, by suppressing microtubule instability and arresting cells in prometaphase[143]. During mitosis, the contacts between chromosomes and kinetochore microtubules are essential for a correct assembly of the mitotic spindle. It has been observed that noscapines cause mitotic arrest, DNA damage and subsequently activation of cell cycle and spindle checkpoints[148]. Abnormalities in spindle organization, multipolarity and centrosome amplification occur after treatment, and Aurora B activity results upregulated, indicating that the attachment of kinetochore to microtubules is disrupted. Multipolar spindle causes cytokinesis failure and consequently multinucleation and aneuploidy[149]. This phenomenon is called "mitotic slippage", and cells are arrested in a pseudo G1-like interphase state[150]. Noscapines induce a chronic mitotic delay and multiple cellular catastrophic events, culminating in apoptosis activation. Survivin, a pro-survival signal, is reduced, while PARP and cleaved caspase-3 are activated, leading to a mitochondrial-mediated cell death[146,144,151].
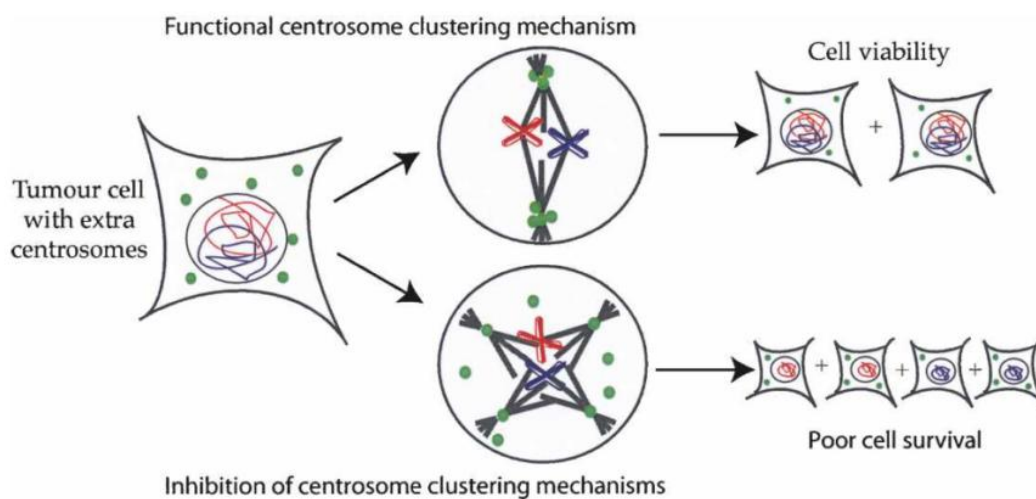
Figure 4. Centrosome amplification and cancer therapy (adapted from Ref.[152])

2.2. AIM OF THE STUDY

Noscapines represent a class of tubulin binding agents with anticancer activity and low toxicity. They cause mitotic spindle dysregulation, arrest in mitosis and consequently apoptosis.

Here we reported an efficient strategy for chemical synthesis based on Suzuki coupling method, and the biological evaluation of a series of novel 9'-alkyl and 9'-aryl derivatives from noscapine. We studied their antiproliferative activity on a panel of cancer cell lines, and the mechanism of action in cell cycle impairment and apoptosis induction.

2.2. AIM OF THE STUDY

2.3. RESULTS

2.3.1. NOVEL 9'-SUBSTITUTED-NOSCAPINES: SYNTHESIS WITH SUZUKI CROSS-COUPLING, STRUCTURE ELUCIDATION AND BIOLOGICAL EVALUATION

Elena Porcù*, Attila Sipos*, Giuseppe Basso, Ernest Hamel, Ruoli Bai, Verena Stempfer, Antal , Attila Cs. Bényei, Helmut Schmidhammer, Sándor Antus, Giampietro Viola

*Equal contributing Authors

submitted

2.3.1.1. Abstract

Tubulin is a major molecular target for anticancer drugs. The dynamic process of microtubule assembly and disassembly can be blocked by various agents that bind to distinct sites on tubulin, usually its β-subunit. Among the antimitotic agents that perturb microtubule dynamics, noscapinoids represent an emerging class of agents. In particular, 9'-bromonoscapine (**EM011**) has been identified as a potent noscapine analog. Here we present high yielding, efficient synthetic methods based on Suzuki coupling of 9'-alkyl and 9'-arylnoscapines and an evaluation of their antiproliferative properties. Our results showed that 9'-alkyl and 9'-aryl derivatives inhibit proliferation of human cancer cells. The most active compounds were the 9'-methyl and the 9'-phenyl derivatives, which showed similar cytotoxic potency in comparison to the 9'-brominated derivative. Interestingly these newly synthesized derivatives did not induce cell death in normal human lymphocytes, suggesting that the compounds may be selective against cancer cells. All of these derivatives, except 9'-(2-methoxyphenyl)-noscapine, efficiently induced a cell cycle arrest in the G2/M phase of the cell cycle in HeLa and Jurkat cells. Furthermore, we showed that the most active compounds in HeLa cells induced apoptosis following the mitochondrial pathway with the activation of both caspase-9 and caspase-3. In addition, these compounds significantly reduced the expression of the anti-apoptotic proteins Mcl-1 and Bcl-2.

2.3.1.2. Introduction

Antimitotic agents, primarily of natural origin, are a class of compounds that have been used for the treatment of a variety of malignancies for many years. Although they are sometimes considered "old chemotherapeutics" with respect to current anticancer approaches[67,153], at the present time they still represent valuable drugs that retain high scientific interest. Their impressive success in patients is due to their potent anti-proliferative effects and to their particular mechanism of action of altering microtubule dynamics, whether their detailed mechanism of action involves inhibition of tubulin assembly (vinca alkaloids, eribulin, estramustine, drug-antibody complexes with dolastatin 10 and maytansine analogues) or inhibition of microtubule disassembly (taxoids, epothilones). The importance of microtubules in mitosis and cell division, as well as the clinical success of microtubule targeting drugs, has made these dynamic organelles one of the most attractive targets for anticancer therapy[68]. In 1997, Ye *et al.*[140] discovered the anti-cancer effect of noscapine [**1**, (-)-α-noscapine, (*S*)-6,7-dimethoxy-3-((*R*)-4'-methoxy-6'-methyl-5',6',7',8'-tetrahydro[1,3]dioxolo-[4,5]isoquinolin-5'-yl) isobenzofuran-1(*3H*)-one], formerly known as narcotine (Figure 1), a phthalide isoquinoline alkaloid constituting 1–10% of the alkaloid content of opium. The antimitotic activity of noscapine was characterized, and it was demonstrated that the compound could inhibit tubulin assembly. These workers therefore embarked on an intensive search for more potent analogues of noscapine[140,146].
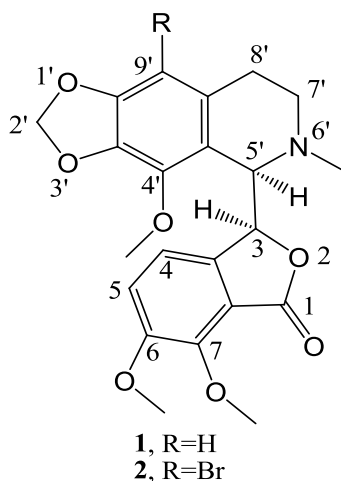
Figure 1. The structure of natural noscapine (**1**) and its 9'-bromo derivative (**2**).

Most importantly, 9'-bromonoscapine (**2**, **EM011**) was patented[154], characterized, and introduced into clinical trials against non-Hodgkin's lymphoma and chronic lymphocytic leukemia. A few other 9'-substituted noscapine derivatives were reported recently[144,148,155,156]. For instance 9'-nitronoscapine was found to be active against drug-resistant ovarian cancer and T-cell lymphoma cells[144], and its reduced congener, 9'-aminonoscapine, has good activity as a tubulin inhibitor[156].

Considering the increased cytotoxic activity of the 9'-bromo derivative of **1** as compared with the parent molecule, it is important to know whether the substitution of the phtalideisoquinoline backbone in position 9' contributes to a conformational change. Besides that, it is known from previous reports that phtalideisoquinoline derivatives are sensitive to acidic or basic media, and in numerous cases epimerization occurs[157,158]. Therefore, it was considered important to unambiguously determine whether or not there is an epimerization reaction during the relatively harsh bromination procedure. Thus, we obtained crystals of 9'-bromonoscapine (**2**) for X-ray crystallography and investigated the circular dichroism of compound **2** in solution. In addition, 9'-bromonoscapine (**2**) prepared

by a modified procedure, was identified as a starting agent for the synthesis of new analogues through the application of modern Pd-catalyzed cross-coupling reactions (Scheme 1)[159]. These new 9'-alkyl and 9'-arylnoscapines were evaluated for their antiproliferative and anti-tubulin properties, as well as their apoptotic mechanism of action.

	R
3	Me
4	Ph
5	4-Me-Ph
6	2-OMe-Ph
7	3-OMe-Ph
8	4-OMe-Ph
9	2-naphthyl
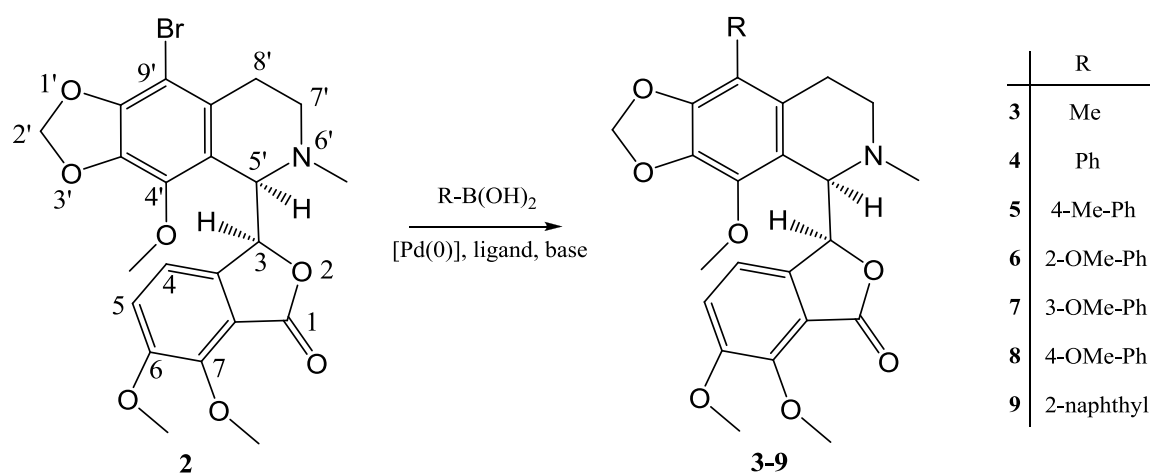
Scheme 1. Synthesis of targeted 9'-alkyl- and arylnoscapines **3-9**

Chemistry

The literature procedure for the preparation of 9'-bromonoscapine (**2**) was published in 2003 by Zhou *et al.*[148]. This procedure began with noscapine free base and used the 48% HBr-bromine water reactant mixture for the bromination of noscapine at position 9'. Afterwards, the alkalinization of the reaction mixture was performed with cc. NH_3 solution. The filtration of the crude product was followed by recrystallization from 96% ethanol. In our hands, this procedure gave rise to the desired 9'-bromonoscapine in a considerably lower yield (<10%), so we optimized the procedure in several steps. The application of extraction after filtration of the

aqueous phase of the crude product resulted in a significant amount of off-white product that was a mixture of 9'-bromonoscapine (**2**) and a large amount of unreacted noscapine (**1**). Recrystallization from 96% ethanol yielded only a very small amount of **2**. The separation of noscapine **1** and its bromo derivative **2** was also attempted several times by column chromatography, but the highly similar retention times of the two compounds prevented their separation, even after trying many different mobile phases. 9-Bromonoscapine was prepared. The Zhou *et al.*[148]. procedure was modified and began with noscapine hydrochloride hydrate. This approach was found to be superior as solvation required less HBr, and this led to an increase in product purity and yield. The yield was further improved by processing the mother liquor and using less base for the neutralization step. The concentration of the mother liquor resulted in a significant amount of a light yellow residue that was found to be 9'-bromonoscapine (**2**) containing a small amount of noscapine impurity. These modifications combined afforded a total yield of 50% on average. The pure 9'-bromonoscapine (**2**) we obtained, confirmed by ^{1}H-NMR, showed a higher melting point than the reported value (174-175℃ instead of 169-170℃). The 9'-bromonoscapine (**2**) obtained was used as a starting agent for its transformation by the application of modern Pd-catalyzed cross-coupling reactions (Suzuki reaction) into new 9'-noscapine derivatives. The application of Suzuki cross-coupling reaction in the synthesis and derivatization of alkaloids is an excellent choice for the formation of new C-C bonds. For example, substitutions in morphinans and aporphinoids were successfully realized at different positions of the two alkaloid backbones[160–162]. The first tested protocol with **2** was adapted from these earlier procedures using K_2CO_3 as a base and $Pd[P(Ph)_3]_4$ as the Pd-source combined with ligands. As summarized in Table 1, this combination of reagents and reaction conditions (heating at 90℃ for 2hours) led to 4-12% percent yields after isolation by means of column chromatography. After testing other generally used

reagents and conditions, we found no significant improvement with these common coupling methodologies. After examining the single crystal structure of compound **2** *(vide infra)*, especially the steric hindrance in the proximity of the bromine substituent, we turned to methods developed for the cross-coupling of hindered aromatic bromides[163]. The application of $Pd(OAc)_2$ as the Pd-source, K_3PO_4 as the base and XPhos, a specific biphenyl phosphine, made possible the isolation of the desired products **3-8** in significantly higher yields (Table 1).

Structural analysis of 9'-bromonoscapine (2) and Suzuki products 3-8

The structure of compound **2** in solution was investigated with the use of circular dichroism (CD). In Figure 2 (Panel A) the CD spectra of parent compound **1** and its brominated congener **2** are presented. The spectrum of (-)-α-isomer **1** shows Cotton effects around 320 and 225nm. These data are in accordance with the most relevant and detailed evaluation of the circular dichroism characteristics of phthalide isoquinoline alkaloids by Snatzke *et al.*[164]. As concluded in this fundamental work, the configuration of the C5' asymmetric centre could be associated with Cotton effects at around 290 (^1L_B transition) and 205nm (^1B aromatic transition), while the data related to the configuration of the C3 carbon appear in the regions of 320 and 225nm (aromatic transitions). Comparing the CD specta obtained for compounds **1** and **2,** it can be unambigously stated that the characteristics, the types and the positions of Cotton-effects confirm the high conformational similarity between the two molecules. On the basis of the X-ray crystal structure, the torsion angle between the H3-C3-C5'-H5' atoms can be measured (Figure 3, panel A). These data are considered an efficient indicator for showing the relative positions of the tetrahydroisoquinoline and isobenzofuranone ring systems of the phthalide isoquinoline derivatives. The angle for natural noscapine base (**1**) was reported to be -66°[165]. Interestingly, the protonation of the

tertiary amino function (formation of noscapine hydrochloride) is followed by a remarkable conformational change characterized by the important torsional angle of +78° for the H3-C3-C5'-H5' atomic connections[166]. As presented in Figure 3 (panel B), the protonation evokes a significant twisting of the isobenzofuranone moiety relative to the tetrahydroisoquinoline group. The modified synthesis of 9'-bromonoscapine (**2**) allowed us to obtain crystals of the compounds appropriate for single crystal X-ray structural analysis (CCDC deposition # 955643) (Figure 3, panel C). It was determined that the indicative torsion angle between H3-C3-C5'-H5' for the 9'-bromonoscapine was -80.1°. A recent study on the three dimensional chemical space of a pharmacophore model for noscapinoids[167] allows us to determin that the relative positions of hydrogen bond acceptor O1' and C7-OCH$_3$ oxygen atoms and the hydrophobic C4'-OCH$_3$ and C6-OCH$_3$ methyl centres are within 1.2 Å of maximal distance. This was done after performing the overlay of the X-ray structures of the free bases of noscapine (**1**) and 9'-bromonoscapine (**2**) by overlaying the structures of both the tetrahydroisoquinoline and isobenzofuranone ring systems. In order to prove that the Suzuki cross-coupling conditions did not lead to epimerization of the original phthalide isoquinoline structure (i.e., that the conformations of the synthesized compounds were similar to the pharmacologically promising precursor **2**), the circular dichroism spectra of compounds **3**-**8** were recorded. The α-isomers of phthalide isoquinoline alkaloids show Cotton effects typically around 320 and 225nm. It can be concluded from the set of CD spectra presented in Figure 2 (panel B), that in these regions the spectra show similar characteristics, which is a proof of the retention of configuration at the two chiral centers.

Table 1. Optimization of the Suzuki coupling of compound **2**

Compounds	Pd-source	Ligand	Base	Solvents	Yields (%)
3	$Pd[P(Ph)_3]_4$	-	K_2CO_3	THF/MeOH	4
3	$Pd(OAc)_2$	XPhos[a]	K_3PO_4	THF/MeOH	44
4	$Pd[P(Ph)_3]_4$	-	K_2CO_3	THF/MeOH	12
4	$Pd(OAc)_2$	Xphos[a]	K_3PO_4	THF/MeOH	53
5	$Pd[P(Ph)_3]_4$	-	K_2CO_3	THF/MeOH	8
5	$Pd(OAc)_2$	Xphos[a]	K_3PO_4	THF/MeOH	61
6	$Pd[P(Ph)_3]_4$	-	K_2CO_3	THF/MeOH	4
6	$Pd(OAc)_2$	XPhos[a]	K_3PO_4	THF/MeOH	41
7	$Pd[P(Ph)_3]_4$	-	K_2CO_3	THF/MeOH	9
7	$Pd(OAc)_2$	Xphos[a]	K_3PO_4	THF/MeOH	55
8	$Pd[P(Ph)_3]_4$	-	K_2CO_3	THF/MeOH	4
8	$Pd(OAc)_2$	XPhos[a]	K_3PO_4	THF/MeOH	42
9	$Pd[P(Ph)_3]_4$	-	K_2CO_3	THF/MeOH	7
9	$Pd(OAc)_2$	Xphos[a]	K_3PO_4	THF/MeOH	57

[a] XPhos: (2-biphenylyl)-dicyclohexyl-phosphine

A

121
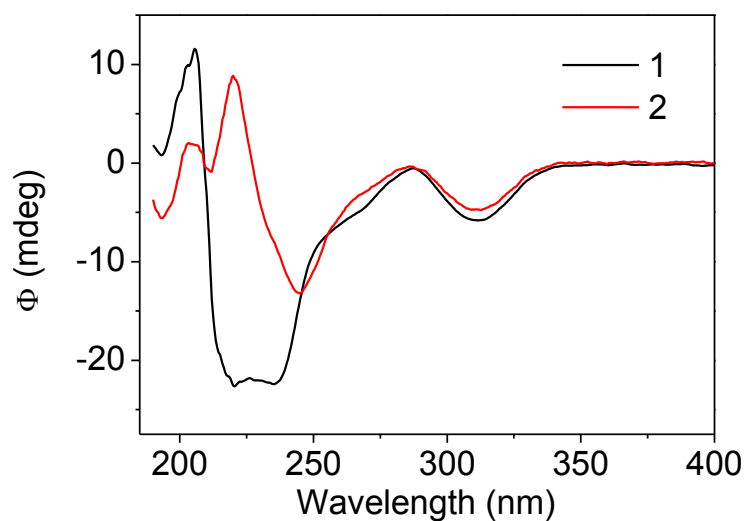
B
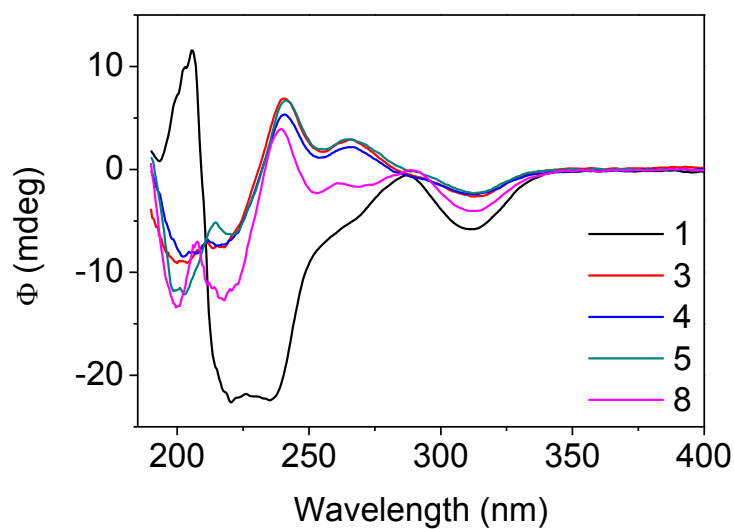
Figure 2. Panel A. CD spectra for natural noscapine **1** and its 9'-bromo derivative **2** in acetonitrile. Panel B. CD spectra for natural (-)-α-noscapine **1** and for representative novel 9'-alkyl and 9'-arylnoscapines in acetonitrile.
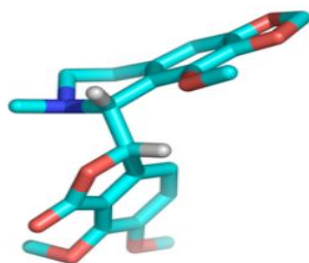
A   **B**
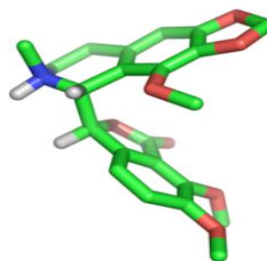
C
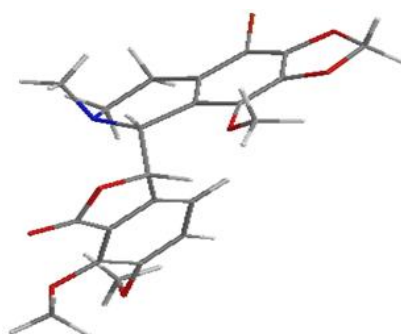
Figure 3. The X-ray crystal structures of natural noscapine free base (**1**, Panel A), its HCl salt (Panel B) and 9'-bromonoscapine (**2**, Panel C).

2.3.1.3. Results

Evaluation of antiproliferative activity

The newly synthesized noscapine derivatives, in comparison with reference compound **2**, were tested for their antiproliferative activity in a panel of human cancer cell lines. As shown in Table 2, 9'-aryl derivatives **4** and **5** and the 9'-alkyl derivative **3** were generally equipotent with 9'-bromonoscapine (**2**). Generally less active than **2**, the three methoxyphenyl derivatives **6-8**, as well as the 9'-alkyl derivative **9**, showed similar potencies to each other. To obtain more insight into the potential cytotoxic activity of these new compounds for normal human cells, they were assayed *in vitro* against peripheral blood lymphocytes (PBL) from healthy donors (Table 3). All the compounds were ineffective in resting lymphocytes, having IC_{50} values over 200μM, in well agreement with previous reports[146,148]. Only some compounds (**2**, **4** and **6**) proved cytotoxic in PHA-stimulated PBL, but only at higher concentrations (generally, 5-30 fold higher) than against the lymphoblastic cell lines Jurkat and CCRF-CEM. Together, these data suggest these compounds may have cancer cell selective killing properties.

Table 2. *In vitro* cell growth inhibitory effects of compounds **2-9**

				IC$_{50}$ [a] (μM)					
Compounds	HeLa	Jurkat	SEM	RS4;11	CEM	LoVo	HT29	A549	IGROV-1
2	2.6±0.4	3.0±0.6	1.8±0.3	1.4±0.6	2.8±0.19	42.8±16.7	18.7±7.0	73.9±7.6	78.2±6.9
3	5.2±0.8	5.9±0.8	4.3±0.7	15.8±2.0	8.8±3.1	66.3±10.1	34.0±10.4	>100	62.4±3.5
4	7.4±1.6	5.4±2.1	3.2±0.4	2.4±0.7	5.2±0.8	42.8±2.8	36.5±7.1	55.3±3.2	68.1±6.1
5	12.8±3.8	5.1±0.9	7.4±1.1	16.4±3.5	11.8±2.2	41.8±3.6	24.9±7.3	22.2±7.9	66.3±7.3
6	30.8±1.9	33.6±5.1	22.2±3.2	13.8±5.4	6.9±1.5	57.1±4.4	72.7±12.0	59.7±5.3	90.9±11.7
7	8.9±0.3	13.2±4.2	13.0±4.0	7.1±2.9	22.3±4.7	29.4±2.7	36.1±5.8	>100	57.2±9.3
8	15.6±5.3	11.3±4.7	15.1±3.9	12.6±1.9	25.8±1.7	28.8±1.5	47.8±4.2	>100	55.6±2.8
9	27.4±3.5	20.0±4.7	8.4±2.1	30.8±0.9	23.3±3.4	60.3±4.5	58.5±10.3	48.1±6.2	67.0±8.4

[a]IC$_{50}$= compound concentration required to inhibit tumor cell proliferation by 50%. Data are presented as the mean ± SEM from the dose-response curves of at least three independent experiments.

Table 3. Cytotoxicity of noscapine derivatives for human peripheral blood lymphocytes (PBL)

Compound	IC$_{50}$ (µM) [a]	
	PBL$_{resting}$[b]	PBL$_{PHA}$[c]
2	>200	92.2±13.8
3	>200	>200
4	>200	54.9±7.6
5	>200	>200
6	>200	42.4±5.0
7	>200	>200
8	>200	>200
9	>200	>200

[a] Compound concentration required to reduce cell growth by 50%. [b] PBL not stimulated with PHA [c] PBL stimulated with PHA. Values are the mean ± SEM for three separate experiments.

Inhibition of tubulin polymerization and colchicine binding

The series of new noscapine analogues was first evaluated for potential inhibition of tubulin assembly in comparison with the potent colchicine site agent combretastatin A-4 (**CA-4**), using a GTP- and glutamate-dependent polymerization assay that measured extent of assembly after 20min at 30°C (Table 1)[119]. It was quickly apparent that, while some activity was observed with several of the noscapine analogues, they were far less potent than **CA-4**, which yielded an IC$_{50}$ value of 1.2µM. In fact, when concentrations up to 400µM were evaluated, an IC$_{50}$ value was obtained only with compound **5**. At the 400µM concentration, two of the compounds, **4** and **6**, appeared to precipitate in the reaction mixture. The inhibition

observed with **5** (IC$_{50}$, 120μM) was 100-fold weaker than the inhibition observed with **CA-4**. However, besides IC$_{50}$ values based on inhibition of the extent of assembly, it is also possible to change the parameter measured from the extent to the rate of assembly[119,168,169]. In our experience, this has the effect of reducing the IC$_{50}$ value for compounds 2-4-fold, thus permitting measurements of IC$_{50}$'s for weakly active compounds and, potentially, for compounds that induce aberrant polymer formation at higher concentrations, which is generally associated with turbidity development that can only be distinguished from "normal" assembly by electron microscopy[170,171]. Our concentration studies with the noscapine analogues did not provide any evidence for an aberrant assembly reaction, since we only observed progressive inhibition, albeit very weak. In addition, it should be noted that the typical microtubule assembly curve, as measured by turbidimetry, has a sigmoidal shape. We therefore measured the maximum rate of assembly at the inflection points of the turbidity curves. This resulted in our obtaining 3-fold reductions in the IC$_{50}$ values for **CA-4** (0.44μM) and **5** (45μM), but, in addition, we obtained maximum rate IC$_{50}$ values for two compounds (**3** and **7**) (Table 4). Only, **2**, **4**, and **6** failed to yield rate IC$_{50}$ values.

Because noscapine has structural similarity to colchicine, it was evaluated without success as a potential inhibitor of [^{3}H]colchicine binding to tubulin[140]. With most active colchicine site inhibitors, we have been able to demonstrate significant inhibition of the binding of [^{3}H]colchicine to tubulin, with tubulin at 1μM and colchicine and the inhibitor at 5μM. This is shown in Table 4 for **CA-4**, although few compounds are as potent as **CA-4** in inhibiting this reaction. With the noscapine analogues, in agreement with the findings with noscapine[140], in a preliminary experiment we found no significant activity when they were added to the reaction mixture at 5μM (data not shown). However, we decided to evaluate the compounds for potential inhibition at 500μM (Table 4). Although an additional two compounds

(**2** and **3**) appeared to precipitate in the reaction mixture, we did observe inhibition reasonably concordant with the effects on tubulin assembly. Thus, the best inhibition was observed with **5**, and the worst with the three compounds that had assembly rate IC_{50} values over 400μM (**2**, **4**, and **6**). We should note here that this assembly assay uses reaction conditions that strongly stabilize the colchicine binding activity of tubulin[160]. Nevertheless, we generally measure inhibition of colchicine binding at short reaction times, such as 10min, when the reaction is 40-60% complete, because we have found that inhibition by weakly active compounds is maximal at shorter incubation times[172]. This is probably because most colchicine site agents dissociate from tubulin much more rapidly than colchicine itself[172,173]. Consequently, once bound, [³H]colchicine in effect locks other agents out of the binding site. Under the reaction conditions used here, the half-life of the colchicine-tubulin complex is about 24hours[173]. The difference in reaction conditions and incubation time probably explains the limited effects reported for noscapine on the binding of [³H]colchicine to tubulin[140]. We should note, however, that a recent report[174] described inhibition of colchicine binding, measured by inhibition of the fluorescence that occurs when colchicine binds to tubulin[175], by 9'-bromonoscapine (**2**), although noscapine (**1**) itself had no activity at the highest concentration examined (100μM).

Table 4. Inhibition of tubulin polymerization and colchicine binding by compounds **1-7** and **CA-4**

Compound	Tubulin assembly[a] $IC_{50}\pm S.D$ (μM)		Colchicine binding[b] % $\pm S.D.$	
	Extent	Rate	5μM drug	500μM drug
1	>400	170±4	n.d.	44±4
2	>400	>400	n.d.	34 ± 4 T
3	>400	220±50	n.d.	39 ± 2 T
4	>400	>400	n.d.	14 ± 1 T
5	120±3	45±8	n.d.	64 ± 4
6	>400	>400	n.d.	13 ± 5 T
7	>400	170±20	n.d.	38±4
CA-4	1.2±0.09	0.44±0.03	99±0.4	n.d.

[a] Inhibition of tubulin polymerization. Tubulin was at 10μM. [b] Inhibition of [^{3}H]colchicine binding. Tubulin and colchicine were at 1 and 5μM, respectively, and the tested compound was at the indicated concentration. n.d. not determined; T = reaction mixture turbid before incubation, implying compound precipitation

Effects of 9'-noscapine derivatives on the cellular microtubule network

We investigated the effects of the new derivatives on the cytoskeletal microtubule and microfilament networks by immunofluorescence in HeLa cells. As shown in Figure 4, the microtubule network exhibited normal arrangement and organization in HeLa cells in the absence of drug treatment. In contrast, 24hours of exposure to compounds **2**, **3** or **7** at 25μM caused extensive microtubule rearrangement, with induction of spherical morphology in 70-80% of the cells. In addition, the treatment

also induced mitotic arrest, characterized at the concentrations and time studied, by an increase in the number of cells with typical bipolar spindles with chromosomes arranged along the metaphase plate. We also observed abnormal microtubule spindles with astral or multipolar configurations as well as a disorganized or spherical arrangement of chromosomes.
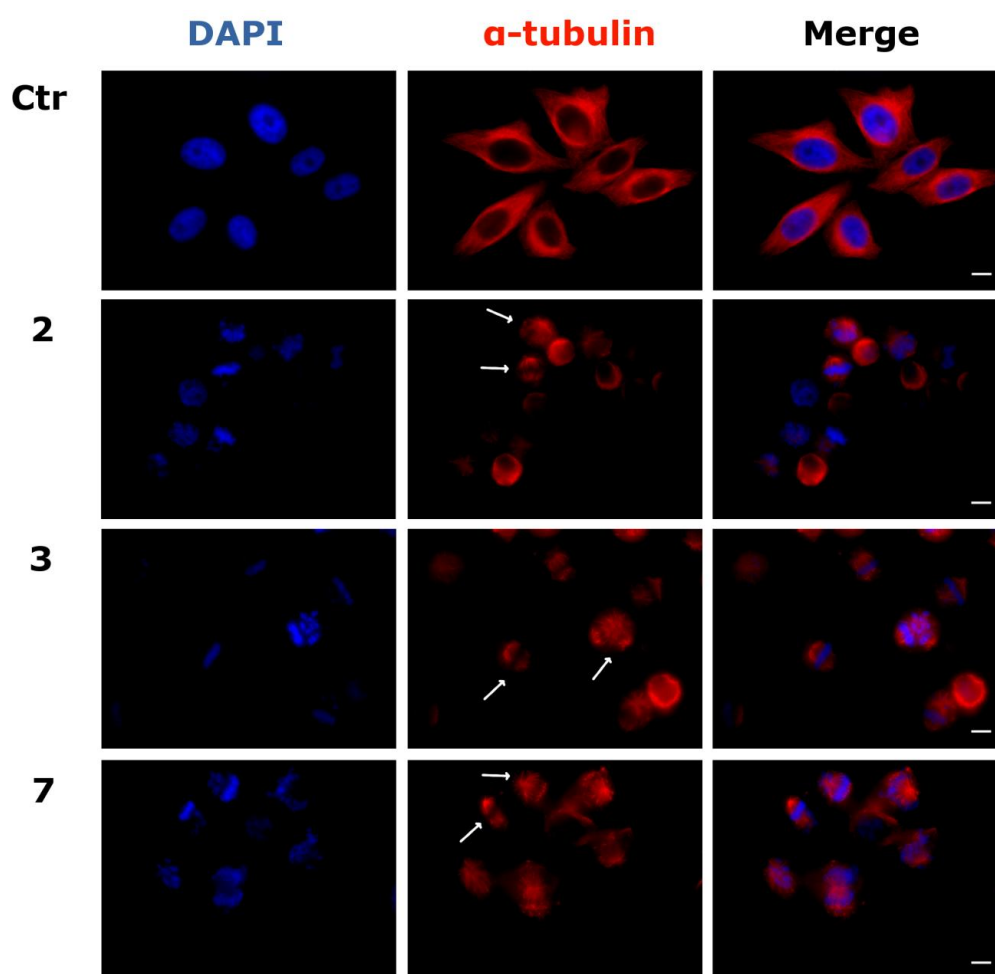
Figure 4. Effects of compounds 2, 3 and 7 on microtubule networks in HeLa cells. Cells were incubated with 25μM compound for 24hours and then stained with anti-β-tubulin primary antibody and secondary Alexa-conjugated antibody and then observed by confocal microscopy (magnification 20x, bar = 10μm). Cells were also counterstained with DAPI to visualize the nuclei. Arrows indicate cells with disorganized spherical arrangements of chromosomes or multipolar microtubules.

In good agreement with microtubule rearrangement, we also observed PCM1 alteration, after treatment of cells with the new compounds (effects of compounds **2**, **3** and **5** shown in Figure 5). PCM1 is a pericentriolar protein involved in recruiting proteins necessary for centrosome replication, and it dynamically fluctuates during the cell cycle. Late in G2, the protein dissociates from the centrosome remaining dispersed throughout the cell during mitosis. The mechanism is cell cycle dependent, with PCM1 aggregates disassembling during mitosis and reassembling in interphase[176,177].

As shown in Figure 5, PCM1 staining revealed an accumulation of the pericentriolar material in some treated cells, similar to the effects observed after treatment with nocodazole and other antimitotics[178]. Moreover, cells arrested in mitosis showed the characteristic rounded shape, and PCM1 was scattered and dispersed throughout the cell. The derivatives induced a depletion of PCM1 function, affecting its localization and the organization of cell cycle machinery, resulting in microtubules anchoring to the centrosome. The derivatives also induced a change in cell morphology detectable by staining with phalloidin (Figure 5). Actin filaments were intact but disorganized as compared with the control cells, contributing to impairment of cell organization.
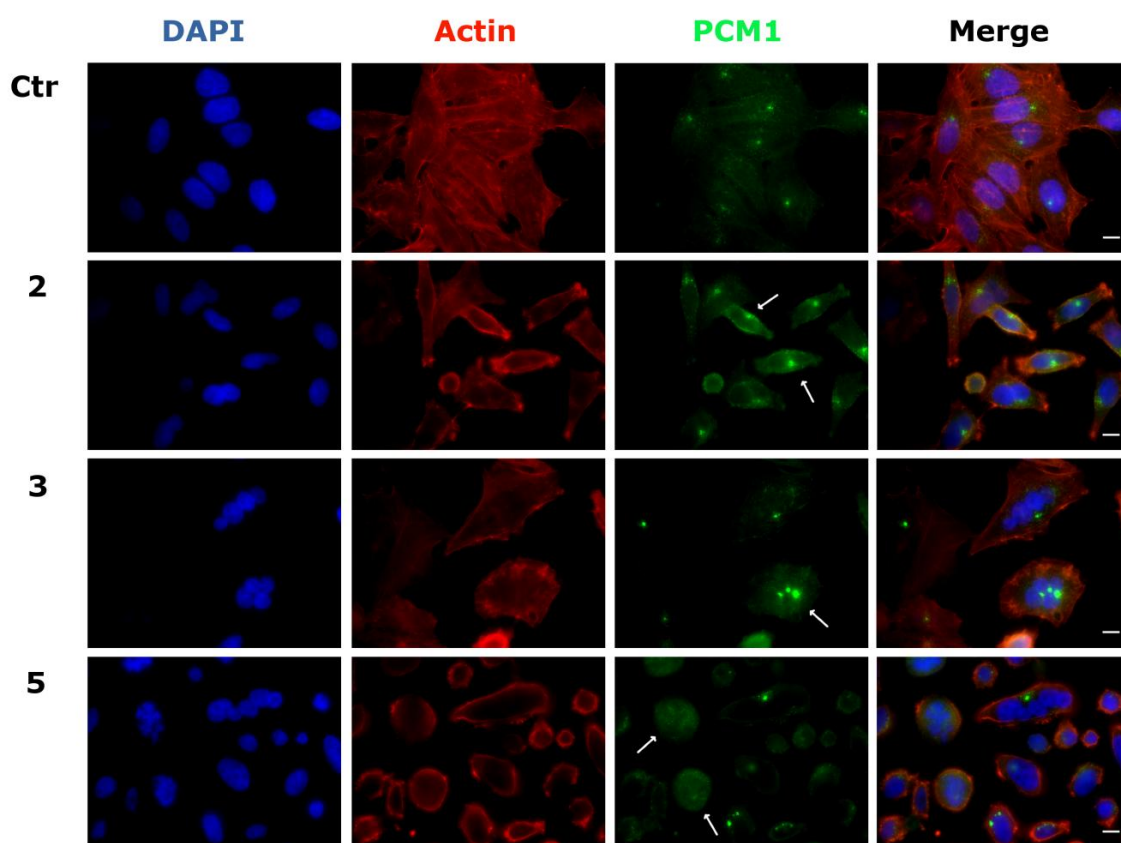
Figure 5. Effects of indicated compounds on PCM1 in HeLa cells. Cells were incubated for 24hours with the indicated compounds (25μM) and stained with anti-PCM1-primary antibody and secondary Alexa-conjugated antibody, phalloidin-tetramethylrhodamine B to visualize actin microfilaments and DAPI. Images were captured by confocal microscopy (magnification 60x, bar = 10μm). Arrows indicate points of PCM1 accumulation or diffused in mitotic cells.

9'-noscapine derivatives induce G2/M arrest of the cell cycle

The effects of a 24hours treatment with different concentrations of compounds **2-7** on cell cycle progression in HeLa (Figure 6) and Jurkat cells (Figure 7), were determined by flow cytometry. All compounds, except **6**, caused a significant G2/M arrest in a concentration-dependent manner in both cell lines, with the new compounds having effects essentially identical to those observed with the reference compound **2**. In HeLa cells (Figure 6), the rise in G2/M cells occurred maximally at a concentration between 10-25μM, while at higher concentrations more than 80% of

the cells were arrested in G2/M. A similar behavior was observed with the Jurkat cells (Figure 7), but, except with compound **2**, maximal effects required higher compound concentrations. As would be expected, the cell cycle arrest in G2/M phase was accompanied by a commensurate reduction in cells in the other phases of the cell cycle. We also examined several of the compounds, in comparison with **CA-4**, in human Burkitt lymphoma CA46 cells since this cell line generally yield a very high mitotic index when treated with antitubulin agents. Compounds **3** and **7** yielded IC$_{50}$ values of 18 ± 8μM and 20 ± 4μM, respectively (the contemporaneously obtained value for **CA-4** was 20 ± 7nM. At five times the IC$_{50}$ concentrations, there was over 80% G2/M cells with all three compounds. Morphological examination of parallel cultures stained with Giemsa yielded mitotic indices of 46% with **CA-4**, 38% with compound **3**, and 28% with compound **7** indicating that they acted like antitubulin agents.
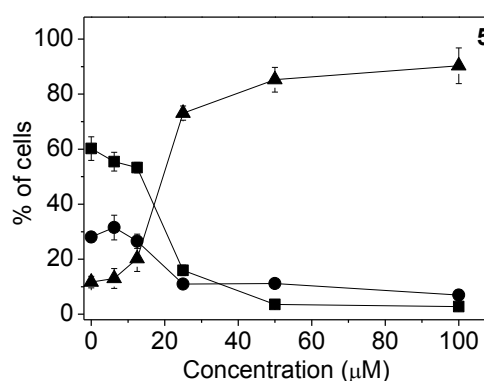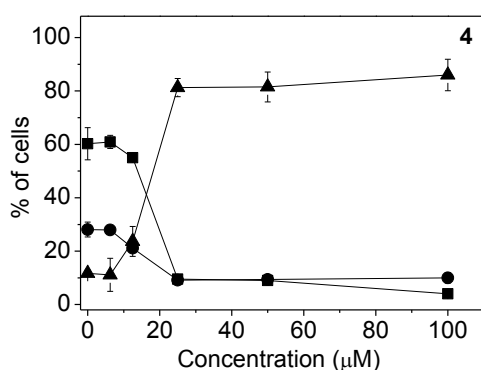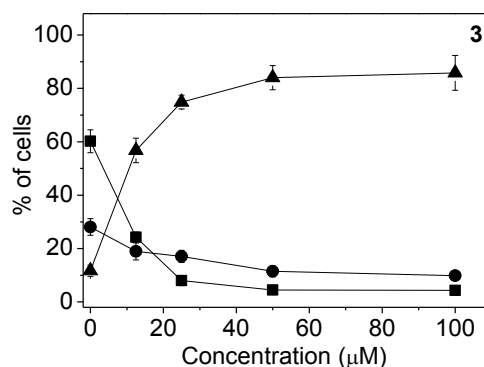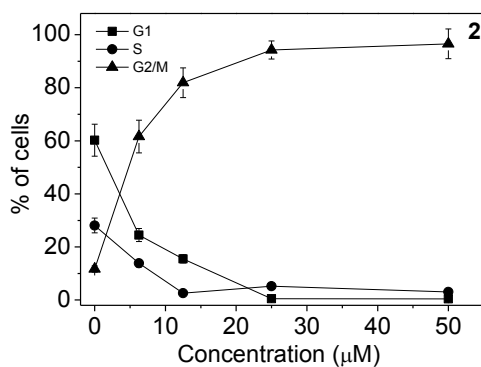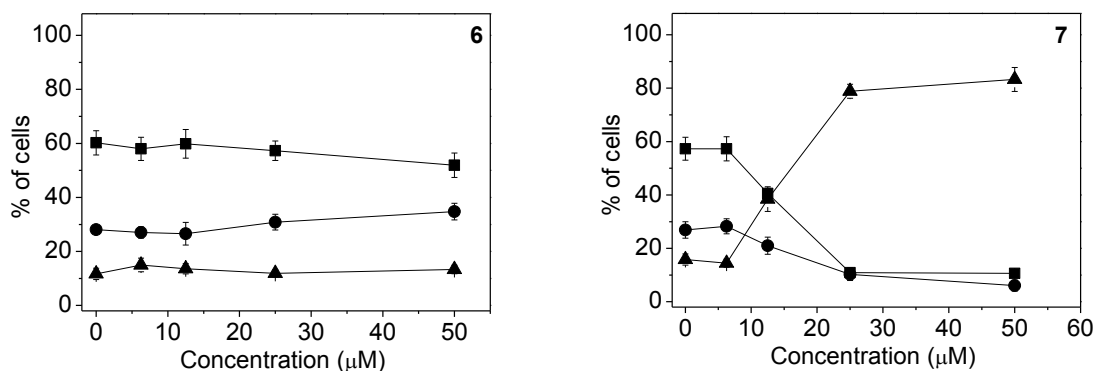
Figure 6. Percentage of cells in each phase of the cell cycle in HeLa cells, treated with the indicated compound at different concentrations for 24hours. Cells were fixed and labeled with PI and analyzed by flow cytometry as described in the experimental section. Data are presented as mean ± SEM of three independent experiments.
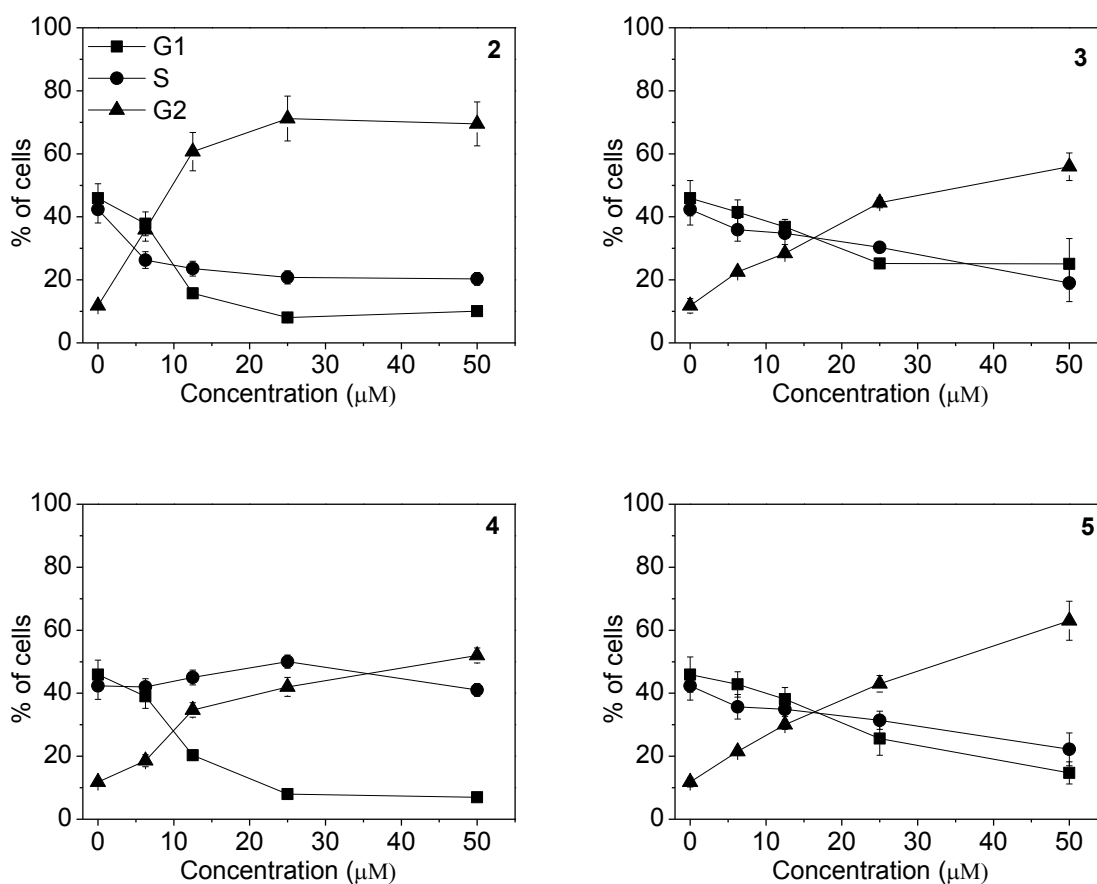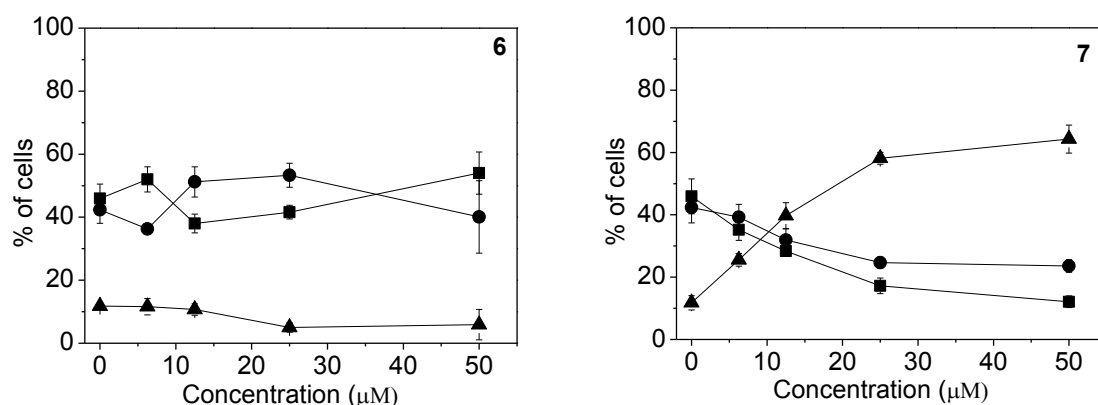
Figure 7. Percentage of cells in each phase of the cell cycle in Jurkat cells, treated with the indicated compound at different concentrations for 24hours. Cells were fixed and labeled with PI and analyzed by flow cytometry as described in the experimental section. Data are presented as mean ± SEM of three independent experiments.

We next studied the effects of compounds **2-5**, on alterations in the expression of proteins that regulate cell division. The cdc2/cyclin B complex controls both entry into and exit from mitosis. Phosphorylation of cdc2 on Tyr15 and phosphorylation of cdc25c phosphatase on Ser216 negatively regulate the activation of the cdc2/cyclin B complex[134,179,180]. Thus, dephosphorylation of these proteins is needed to activate the cdc2/cyclin B complex. Cdc25c is a major phosphatase that dephosphorylates the site on cdc2 and autodephosphorylates itself. Phosphorylation of cdc25C directly stimulates both its phosphatase and autophosphatase activities, a condition necessary to activate cdc2/cyclin B on entry of cells into mitosis[134,179,180]. As shown in Figure 8 in HeLa cells, treatment with **3**, **4** or **5** at 25μM for 24 or 48hours caused an increased expression of cyclin B at 24hours, in particular for compounds **5**, followed by its disappearance at 48hours. Similarly, slower migrating forms of phosphatase cdc25C appeared at 24hours following treatment with **4** or **5**, indicating changes in the phosphorylation state of this protein, while at 48hours with these compounds, as well as compound **2**, the expression of cdc25c strongly

decreased. We also observed a dramatic reduction in the expression of the phosphorylated form of cdc2 (Tyr15) with all tested compounds. We also examined the effect of the new derivatives on the expression of aurora kinase A and its phosphorylated form at Thr288 since the phosphorylation of aurora kinase A is a hallmark of the G2/M phase[181]. As shown in Figure 8, aurora kinase levels increased after a 24hours treatment with compounds **3**, **4** and **5**, but not **2.** Altogether these data suggest, as did the immunofluorescence studies, that the observed G2/M arrest was not due to a defect in G2 to M phase progression but instead was caused by aberrant execution of mitosis.

Prolonged mitotic arrest can lead to DNA damage[182,183]. We identified DNA damage through the detection of the phosphorylated histone γ-H2A.X. Compounds **3**, **4** and **5** induced a marked increase in the expression of γ-H2A.X after a 24hours treatment, while a similar increase was observed after 48hours with compound **2**, suggesting that these compounds induce major DNA damage during mitotic arrest that could contribute to their antiproliferative activity. Since DNA damage is often linked to p53 induction, we evaluated the expression of p53. The immunoblot analysis showed an increased level of p53 expression that occurred at 48hours, as the increased expression of γ-H2A.X was declining.
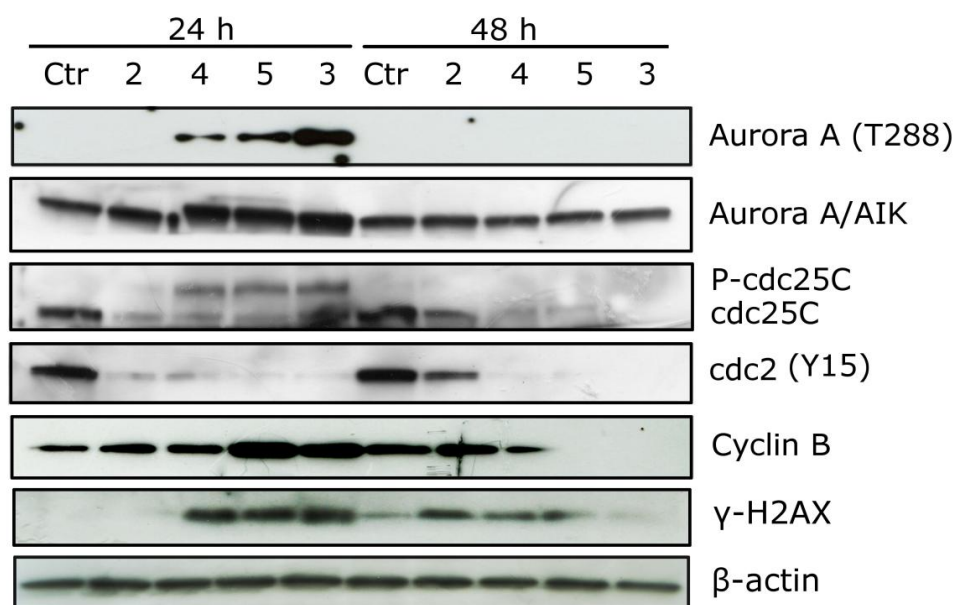
Figure 8. Effects of **2-5** on G2/M regulatory proteins and p53. HeLa cells were treated for 24 or 48hours with the indicated compound at 25µM. The cells were harvested and lysed for the detection of cyclin B, p-cdc2^{Tyr15}, cdc25C, γH2A.X and p53 expression by western blot analysis. To confirm equal protein loading, each membrane was stripped and reprobed with anti-β-actin antibody.

9'-noscapine derivatives induce apoptosis.

To characterize the mode of cell death induced by these compounds, a biparametric cytofluorimetric analysis was performed using PI, which stains DNA and enters only dead cells, and fluorescent immunolabeling of the protein annexin-V, which binds to PS in a highly selective manner[184]. Compounds **2-5** were incubated with HeLa cells for 24 or 48hours and then stained with the two dyes. Dual staining with annexin-V and with PI permits discrimination between live cells (annexin-V$^-$/PI$^-$), early apoptotic cells (annexin-V$^+$/PI$^-$), late apoptotic cells (annexin-V$^+$/PI$^+$) and necrotic cells (annexin-V$^-$/PI$^+$). As depicted in Figure 9 (Panels A-E), the treated HeLa cells showed an accumulation of annexin-V positive cells in comparison with the control, in a concentration and time-dependent manner. In good agreement with MTT data, the reference compound **2** was slightly more active than the other three compounds.
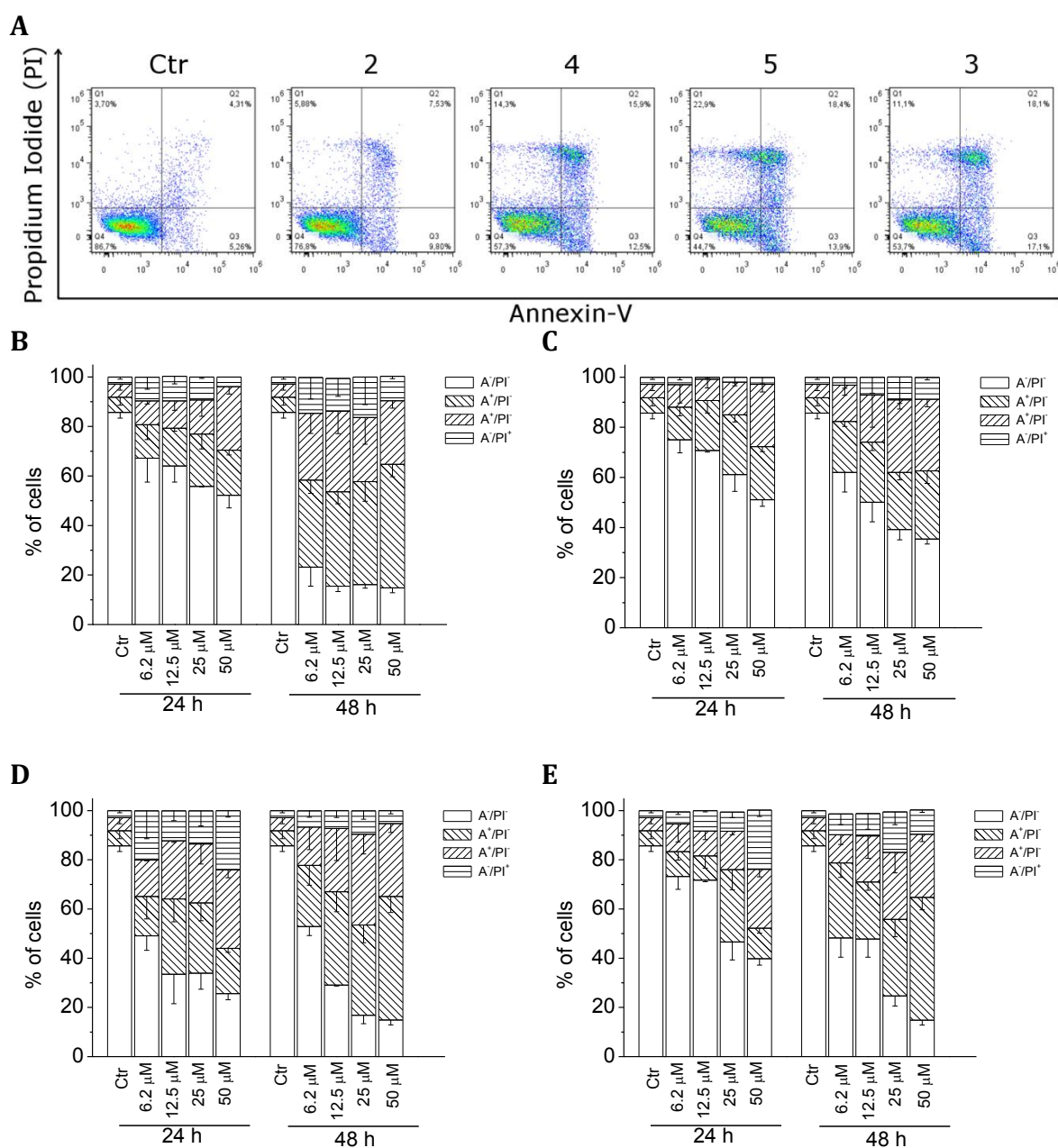
Figure 9. Flow cytometric demonstration of apoptosis by compounds **2**, **3**, **4** and **5**. A. Representative biparametric histograms obtained after a 24hours incubation of HeLa cells with the indicated compound at 25μM. The cells were harvested and labeled with annexin-V-FITC and PI and analyzed by flow cytometry. In these histograms, the lower left-hand segment represents the annexin-V⁻/PI⁻ cells, the lower right-hand segment the annexin-V⁺/PI⁻ cells, the upper right-hand segment the annexin-V⁺/PI⁺ cells, and the upper left-hand segment the annexin-V⁻/PI⁺ cells. Percentage of cells found in the different regions of the biparametric histograms shown in panel A and analogous histograms obtained after 48hours incubations are shown for compounds **2** (Panel B), **4** (panel C), **5** (panel D) or **3** (panel E) at the indicated concentrations. Data shown in panels B-E are presented as mean ± SEM of three independent experiments.

9'-noscapine derivatives induce apoptosis through the mitochondrial pathway

Mitochondria play an essential role in the propagation of apoptosis[123]. It is well established that, at an early stage, apoptotic stimuli alter the mitochondrial transmembrane potential $(\Delta\psi_{mt})$[122]. $\Delta\psi_{mt}$ was monitored by the fluorescence of the dye JC-1. As shown in Figure 10 (Panels A-D), compounds **2-5** induced a time and concentration–dependent increase in the proportion of cells with depolarized mitochondria.

A

B

C

D
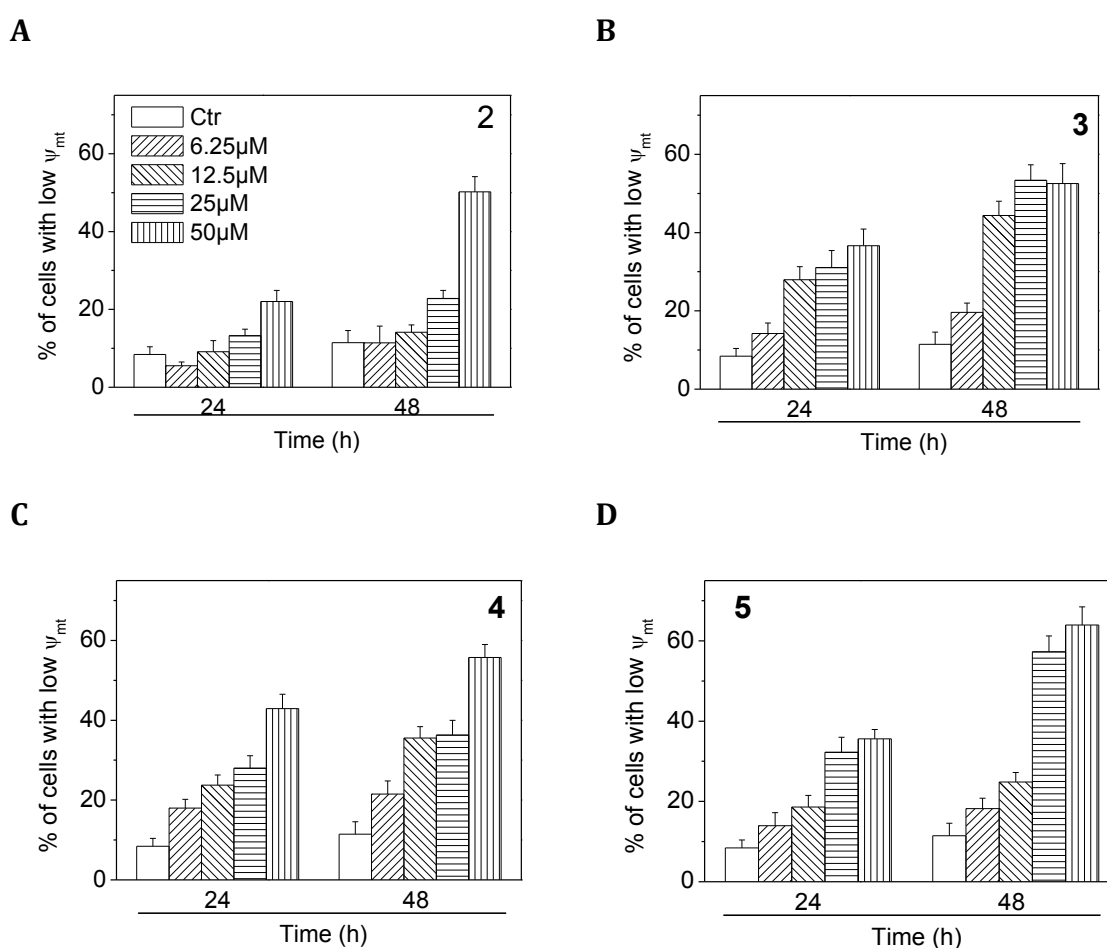
Figure 10. Assessment of mitochondrial membrane potential $(\Delta\psi_{mt})$ after treatment of HeLa cells with compounds **2-5**. Cells were treated with different concentration of the indicated compounds for 24 or 48hours and then stained with the fluorescent probe JC-1. Data are expressed as mean ± SEM for three independent experiments.

Mitochondrial membrane depolarization is associated with mitochondrial production of ROS[125]. Therefore, we investigated whether ROS production increased after treatment with **2-5**. We analyzed the production of ROS by flow cytometry utilizing the fluorescence indicator H_2-DCFDA. The results presented in Figure 11 (Panels A-D) show that all the tested compounds induced the production of significant amounts of ROS in comparison with control cells, which agrees with the previously described dissipation of $\Delta\psi_{mt}$. Altogether, these results indicate that these compounds induced apoptosis through the mitochondrial pathway in good agreement with previous reports[91,132,185].
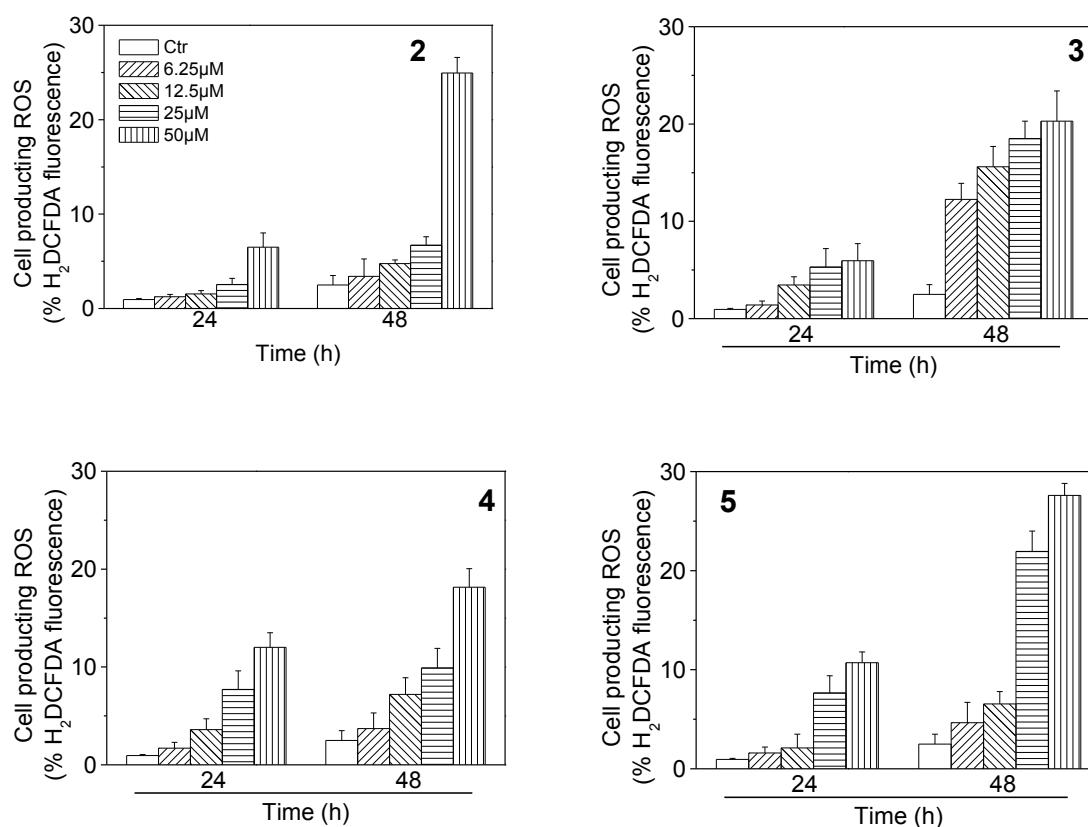
Figure 11. Mitochondrial production of ROS in HeLa cells following treatment with compounds **2**-**5**. After 24 or 48hours incubations with the indicated compounds at the indicated concentration, HeLa cells were stained with H_2-DCFDA and analyzed by flow cytometry. Data are expressed as mean ± SEM of three independent experiments.

Effect of 9'-alkyl and 9'-arylnoscapines on caspase activation.

The activation of caspases plays a central role in the process of apoptotic cell death[186]. Synthesized as proenzymes, caspases are themselves activated by specific proteolytic cleavage reactions. Caspases-2, -8, -9, and -10 are termed initiator caspases and are usually the first to be activated in the apoptotic process. Following their activation, they in turn activate effector caspases, in particular caspase-3[128]. As shown in Figure 12 (Panel A), all tested compounds induced proteolytic cleavage of caspase-9 and caspase-3, in good agreement with the mitochondrial depolarization described above. The DNA repair enzyme PARP is cleaved by caspase-3 from its full length 116 kDa form to an inactive 85 kDa form. We also observed that PARP cleavage was detectable after 24 and 48hours treatments. Altogether, these results showed that apoptosis induced by the 9'-noscapine derivatives was caspase-dependent and followed the intrinsic (mitochondrial) pathway. These findings are in good agreement with those of Aneja *et al.* who found that 9'-bromonoscapine induces mitochondrial depolarization followed by caspase-dependent apoptosis in both human prostate cancer cells and leukemia cells[144,145].

A

B
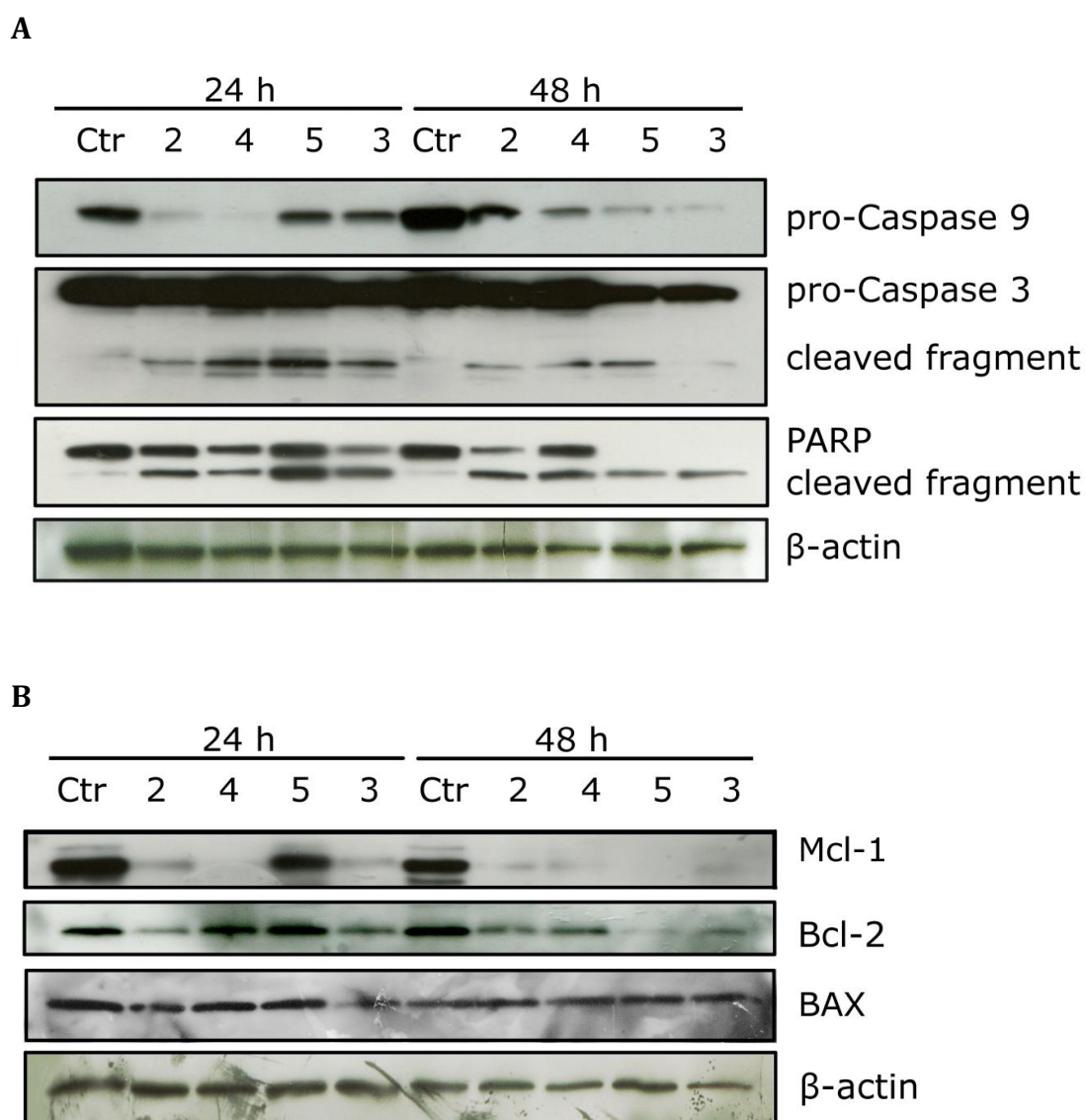
Figure 12. Effect of **2-5** on caspase activation (panel A) and on Bcl-2, Mcl-1 and Bax proteins (panel B) in HeLa cells. Cells were treated for 24 or 48hours with the indicated compounds at 25µM. The cells were harvested and lysed for the detection of pro-caspase-9, pro-caspase-3, PARP, Mcl-1, Bcl-2 and Bax expression by western blot analysis. To confirm equal protein loading, each membrane was stripped and reprobed with anti-β-actin antibody.

Effect on proapoptotic proteins and IAP expression.

There is increasing evidence that regulation of the Bcl-2 family proteins shares the signalling pathways induced by antimicrotubule compounds[91]. Several pro-apoptotic family proteins (e.g., Bax, Bid, Bim and Bak) promote the release of cytochrome *c*, whereas anti-apoptotic members (Bcl-2, Bcl-XL and Mcl-1) are capable of antagonizing the pro-apoptotic proteins and preventing the loss of mitochondrial membrane potential[91]. As shown in Figure 12 (Panel B), after a 24hours treatment, Bcl-2 expression was reduced with compounds **2** and **3**, but not with compounds **4** and **5**. After a 48hours treatment, however. Bcl-2 expression was decreased with all four compounds (**2-5**). The pro-apoptotic protein Bax was essentially unchanged after either 24 or 48hours treatments. Mcl-1 is an anti-apoptotic member of the Bcl-2 family, and recently it was reported that sensitivity to antimitotic drugs is regulated by Mcl-1 levels[130,187]. As shown in Figure 12 (Panel B), the Mcl-1 band was strongly reduced after the 24hours treatment with compounds **2**, **3** and **4,** but not **5**. After the 48hours treatment, the Mcl-1 band disappeared with all four compounds. It has recently emerged that Mcl-1 acts as a controller of the apoptotic timing response during mitotic arrest[130,187]. When Mcl-1 levels fall, Bak and Bax form pores in the mitochondrial membrane, resulting in the release of cytochrome *c*, mitochondrial depolarization and caspase activation that ultimately lead to apoptosis[130].

2.3.1.4. Conclusion

We devised an efficient new synthesis for noscapine derivatives modified at position 9', using Suzuki cross-coupling, a specific palladium-catalyzed carbon-carbon bond formation reaction, on the phthalide isoquinoline backbone. The ligands examined here were chosen to study the general utility of the reaction and, equally importantly, to obtain new, potentially cytotoxic noscapine derivatives. As shown above, 9'-bromonoscapine (**2**) has a very similar conformation in solid phase as the noscapine free base (**1**). This suggests that cytotoxic activity is a consequence of electronic rather than structural effects.

We also showed that the new 9'-substituted noscapines shared common properties with the lead compound **2** and are efficacious as antiproliferative agents in different cancer cell lines. Moreover, they are also strong apoptosis inducers that follow the mitochondrial intrinsic pathway. They did not show any appreciable activity on normal human lymphocytes, suggesting a low toxicity profile. It is worth noting that the replacement of bromine with a methyl group or a more bulky substituent such as 4-methylphenyl (compound **5**) did not substantially modify the cytotoxic potency in comparison with **2**, suggesting the existence of a large binding pocket in tubulin. From the point of view of the inhibition of tubulin polymerization *in vitro*, 9'-bromonoscapine and related derivatives did not show potent activity. The most active compound had an IC_{50} of 120μM, 100 fold weaker than that observed for **CA-4**. However, our results indicate, as have those presented by other workers, that noscapine and, in particular, 9'-bromonoscapine may produce subtle effects on microtubule dynamics that could interfere, for example, with the proper attachment of chromosomes to the kinetochore microtubules[149] instead of strongly binding to tubulin as do most well-studied antimitotic drugs. In accord with this idea, it was recently shown[149] that 9'-bromonoscapine did not perturb the morphology of

microtubules but rather induced alterations in the centrosome duplication cycle and caused inappropriate centrosome amplification. Our data showed that 9'-substituted noscapine induce accumulation of round cells with condensed DNA indicative of mitotic arrest and in addition, PCM1 alteration disrupted the radial organization of microtubules. We also found that compounds **3-5** induced a substantial increase in the expression of the phosphorylated form of H2A.X that is indicative of DNA damage. This could be due to a protracted mitotic arrest that ultimately led to cell death. In line with these findings, we observed an activation of the tumor suppressor p53. In conclusion, all these findings indicate that the noscapine derivatives have good therapeutic potential and merit further investigation.

2.4. CONCLUSIONS

Tubulin binding agents represent a class of drugs commonly used in chemotherapy. Nevertheless TBAs induce many side effects by altering the overall structure of microtubules. Noscapines, particularly **EM011**, are molecules which bind to tubulin with low toxic side effects, because they act without impairing the microtubule polymer mass.

They reduce the dynamic instability, necessary for continuous growth and shrinking of tubulin cytoskeleton. Noscapines disrupt the normal association of microtubule to kinetochore, inducing abnormalities in mitotic spindle, cell cycle arrest in mitosis and consequent apoptosis following the mitochondrial pathway.

Recently some derivatives were synthesized in order to find new molecules with increased antitumoral effects. Accordingly to the activity described for **EM011**, our 9'-alkyl and 9'-arylnoscapines showed high antiproliferative effect on a panel of cancer cell lines, with GI_{50} which ranged between 1.4μM and 100μM, while in normal human lymphocytes they resulted ineffective, confirming the low toxicity of noscapines. The observed mechanism of action was in well agreement with lead compound. The more potent derivatives studied in this work endowed the ability to arrest cell cycle in mitosis, and to alter the radial organization of microtubules, with multipolar spindles. DNA damage and subsequent apoptosis occurred after treatment with the 9'-substituted noscapines. The intrinsic pathway was activated, by the involvement of caspase-9 and PARP.

The balance between cell cycle arrest and apoptosis induction resulted in the activation of the cell death program, and the anticancer activity was carried out.

Noscapine derivatives have many advantages as concern the molecular structure. They have similar structure to colchicine, but they demonstrated low toxicity, and

they are water-soluble. For these aspects, noscapines are more appealing molecules for delivery and specific drug therapy. Finally, although our derivatives did not show higher antiproliferative activity respect to other noscapines, we reported the Suzuki cross-coupling, an effective method for their chemical synthesis.

3. SMALL MOLECULES AS WNT INHIBITORS IN COLON CANCER

3.1. INTRODUCTION

3.1.1 Wnt/β-catenin signaling pathway: discovery and molecular cascade

Since when the Wnt/β-catenin signaling pathway was discovered, it raised great interest, and it seems to be one of the major involved pathways in embryonic development, in regulation of homeostatic self-renewal of many adult tissues, and in carcinogenesis.

It is represented by a number of molecules which allow the communication of extracellular signals through membrane receptors, to the inside of the cell. Three signaling cascades were characterized as those which are activated upon the binding of Wnt ligands to their receptors. The best understood pathway is the "canonical" Wnt/β-catenin cascade, while the other "non-canonical" ones are the planar cell polarity (PCP) pathway, and the Wnt/Ca^{2+} pathway[188].

Firstly, in 1982, the *Int-1* gene was identified in murine tumor cells, and in parallel, the homologous gene *Wingless* (*Wg*) was characterized in Drosophila melanogaster. A spontaneous loss-of-function mutation in mammalian *Int1* originated a mouse lacking the anterior cerebellum, while mutated *Wingless* gave rise to a Drosophila melanogaster without wings. These discoveries led to the study of a lot of mutants, resulting in the definition of the term Wnt, as the combination of Wg and Int[189,190]. The Wnt signaling regulates different processes, such as development and cancer, and it is represented by a series of secreted Cysteine-rich proteins which trigger the transduction of signal. As already outlined, three signaling pathways were described: the Wnt/β-catenin mediated "canonical" way, the "non-canonical" PCP cascade, and the calcium-mediated pathway. They are differently activated on the basis of the ligand interaction to specific receptors. In fact more than 15 receptors

and co-receptors were described, and the particular combination between these and Wnt ligands triggers the activation of different pathways[191],[188],[192]. The PCP cascade is involved in cell polarity and morphogenesis regulation, acting on cell cytoskeleton through particular molecular mediators, such as c-Jun N-terminal kinases (JNK) and small GTPases[193].

The Wnt-Ca^{2+} pathway results in the activation of Ca^{2+} effectors, and triggers the transcriptional regulation by NFAT (nuclear factor associated with T cells), controlling processes like cancer, inflammation and neurodegeneration[194],[195].
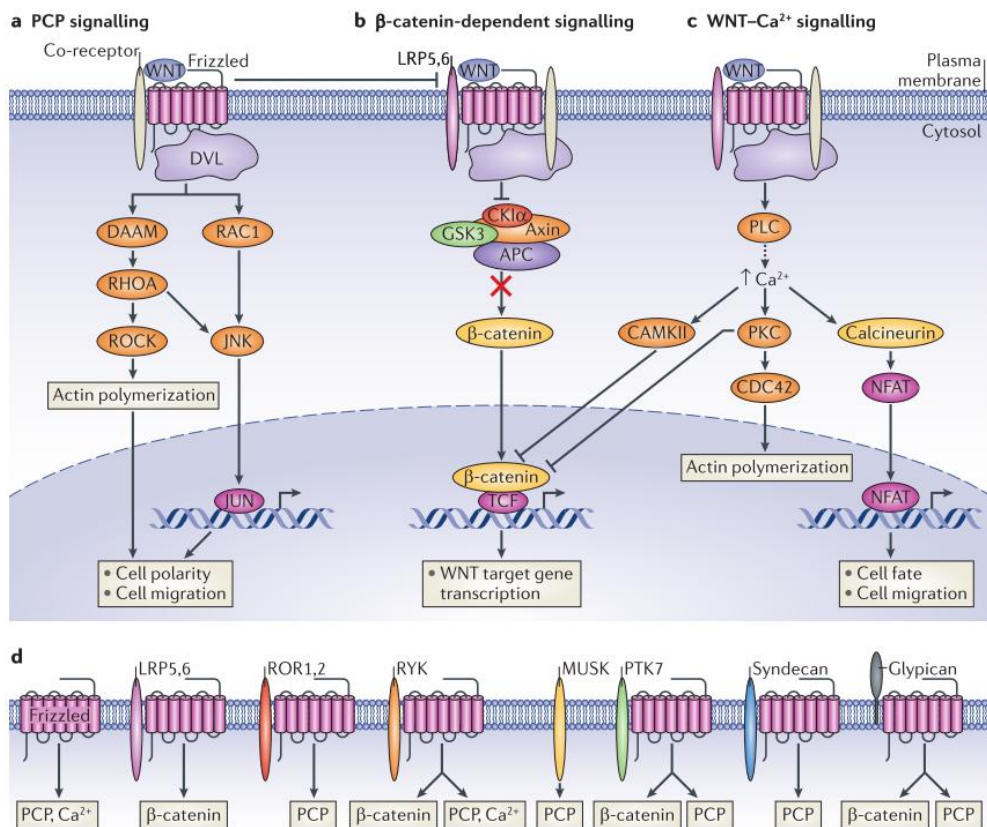
Figure 1. Wnt signaling pathways (adapted from Ref.[192])

The best known and more frequently activated Wnt pathway is the canonical cascade, and principally we will focus on it.

The central protein of this molecular pathway is β-catenin, a protein which, in this case, acts as a transcription factor. The cascade is triggered by the Wnt ligand binding to the receptor Frizzled, a serpentine transmembrane receptor, and its co-factors LRP5/6. Once activated, the intracellular signaling cascade is initiated by dishevelled proteins (DVL) which in turn cooperate with the sequestration of a series of molecules. In these conditions β-catenin carries out its role, translocating from the cytoplasm into the nucleus. Here it associates with the DNA-binding proteins of the TCF/LEF family, and converts them into transcriptional activators[196].

When the ligand is not associated with the receptor, the signaling pathways is in an "off-state". An inhibitory signal is activated, and a degradation complex of β-catenin is engaged. The tumor suppressor adenomatous polyposis coli (APC) and Axin2 create a scaffold for the kinases CK1 (casein kinase 1) and GSK3 (glycogen synthase kinase 3), which successively phosphorylate β-catenin. Several Ser and Thr residues sites are phosphorylated and β-catenin is recluted by E3 ubiquitin ligase and sequestered into the proteasome.

The co-repressor Groucho, or other repressor proteins, assembles with TCF/LEF proteins and represses the Wnt/β-catenin target genes[197].

 A wide list of target genes is transcribed as a consequence of the Wnt/β-catenin pathway activation. Cyclin D1 and c-myc are largely described as Wnt targets, and they regulate cell cycle progression and induce cell proliferation[198]. The Wnt cascade is strictly controlled by numerous proteins and feedback loops, and it is able to self-maintain or auto-inhibit[199,200].
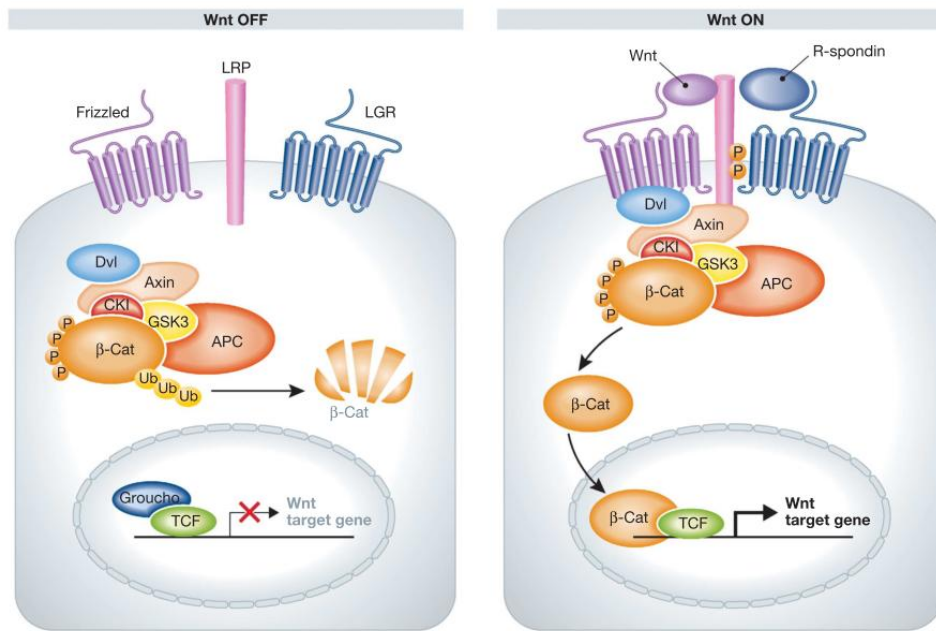
Figure 2. The canonical Wnt signaling pathway (adapted from Ref.[201])

3.1.2 Wnt pathway and stem cells

The canonical Wnt cascade is a key regulator in stemness maintenance and differentiation processes, both during embryonic development and in regeneration or damage repair in adult tissues[201]. At physiological level, numerous mechanisms were described in which both canonical and non-canonical Wnt cascades are mediators of commitment phenomena for the development of different tissues, such as osteogenesis[202].

Moreover, the intestinal epithelium is a physiological model of stem cells regulation by mutual activation of Wnt signals. Wnt/β-catenin target genes control the rapid and continuous proliferation of stem cells in the niche, and their commitment to epithelial cells[203,204].

Since the Wnt pathway has a great relevance in the tightly regulation of self-renewal in stem cells and progenitor cells, any alteration in the recruited molecules can give rise to cancer stem cells development and their progression to malignancy[205].

3.1.3 Wnt pathway is hyperactivated in cancer and other diseases

Any dysregulation in Wnt/β-catenin signaling pathway leads to aberrant homeostasis, cell proliferation or embryonic development. Many diseases are related to genetic mutations or environmental perturbation of the Wnt pathway, particularly cancer and birth defects[206],[190].

Colon cancer is the mostly described tumor induced by mutations in the Wnt pathway, but other pathologies are caused by Wnt deregulations, such as hepatocellular carcinoma, medulloblastoma, melanoma, prostate cancer and ovarian cancer[207],[208].

Beyond cancers, other human diseases are associated to altered expression or mutations of components of the canonical Wnt pathway. Bone malformations, like osteoarthritis or osteoporosis-pseudogliome syndrome are due to an increased Wnt activity, as well as eye defects (familiar exudative vitreoretinopathy), acute renal failure (polycystic kidneys), cardiovascular diseases (cardiac hypertrophy), or neurodevelopment and neurogenerative diseases (schizophrenia or Alzheimer disease)[190],[209].

Finally, given the role of Wnt signaling for stemness maintenance, and the involvement of stem cells in tumors and aggressiveness, it is not surprising that numerous mutations in this cascade occur in cancers[210]. Frequently, the hit tissues are which ones depending on Wnt regulation for their homeostasis repair. Several mutations take place in proteins of the degradation complex, or in β-catenin, but the majority of them lead to a more stabilized form of β-catenin, which shuttles into the nucleus to transcribe for prosurvival and self-renewal genes. In particular loss of

function mutations occur in APC. Generally, patients with adenomatous polyposis, a familiar cancer syndrome caused by APC mutations, were subjected to a first germline heterozygous mutation, and successively to a second hit in individual cells, belonging to colorectal tissues[211],[212],[213].

3.1.4 Wnt pathway in colon cancer

One of the most aggressive tumor is represented by colorectal carcinoma, which is associated to high frequency of death due to neoplastic disease, in Western world. In the last years many advances in colon cancer knowledge were improved, but patients mortality is still around 40%[214]. 80%-85% of colorectal cancers is related to alterations in the canonical Wnt pathway, and they derived from adenomas. A precisely sequence of events and genetic alterations were described and a model for carcinogenesis was proposed[215],[216]. Here APC mutations represented the first event initiating the tumorigenesis. Over the years, more evidences regarding colon cancer were examined in depth, and the cancer stem cell definition has been helpful. In fact the development of intestine is strictly dependent on the differentiation and proliferation of stem cells, localized into the bottom of intestinal crypts. Differentiated cells progressively go up and constitute the top of crypts, giving rise to a stem cell regeneration cycle, and to a migration phenomenon of differentiated cells on the villus, creating a crypt-villus axis. This axis is finely regulated by the Wnt signaling pathway, which is required physiologically to preserve the stem phenotype of crypt epithelial progenitors[217],[197].

In addition to APC, other molecules are dysregulated in colon cancer stem cells, such as Axin2 or β-catenin itself. In fact the closing effect of the overall mutations is an upregulation of β-catenin transcriptional activity, and its binding to co-factors like TCF4[218],[219].
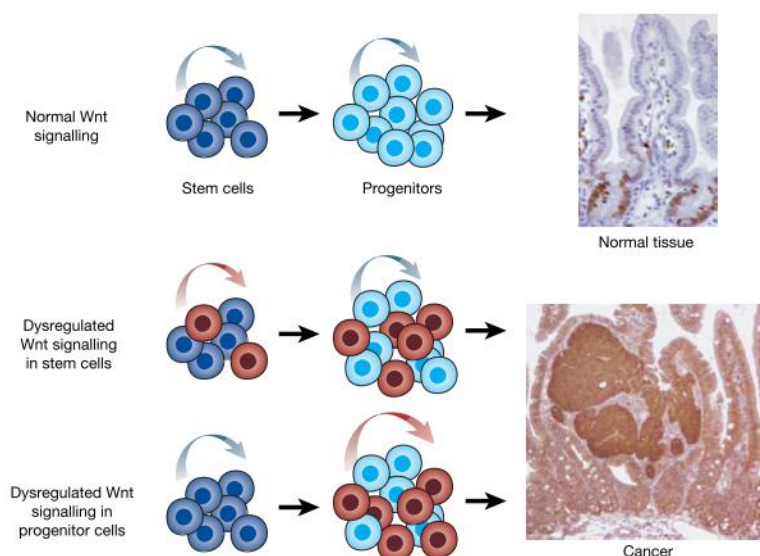
Figure 3. Wnt signaling influences on stem cells proliferation and self-renewal (adapted from Ref.[197])

3.1.5 Wnt inhibitors

Aberrations in Wnt/β-catenin pathway play an important role in carcinogenesis and in some pathological conditions, as well as numerous target genes and proteins were identified in this signaling cascade, to improve pharmacological treatment.

Several therapeutic approaches aimed to inhibit Wnt were studied, and a series of different molecules was developed. These molecules can perform their inhibitory activity on the Wnt pathway acting upstream or downstream along the signaling cascade. **IWP** is a porcupine inhibitor and prevents the secretion of Wnt ligands, required to preserve the iperactivated Wnt signals in cancer[220]. Secondly it is possible to interfere with the binding of the ligand to the receptor/co-receptor, arresting the signal transduction. For example, recombinant DKK proteins mimic the namesake Wnt ligand competitor, binding the LRP5/6 with high affinity[221].

Signal transduction is avoided also by interfering with the intracellular domain of the receptor preventing the interaction with DVL proteins, signaling intermediates for the intracellular regulation of β-catenin[222].

Other identified targets for therapy in Wnt-related cancers are the proteins of the degradation complex. The goal of this approach is to stabilize the degradation complex in order to stimulate β-catenin degradation. Axin stabilizers, such as the tankyrase inhibitors (**IWR1** or **XAV939**), are effective also in APC-mutated tumors, because they act independently of APC[223]. CK1 are modulated and several isoforms could be targeted. An example is pyrvinium which induces the CK1α kinase activity although it binds all CK1 isoforms, resulting in a reduced Wnt signaling[224].

Finally, the Wnt cascade converges to the β-catenin activation and TCF/LEF-dependent transcription of its target genes. A series of other co-factors, such as hystone acetylases (CBP or p300) and chromatin remodeling proteins, were recruited to modulate specific gene transcription. The direct inhibition of β-catenin or the prevention of the binding to its partners cause the arrest of Wnt transduction signal. **ICG001** and **IQ-1** respectively act inhibiting CBP and p300 respectively, and they affect the binding of β-catenin to TCF/LEF[222],[208].

Since drugs targeting the Wnt/β-catenin signaling pathway can modulate many cellular processes and are implicated in several human diseases, effective pharmacological treatments are required[225]. High-throughput screening methods were optimized to find new small molecules, comprehending both inhibitors and agonists of the Wnt/β-catenin signals, with different applications in a broad-spectrum of pathologies[226],[227].

Table I. Small-molecule Wnt pathway modifiers (adapted from Ref.[211])

Small Molecule	Molecular Target	Function	Effect on Wnt Pathway Output
IWP	Porcupine	inhibitor	inhibits
XAV939	tankyrase 1/Axin	activates Axin	inhibits
IWR	Axin	activates Axin	inhibits
Pyrvinium	CK1	inhibitor	inhibits
SB-216763	GSK3	inhibitor	activates
BIO(6-bromo indirubin-30-oxime)	GSK3	inhibitor	activates
ICG001	CREB-binding protein	inhibitor	inhibits
PKF115-584 (and other compounds)	TCF/β-catenin	inhibitor	inhibits

3.2. AIM OF THE STUDY

Wnt/β-catenin pathway is involved in the regulation of embryonic development and tumorigenesis. Since aberrant Wnt signals give rise to severe human diseases, targeting this pathway is a suitable strategy with numerous implications.

In this study we focused on Wnt-related cancers, especially APC-mutated colon cancer, and we identified some imidazo[1,2-*a*]pyrimidines and imidazo[1,2-*a*]pyridines derivatives that were able to inhibit the Wnt/β-catenin signaling cascade.

3.2. AIM OF THE STUDY

3.3. RESULTS

3.3.1. SYNTHESIS AND BIOLOGICAL EVALUATION OF IMIDAZO[1,2-*a*]PYRIMIDINES AND IMIDAZO[1,2-*a*]PYRIDINES AS NEW INHIBITORS OF THE WNT/β-CATENIN SIGNALING

Barbara Cosimelli, Sonia Laneri, Carmine Ostacolo, Antonia Sacchi, Elda Severi, Elena Porcù, Elena Rampazzo, Enrico Moro, Giuseppe Basso, Giampietro Viola

submitted

3.3.1.1. Abstract

Wnt/β-catenin signaling plays an important role in the regulation of embryonic development and tumorigenesis. Since its deregulation results in severe human diseases, especially cancer, the Wnt signaling pathway constitutes a promising platform for pharmacological targeting of cancer. In this study we synthesized a series of imidazo[1,2-*a*]pyrimidines and imidazo[1,2-*a*]pyridines and identified some derivatives that were able to inhibit the Wnt/β-catenin signaling pathway in a luciferase reporter assay and cell proliferation in selected cancer cell lines, endowed with APC or β-catenin gene mutations. The most active compounds significantly downregulate the expression of Wnt target genes such as c-myc and cyclin D1. Further studies indicated that these compounds function independently of GSK-3β activity. More importantly, *in vivo* experiments, carried out on a Wnt-reporter zebrafish model indicate, in particular for compounds **4c** and **4i** as the most active compounds, an activity comparable to that of the reference compound **IWR1**, suggesting their potential use not only as small molecule inhibitors of the Wnt/β-catenin signal in Wnt driven cancers, but also in other Wnt-related diseases.

3.3.1.2. Introduction

Wnt signaling pathway is a highly conserved system which has a crucial role in embryogenesis of all metazoan, in tissue regeneration in adult organisms and in many other processes[190], including cellular proliferation, differentiation, migration and polarity[228]. Wnt ligands are a large family of secreted, hydrophobic glycoproteins which have many receptors on a variety of cell types[191]. Three different pathways have been described as signaling cascades activated upon the binding of Wnts to the receptor: the canonical Wnt/β-catenin pathway, the non-canonical planar cell polarity (PCP) cascade, and the Wnt/Ca^{2+} pathway[188]. This work is focused on the best understood canonical pathway. Downstream effect of activation of this cascade is transcription of a new set of genes through the β-catenin-T cell factor (TCF) complex, which regulates cell proliferation and differentiation[219]. In canonical pathway, when Wnts are associated to their cell-surface receptor Frizzled, signal cascade is active and stable β-catenin forms a complex with TCF in the nucleus, recruiting transcriptional coactivators like cyclic AMP response element-binding protein (CBP). Such complex activates the transcription of Wnt target genes. If Wnt ligands are not associated to Frizzled, the cytoplasmic complex APC–Axin2 provides a scaffold for GSK-3β which phosphorylates β-catenin[213]. Phosphorylation is a destabilizing process for β-catenin which is rapidly degraded through the ubiquitin-proteasome pathway. Wnts and Frizzled interaction induces Dishevelled phosphorylation which, in that form, triggers GSK-3β inhibition[229,230]. Subsequently the balance between Axin2 and β-catenin favors the latter protein and Wnt signaling is turned on[231]. A critical role of canonical cascade has been described in regulation of stem cells, and in many tissues impairment of Wnt signaling is associated with cancer[197]. Wnt involvement in human cancer is not surprising given its fundamental role in homeostasis in adult

tissue[232], and it has since been buttressed by the identification of mutations in genes coding for the Wnt pathway components Axin2, Adenomatous polyposis coli (APC), and β-catenin[233]. Indeed, loss of function of Wnt components (such as the inactivation of the APC gene) or activating mutations of β-catenin are believed to be the critical initiating steps in malignant transformation[214]. Specific genetic hit mutations in a series of oncogenes and tumor-suppressor genes (APC, KRAS, SMAD2/4, TP53) give rise to colorectal carcinomas through a series of well-characterized histopathological changes[234]. Particularly, deregulation of canonical Wnt/β-catenin signaling through mutations in APC was recognized to be an initiating event in colon carcinogenesis[217,235]. However, despite the presence of constitutively activating mutations in APC or β-catenin, most colorectal cancers show cellular heterogeneity when β-catenin localization is analyzed, indicating a more complex regulation of Wnt signaling[210]. Anyway, the Wnt/β-catenin signaling pathway could be qualified as one of the promising target for innovative treatment strategies of colorectal cancer[236]. Moreover, given the fact that Wnt/β-catenin signaling is tightly regulated at multiple cellular levels, the pathway itself offers ample targeting nodal points for cancer drug development[237]. Recently, several Wnt inhibitors were identified in high-throughput screening that target the upstream signaling of β-catenin in order to promote β-catenin degradation[223]. Although these agents efficiently inhibit Wnt signaling in normal cells and some APC-mutated colon cancer cells, they may not be effective in cells containing β-catenin mutations[238]. Despite in the last years many advances have been achieved in that field, the majority of patients relapses and the survival with metastatic disease remains approximately two years, indicating the need for new therapies that may produce dramatic improvements[239]. As just noted, high-throughput screening of synthetic compounds libraries was used to identify several WNT inhibitors[223,240,241], as well as agonists[242,243]. This method efforts several structures all characterized by a

pyrimidine ring decorated with a large variety of substituents or, also, condensed with other heterocycle rings.

In the past years we have been engaged in the synthesis of pyrimidines derivatives[244], imidazo[1,2-*a*]pyrimidines and imidazo[1,2-*a*]pyridines[245], now we used our knowledge in the synthesis of these heterocycles to prepare a small library of 2,4,6-substituted pyrimidines and a small library of imidazo[1,2-*a*]pyrimidines and imidazo[1,2-*a*]pyridines that resemble geometry or functional groups of the known active compounds; indeed it has been reported that some NSAIDs are potential WNT pathway therapeutics[246], and the imidazo[1,2-*a*]pyridine derivatives are often compared to indomethacin that is active on WNT pathway[247]. A series of the synthesized molecules were then evaluated for their biological activity on WNT pathway.

3.3.1.3. Results and Discussion

Newly synthesized compounds impaired TCF/LEF transcriptional activity

In order to evaluate the effect of the new compounds on the Wnt/β-catenin signaling cascade, we used a luciferase-reporter system. After liposomal transfection to insert into HT-29 cells the BAT-LUX vector, containing luciferase gene downstream the TCF/LEF promoter[248], we treated the transfected cells with our derivatives for 24hours. Then, the cells were assayed for the β-catenin/TCF mediated activity. The data are depicted in Table 1 in which the IC_{50} values represent the concentrations that cause 50% inhibition of β-catenin transcriptional activity. Two known inhibitors of the Wnt signaling response were used as reference compounds: **IWR1**, an Axin stabilizer[240], and **ICG001** which is endowed with an effect downstream the β-catenin degradation complex, disrupting the CBP-β-catenin interaction[249]. Pyrimidine derivatives **1a-d** and **2a-2d** were inactive. Among the imidazo[1,2-*a*]pyridine derivatives compounds **4c**, **4d**, **4h** and **4i** showed a moderate activity, similar to that of the two reference compounds. The most active compound **4a** has a *p*-nitrophenyl while the activity disappeared in **4b** where an aminophenyl is present. Interestingly, **4f**, that is the isomer of **4a**, had reduced activity pointing out that the position of methyl group has an important role in modulating the activity. On the contrary **4g**, the isomer of **4b,** remained inactive.

Table 1. Wnt inhibitory effect in BAT-LUX system into HT-29 cells, of the newly investigated compounds.

Compound	IC$_{50}$ (µM)[a]	Compound	IC$_{50}$ (µM)[a]
1a	> 25	3e	> 25
1b	> 25	3f	10.4 ± 0.02
1c	> 25	3g	16.1 ± 0.01
1d	> 25	4a	6.2 ± 0.003
1e	22.3 ± 0.2	4b	> 25
1f	> 25	4c	11.1 ± 0.005
2a	> 25	4d	19.5 ± 0.03
2b	> 25	4e	9.7 ± 0.007
2c	> 25	4f	23.1 ± 0.03
2d	> 25	4g	> 25
3a	> 25	4h	17.8 ± 0.1
3b	14.3 ± 0.04	4i	24.1 ± 0.02
3c	> 25	4j	> 25
3d	34.6 ± 0.04	IWR1	24.4 ± 0.6
		ICG001	18.7 ± 0.3

[a] IC$_{50}$ values represent the concentration necessary to inhibit TCF/LEF transcriptional activity by 50%.

The 5,7-dimethoxy-2-(4-nitrophenyl)imidazo[1,2-*a*]pyridimidine derivatives **3a**, **3c**, **3d** and **3e** were inactive except **3b** whereas 5-(hydroxyl)-7-methyl-2-(4-nitrophenyl)imidazo[1,2-*a*]pyrimidine **(3f)** and 5-(benzyloxy)-7-methyl-2-(4-nitrophenyl)imidazo[1,2-*a*]pyrimidine **(3g)** exhibit a value of IC$_{50}$ lower than both **IWR1** and **ICG001**.

Biological in vitro activity: antiproliferative studies

All derivatives were tested in a panel of four human cancer cell lines to determine their antiproliferative activity after 72hours of treatment. We used two human colon adenocarcinoma cell lines, HT-29 and LoVo, with mutated APC gene and the liver hepatocellular carcinoma HepG2 cell line, endowed with endogenously mutated β-catenin gene. In addition, the pulmonary epithelial cancer cells A549, endowed with high levels of Wnt2 were also used. All of the reported mutations result in an upregulated Wnt signaling[250,251]. As shown in Table 2, GI_{50} values in all cell lines ranging from 5.7 to more than 100μM, and the more active compounds against all cell lines are **4i** and **4c** which exhibited a lower GI_{50} values in comparison to the reference compounds **IWR1** and **ICG001**, in the two colon adenocarcinoma cell lines (HT-29 and LoVo). Compound **4i** on HepG2 and A549 cells presented an higher activity respect to **IWR1** but slightly lower than **ICG001**. On the other hand, **4c** was ineffective in HepG2 and was endowed with a higher value of GI_{50} in A549 cells.

Table 2. *In vitro* cell growth inhibition after 72hours treatment of the newly investigated compounds.

Compound			GI_{50} (μM)[a]	
	HT-29	LoVo	HepG2	A549
1a	40.0 ± 24.7	54.5 ± 4.9	60.8 ± 2.5	18.7 ± 12.6
1b	35.7 ± 11.7	53.9 ± 7.2	64.4 ± 3.4	19.9 ± 12.7
1c	53.9 ± 7.1	53.7 ± 3.8	49.0 ± 7.0	46.2 ± 3.9
1d	65.8 ± 1.5	40.0 ± 2.1	42.9 ± 22.1	35.2 ± 19.5
1e	88.2 ± 2.9	54.2 ± 13.2	87.1 ± 6.3	51.0 ± 29.4
1f	59.9 ± 7.9	54.9 ± 8.8	75.1 ± 3.8	75.7 ± 3.6
2a	> 100	68.0 ± 2.5	77.0 ± 11.9	83.3 ± 9.1
2b	68.4 ± 9.4	58.5 ± 5.2	67.6 ± 19.9	46.4 ± 19.2
2c	> 100	84.9 ± 15.1	97.8 ± 1.9	> 100
2d	79.3 ± 4.8	56.3 ±6.1	71.7 ± 9.1	50.4 ± 9.0
3a	> 100	70.6 ± 29.4	35.9 ± 27.0	36.6 ± 7.6
3b	> 100	> 100	> 100	> 100

3c	> 100	> 100	> 100	> 100
3d	> 100	> 100	> 100	> 100
3e	> 100	61.9 ± 16.5	> 100	7.0 ± 1.0
3f	90.1 ± 5.0	87.6 ± 6.0	> 100	38.9 ± 12.0
3g	> 100	74.9 ± 10.6	> 100	71.0 ± 3.8
4a	> 100	> 100	> 100	> 100
4b	82.9 ± 9.0	65.2 ± 2.0	> 100	> 100
4c	8.8 ± 0.4	42.6 ± 3.5	> 100	56.1 ± 11.2
4d	37.6 ± 4.0	n.d.	n.d.	60.0 ± 6.1
4e	> 100	90.7 ± 9.3	> 100	> 100
4f	> 100	n.d.	n.d.	62.4 ± 6.5
4g	93.6 ± 5.2	n.d.	n.d.	> 100
4h	17.5 ± 2.6	n.d.	n.d.	5.1 ± 0.7
4i	6.9 ± 1.2	5.7 ± 0.5	18.4 ± 10.0	17.2 ± 6.9
4j	> 100	n.d.	n.d.	> 100
IWR1	> 100	63.1 ± 7.7	95.4 ± 4.5	> 100
ICG001	17.2 ± 2.9	15.6. ± 2.8	12.7 ± 1.5	6.1 ± 0.1

[a] GI_{50} indicates the required concentration to inhibit tumor cell proliferation by 50%. Data are expressed as the mean ± SEM from the dose–response curves of at least three independent experiments. n.d. not determined

Interestingly, some of the most active compounds (**3f**, **4c**, **4h**, **4i**) exhibited a lower activity or were ineffective in a primary cell line of human fibroblast, in which the Wnt/β-catenin signaling status is inactive (Table 3), suggesting that these compounds are selectively toxic to cell lines harboring deregulation of the Wnt/β-catenin pathway. On the basis of the results obtained both in the luciferase-based assay and in the antiproliferative studies, we selected five molecules (**3f**, **4a**, **4c**, **4e**, **4i**), within the more active compounds that induce antiproliferative effects and antagonist action to β-catenin transcriptional activity, that were further evaluated for their ability to decrease the expression of Wnt target genes in HT-29 cell line.

Table 3. *In vitro* cell growth inhibition after 72hours treatment of the newly investigated compounds.

Compound	GI$_{50}$ (µM)[a]
	Human Primary Fibroblasts
3f	> 100
4c	> 100
4h	> 100
4i	52.3 ± 3.2

[a] GI$_{50}$ indicates the required concentration to inhibit tumor cell proliferation by 50%. Data are expressed as the mean ± SEM from the dose–response curves of at least three independent experiments. n.d. not determined

β-catenin transcriptional activity was modulated independently by GSK-3β

To evaluate on which step of Wnt/β-catenin signaling these compounds act, we treated HT-29 cells transfected with BAT-LUX plasmid, with selected compounds in the presence or absence of LiCl, a GSK-3β inhibitor. LiCl avoids β-catenin degradation by GSK-3β enzyme, thus the effect on luciferase activity resulted independent by this enzyme. As reported in Figure 1, LiCl increased the TCF/LEF transcriptional activity by four times respect to the untreated cells, while the selected compounds, at the concentration of 25µM, remarkably reduced luciferin luminescence both in absence and in presence of LiCl, after 24hours of treatment, indicating that their effect did not depend on GSK-3β activity.
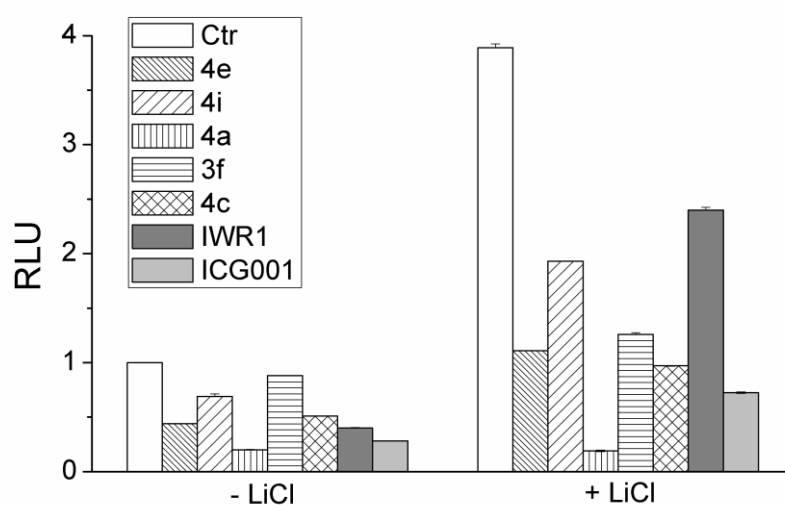
Figure 1. Effect on TCF/LEF transcriptional activity in BAT-LUX system after 24hours of treatment with **4e**, **4i**, **4a**, **3f**, **4c** compounds, at the concentration of 25μM alone or in combination with the GSK-3 inhibitor, LiCl (25mM). Relative Luminescence Unit (RLU) indicates the relative intensity of luciferine signal. Data are expressed as mean ± SEM of three independent experiments.

Moreover, as shown in Figure 2, the mRNA expression of Axin2 was generally upregulated in particular by **4i** and **3f** as well as the reference compounds, confirming an inhibitory effect on Wnt pathway. In this context, it is worthwhile to note that new molecules have been described as Axin2 inducers or stabilizers[240], given its role as Wnt signaling repressor. On the other hand Axin2 itself is also a direct target of the Wnt signaling and regulates the pathways through a negative feedback loop. Its upregulation after treatment with our compounds, suggest that a repressive mechanism on Wnt pathway has been activated.
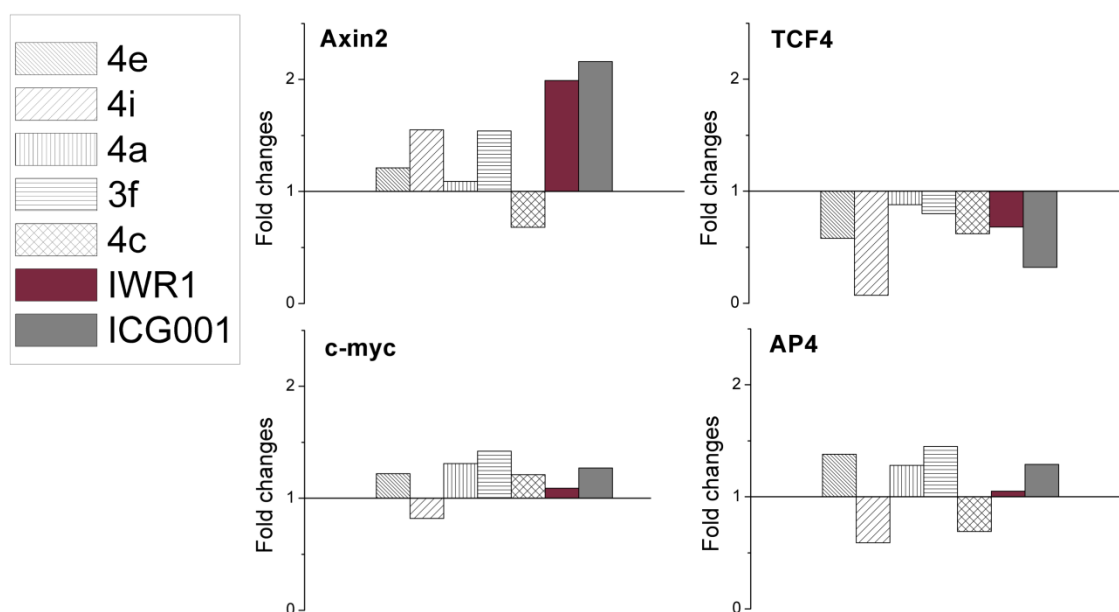
Figure 2. Fold changes of mRNA expression of Axin2, TCF4, c-myc, AP4. Cells were treated with indicated compounds at the concentration of 25μM, as well as the two reference compounds **IWR1** and **ICG001**. After 24hours total RNA was exctracted and transcribed as described in the experimental section. Quantitative real-time PCR was then performed and the results were calibrated to untreated cells mRNA (RQ = 1), used as control.

Upstream β-catenin modulators were differently regulated by selected compounds

We investigated if the most active compounds alter the expression of the main molecules of the canonical Wnt pathway, that trigger β-catenin translocation into the nucleus. Immunoblot analysis depicted in Figure 3, shows that total levels of β-catenin protein were not modified after treatment. On the other hand we observed β-catenin dephosphorylation in Ser33/37/Thr41 induced by **4e**, **4i** and particularly **4c**. Interestingly, treatment with the new compounds led to modifications in β-catenin localization, mainly sited into the cytoplasm in its inactive form (shown in red, Figure 4). None of the tested compounds impaired GSK-3α/β phosphorylation

in Ser21/Ser9. T-cell Factors (TCF) have essential nuclear functions, they consist in several isoforms, and the major transducers of Wnt signaling in the intestine and the oncogenic drivers of colon cancer are TCF-1 and TCF4[252]. It is also known that TCF-1 expression is regulated by APC and β-catenin–TCF4[253]. As shown in Figure 3, it appears that **3f**, **4c** and **4e** induced an increased TCF-1 protein level, but on the contrary, **4i** particularly reduced TCF-1, preventing its co-activation effect on β-catenin. Moreover, all the selected compounds remarkably reduced the mRNA expression of TCF4 (Figure 2), being the more effective compound **4i**. Altogether these effects contributed to make **4i** one of the most active compounds in the antiproliferative assay.
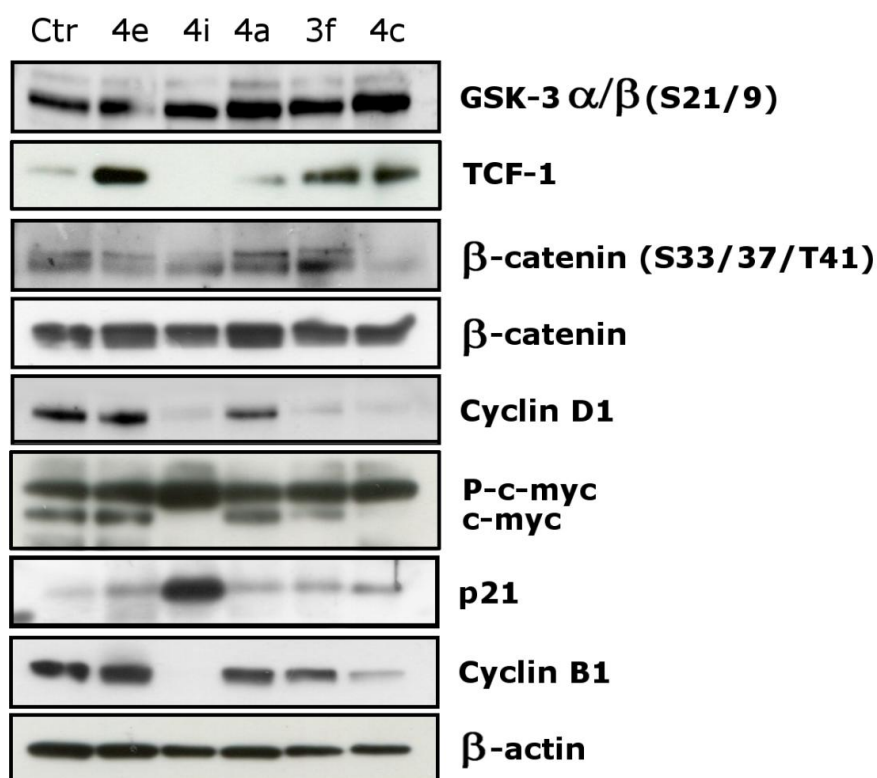
Figure 3. Effects of **4e**, **4i**, **4a**, **3f**, **4c** on the main molecules implicated in Wnt/β-catenin cascade. HT-29 cells were treated with the indicated compounds at 25μM concentration for 24hours, harvested and lysed for Western blot analysis. To confirm equal protein loading, each membrane was stripped and reprobed with anti-β-actin antibody.
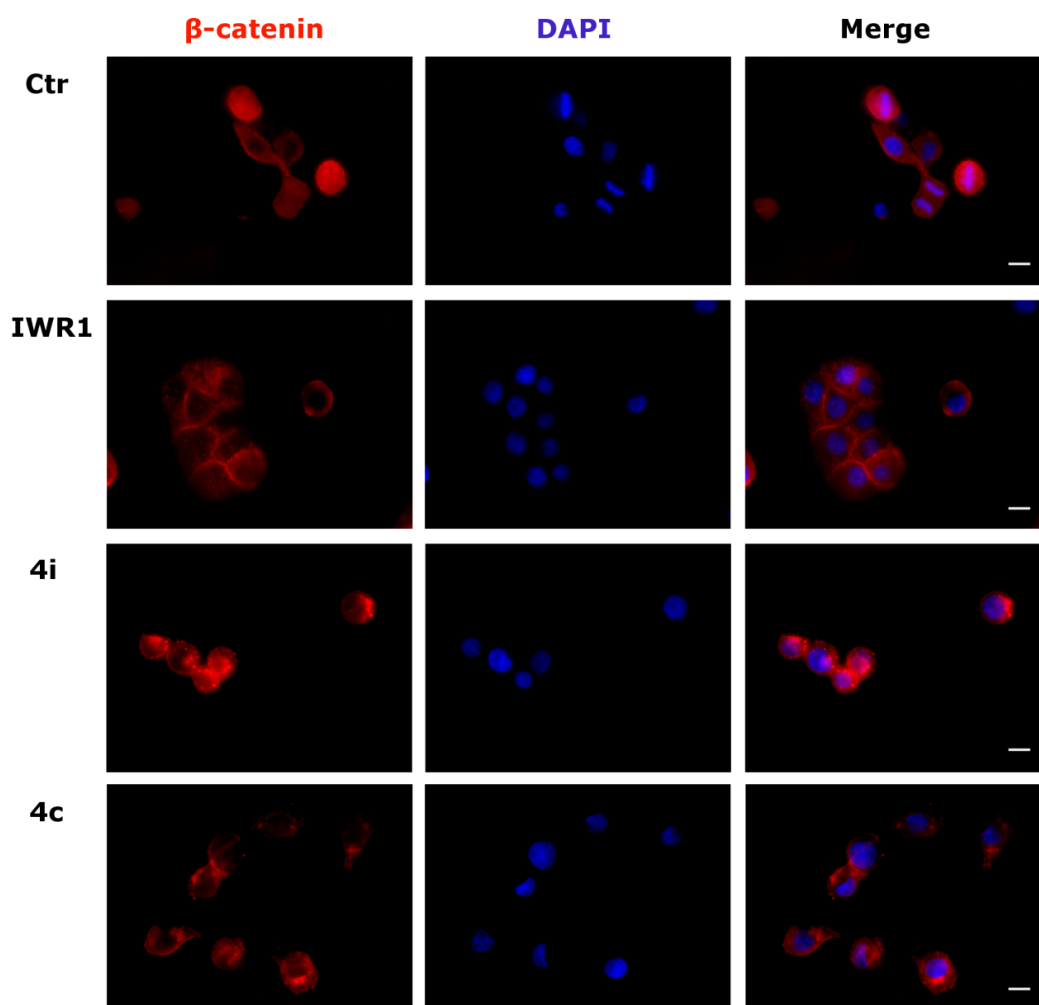
Figure 4. Representative images of HT-29 cells treated with the indicated compounds at 25µM for 24hours. Immunostaining was performed for β-catenin (red), and with DAPI to stain the nuclei (blue). Pictures were acquired by fluorescent microscope using a 60x objective (Bar=100µm).
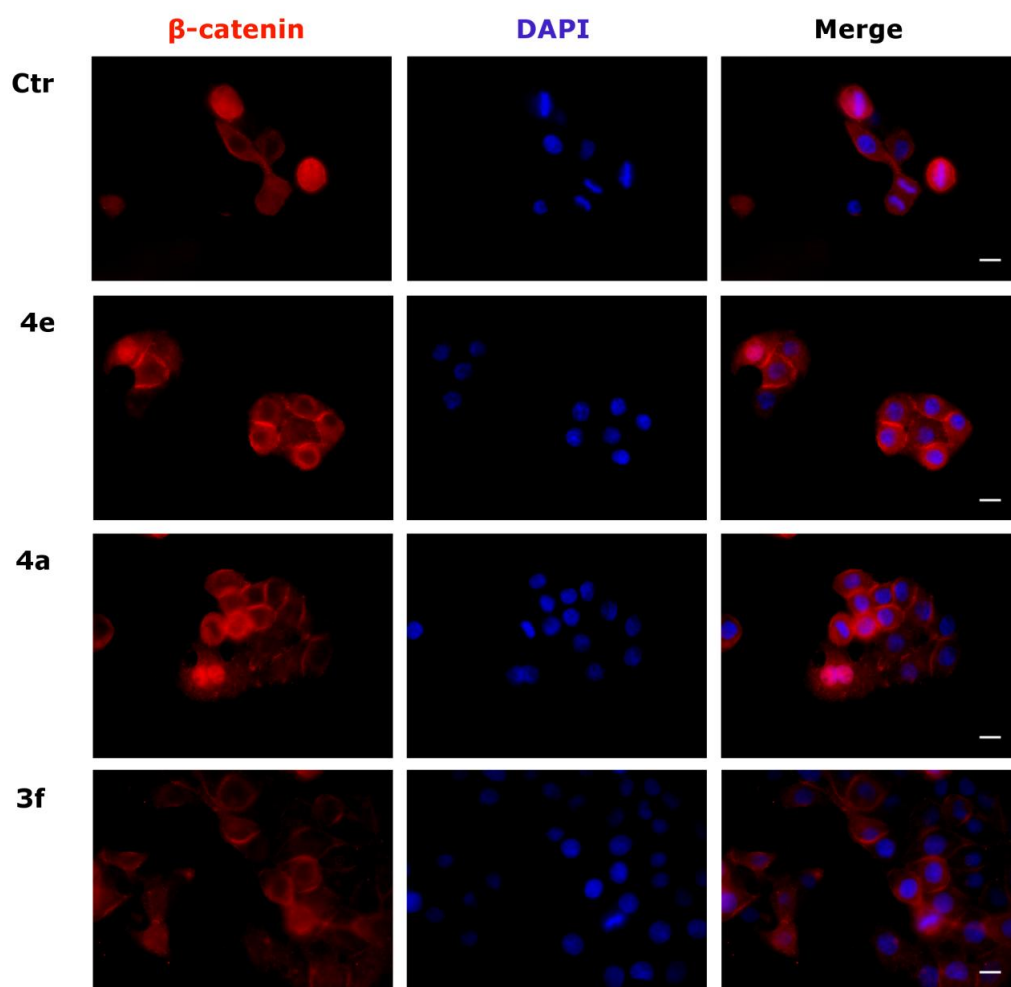
Figure 4b. Representative images of HT-29 cells treated with the indicated compounds at 25μM for 24hours. β-catenin (red) when it is detectable into the nucleus, otherwise it is localized in the cytoplasm. DAPI stained the nuclei (blue). Pictures were acquired by fluorescent microscope using a 60x objective (Bar=100μm).

4c and 4i compounds negatively modulated the downstream Wnt/β-catenin targets cyclin D1, cyclin B1 and c-myc

Cyclin D1 is a β-catenin direct target gene, required for G1/S transition, in cell cycle regulation, and involved in proliferation process. We investigated its regulation through Western blot analysis (Figure 3), and we observed a strong impairment in protein levels after **3f**, **4c**, and **4i** treatment. Cyclin B1 is highly expressed in the majority of colorectal cancers[254], may promote carcinogenesis and later metastasis to lymph nodes[255]. It is essential for the transition from G2 phase to mitosis and it is linked to a high rate of cell proliferation. Also in this case a strong downregulation of cyclin B1 expression was noted by **3f**, **4c**, and **4i**. In this way, both inhibition of cyclin D1 and cyclin B1 could contribute to reduce cell growth induced by the compounds. To further evaluate the consequence of cyclins downregulation we analyzed the effect of the compounds on cell cycle in HT-29 cells. As showed in Figure 5, compound **4i** but not **3f** and **4c**, induced a significant accumulation in G1 along with a reduction of both S and G2/M phase. These results are in well agreement with the reduction of cyclin D1 and the remarkable increase of p21 (see Figure 3).

Another important gene directly transcribed by β-catenin after Wnt signaling activation is c-myc, an oncogenic transcription factor. As shown in Figure 2, mRNA expression was not significantly modified by the selected compounds. On the contrary, in Western blot (Figure 3), the c-myc protein migrated as two bands. The upper band is probably the phosphorylated and inactive form whereas the lower band is the unphosphorylated and activated form of the protein[256]. Interestingly, with **4i**, **4c** and **3f**, the lower band disappeared while the upper band remain substantially unmodified except for **4i** in which we observed a slight increase.
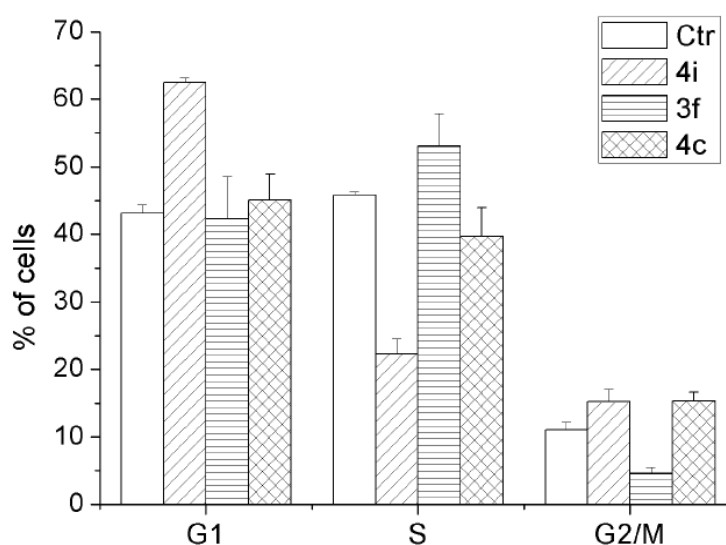
Figure 5. Cell cycle analysis after 24hours of treatment with the indicated compounds at the concentration of 25µM in HT-29. Significative effects were detectable for **4i** compound which arrested cell cycle in G1 and decreased S phase. Data are expressed as mean ± SEM of three independent experiments.*p<0.01 vs control cells.

4c and 4i acted as WNT inhibitors in vivo zebrafish models

We investigated the effects on Wnt/β-catenin pathway also *in vivo*, using a Wnt-reporter zebrafish model, in order to explore the TCF/LEF functions[257]. These transgenic animals expressed a fluorescent reporter (GFP) under the control of Wnt-responsive promoters, and they showed high levels of signal in embryonic head and intestine. Therefore Wnt/β-catenin signaling deregulation is easily detectable by fluorescence reduction. At 96hours post fertilization, zebrafish were maintained in E3 medium in which the compounds were solubilized and treated for 7 days at

different concentrations, to determine the survival rate. As shown in Figure 6 (panel A) compounds **2d** and **4c** showed high toxicity in the concentration range 5-25μM while at 1μM they did not appear toxic. On the contrary, compound **4i**, showed high mortality only at the highest concentration used (25μM). On the basis of these results we set the concentration at which we investigated the GFP signal after 72hours of treatment. The representative images concerning these experiments are reported in Figure 6 (panels B-C). In well agreement with Wnt inhibitory activity in BAT-LUX system **4c** and **4i** represent the most active compounds *in vivo*, and they strongly reduced the TCF/LEF transcription, in the intestinal zone. In Figure 6 (panel B), bright field images demonstrated as larvae treated with **4i** compound developed pericardial edema and dysmorphic craniofacial features. These peculiarities were described in embryos carrying null mutations in LEF1/TCF4 and they are typical in cases where WNT/β-catenin cascade is inhibited. Moreover, as reported in the magnified fluorescence images of intestine (Figure 6 panel B), **2d** reduced the expression of TCF/LEF green signal, and the intestine resulted thinner than control, and in **4i** treated, Wnt signal totally disappeared. A GFP signal quantification is depicted in Figure 6 (panel C) in which we can observe that **4i** strongly reduced the fluorescence signal comparable to that of **IWR1**.
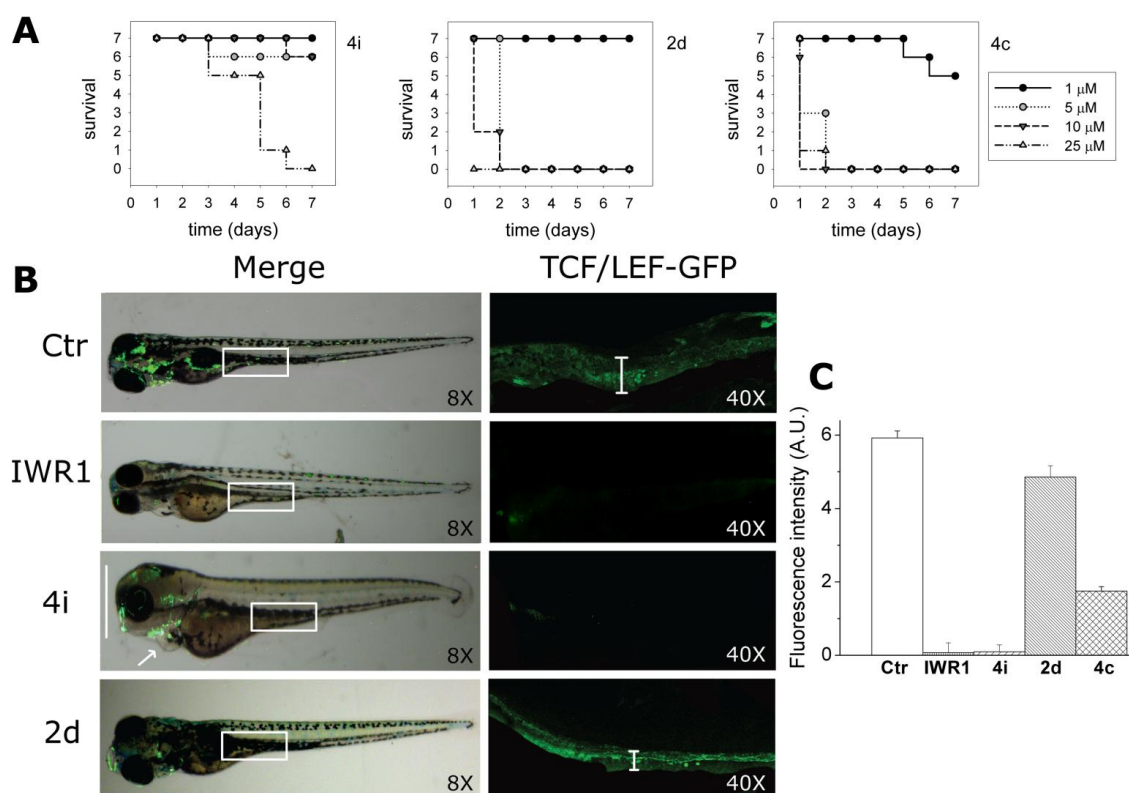
Figure 6. Panel A: survival curves of zebrafish larvae treated for 7 days starting at 72hours post-fertilization. Panel B: representative images of Wnt-reporter zebrafish treated with **IWR1** and **4i** at 10μM, **2d** and **4c** at 1μM for 72hours, starting at 24hours after fertilization. On the left side, bright field images, merged with GFP signal, were reported. The white rectangles indicate the portions reported on the right side, representing the intestinal zone. In control larvae TCF/LEF-GFP signal, characterizing the intestine, is wide and strewn, while treated zebrafish by **2d** showed a thinner intestine. After **4i** treatment the reporter signal totally disappeared, and the fish phenotype was characterized by pericardial edema (indicated by the arrow), and craniofacial dysmorphism. Panel C: the graph summarized the fluorescence intensity measured in the intestinal zone, after compounds treatment. Data represented as mean ± SEM of three independent experiments.

Proposed mechanism of action for compound 4i

4i compound was the most antiproliferative compound in tested cell lines, and it was able to inactivate c-myc. Moreover, after **4i** treatment, AP4 mRNA is strongly reduced and p21 is highly expressed, as shown in Figure 2 and Figure 3 respectively.

Therefore **4i** compound inhibits Wnt/β-catenin cascade, leading not only to cyclin D1 repression, but also to c-myc inactivation, and consequently to AP4 inhibition and p21 upregulation. This hypothesis is supported by the findings of Jung and Hermeking[258] which reported that c-myc directly regulates the expression of AP4, a transcription factor which binds to recognition motifs located in the vicinity of the p21 promoter mediating transcriptional repression of p21 itself[259]. The resulting event is an impairment of cellular proliferation. Finally cyclin D1 and p21 stimulated cell cycle arrest in G1 and an antiproliferative effect, confirmed by S phase reduction (Figure 5). The hypothetical molecular pathway deregulated after **4i** treatment is summarized in Figure 7.
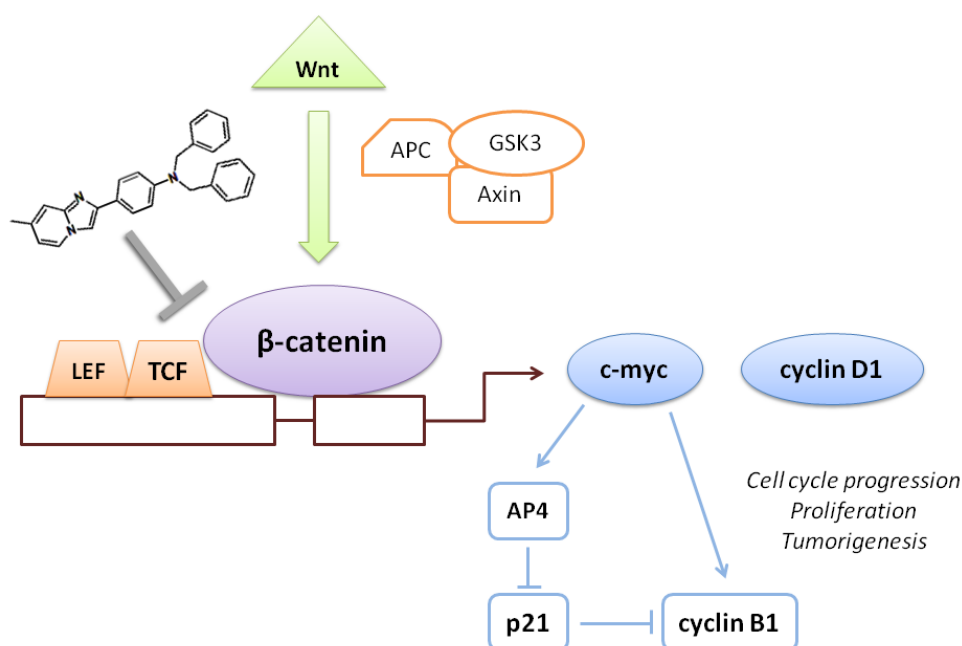
Figure 7. Schematic representation of Wnt signaling pathway and its downstream molecules probably involved in response to **4i** treatment. β-catenin target genes are downregulated after **4i** treatment, independently to GSK-3 action. c-myc deregulation leads to p21 upregulation and cyclin B1 reduction, resulting in cell cycle arrest and inhibited proliferation.

3.3.1.4. Conclusion

Among the synthesized compounds, we found that **4i** repressed Wnt signaling downstream of β-catenin and efficaciously inhibited the proliferation of selected cancer cell lines. The remarkable inhibition of our compounds on Wnt/β-catenin targets suggests that these derivatives may downregulate Wnt signaling independently by β-catenin levels. Nevertheless Wnt target genes activation, like c-myc and cyclin D1, is severely impaired after treatment, leading to a reduced proliferation. Preliminary results have also indicated that these compounds are ineffective in normal cells suggesting that they could be selective toward cancer cells endowed with deregulation of the Wnt pathway.

The Wnt-reporter zebrafish model provides an excellent experimental mean to test the ability of a compound to modulate Wnt signaling *in vivo*. The results obtained in this model clearly showed that our compounds are strongly inhibitors of the Wnt signaling, with an activity comparable to that of reference compound **IWR1**, suggesting that these compounds hold promise for potential use in the therapy of Wnt driven cancers but also for other Wnt related diseases. Studies are currently underway to identify the direct target(s) of these promising new molecules.

3.4. CONCLUSIONS

The screening of new molecules which target the Wnt/β-catenin pathway is an exciting field for the broad use in numerous diseases. Wnt signals are key proteins regulating both embryonic development and adult tissues regeneration, so alterations in signal transduction lead to aberrant processes such as tumorigenesis. Colorectal cancers represent tumors which are common in the Western world, and although many advances in the colon carcinogenesis were discovered, resistance mechanisms and patient relapses occur. New therapeutic approaches are required to overcome these phenomena, and several studies for the optimization of small molecules are currently under developing.

The Wnt signaling pathways has been well studied, but some molecular mechanisms still should be explained. However, a wide series of molecular targets has been identified, and numerous upstream/downstream inhibitors of the Wnt cascade have been found. Some pharmacological strategies comprehend recombinant proteins, but the use of small molecules can improve the efficacy of delivery and the costs of production.

Here we studied a series of small molecules, in order to identify new structures able to significantly inhibit the Wnt pathway. The imidazo[1,2-*a*]pyridine structures showed a good activity, comparable to that of the reference compounds (**IWR1** and **ICG001**), in inducing Wnt repression. *In vitro* experiments on colon cancer cell lines demonstrated as our compounds reduced proliferation and decreased β-catenin translocation into the nucleus. TCF-1/4 co-factors, as well as target genes such as cyclin D1 and c-myc were downregulated by the treatment. The inhibition of the Wnt pathway was confirmed also *in vivo* in Wnt-reporter zebrafish models, where β-catenin transcriptional activity was significantly reduced. Moreover, the treatment

with the most active compound (**4i**) gave rise to the appearance of a craniofacial dysmorphism, a typical phenotype related to embryonic development defects, due to Wnt signaling repression.

Although some studies to find the direct target of these structures are underway, these new small molecules have strong inhibitory effects on the Wnt/β-catenin signaling pathway, and are promising for cancer therapy.

MATERIALS AND METHODS

Drugs

TR-644, **TR-764**, **3b** were synthesized as previously described[63,79,132]. Combretastatin A4 (**CA-4**) and **CA-4P** were synthesized as described[112,260,261]. Noscapine derivatives were newly synthesized with the Suzuki cross-coupling method, by Dott. Attila Sipos at University of Debrecen, Hungary. Imidazo[1,2-*a*]pyridine were newly synthesized by Prof. Barbara Cosimelli, at University of Napoli, Italy.

Stock solutions (10mM) of the different compounds were obtained by dissolving them in DMSO.

Molecular modeling

All molecular modeling studies were performed on a MacPro dual 2.66GHz Xeon running Ubuntu 10. The tubulin structure was downloaded from the PDB data bank (http://www.rcsb.org/ - PDB code: 3HKC)[262]. Hydrogen atoms were added to the protein, using the Protonate3D function of Molecular Operating Environment (MOE)[263]. Ligand structures were built with MOE and minimized using the MMFF94x forcefield until a RMSD gradient of 0.05kcal mol^{-1} Å^{-1} was reached. The docking simulations were performed using PLANTS[264].

Cell cultures

HUVECs were prepared from human humbelical cord veins, as previously described[265], and they were maintained in M200 medium additioned by LSGS (Low Serum Growth Supplement), containing FBS, Hydrocortisone, hEGF, bFGF, heparin, gentamycin/amphotericin (Life technologies). Once confluent, the cells were

detached by trypsin–EDTA solution and used in experiments from the first to sixth passages.

Human promyelocytic leukemia (HL-60), human T-cell (Jurkat) and B-cell leukemia cell lines (SEM and RS4;11) were grown in RPMI-1640 medium (Gibco). Breast adenocarcinoma (MCF-7), human non-small cell lung carcinoma (A549), human cervix carcinoma (HeLa), human colon adenocarcinoma (HT-29), human hepatocellular liver carcinoma (HepG2), ovarian carcinoma (IGROV-1) cell lines were grown in DMEM medium (Gibco). Both media were supplemented with 115units/mL of penicillin G (Gibco), 115µg/mL of streptomycin (Invitrogen) and 10% fetal bovine serum (Invitrogen). LoVo[Doxo] cells are a doxorubicin resistant subclone of LoVo cells[116] and were grown in complete Ham's F12 medium supplemented with doxorubicin (0.1µg/mL). CEM[Vbl-100] cells are a multidrug-resistant line selected against vinblastine[117]. A549-T12 cells are a non-small cell lung carcinoma line exhibiting resistance to taxol[118]. They were grown in complete DMEM medium supplemented with taxol (12nM).

BL6-B16 murine melanoma cells were maintained in DMEM supplemented with 10% fetal calf serum (FCS).

Antiproliferative assay (MTT test)

Individual wells of a 96-well tissue culture microtiter plate were inoculated with 100 µL of complete medium containing 8×10^3 cells. The plates were incubated at 37°C in a humidified 5% CO_2 incubator for 18hours prior to the experiments. After medium removal, 100µL of fresh medium containing the test compound at different concentrations was added to each well and incubated at 37°C for 72hours. The percentage of DMSO in the medium never exceeded 0.25%. Cell viability was assayed by the 3-(4,5-dimethylthiazol-2-yl)-2,5-diphenyl tetrazolium bromide (MTT,

184

Sigma-Aldrich) test as previously described[124]. The IC_{50} was defined as the compound concentration required to inhibit cell proliferation by 50%.

Cytotoxicity assay (trypan blue)

Cytotoxicity assay were carried out with trypan blue test as described previously[266]. Cells were treated with the compounds at different concentrations and times. After incubation time, an aliquot of cell suspension was taken and marked with trypan blue. Cells were counted with Burker/Neubauer chamber under an optical microscope.

Evaluation of mitotic index

The Burkitt lymphoma CA46 cells were grown in RPMI 1640 medium supplemented with 17% fetal bovine serum and 2mM l-glutamine at 37°C 5%CO_2 atmosphere. The mitotic index in the Burkitt cell cultures was determined at 16hours, the time that produces a near-maximal value after treatment with antitubulin drugs. About 4.5mL of cell culture medium was centrifuged at 1000 rpm for 1min. The pelleted cells were resuspended in 5mL of phosphate-buffered saline at room temperature, and the cells were harvested by centrifuging the suspension as before. The cell pellet was suspended in 0.5mL of half-strength phosphate-buffered saline, and the cells were allowed to swell for 10min. The cells were then fixed by adding 6mL of 0.5% acetic acid-1.5% ethanol. After 30min, the cells were harvested by centrifuging as before. The cells were resuspended in 25% acetic acid/75% ethanol, and a droplet of the cell suspension was spread on the slide. The slide was air-dried and stained with Giemsa. The slide was examined under a light microscope, with mitotic cells defined as those with condensed chromosomes and no nuclear membrane. At least 200 cells were counted for each condition examined.

Colony forming assay

HUVECs were plated at 1×10^3 cells/well in six-well plates to provide an optimal counting density. Cells were treated with compounds at different concentration for 24hours. After 24hours, medium was replaced with fresh one and cells were cultured for 1-2 weeks until well-defined colonies had formed (replacing culture medium every 2 to 3 days). Cells were briefly washed with 0.9% saline solution and stained with 0.5% crystal violet in 20% methanol. Colonies of ≥50 cells were then counted visually.

Effects on tubulin polymerization and on colchicine binding to tubulin

To evaluate the effect of the compounds on tubulin assembly *in vitro*[119], varying concentrations of compounds were preincubated with 10μM bovine brain tubulin in glutamate buffer at 30 ℃ and then cooled to 0 ℃. After addition of 0.4mM GTP, the mixtures were transferred to 0°C cuvettes in a recording spectrophotometer and warmed to 30°C. Tubulin assembly was followed turbidimetrically at 350nm. The IC_{50} was defined as the compound concentration that inhibited the extent of assembly by 50% after a 20min incubation. The capacity of the test compounds to inhibit colchicine binding to tubulin was measured as described[120], except that the reaction mixtures contained 1μM tubulin, 5μM [^{3}H]colchicine and 5μM test compound.

Flow cytometric analysis of cell cycle distribution

For flow cytometric analysis of DNA content, 5×10^5 cells were treated with different concentrations of the test compounds. After the incubation period, the cells were collected, centrifuged and fixed with ice-cold ethanol (70%). The cells were then treated with lysis buffer containing RNAse A and 0.1% Triton X-100 and stained with propidium iodide (PI). Samples were analyzed on a Cytomic FC500 flow

cytometer (Beckman Coulter). DNA histograms were analyzed using MultiCycle® for Windows (Phoenix Flow Systems).

Annexin-V assay for testing apoptosis

Surface exposure of phosphatidyl serine (PS) on apoptotic cells was measured by flow cytometry with a Coulter Cytomics FC500 (Beckman Coulter) by adding annexin-V-FITC to cells according to the manufacturer's instructions (Annexin-V Fluos, Roche Diagnostic). Simultaneously, the cells were stained with PI. Excitation was set at 488nm, and the emission filters were at 525nm and 585nm, respectively, for FITC and PI.

Assessment of mitochondrial changes

The mitochondrial membrane potential was measured with the fluorescent lipophilic cationic 5,5',6,6'-tetrachlo-1,1',3,3'-tetraethylbenzimidazolcarbocyanine dye (JC-1) (Molecular Probes) by flow cytometry, as described previously[124]. The production of reactive oxygen species (ROS) was measured by flow cytometry using either hydroethidine (HE) (Molecular Probes) or 2,7-dichlorodihydrofluorescein diacetate (H_2DCFDA) (Molecular Probes). The fluorescence was recorded with the flow cytometer, using as excitation wavelength 488nm and emission at 585nm and 530nm for HE and H_2DCFDA, respectively, as previously described[267].

Luciferase reporter gene assay

Cells were transfected with the luciferase reporter plasmid BAT-LUX (kindly provided by Prof. Stefano Piccolo, University of Padova) which codified for LEF/TCF transcription factors. BAT-LUX plasmid constitutes seven repeats of TCF binding element and siamois minimal promoter, cloned upstream of Luciferase gene in pGL3 backbone[268]. Cells (1.4 x 10^4) were transfected using HiPerFect Transfection

Reagent (Qiagen) with 1μg BAT-LUX construct and 1μg Renilla vector as an internal transfection control, and incubated with various concentrations of selected compounds at 37°C. After 24hours, the cells were lysed in 50μL passive lysis buffer (Promega). Firefly luciferase and Renilla luciferase activity were determined using the Dual-Glo Luciferase Assay System (Promega). Results are expressed as the mean of normalized ratios of firefly luciferase activity and Renilla luciferase activity measurements.

Quantitative real-time RT-PCR

To quantify Axin2, TCF4, c-myc, AP4 mRNA levels we designed real-time RT-PCR assays, using GUS as reference gene. Total RNA was isolated using TRIzol (Invitrogen) from cells treated for 24hours with the compounds. 1μg of RNA was transcribed using the Superscript II system (Invitrogen-Gibco) in 25μL final volume according to the manufacturer's instructions. Quantitative real-time PCR (qRT-PCR) was performed with 1μL cDNA in 20μL using the Sybr Green method (Invitrogen-Gibco) and analyzed on an ABI PRISM 7900HT Sequence detection system (Applied Biosystems).

The oligonucleotides to amplify mRNA fragments were Axin2 (forward 5'-CAAGGGCCAGGTCACCAA, reverse 3'-CCCCCAACCCATCTTCGT), TCF4 (forward 5'-GACGACAAGAAGGATATCAAATCA, reverse 3'-ATCCTCCGCTCCTTCTCAC), c-myc (forward 5'-AGGACCCGCTTCTCTGAAA, reverse 3'-TTCCTGTTGGTGAAGCTAACG), AP4 (forward 5'-GAGCCAGCCTGGGATTGTC, reverse 3'-GTGCTTAAAGGAGAAAGAAGAAAACC) and GUS (forward 5'-GAAAATATTGTGGTTGGAGAGC, reverse 3'-CGAGTGAAGATCCCCTTTTTA). After normalization on GUS, expression regulation was calculated respect to untreated cells.

188

Western Blot Analysis

Cells were incubated in the presence of test compounds and, after different times, were collected, centrifuged and washed two times with ice cold phosphate-buffered saline (PBS). The pellet was resuspended in lysis buffer. After the cells were lysed on ice for 30min, lysates were centrifuged at 15000 x g at 4°C for 10min. The protein concentration in the supernatant was determined using BCA protein assay reagents (Pierce, Italy). Equal amounts of protein (10μg) were resolved using sodium dodecyl sulfate polyacrylamide gel electrophoresis (SDS-PAGE) (7.5-15% acrylamide gels) and transferred to a PVDF Hybond-p membrane (GE Healthcare). Membranes were blocked with I-block (Tropix), the membrane being gently rotated for 3hours at room temperature. Membranes were incubated overnight at 4°C with primary antibodies against, Bcl-2, cleaved PARP, cdc25C, Bax, phospho-histone γH2AX, cdc2, cdc2^{Tyr15}, cdc25c, TCF-1, β-catenin, β-catenin$^{Ser33/37/Thr41}$, GSK-3α/β$^{Ser21/9}$, p21$^{Waf1/Cip1}$ (DCS60), cyclin D1, Src family^{Tyr416} (Cell Signaling), c-myc (Calbiochem), cyclin B, FAK^{Tyr397} (BD Biosciences), VE-cadherin^{Tyr658}, β-catenin^{Tyr142} (Abcam), FAK (C-20), Src-1 (M341) (Santa Cruz), HIF-1α (GeneTex), β-actin (Sigma-Aldrich). Membranes were next incubated with peroxidase-labeled goat anti-rabbit IgG (1:100000, Sigma-Aldrich) or peroxidase-labeled goat anti-mouse IgG (1:100000, Sigma-Aldrich) for 1hour. All membranes were visualized using ECL Advance (GE Healthcare) and exposed to Hyperfilm MP (GE Healthcare). To ensure equal protein loading, each membrane was stripped and reprobed with anti-β-actin antibody.

Immunofluorescence analysis

Cells were fixed in cold 4% formaldehyde for 15min, rinsed and stored prior to analysis. Primary antibody staining was performed for α-tubulin (Millipore), β-tubulin (Sigma-Aldrich), β-catenin, FAK^{Tyr397} (BD Biosciences), VE-cadherin^{Tyr658}

(Abcam), PCM1 (Abnova). After incubation, cells were washed and incubated with an Alexa conjugated secondary antibody (1:2000, Life Technologies).

For F-actin visualization the cells were fixed as above and stained with phalloidin-tetramethylrhodamine B isothiocyanate conjugate (Sigma-Aldrich).

Cells were counterstained with 4',6-diamidin-2-fenilindole (DAPI) (Sigma-Aldrich). Images were obtained on a video-confocal microscope (Vico, Eclipse Ti80, Nikon), equipped with a digital camera.

Motility assay

Motility assay for HUVECs was based on "scratch" wounding of a confluent monolayer[131]. Briefly, HUVECs (1×10^5) were seeded onto 0.1% collagen type I (BD Biosciences)-coated twelve well plates in complete medium until a confluent monolayer was formed. The cells were scratch wounded using a pipette tip and wells were washed with PBS to remove the undetached cells. Then, the cells were treated with the test compounds and at different times from the scratch, the cells were photographed under a light microscope (10x magnification). At all indicated time points, the wound width was measured in four areas and compared with the initial width.

Endothelial cell vessel formation on Matrigel matrix

Matrigel matrix (Basement membrane matrix, BD Biosciences) was kept at 4°C for 3hours. 230μL of Matrigel were added to each well of a 24-well plate. After gelling at 37°C for 30min, gels were overlaid with 500μL of medium containing 6×10^4 HUVEC cells, incubated over Matrigel for 6hours to allow the capillary tubes to form. Different concentrations of compound were added in the cultures and incubated for different times and the disappearance of existing vasculature was monitored and photographed (five fields for each well: the four quadrants and the center) at a 10x magnification. Phase contrast images were recorded using a digital camera and save

as TIFF files. Image analysis was carried out using the ImageJ image analysis software and the following dimensional parameters (percent area covered by HUVECs and total length of HUVECs network per field), and topological parameters (number of meshes and branching points per fields) were estimated[269]. Values were expressed as percent change from control cultures grown with complete medium.

Endothelial cell permeability assay

HUVEC cells were seeded at a density of 3 x 10^5 cells per well into 24-well cell culture inserts (1.0µm, Falcon) and incubated for 24hours to allow a confluent cell monolayer to form. Drugs at varying concentrations were added to the cells at the upper chamber and incubated for different times at 37°C. At the same time, FITC-dextran (Fluorescein Isothiocyanate-dextran 40kDa, Sigma-Aldrich) was added to the upper chamber. The effects of the compounds on HUVEC monolayer permeability were monitored using a fluorescent plate reader (Victor^3 Perkin Elmer) as measured by increased fluorescent signal in the lower chamber as a function of time.

Cell adhesion assay

HUVECs were seeded in six-well plates to provide an optimal density and treated with compounds at different concentrations. After 24hours, cells were trypsinized and plated in quadruplicate on a 96-well plate at 5x10^4 cells per well. Cells were allowed to attach for 30min at 37°C, and then unattached cells were gently removed. Adherent cells were washed three times with PBS and incubated with (3-(4,5-dimethylthiazol-2-yl)-2,5-diphenyl tetrazolium bromide (Sigma-Aldrich). MTT test was performed as previously described[124] to quantify the attached cells.

CAM assay in fertilized chicken eggs

Alginate pellets containing the compounds were grafted on the chorioallantoic membrane (CAM) of fertilized chicken eggs at day 11[270]. After 72hours new blood vessels converging toward the implant were counted at 5x magnification under a stereomicroscope.

3b antitumor activity *in vivo*

Four week old female BALB/c-nu nude mice (15–18 g) were obtained from Shanghai SLAC Laboratory Animal Co., Ltd (Shanghai, China). The animals were maintained under specific pathogen-free conditions with food and water supplied ad libitum in Zhejiang University of Traditional Chinese Medicine Laboratory Animal Center. Human colon adenocarcinoma HT-29 cells in logarithmic growth phase were resuspended in RPMI 1640 without fetal bovine serum at 1×10^7cells/mL and inoculated (0.2mL) in the hypodermis of the pars dorsalis of each mouse. Once the HT-29 xenografts reached a size of $\sim$300mm^3, twelve mice were randomly assigned to two groups: For the first group, compound **3b** was prepared in DMSO and injected intraperitoneally at volumes of 0.01mL/g body weight to give a dose of 100mg/kg to each mouse. The compound was administered three times a week for one week. After completing the treatment schedule and the evaluation period, tumor-bearing mice were euthanized. Tumor volume was calculated by the formula: $V=(L \times W^2)/2$ where L is the length and W is the width of the tumor nodules measured by vernier caliper. The study was approved by the Institutional Animal Ethical Committee of the Second Affiliated Hospital, School of Medicine, Zhejiang University (PRC).

Tumorigenesis studies (TR-644, TR-764, CA-4P)

Procedures involving animals and their care conformed with institutional guidelines that comply with national and international laws and policies (EEC Council Directive 86/609, OJ L 358, 12 December 1987). Six week old C57BL/6 mice (Charles River,

192

Calco, Italy) were injected s.c. into the dorsolateral flank with 10^5 BL6-B16 murine melanoma cells in 200μL of total volume of PBS. When tumor volume reached 300mm^3 of volume, animals were treated i.p with 50μL of the compounds dissolved in DMSO. Twenty-four hours later tumors where harvested, embedded in OCT-compound (Bio-Optica) and immediately frozen in liquid nitrogen for immunohistochemical analysis.

Immunohistochemistry and immunofluorescence of tumor tissues

Excised tumors were cut with a cryostat in 4-5μm sections. Immunohistochemistry was performed by staining samples with rat anti-mouse CD31 antibody (1:200; BD Biosciences) and biotinylated goat anti-rat secondary antibody (1:100; BD Biosciences). The detection of tumor vasculature was performed using HRP-conjugated streptavidin (1:500; Jackson ImmunoResearch Laboratories). The microvessel density (MVD) was evaluated by counting the number of vessels in 5 fields per section, using a 40x objective. For subsequent experiments, samples were formalin-fixed and paraffin embedded and then stained with mouse primary antibody against proliferating cell nuclear antigen PCNA (1:100; Santa Cruz) and Alexa-Fluor secondary antibody (1:2000, Life technologies, Monza, Italy). Proliferating cells were determined by counting the number of PCNA-positive cells on DAPI-positive cells (values expressed as percent of PCNA+ cells/DAPI+ cells), in 3 fields for each section, with a 40x objective. A staining with hematoxylin and eosin (HE) was also performed to visualize the histological features of tumors. All specimens were viewed under a video-confocal microscope (Vico, Ecliple Ti80, Nikon), equipped with a digital camera, and images were captured using a 10x objective.

In vivo treatment on zebrafish model

We used wild type zebrafish, raised and maintained under standard conditions, to test our chemical compounds. Larvae were treated at 72hours post-fertilization, until 7 days after treatment, in order to investigate compound toxicity and the survival rate. The compounds were solubilized in E3 medium, replaced every day with new medium with containing compounds. The effect on Wnt/β-catenin signaling was investigated using TCF/LEF-GFP reporter zebrafish. They were treated at 24hours post-fertilization, for 72hours. Reporter expression was visualized using the fluorescent microscope (Nikon SMZ 1500) with a GFP filter and objective 8x. 40x images were captured by a confocal microscope (Nikon A1R-A1). The quantification of fluorescence emission was carried out by ImageJ software.

Statistical Analysis

Unless indicated otherwise, results are presented as mean ± S.E.M. The differences between different treatments were analyzed using the two-sided Student's *t* test. P values lower than 0.05 were considered significant.

ABBREVIATIONS

AI	angiogenic inhibitor
ANG	angiopoietin
APC	adenomatous polyposis coli
ATP	adenosine triphosphate
Bcl-2	B-cell lymphoma 2
BMP	bone morphogenetic protein
CA-4	combretastatin-A4
CAM	chicken embryo chorioallantoic membrane
CBP	cyclic AMP response element-binding protein
Cdk	cyclin-dependent kinase
CK1	casein kinase 1
DCFDA	dichlorodihydrofluorescein diacetate
DVL	dishevelled
ECM	extracellular matrix
EGFR	epidermal growth factor receptor
FAK	focal adhesion kinase
bFGF	basal fibroblast growth factor
GFP	green fluorescent protein
GSK3	glycogen synthase kinase 3
GTP	guanosine triphosphate
HE	hydroethidine
HIF	hypoxia-inducible factor
HUVEC	human umbilical endothelial cell
JNK	c-Jun N-terminal kinase
LEF	lymphoid enhancer factor

MAPK	mitogen-activated protein kinases
Mcl-1	myeloid cell leukemia-1
mTOR	mammalian target of rapamycin
NFAT	nuclear factor associated with T cells
PARP	poly ADP-ribose polymerase
PBL	peripheral blood lymphocytes
PCM1	pericentriolar material 1
PCP	planar cell polarity
PDGF	platelet-derived growth factor
PHA	phytohaemagglutinin
PI	propidium iodide
PI3K	phosphoinositide 3-kinase
PKC	protein kinase C
ROS	reactive oxygen species
SAC	spindle assembly checkpoint
SRC	steroid receptor coactivator
TBA	tubulin binding agent
TCF	T cell factor
TGF-β	transforming growth factor-beta
TKI	tyrosine kinase inhibitor
TNF-α	tumor necrosis factor-alpha
VDA	vascular disrupting agent
VEGF	vascular endothelial growth factor

REFERENCES

1. Marcelo, K., Goldie, L. & Hirschi, K. Regulation of Endothelial Cell Differentiation and Specification. *Circ. Res.* **112,** 1272–87 (2013).

2. Carmeliet, P. & Jain, R. K. Molecular mechanisms and clinical applications of angiogenesis. *Nature* **473,** 298–307 (2011).

3. Conway, E. M., Collen, D. & Carmeliet, P. Molecular mechanisms of blood vessel growth. *Cardiovasc. Res.* **49,** 507–21 (2001).

4. Kushner, E. & Bautch, V. Building blood vessels in development and disease. *Curr. Opin. Hematol.* **20,** 231–6 (2013).

5. Ucuzian, A. a, Gassman, A. a, East, A. T. & Greisler, H. P. Molecular mediators of angiogenesis. *J. Burn Care Res.* **31,** 158–75 (2010).

6. Koch, S. & Claesson-Welsh, L. Signal transduction by vascular endothelial growth factor receptors. *Cold Spring Harb. Perspect. Med.* **2,** 169–83 (2012).

7. Mettouchi, A. The role of extracellular matrix in vascular branching morphogenesis. *Cell Adh. Migr.* **6,** 528–34 (2012).

8. Buganza Tepole, A. & Kuhl, E. Systems-based approaches toward wound healing. *Pediatr. Res.* **73,** 553–63 (2013).

9. Senger, D. R. & Davis, G. E. Angiogenesis. *Cold Spring Harb. Perspect. Biol.* **3,** (2011).

10. Rüegg, C. & Alghisi, G. C. Vascular integrins: therapeutic and imaging targets of tumor angiogenesis. *Recent Results Cancer Res.* **180,** 83–101 (2010).

11. Zhao, X. & Guan, J. Focal adhesion kinase and its signaling pathways in cell migration and angiogenesis. *Adv. Drug Deliv. Rev.* **63,** 610–5 (2011).

12. Tomar, A., Lim, S., Lim, Y. & Schlaepfer, D. A FAK-p120RasGAP-p190RhoGAP complex regulates polarity in migrating cells. *J. Cell Sci.* **122,** 1852–1862 (2009).

13. Bryan, B. a & D'Amore, P. a. What tangled webs they weave: Rho-GTPase control of angiogenesis. *Cell. Mol. Life Sci.* **64,** 2053–65 (2007).

14. Thurston, G. & Kitajewski, J. VEGF and Delta-Notch: interacting signalling pathways in tumour angiogenesis. *Br. J. Cancer* **99,** 1204–9 (2008).

15. Ridgway, J. *et al.* Inhibition of Dll4 signalling inhibits tumour growth by deregulating angiogenesis. *Nature* **444,** 1083–7 (2006).

16. Dejana, E. & Vestweber, D. The role of VE-cadherin in vascular morphogenesis and permeability control. *Prog. Mol. Biol. Transl. Sci.* **116,** 119–44 (2013).

17. Axnick, J. & Lammert, E. Vascular lumen formation. *Curr. Opin. Hematol.* **19,** 192–8 (2012).

18. Sullivan, D. C. & Bicknell, R. New molecular pathways in angiogenesis. *Br. J. Cancer* **89,** 228–31 (2003).

19. Folkman, J. & Hanahan, D. Switch to the angiogenic phenotype during tumorigenesis. *Princess Takamatsu Symp.* **22,** 339–47 (1991).

20. Raica, M., Cimpean, A. M. & Ribatti, D. Angiogenesis in pre-malignant conditions. *Eur. J. Cancer* **45,** 1924–34 (2009).

21. Folkman, J. Angiogenesis: an organizing principle for drug discovery? *Nat. Rev. Drug Discov.* **6,** 273–286 (2007).

22. Baeriswyl, V. & Christofori, G. The angiogenic switch in carcinogenesis. *Semin. Cancer Biol.* **19,** 329–337 (2009).

23. Siemann, D. The unique characteristics of tumor vasculature and preclinical evidence for its selective disruption by Tumor-Vascular Disrupting Agents. *Cancer Treat. Rev.* **37,** 63–74 (2011).

24. Bergers, G. & Benjamin, L. E. Tumorigenesis and the angiogenic switch. *Nat. Rev. Cancer* **3,** 401–10 (2003).

25. Ribatti, D. & Crivellato, E. "Sprouting angiogenesis", a reappraisal. *Dev. Biol.* **372,** 157–65 (2012).

26. Kume, T. Novel insights into the differential functions of Notch ligands in vascular formation. *J. Angiogenes. Res.* **1,** 8 (2009).

27. Asahara, T. & Kawamoto, A. Endothelial progenitor cells for postnatal vasculogenesis. *Am. J. Physiol. Cell Physiol.* **287,** C572–9 (2004).

28. Djonov, V., Baum, O. & Burri, P. H. Vascular remodeling by intussusceptive angiogenesis. *Cell Tissue Res.* **314,** 107–17 (2003).

29. Makanya, A. N., Hlushchuk, R. & Djonov, V. G. Intussusceptive angiogenesis and its role in vascular morphogenesis, patterning, and remodeling. *Angiogenesis* **12,** 113–23 (2009).

30. Gianni-Barrera, R., Trani, M., Reginato, S. & Banfi, A. To sprout or to split? VEGF, Notch and vascular morphogenesis. *Biochem. Soc. Trans.* **39,** 1644–8 (2011).

31. Leenders, W. P. J., Küsters, B. & de Waal, R. M. W. Vessel co-option: how tumors obtain blood supply in the absence of sprouting angiogenesis. *Endothelium* **9,** 83–7 (2002).

32. Donnem, T. *et al.* Vessel co-option in primary human tumors and metastases: an obstacle to effective anti-angiogenic treatment? *Cancer Med.* **2,** 427–36 (2013).

33. Paulis, Y. W. J., Soetekouw, P. M. M. B., Verheul, H. M. W., Tjan-Heijnen, V. C. G. & Griffioen, A. W. Signalling pathways in vasculogenic mimicry. *Biochim. Biophys. Acta* **1806,** 18–28 (2010).

34. Bussolati, B., Grange, C. & Camussi, G. Tumor exploits alternative strategies to achieve vascularization. *FASEB J.* **25,** 2874–82 (2011).

35. Bunn, H. F. & Poyton, R. O. Oxygen sensing and molecular adaptation to hypoxia. *Physiol. Rev.* **76,** 839–85 (1996).

36. Pugh, C. W. & Ratcliffe, P. J. Regulation of angiogenesis by hypoxia: role of the HIF system. *Nat. Med.* **9,** 677–84 (2003).

37. Semenza, G. L. HIF-1 mediates metabolic responses to intratumoral hypoxia and oncogenic mutations. *J. Clin. Invest.* **123,** 3664–71 (2013).

38. Philip, B., Ito, K., Moreno-Sánchez, R. & Ralph, S. J. HIF expression and the role of hypoxic microenvironments within primary tumours as protective sites driving cancer stem cell renewal and metastatic progression. *Carcinogenesis* **34,** 1699–707 (2013).

39. Cesca, M., Bizzaro, F., Zucchetti, M. & Giavazzi, R. Tumor delivery of chemotherapy combined with inhibitors of angiogenesis and vascular targeting agents. *Front. Oncol.* **3,** 259 (2013).

40. Bellou, S., Pentheroudakis, G., Murphy, C. & Fotsis, T. Anti-Angiogenesis in Cancer Therapy: Hercules And Hydra. *Cancer Lett.* **338,** 219–28 (2013).

41. Cook, K. M. & Figg, W. D. Angiogenesis inhibitors: current strategies and future prospects. *CA. Cancer J. Clin.* **60,** 222–43 (2010).

42. Shojaei, F. & Ferrara, N. Antiangiogenic therapy for cancer: an update. *Cancer J.* **12,** 1095–111 (2007).

43. Siemann, D., Bibby, M. & Dark, G. Differentiation and definition of vascular-targeted therapies. *Clin. cancer Res.* **2,** 416–420 (2005).

44. Heath, V. L. & Bicknell, R. Anticancer strategies involving the vasculature. *Nat. Rev. Clin. Oncol.* **6,** 395–404 (2009).

45. Hollebecque, A. Vascular disrupting agents: a delicate balance between efficacy and side effects. *Curr Opin Oncol.* **24,** 305–15 (2012).

46. Tozer, G. M. *et al.* Tumour vascular disrupting agents: combating treatment resistance. *Br. J. Radiol.* **81 Spec No,** S12–20 (2008).

47. Kanthou, C. & Tozer, G. Selective destruction of the tumour vasculature by targeting the endothelial cytoskeleton. *Drug Discov. Today Ther. Strateg.* **4,** 237–243 (2008).

48. III, J. L. Vascular disrupting agents. *Bioorg. Med. Chem.* **15,** 605–615 (2007).

49. Kim, S., Peshkin, L. & Mitchison, T. Vascular Disrupting Agent Drug Classes Differ in Effects on the Cytoskeleton. *PLoS One* **7,** e40177 (2012).

50. Patterson, D. & Rustin, G. Vascular damaging agents. *Clin. Oncol.* **19,** 443–456 (2007).

51. Schwartz, E. L. Antivascular actions of microtubule-binding drugs. *Clin. Cancer Res.* **15,** 2594–601 (2009).

52. Jordan, M. & Wilson, L. Microtubules as a target for anticancer drugs. *Nat. Rev. Cancer* **4,** (2004).

53. Kanthou, C. & Tozer, G. M. The tumor vascular targeting agent combretastatin A-4-phosphate induces reorganization of the actin cytoskeleton and early membrane blebbing in human endothelial cells. *Blood* **99,** 2060–9 (2002).

54. Kanthou, C. & Tozer, G. M. Microtubule depolymerizing vascular disrupting agents: novel therapeutic agents for oncology and other pathologies. *Int. J. Exp. Pathol.* **90,** 284–94 (2009).

55. Honoré, S. *et al.* Antiangiogenic vinflunine affects EB1 localization and microtubule targeting to adhesion sites. *Mol. Cancer Ther.* **7,** 2080–9 (2008).

56. Giannotta, M., Trani, M. & Dejana, E. VE-cadherin and endothelial adherens junctions: active guardians of vascular integrity. *Dev. Cell* **26,** 441–54 (2013).

57. Millán, J. *et al.* Adherens junctions connect stress fibres between adjacent endothelial cells. *BMC Biol.* **8,** 11 (2010).

58. Vincent, L. *et al.* Combretastatin A4 phosphate induces rapid regression of tumor neovessels and growth through interference with vascular endothelial-cadherin signaling. *J. Clin. Invest.* **115,** 2992–3006 (2005).

59. Dark, G. G. *et al.* Combretastatin A-4, an agent that displays potent and selective toxicity toward tumor vasculature. *Cancer Res.* **57,** 1829–34 (1997).

60. Tozer, G. M. *et al.* Combretastatin A-4 phosphate as a tumor vascular-targeting agent: early effects in tumors and normal tissues. *Cancer Res.* **59,** 1626–34 (1999).

61. Tozer, G. M., Kanthou, C. & Baguley, B. C. Disrupting tumour blood vessels. *Nat. Rev. Cancer* **5,** 423–35 (2005).

62. Pasquier, E. & Kavallaris, M. Microtubules: a dynamic target in cancer therapy. *IUBMB Life* **60,** 165–70 (2008).

63. Romagnoli, R. *et al.* Discovery and optimization of a series of 2-aryl-4-amino-5-(3',4',5'-trimethoxybenzoyl)thiazoles as novel anticancer agents. *J. Med. Chem.* **55,** 5433–45 (2012).

64. Abdollahi, A. & Folkman, J. Evading tumor evasion: current concepts and perspectives of anti-angiogenic cancer therapy. *Drug Resist. Updat.* **13,** 16–28 (2010).

65. Soda, Y., Myskiw, C., Rommel, A. & Verma, I. Mechanisms of neovascularization and resistance to anti-angiogenic therapies in glioblastoma multiforme. *J. Mol. Med.* **91,** 439–48 (2013).

66. Porcù, E. *et al.* TR-644 a novel potent tubulin binding agent induces impairment of endothelial cells function and inhibits angiogenesis. *Angiogenesis* **16,** 647–62 (2013).

67. Jordan, M. A. & Wilson, L. Microtubules as a target for anticancer drugs. *Nat. Rev. Cancer* **4,** 253–65 (2004).

68. Dumontet, C. & Jordan, M. A. Microtubule-binding agents: a dynamic field of cancer therapeutics. *Nat. Rev. Drug Discov.* **9,** 790–803 (2010).

69. Grosios, K., Holwell, S. E., McGown, a T., Pettit, G. R. & Bibby, M. C. In vivo and in vitro evaluation of combretastatin A-4 and its sodium phosphate prodrug. *Br. J. Cancer* **81,** 1318–27 (1999).

70. Gaukroger, K., Hadfield, J. A., Lawrence, N. J., Nolan, S. & McGown, A. T. Structural requirements for the interaction of combretastatins with tubulin: how important is the trimethoxy unit? *Org. Biomol. Chem.* **1,** 3033–7 (2003).

71. Tron, G. C. *et al.* Medicinal chemistry of combretastatin A4: present and future directions. *J. Med. Chem.* **49,** 3033–44 (2006).

72. Wang, L. *et al.* Potent, orally active heterocycle-based combretastatin A-4 analogues: synthesis, structure-activity relationship, pharmacokinetics, and in vivo antitumor activity evaluation. *J. Med. Chem.* **45,** 1697–711 (2002).

73. Schobert, R. *et al.* 4-(3-Halo/amino-4,5-dimethoxyphenyl)-5-aryloxazoles and -N-methylimidazoles that are cytotoxic against combretastatin A resistant tumor cells and vascular disrupting in a cisplatin resistant germ cell tumor model. *J. Med. Chem.* **53,** 6595–602 (2010).

74. Ohsumi, K. *et al.* Syntheses and antitumor activity of cis-restricted combretastatins: 5-membered heterocyclic analogues. *Bioorg. Med. Chem. Lett.* **8,** 3153–8 (1998).

75. Tron, G. C., Pagliai, F., Del Grosso, E., Genazzani, A. A. & Sorba, G. Synthesis and cytotoxic evaluation of combretafurazans. *J. Med. Chem.* **48,** 3260–8 (2005).

76. Liu, T. *et al.* Synthesis and biological evaluation of 3,4-diaryl-5-aminoisoxazole derivatives. *Bioorg. Med. Chem.* **17,** 6279–85 (2009).

77. Wu, M. *et al.* Synthesis and activity of Combretastatin A-4 analogues: 1,2,3-thiadiazoles as potent antitumor agents. *Bioorg. Med. Chem. Lett.* **17,** 869–73 (2007).

78. Romagnoli, R. *et al.* Synthesis and antitumor activity of 1,5-disubstituted 1,2,4-triazoles as cis-restricted combretastatin analogues. *J. Med. Chem.* **53,** 4248–58 (2010).

79. Romagnoli, R. *et al.* Convergent synthesis and biological evaluation of 2-amino-4-(3',4',5'-trimethoxyphenyl)-5-aryl thiazoles as microtubule targeting agents. *J. Med. Chem.* **54,** 5144–53 (2011).

80. Dejana, E. & Giampietro, C. Vascular endothelial-cadherin and vascular stability. *Curr. Opin. Hematol.* **19,** 218–23 (2012).

81. Vittet, D., Buchou, T., Schweitzer, A., Dejana, E. & Huber, P. Targeted null-mutation in the vascular endothelial-cadherin gene impairs the organization of vascular-like structures in embryoid bodies. *Proc. Natl. Acad. Sci. U. S. A.* **94,** 6273–8 (1997).

82. Feraud, O., Cao, Y. & Vittet, D. Embryonic stem cell-derived embryoid bodies development in collagen gels recapitulates sprouting angiogenesis. *Lab. Invest.* **81,** 1669–81 (2001).

83. Dejana, E., Orsenigo, F. & Lampugnani, M. G. The role of adherens junctions and VE-cadherin in the control of vascular permeability. *J. Cell Sci.* **121,** 2115–22 (2008).

84. Bogatcheva, N. V & Verin, A. D. The role of cytoskeleton in the regulation of vascular endothelial barrier function. *Microvasc. Res.* **76,** 202–7 (2008).

85. Mitra, S. K., Hanson, D. A. & Schlaepfer, D. D. Focal adhesion kinase: in command and control of cell motility. *Nat. Rev. Mol. Cell Biol.* **6,** 56–68 (2005).

86. Herzog, B., Pellet-Many, C., Britton, G., Hartzoulakis, B. & Zachary, I. C. VEGF binding to NRP1 is essential for VEGF stimulation of endothelial cell migration, complex formation between NRP1 and VEGFR2, and signaling via FAK Tyr407 phosphorylation. *Mol. Biol. Cell* **22,** 2766–76 (2011).

87. Chen, X. L. *et al.* VEGF-induced vascular permeability is mediated by FAK. *Dev. Cell* **22,** 146–57 (2012).

88. Andrés, G. *et al.* A pro-inflammatory signature mediates FGF2-induced angiogenesis. *J. Cell. Mol. Med.* **13,** 2083–108 (2009).

89. Atherton-Fessler, S. *et al.* Cell cycle regulation of the p34cdc2 inhibitory kinases. *Mol. Biol. Cell* **5,** 989–1001 (1994).

90. Choi, H. J., Fukui, M. & Zhu, B. T. Role of cyclin B1/Cdc2 up-regulation in the development of mitotic prometaphase arrest in human breast cancer cells treated with nocodazole. *PLoS One* **6,** e24312 (2011).

91. Mollinedo, F. & Gajate, C. Microtubules, microtubule-interfering agents and apoptosis. *Apoptosis* **8,** 413–50 (2003).

92. Lu, H., Murtagh, J. & Schwartz, E. L. The microtubule binding drug laulimalide inhibits vascular endothelial growth factor-induced human endothelial cell migration and is synergistic when combined with docetaxel (taxotere). *Mol. Pharmacol.* **69,** 1207–15 (2006).

93. Murtagh, J., Lu, H. & Schwartz, E. L. Taxotere-induced inhibition of human endothelial cell migration is a result of heat shock protein 90 degradation. *Cancer Res.* **66,** 8192–9 (2006).

94. Qin, L. & Zhang, M. Maspin regulates endothelial cell adhesion and migration through an integrin signaling pathway. *J. Biol. Chem.* **285,** 32360–9 (2010).

95. Dalyot-Herman, N., Delgado-Lopez, F., Gewirtz, D. A., Gupton, J. T. & Schwartz, E. L. Interference with endothelial cell function by JG-03-14, an agent that binds to the colchicine site on microtubules. *Biochem. Pharmacol.* **78,** 1167–77 (2009).

96. Katz, M. *et al.* A reciprocal tensin-3-cten switch mediates EGF-driven mammary cell migration. *Nat. Cell Biol.* **9,** 961–9 (2007).

97. Presta, M., Andrés, G., Leali, D., Dell'Era, P. & Ronca, R. Inflammatory cells and chemokines sustain FGF2-induced angiogenesis. *Eur. Cytokine Netw.* **20,** 39–50 (2009).

98. Iversen, A., Busk, M. & Horsman, M. Induction of hypoxia by vascular disrupting agents and the significance for their combination with radiation therapy. *Acta Oncol. (Madr).* **52,** 1320–6 (2013).

99. Romagnoli, R. *et al.* Discovery and optimization of a series of 2-aryl-4-amino-5-(3′, 4′, 5′-trimethoxybenzoyl) thiazoles as novel anticancer agents. *J. Med. Chem.* **55,** 5433–45 (2012).

100. Aplin, a E., Howe, a, Alahari, S. K. & Juliano, R. L. Signal transduction and signal modulation by cell adhesion receptors: the role of integrins, cadherins, immunoglobulin-cell adhesion molecules, and selectins. *Pharmacol. Rev.* **50,** 197–263 (1998).

101. Quadri, S. K. Cross talk between focal adhesion kinase and cadherins: role in regulating endothelial barrier function. *Microvasc. Res.* **83,** 3–11 (2012).

102. Bolós, V., Gasent, J. M., López-Tarruella, S. & Grande, E. The dual kinase complex FAK-Src as a promising therapeutic target in cancer. *Onco. Targets. Ther.* **3,** 83–97 (2010).

103. Claesson-Welsh, L. & Welsh, M. VEGFA and tumour angiogenesis. *J. Intern. Med.* **273,** 114–27 (2013).

104. Amos, L. A. Microtubule structure and its stabilisation. *Org. Biomol. Chem.* **2,** 2153–60 (2004).

105. Walczak, C. E. Microtubule dynamics and tubulin interacting proteins. *Curr. Opin. Cell Biol.* **12,** 52–6 (2000).

106. Risinger, A. L., Giles, F. J. & Mooberry, S. L. Microtubule dynamics as a target in oncology. *Cancer Treat. Rev.* **35,** 255–61 (2009).

107. Downing, K. H. & Nogales, E. Tubulin structure: insights into microtubule properties and functions. *Curr. Opin. Struct. Biol.* **8,** 785–91 (1998).

108. Honore, S., Pasquier, E. & Braguer, D. Understanding microtubule dynamics for improved cancer therapy. *Cell. Mol. Life Sci.* **62,** 3039–56 (2005).

109. Pellegrini, F. & Budman, D. R. Review: tubulin function, action of antitubulin drugs, and new drug development. *Cancer Invest.* **23,** 264–73 (2005).

110. Screpanti, E. *et al.* A screen for kinetochore-microtubule interaction inhibitors identifies novel antitubulin compounds. *PLoS One* **5,** e11603 (2010).

111. Kingston, D. G. I. Tubulin-interactive natural products as anticancer agents. *J. Nat. Prod.* **72,** 507–15 (2009).

112. Pettit, G. R. *et al.* Isolation and structure of the strong cell growth and tubulin inhibitor combretastatin A-4. *Experientia* **45,** 209–11 (1989).

113. Lin, C. M., Ho, H. H., Pettit, G. R. & Hamel, E. Antimitotic natural products combretastatin A-4 and combretastatin A-2: studies on the mechanism of

their inhibition of the binding of colchicine to tubulin. *Biochemistry* **28,** 6984–91 (1989).

114. McGown, A. T. & Fox, B. W. Differential cytotoxicity of combretastatins A1 and A4 in two daunorubicin-resistant P388 cell lines. *Cancer Chemother. Pharmacol.* **26,** 79–81 (1990).

115. Romagnoli, R. *et al.* One-pot synthesis and biological evaluation of 2-pyrrolidinyl-4-amino-5-(3',4',5'-trimethoxybenzoyl)thiazole: a unique, highly active antimicrotubule agent. *Eur. J. Med. Chem.* **46,** 6015–24 (2011).

116. Toffoli, G. *et al.* Pleiotropic-resistant phenotype is a multifactorial phenomenon in human colon carcinoma cell lines. *Br. J. Cancer* **63,** 51–6 (1991).

117. Dupuis, M. L., Flego, M., Molinari, A. & Cianfriglia, M. Saquinavir induces stable and functional expression of the multidrug transporter P-glycoprotein in human CD4 T-lymphoblastoid CEMrev cells. *HIV Med.* **4,** 338–45 (2003).

118. Martello, L. A. *et al.* Elevated levels of microtubule destabilizing factors in a Taxol-resistant/dependent A549 cell line with an alpha-tubulin mutation. *Cancer Res.* **63,** 1207–13 (2003).

119. Hamel, E. Evaluation of antimitotic agents by quantitative comparisons of their effects on the polymerization of purified tubulin. *Cell Biochem. Biophys.* **38,** 1–22 (2003).

120. Verdier-Pinard, P. *et al.* Structure-activity analysis of the interaction of curacin A, the potent colchicine site antimitotic agent, with tubulin and effects of analogs on the growth of MCF-7 breast cancer cells. *Mol. Pharmacol.* **53,** 62–76 (1998).

121. Massarotti, A., Coluccia, A., Silvestri, R., Sorba, G. & Brancale, A. The tubulin colchicine domain: a molecular modeling perspective. *ChemMedChem* **7,** 33–42 (2012).

122. Ly, J. D., Grubb, D. R. & Lawen, A. The mitochondrial membrane potential (deltapsi(m)) in apoptosis; an update. *Apoptosis* **8,** 115–28 (2003).

123. Green, D. R. & Kroemer, G. The pathophysiology of mitochondrial cell death. *Science* **305,** 626–9 (2004).

124. Viola, G. *et al.* Central role of mitochondria and p53 in PUVA-induced apoptosis in human keratinocytes cell line NCTC-2544. *Toxicol. Appl. Pharmacol.* **227,** 84–96 (2008).

125. Cai, J. & Jones, D. P. Superoxide in apoptosis. Mitochondrial generation triggered by cytochrome c loss. *J. Biol. Chem.* **273,** 11401–4 (1998).

126. Nohl, H., Gille, L. & Staniek, K. Intracellular generation of reactive oxygen species by mitochondria. *Biochem. Pharmacol.* **69,** 719–23 (2005).

127. Rothe, G. & Valet, G. Flow cytometric analysis of respiratory burst activity in phagocytes with hydroethidine and 2',7'-dichlorofluorescin. *J. Leukoc. Biol.* **47,** 440–8 (1990).

128. Porter, A. G. & Jänicke, R. U. Emerging roles of caspase-3 in apoptosis. *Cell Death Differ.* **6,** 99–104 (1999).

129. Kuo, L. J. & Yang, L.-X. Gamma-H2AX - a novel biomarker for DNA double-strand breaks. *In Vivo* **22,** 305–9 (2008).

130. Matson, D. R. & Stukenberg, P. T. Spindle poisons and cell fate: a tale of two pathways. *Mol. Interv.* **11,** 141–50 (2011).

131. Liang, C.-C., Park, A. Y. & Guan, J.-L. In vitro scratch assay: a convenient and inexpensive method for analysis of cell migration in vitro. *Nat. Protoc.* **2,** 329–33 (2007).

132. Romagnoli, R. *et al.* Synthesis and biological evaluation of 2-(alkoxycarbonyl)-3-anilinobenzo[b]thiophenes and thieno[2,3-b]pyridines as new potent anticancer agents. *J. Med. Chem.* **56,** 2606–18 (2013).

133. Gascoigne, K. E. & Taylor, S. S. How do anti-mitotic drugs kill cancer cells? *J. Cell Sci.* **122,** 2579–85 (2009).

134. Clarke, P. R. & Allan, L. a. Cell-cycle control in the face of damage--a matter of life or death. *Trends Cell Biol.* **19,** 89–98 (2009).

135. Luch, A. Cell cycle control and cell division: implications for chemically induced carcinogenesis. *Chembiochem* **3,** 506–16 (2002).

136. Jin, Z. & El-Deiry, W. Overview of cell death signaling pathways. *Cancer Biol. Ther.* **2,** 139–63 (2005).

137. Marzo, I. & Naval, J. Antimitotic drugs in cancer chemotherapy: promises and pitfalls. *Biochem. Pharmacol.* **86,** 703–10 (2013).

138. Zhou, J. & Giannakakou, P. Targeting microtubules for cancer chemotherapy. *Curr. Med. Chem. Anticancer. Agents* **5,** 65–71 (2005).

139. Schmidt, M. & Bastians, H. Mitotic drug targets and the development of novel anti-mitotic anticancer drugs. *Drug Resist. Updat.* **10,** 162–81 (2007).

140. Ye, K. *et al.* Opium alkaloid noscapine is an antitumor agent that arrests metaphase and induces apoptosis in dividing cells. *Proc. Natl. Acad. Sci. U. S. A.* **95,** 1601–6 (1998).

141. Bughani, U., Li, S. & Joshi, H. C. Recent patents reveal microtubules as persistent promising target for novel drug development for cancers. *Recent Pat. Antiinfect. Drug Discov.* **4,** 164–82 (2009).

142. Hagel, J. M. & Facchini, P. J. Benzylisoquinoline alkaloid metabolism: a century of discovery and a brave new world. *Plant Cell Physiol.* **54,** 647–72 (2013).

143. Manchukonda, N. K. *et al.* Rational Design, Synthesis, and Biological Evaluation of Third Generation α-Noscapine Analogues as Potent Tubulin Binding Anti-Cancer Agents. *PLoS One* **8,** e77970 (2013).

144. Aneja, R. *et al.* Drug-resistant T-lymphoid tumors undergo apoptosis selectively in response to an antimicrotubule agent, EM011. *Blood* **107,** 2486–92 (2006).

145. Aneja, R. *et al.* A novel microtubule-modulating agent induces mitochondrially driven caspase-dependent apoptosis via mitotic checkpoint activation in human prostate cancer cells. *Eur. J. Cancer* **46,** 1668–78 (2010).

146. Mahmoudian, M. & Rahimi-Moghaddam, P. The anti-cancer activity of noscapine: a review. *Recent Pat. Anticancer. Drug Discov.* **4,** 92–7 (2009).

147. Aneja, R. *et al.* Development of a novel nitro-derivative of noscapine for the potential treatment of drug-resistant ovarian cancer and T-cell lymphoma. *Mol. Pharmacol.* **69,** 1801–9 (2006).

148. Zhou, J. *et al.* Brominated derivatives of noscapine are potent microtubule-interfering agents that perturb mitosis and inhibit cell proliferation. *Mol. Pharmacol.* **63,** 799–807 (2003).

149. Karna, P. *et al.* A novel microtubule-modulating noscapinoid triggers apoptosis by inducing spindle multipolarity via centrosome amplification and declustering. *Cell Death Differ.* **18,** 632–44 (2011).

150. Karna, P., Sharp, S. M., Yates, C., Prakash, S. & Aneja, R. EM011 activates a survivin-dependent apoptotic program in human non-small cell lung cancer cells. *Mol. Cancer* **8,** 93 (2009).

151. Ajeawung, N. F., Joshi, H. C. & Kamnasaran, D. The microtubule binding drug EM011 inhibits the growth of paediatric low grade gliomas. *Cancer Lett.* **335,** 109–18 (2013).

152. Gergely, F. & Basto, R. Multiple centrosomes: together they stand, divided they fall. *Genes Dev.* **22,** 2291–6 (2008).

153. Hadfield, J. A., Ducki, S., Hirst, N. & McGown, A. T. Tubulin and microtubules as targets for anticancer drugs. *Prog. Cell Cycle Res.* **5,** 309–25 (2003).

154. Liu., H.C. Joshi, K. Ye, J. Kapp, F. Noscapine and noscapine derivatives, useful as anticancer agents - U.S. Patent 6376516. (2002).

155. Manchukonda, N. K., Sridhar, B., Naik, P. K., Joshi, H. C. & Kantevari, S. Copper(I) mediated facile synthesis of potent tubulin polymerization inhibitor, 9-amino-α-noscapine from natural α-noscapine. *Bioorg. Med. Chem. Lett.* **22,** 2983–7 (2012).

156. Naik, P. K. *et al.* Rational design, synthesis and biological evaluations of amino-noscapine: a high affinity tubulin-binding noscapinoid. *J. Comput. Aided. Mol. Des.* **25,** 443–54 (2011).

157. Bognár, R., Gaál, G., Kerekes, P. & Szabó, S. [On the accompanying alkaloids of morphine. 1. Isolation of codeine, thebaine and narcotine]. *Pharmazie* **22,** 452–4 (1967).

158. Baradarani, M. M. & Prager, R. H. The specific epimerisation of phthalideisoquinoline alkaloids. *Tetrahedron Lett.* **40,** 7403–7406 (1999).

159. Miyaura, N. & Suzuki, A. Palladium-Catalyzed Cross-Coupling Reactions of Organoboron Compounds. *Chem. Rev.* **95,** 2457–2483 (1995).

160. Sipos, A., Kiss, B., Schmidt, E., Greiner, I. & Berényi, S. Synthesis and neuropharmacological evaluation of 2-aryl- and alkylapomorphines. *Bioorg. Med. Chem.* **16,** 3773–9 (2008).

161. Berenyi, S., Sipos, A., Szabo, I. & Kalai, T. Novel Route to 2-Arylapomorphines. *ChemInform* **38,** (2007).

162. Sipos, A., Debreceni, S., Szabó, R., Gyulai, Z. & Berényi, S. Synthesis of 3-Alkyl and Arylapomorphines. *Synth. Commun.* **37,** 2549–2558 (2007).

163. Martin, R. & Buchwald, S. L. Palladium-catalyzed Suzuki-Miyaura cross-coupling reactions employing dialkylbiaryl phosphine ligands. *Acc. Chem. Res.* **41,** 1461–73 (2008).

164. Snatzke, G. *et al.* The optical rotatory dispersion and circular dichroism of the phthalideisoquinoline alkaloids and of their α-hydroxybenzyltetrahydroisoquinoline derivatives. *Tetrahedron* **25,** 5059–5086 (1969).

165. Von Langermann, J. *et al.* (3R*,5'S*)-6,7-Dimeth-oxy-3-(4'-meth-oxy-6'-methyl-5',6',7',8'-tetra-hydro-1,3-dioxolo[4,5-g]isoquinolin-5'-yl)isobenzofuran-1(3H)-one (racemic α-noscapine). *Acta Crystallogr. Sect. E. Struct. Rep. Online* **66,** o570 (2010).

166. Seetharaman, J. & Rajan, S. S. Crystal and molecular structure of noscapine 1. *Zeitschrift für Krist.* **210,** 111–113 (1995).

167. Naik, P. K., Santoshi, S. & Joshi, H. C. Noscapinoids with anti-cancer activity against human acute lymphoblastic leukemia cells (CEM): a three dimensional chemical space pharmacophore modeling and electronic feature analysis. *J. Mol. Model.* **18,** 307–18 (2012).

168. Pinney, K. G. *et al.* A new anti-tubulin agent containing the benzo[b]thiophene ring system. *Bioorg. Med. Chem. Lett.* **9,** 1081–6 (1999).

169. Raffa, D. *et al.* Synthesis, antiproliferative activity, and mechanism of action of a series of 2-{[(2E)-3-phenylprop-2-enoyl]amino}benzamides. *Eur. J. Med. Chem.* **46,** 2786–96 (2011).

170. Hamel, E., Blokhin, A. V., Nagle, D. G., Yoo, H.-D. & Gerwick, W. H. Limitations in the use of tubulin polymerization assays as a screen for the identification of new antimitotic agents: The potent marine natural product curacin A as an example. *Drug Dev. Res.* **34,** 110–120 (1995).

171. Edler, M. C. *et al.* Demonstration of microtubule-like structures formed with (-)-rhazinilam from purified tubulin outside of cells and a simple tubulin-based assay for evaluation of analog activity. *Arch. Biochem. Biophys.* **487,** 98–104 (2009).

172. Lin, C. M. *et al.* Investigation of the mechanism of the interaction of tubulin with derivatives of 2-styrylquinazolin-4(3H)-one. *Mol. Pharmacol.* **40,** 827–32 (1991).

173. Kang, G. J., Getahun, Z., Muzaffar, A., Brossi, A. & Hamel, E. N-acetylcolchinol O-methyl ether and thiocolchicine, potent analogs of colchicine modified in the C ring. Evaluation of the mechanistic basis for their enhanced biological properties. *J. Biol. Chem.* **265,** 10255–9 (1990).

174. Naik, P. K., Santoshi, S., Rai, A. & Joshi, H. C. Molecular modelling and competition binding study of Br-noscapine and colchicine provide insight into noscapinoid-tubulin binding site. *J. Mol. Graph. Model.* **29,** 947–55 (2011).

175. Bhattacharyya, B. & Wolff, J. Promotion of fluorescence upon binding of colchicine to tubulin. *Proc. Natl. Acad. Sci. U. S. A.* **71,** 2627–31 (1974).

176. Kubo, A. & Tsukita, S. Non-membranous granular organelle consisting of PCM-1: subcellular distribution and cell-cycle-dependent assembly/disassembly. *J. Cell Sci.* **116,** 919–28 (2003).

177. Balczon, R., Bao, L. & Zimmer, W. E. PCM-1, A 228-kD centrosome autoantigen with a distinct cell cycle distribution. *J. Cell Biol.* **124,** 783–93 (1994).

178. Didier, C., Merdes, A., Gairin, J.-E. & Jabrane-Ferrat, N. Inhibition of proteasome activity impairs centrosome-dependent microtubule nucleation and organization. *Mol. Biol. Cell* **19,** 1220–9 (2008).

179. Kiyokawa, H. & Ray, D. In vivo roles of CDC25 phosphatases: biological insight into the anti-cancer therapeutic targets. *Anticancer. Agents Med. Chem.* **8,** 832–6 (2008).

180. Donzelli, M. & Draetta, G. F. Regulating mammalian checkpoints through Cdc25 inactivation. *EMBO Rep.* **4,** 671–7 (2003).

181. Walter, A. O., Seghezzi, W., Korver, W., Sheung, J. & Lees, E. The mitotic serine/threonine kinase Aurora2/AIK is regulated by phosphorylation and degradation. *Oncogene* **19,** 4906–16 (2000).

182. Quignon, F. *et al.* Sustained mitotic block elicits DNA breaks: one-step alteration of ploidy and chromosome integrity in mammalian cells. *Oncogene* **26,** 165–72 (2007).

183. Ganem, N. J. & Pellman, D. Linking abnormal mitosis to the acquisition of DNA damage. *J. Cell Biol.* **199,** 871–81 (2012).

184. Vermes, I., Haanen, C., Steffens-Nakken, H. & Reutelingsperger, C. A novel assay for apoptosis. Flow cytometric detection of phosphatidylserine expression on early apoptotic cells using fluorescein labelled Annexin V. *J. Immunol. Methods* **184,** 39–51 (1995).

185. Chiang, N.-J. *et al.* A novel synthetic microtubule inhibitor, MPT0B214 exhibits antitumor activity in human tumor cells through mitochondria-dependent intrinsic pathway. *PLoS One* **8,** e58953 (2013).

186. Denault, J.-B. & Salvesen, G. S. Caspases: keys in the ignition of cell death. *Chem. Rev.* **102,** 4489–500 (2002).

187. Wertz, I. E. *et al.* Sensitivity to antitubulin chemotherapeutics is regulated by MCL1 and FBW7. *Nature* **471,** 110–4 (2011).

188. Clevers, H. Wnt/beta-catenin signaling in development and disease. *Cell* **127,** 469–80 (2006).

189. Nusse, R. *et al.* A new nomenclature for int-1 and related genes: The Wnt gene family. *Cell* **64,** 231 (1991).

190. Klaus, A. & Birchmeier, W. Wnt signalling and its impact on development and cancer. *Nat. Rev. Cancer* **8,** 387–98 (2008).

191. Kikuchi, A., Yamamoto, H. & Sato, A. Selective activation mechanisms of Wnt signaling pathways. *Trends Cell Biol.* **19,** 119–29 (2009).

192. Niehrs, C. The complex world of WNT receptor signalling. *Nat. Rev. Mol. Cell Biol.* **13,** 767–79 (2012).

193. Gao, B. Wnt regulation of planar cell polarity (PCP). *Curr. Top. Dev. Biol.* **101,** 263–95 (2012).

194. Sugimura, R. & Li, L. Noncanonical Wnt signaling in vertebrate development, stem cells, and diseases. *Birth Defects Res. C. Embryo Today* **90,** 243–56 (2010).

195. Kohn, A. D. & Moon, R. T. Wnt and calcium signaling: beta-catenin-independent pathways. *Cell Calcium* **38,** 439–46 (2005).

196. Jamieson, C., Sharma, M. & Henderson, B. R. Wnt signaling from membrane to nucleus: β-catenin caught in a loop. *Int. J. Biochem. Cell Biol.* **44,** 847–850 (2012).

197. Reya, T. & Clevers, H. Wnt signalling in stem cells and cancer. *Nature* **434,** 843–50 (2005).

198. Niehrs, C. & Acebron, S. P. Mitotic and mitogenic Wnt signalling. *EMBO J.* **31,** 2705–13 (2012).

199. Nakamura, Y., Tsiairis, C. D., Özbek, S. & Holstein, T. W. Autoregulatory and repressive inputs localize Hydra Wnt3 to the head organizer. *Proc. Natl. Acad. Sci. U. S. A.* **108,** 9137–42 (2011).

200. Wang, G., Burk, O., Stange, E. & Wehkamp, J. Auto-regulation of human Tcf-4 by Wnt-β-catenin-Tcf-4 signaling. *Z. Gastroenterol.* **46,** P276 (2008).

201. Schuijers, J. & Clevers, H. Adult mammalian stem cells: the role of Wnt, Lgr5 and R-spondins. *EMBO J.* **31,** 2685–96 (2012).

202. Fakhry, M., Hamade, E., Badran, B., Buchet, R. & Magne, D. Molecular mechanisms of mesenchymal stem cell differentiation towards osteoblasts. *World J. Stem Cells* **5,** 136–148 (2013).

203. Pinto, D. & Clevers, H. Wnt, stem cells and cancer in the intestine. *Biol. Cell* **97,** 185–96 (2005).

204. Clevers, H. The Intestinal Crypt, A Prototype Stem Cell Compartment. *Cell* **154,** 274–284 (2013).

205. Holland, J. D., Klaus, A., Garratt, A. N. & Birchmeier, W. Wnt signaling in stem and cancer stem cells. *Curr. Opin. Cell Biol.* **25,** 254–64 (2013).

206. Saito-Diaz, K. *et al.* The way Wnt works: components and mechanism. *Growth Factors* **31,** 1–31 (2013).

207. Polakis, P. Wnt signaling and cancer. *Genes Dev.* **15,** 1837–1851 (2000).

208. Anastas, J. N. & Moon, R. T. WNT signalling pathways as therapeutic targets in cancer. *Nat. Rev. Cancer* **13,** 11–26 (2013).

209. MacDonald, B. T., Tamai, K. & He, X. Wnt/beta-catenin signaling: components, mechanisms, and diseases. *Dev. Cell* **17,** 9–26 (2009).

210. Vermeulen, L. *et al.* Wnt activity defines colon cancer stem cells and is regulated by the microenvironment. *Nat. Cell Biol.* **12,** 468–76 (2010).

211. Clevers, H. & Nusse, R. Wnt/β-Catenin Signaling and Disease. *Cell* **149,** 1192–1205 (2012).

212. Korinek, V. *et al.* Constitutive transcriptional activation by a beta-catenin-Tcf complex in APC-/- colon carcinoma. *Science* **275,** 1784–7 (1997).

213. McCartney, B. M. & Näthke, I. S. Cell regulation by the Apc protein Apc as master regulator of epithelia. *Curr. Opin. Cell Biol.* **20,** 186–93 (2008).

214. De Sousa, E. M. F., Vermeulen, L., Richel, D. & Medema, J. P. Targeting Wnt signaling in colon cancer stem cells. *Clin. Cancer Res.* **17,** 647–53 (2011).

215. Fearon, E. R. & Vogelstein, B. A genetic model for colorectal tumorigenesis. *Cell* **61,** 759–67 (1990).

216. Morán, A. *et al.* Differential colorectal carcinogenesis: Molecular basis and clinical relevance. *World J. Gastrointest. Oncol.* **2,** 151–8 (2010).

217. Bienz, M. & Clevers, H. Linking colorectal cancer to Wnt signaling. *Cell* **103,** 311–320 (2000).

218. Tian, W. *et al.* Structure-based discovery of a novel inhibitor targeting the β-catenin/Tcf4 interaction. *Biochemistry* **51,** 724–31 (2012).

219. Giles, R. H., van Es, J. H. & Clevers, H. Caught up in a Wnt storm: Wnt signaling in cancer. *Biochim. Biophys. Acta - Rev. Cancer* **1653,** 1–24 (2003).

220. Voloshanenko, O. *et al.* Wnt secretion is required to maintain high levels of Wnt activity in colon cancer cells. *Nat. Commun.* **4,** 2610 (2013).

221. Cruciat, C.-M. & Niehrs, C. Secreted and transmembrane wnt inhibitors and activators. *Cold Spring Harb. Perspect. Biol.* **5,** a015081 (2013).

222. Baarsma, H. A., Königshoff, M. & Gosens, R. The WNT signaling pathway from ligand secretion to gene transcription: Molecular mechanisms and pharmacological targets. *Pharmacol. Ther.* **138,** 66–83 (2013).

223. Huang, S.-M. a *et al.* Tankyrase inhibition stabilizes axin and antagonizes Wnt signalling. *Nature* **461,** 614–20 (2009).

224. Thorne, C. a *et al.* Small-molecule inhibition of Wnt signaling through activation of casein kinase 1α. *Nat. Chem. Biol.* **6,** 829–36 (2010).

225. Thakur, R. & Mishra, D. P. Pharmacological modulation of beta-catenin and its applications in cancer therapy. *J. Cell. Mol. Med.* **17,** 449–56 (2013).

226. Bialkowska, A. B. & Yang, V. W. High-throughput screening strategies for targeted identification of therapeutic compounds in colorectal cancer. *Future Oncol.* **8,** 259–72 (2012).

227. Voronkov, A. & Krauss, S. Wnt/beta-catenin signaling and small molecule inhibitors. *Curr. Pharm. Des.* **19,** 634–64 (2013).

228. Burgess, A. W., Faux, M. C., Layton, M. J. & Ramsay, R. G. Wnt signaling and colon tumorigenesis--a view from the periphery. *Exp. Cell Res.* **317,** 2748–58 (2011).

229. Taketo, M. M. Shutting down Wnt signal-activated cancer. *Nat. Genet.* **36,** 320–2 (2004).

230. Gao, C. & Chen, Y.-G. Dishevelled: The hub of Wnt signaling. *Cell. Signal.* **22,** 717–27 (2010).

231. Peterson, R. Drug discovery: propping up a destructive regime. *Nature* **461,** (2009).

232. Miyoshi, Y. *et al.* Somatic mutations of the APC gene in colorectal tumors: mutation cluster region in the APC gene. *Hum. Mol. Genet.* **1,** 229–33 (1992).

233. Polakis, P. The many ways of Wnt in cancer. *Curr. Opin. Genet. Dev.* **17,** 45–51 (2007).

234. Fodde, R., Smits, R. & Clevers, H. APC, signal transduction and genetic instability in colorectal cancer. *Nat. Rev. Cancer* **1,** 55–67 (2001).

235. Suzuki, H. *et al.* Epigenetic inactivation of SFRP genes allows constitutive WNT signaling in colorectal cancer. *Nat. Genet.* **36,** 417–22 (2004).

236. Shan, B.-E., Wang, M.-X. & Li, R. Quercetin inhibit human SW480 colon cancer growth in association with inhibition of cyclin D1 and survivin expression through Wnt/beta-catenin signaling pathway. *Cancer Invest.* **27,** 604–12 (2009).

237. Luu, H. & Zhang, R. Wnt/beta-catenin signaling pathway as novel cancer drug targets. *Curr. Cancer Drug Targets* **4,** 653–671 (2004).

238. Zhang, W. *et al.* Fluorinated N,N-dialkylaminostilbenes for Wnt pathway inhibition and colon cancer repression. *J. Med. Chem.* **54,** 1288–97 (2011).

239. Chen, W., Chen, M. & Barak, L. S. Development of small molecules targeting the Wnt pathway for the treatment of colon cancer: a high-throughput screening approach. *Am. J. Physiol. Gastrointest. Liver Physiol.* **299,** G293–300 (2010).

240. Chen, B. *et al.* Small molecule-mediated disruption of Wnt-dependent signaling in tissue regeneration and cancer. *Nat. Chem. Biol.* **5,** 100–7 (2009).

241. Ewan, K. *et al.* A useful approach to identify novel small-molecule inhibitors of Wnt-dependent transcription. *Cancer Res.* **70,** 5963–73 (2010).

242. Liu, J. *et al.* A Small-Molecule Agonist of the Wnt Signaling Pathway. *Angew. Chemie* **117,** 2023–2026 (2005).

243. Pelletier, J. C. *et al.* (1-(4-(Naphthalen-2-yl)pyrimidin-2-yl)piperidin-4-yl)methanamine: a wingless beta-catenin agonist that increases bone formation rate. *J. Med. Chem.* **52,** 6962–5 (2009).

244. Cosimelli, B. *et al.* Derivatives of 4-amino-6-hydroxy-2-mercaptopyrimidine as novel, potent, and selective A3 adenosine receptor antagonists. *J. Med. Chem.* **51,** 1764–70 (2008).

245. Laneri, S. *et al.* Synthesis and Antihypertensive Action of New Imidazo[1,2-a]pyridine Derivatives , non Peptidic Angiotensin II Receptor Antagonists. *Cardiovasc. Hematol. Disord. Targets* **11,** 87–96 (2011).

246. Barker, N. & Clevers, H. Mining the Wnt pathway for cancer therapeutics. *Nat. Rev. Drug Discov.* **5,** 997–1014 (2006).

247. Dihlmann, S., Klein, S. & Doeberitz Mv, M. von K. Reduction of beta-catenin/T-cell transcription factor signaling by aspirin and indomethacin is caused by an increased stabilization of phosphorylated beta-catenin. *Mol. Cancer Ther.* **2,** 509–16 (2003).

248. Rampazzo, E. *et al.* Wnt activation promotes neuronal differentiation of glioblastoma. *Cell Death Dis.* **4,** e500 (2013).

249. Emami, K. H. *et al.* A small molecule inhibitor of beta-catenin/CREB-binding protein transcription [corrected]. *Proc. Natl. Acad. Sci. U. S. A.* **101,** 12682–7 (2004).

250. Li, J., Mizukami, Y., Zhang, X., Jo, W.-S. & Chung, D. C. Oncogenic K-ras stimulates Wnt signaling in colon cancer through inhibition of GSK-3beta. *Gastroenterology* **128,** 1907–18 (2005).

251. Pacheco-Pinedo, E. C. *et al.* Wnt/β-catenin signaling accelerates mouse lung tumorigenesis by imposing an embryonic distal progenitor phenotype on lung epithelium. *J. Clin. Invest.* **121,** 1935–45 (2011).

252. Gregorieff, A. & Clevers, H. Wnt signaling in the intestinal epithelium: from endoderm to cancer. *Genes Dev.* **19,** 877–90 (2005).

253. Roose, J. *et al.* Synergy between tumor suppressor APC and the beta-catenin-Tcf4 target Tcf1. *Science* **285,** 1923–6 (1999).

254. Wang, A., Yoshimi, N., Ino, N., Tanaka, T. & Mori, H. Overexpression of cyclin B1 in human colorectal cancers. *J. Cancer Res. Clin. Oncol.* **123,** 124–7 (1997).

255. Li, J.-Q. *et al.* Cyclin B1, unlike cyclin G1, increases significantly during colorectal carcinogenesis and during later metastasis to lymph nodes. *Int. J. Oncol.* **22,** 1101–10 (2003).

256. Tao, L. *et al.* Altered expression of c-myc, p16 and p27 in rat colon tumors and its reversal by short-term treatment with chemopreventive agents. *Carcinogenesis* **23,** 1447–54 (2002).

257. Moro, E. *et al.* In vivo Wnt signaling tracing through a transgenic biosensor fish reveals novel activity domains. *Dev. Biol.* **366,** 327–40 (2012).

258. Jung, P. & Hermeking, H. The c-MYC-AP4-p21 cascade. *Cell Cycle* **8,** 982–9 (2009).

259. Jung, P., Menssen, A., Mayr, D. & Hermeking, H. AP4 encodes a c-MYC-inducible repressor of p21. *Proc. Natl. Acad. Sci. U. S. A.* **105,** 15046–51 (2008).

260. Pettit, G. R. *et al.* Antineoplastic agents. 291. Isolation and synthesis of combretastatins A-4, A-5, and A-6(1a). *J. Med. Chem.* **38,** 1666–72 (1995).

261. Pettit, G. R. *et al.* Antineoplastic agents 322. synthesis of combretastatin A-4 prodrugs. *Anticancer. Drug Des.* **10,** 299–309 (1995).

262. Dorléans, A. *et al.* Variations in the colchicine-binding domain provide insight into the structural switch of tubulin. *Proc. Natl. Acad. Sci. U. S. A.* **106,** 13775–9 (2009).

263. Group, C. C. Molecular Operating Environment (MOE 2010). *Inc. Montr. Quebec, Canada.* (2010). at <http://www.chemcomp.com>

264. Korb, O., Stützle, T. & Exner, T. PLANTS: Application of Ant Colony Optimization to Structure-Based Drug Design. *Ant Colony Optim. Swarm Intell.* (2006).

265. Mitola, S., Strasly, M., Prato, M., Ghia, P. & Bussolino, F. IL-12 regulates an endothelial cell-lymphocyte network: effect on metalloproteinase-9 production. *J. Immunol.* **171,** 3725–33 (2003).

266. Basili, S. *et al.* Diazoniapolycyclic ions inhibit the activity of topoisomerase I and the growth of certain tumor cell lines. *ChemMedChem* **3,** 1671–6 (2008).

267. Viola, G. *et al.* Induction of gamma-globin mRNA, erythroid differentiation and apoptosis in UVA-irradiated human erythroid cells in the presence of furocumarin derivatives. *Biochem. Pharmacol.* **75,** 810–25 (2008).

268. Wang, X. *et al.* Wnt signaling regulates postembryonic hypothalamic progenitor differentiation. *Dev. Cell* **23,** 624–36 (2012).

269. Guidolin, D., Vacca, A., Nussdorfer, G. G. & Ribatti, D. A new image analysis method based on topological and fractal parameters to evaluate the angiostatic activity of docetaxel by using the Matrigel assay in vitro. *Microvasc. Res.* **67,** 117–24 (2004).

270. Chiodelli, P. *et al.* Heparan sulfate proteoglycans mediate the angiogenic activity of the vascular endothelial growth factor receptor-2 agonist gremlin. *Arterioscler. Thromb. Vasc. Biol.* **31,** e116–27 (2011).